UNIVERSITÀ DEGLI STUDI DI PALERMO

Dottorato di Ricerca in
SISTEMI AGRO-ALIMENTARI E FORESTALI MEDITERRANEI
Dipartimento di Scienze Agrarie, Alimentari e Forestali SAAF
Settore Scientifico Disciplinare AGR/08 Idraulica agraria e sistemazioni idraulico-forestali

IMPACT OF DISTURBANCE AND AMENDMENT ON SOIL HYDRAULIC BEHAVIOUR

IL DOTTORE

FRANCESCO ZANNA

IL COORDINATORE

PROF. MASSIMO IOVINO

IL TUTOR

PROF. VINCENZO BAGARELLO

IL CO-TUTOR

PROF. DARIO GIAMBALVO

Index

Chapter 1– Introduction

The current global economic and environmental context is placing increasing pressure on agri-food and forestry systems, requiring scientific research to address challenges that are complex, interconnected, and rapidly evolving. Among the most critical issues there are the increase in global food demand, driven by population growth and changing consumption patterns, and the wide-ranging impacts of climate change on natural resources, ecosystem functioning, and agricultural productivity (Schneider et al., 2011). These dynamics do not act independently, but rather interact across spatial and temporal scales, amplifying existing vulnerabilities and creating new constraints for land-based production systems.

Responding to these challenges increasingly relies on the integration of technological innovation within agricultural and forestry systems, alongside the refinement of traditional cultivation practices. Advances in precision agriculture, digital monitoring, and alternative cultivation systems have opened new possibilities for improving efficiency and resource use. However, technological progress alone is insufficient if not supported by a solid understanding of the biophysical processes governing agri-forest systems. Among the multiple variables that regulate these systems, soil stands out as a central and irreplaceable interface through which climate variability, land management practices, and technological interventions directly influence both productivity and environmental stability (Seneviratne et al., 2010).

Soil plays a central role in mediating water fluxes, nutrient cycling, and biological activity, thereby sustaining plant growth and ecosystem services (Bauke et al., 2022). Improving the understanding of soil processes and their response to environmental and anthropogenic pressures is therefore a fundamental step toward supporting resilient agroecosystems, preserving ecosystem functions, and ensuring the long-term sustainability of food production systems (Smith et al., 2016). Soil is a non-renewable and increasingly threatened resource, whose degradation has reached alarming levels worldwide. In fact, according to international assessments by the FAO (2015), the progressive loss of arable land due to erosion, soil sealing, and fertility decline represents one of the major environmental emergencies at the global scale (Eswaran et al, 2019). These problems are particularly critical in regions already characterized by environmental fragility and high anthropogenic pressure.

The Mediterranean basin is widely recognized as a hotspot of climate change impacts and land degradation. Here, water availability represents a major limiting factor for agricultural and forest

ecosystems, and this constraint is expected to intensify in the coming decades (Lionello et al., 2014; Tramblay et al., 2020). Although total annual precipitation has remained broadly stable or has slightly decreased in recent decades (Caloiero et al., 2019), rainfall is increasingly concentrated in short, high-intensity events separated by prolonged dry periods (Vallebona et al., 2015). This shift results in greater surface runoff and accentuated erosion risk, especially where vegetation cover is scarce or soils are compacted and poorly structured

In Sicily, these issues are further intensified by socio-economic and land-use dynamics. The progressive conversion of agricultural land to urban areas, infrastructures, and photovoltaic installations has reduced the extent of productive soils, while the widespread abandonment of marginal farmland has favoured the development of degraded and poorly vegetated surfaces. These dynamics, coupled with recurrent drought, loss of soil organic matter, and the advance of desertification processes, are leading to a progressive decline in both soil fertility and ecosystem resilience, with cascading effects on biodiversity and local habitats (Giordano et al., 2007). The relevance of these challenges is clearly reflected in national and regional policy frameworks. In Italy, strategic instruments such as the National Recovery and Resilience Plan (PNRR) and regional development programmes, including the PO FESR Sicilia, explicitly identify innovation in agriculture, sustainable land and forest governance, and hydrogeological risk mitigation as priority objectives.

By controlling water infiltration, storage, and redistribution, soil governs both water availability for vegetation and the partitioning of rainfall between infiltration and surface runoff. As a result, soil hydrological and hydraulic properties play a decisive role in agricultural productivity, ecosystem stability, and landscape resilience (Vereecken et al., 2022). Gaining a deeper understanding of these properties is therefore essential to support both agricultural productivity and environmental protection, particularly in Mediterranean environments characterized by strong climatic variability. From a management perspective, reliable analysis and evidence-based decision-making are crucial to addressing two major and complementary challenges. On one hand, during prolonged dry periods, improving water-use efficiency requires optimized irrigation strategies and soils capable of retaining and transmitting water effectively within the root zone (Evans et al., 2008). On the other hand, during intense rainfall events, reducing runoff and erosion risks depends on the ability to identify soils with limited infiltration capacity or water repellency and to implement targeted environmental engineering and reforestation measures aimed at restoring soil functionality and landscape stability (Martínez-Mena et al., 2020).

However, soil hydrological properties are dynamic and can change over time as a result of both natural processes and human activities (Biddoccu et al., 2017). Natural processes such as the transport and deposition of fine particles over more permeable surfaces can modify the soil texture distribution, reducing infiltration capacity and altering water retention. At the same time, anthropogenic actions, such as the application of organic or mineral amendments, can modify the soil matrix to improve its structure, porosity, and overall hydrological response. Conversely, human activities may also introduce pollutants or microplastics into soils, with potentially adverse effects on infiltration and retention dynamics. Other disturbances, such as wildfires, can also cause significant and often long-lasting changes in soil hydraulic behaviour. In both agricultural and forest environments, fires can lead to surface sealing, loss of organic matter, and the onset of soil water repellency, thereby increasing runoff and erosion risks. Despite their central role, soil hydraulic properties are often characterized under simplified conditions and remain poorly understood in the presence of the multiple disturbances that increasingly affect agricultural and forest soils, particularly in Mediterranean environments. This limits the ability to predict soil–water behaviour under real management and climatic scenarios, thereby reducing the effectiveness of both agronomic practices and environmental mitigation strategies.

It is precisely this knowledge gap that motivates the research activities carried out during the doctoral period. The various forms of disturbance and alteration affecting soils, and consequently their hydraulic behaviour, give rise to a wide range of conditions that are highly heterogeneous and strongly context-dependent. Addressing this complexity requires moving beyond generalized assumptions and focusing on specific, well-defined scenarios that are representative of real agricultural and forest systems. Accordingly, the research adopted a strongly site-oriented approach, working predominantly with local soils and disturbance processes that are characteristic of Sicilian agri-forest environments. For instance, in the case of layered soils resulting from surface compaction or lateral transport and deposition of finer materials, hydraulic responses can vary substantially depending on the contrast between layers and their thickness. Investigating these dynamics in representative agricultural soils allowed a more realistic assessment of how such stratification influences infiltration and near-saturated flow conditions.

An even higher level of complexity emerges when external materials are incorporated into the soil matrix. Microplastics provide a clear example: plastics and microplastics can reach soils through multiple pathways, generating a wide variability in polymer type, shape, and size, which interacts with the inherent variability of soil properties. Much of the existing literature has attempted to address the question of “the effect of microplastics” in a generalized manner, often by testing a large number

of treatments that combine multiple soils, polymers, shapes, and concentrations. In contrast, the research presented here deliberately focused on a limited number of representative combinations, selecting three soils commonly used for herbaceous crops in Sicily, five microplastic types widely employed in mulching films, the main source of microplastics in agricultural soils. and a single, realistic concentration. This approach allowed a clearer interpretation of soil–microplastic interactions under conditions relevant to Mediterranean agriculture. Similarly, with regard to soil amendments, the research addressed a less explored aspect of the literature, namely their influence on soil hydrodynamic and hydrostatic properties. While the agronomic benefits of amendments such as compost, biochar, and zeolite are well documented in terms of soil chemistry and fertility, their effects on water flow and retention, particularly under near-saturated conditions, remain insufficiently quantified. The studies therefore examined these effects using Sicilian agricultural soils and scenarios typical of Mediterranean systems, including surface disturbances such as rill formation, where hydrological processes play a key role in erosion development.

Taken together, these research choices reflect the need to investigate soil hydraulic behaviour under altered but realistic conditions, where natural processes and human interventions intersect. Rather than seeking universal responses, the work aims to contribute detailed, context-specific knowledge that improves understanding of how soils function when subjected to common agricultural and environmental pressures, thereby supporting more informed soil and land management strategies in Mediterranean regions

Equally important is the methodological dimension of soil research. Accurately describing soil hydraulic behaviour requires robust experimental approaches and reliable measurement techniques capable of capturing spatial and temporal variability. Continuous improvement in sampling strategies, measurement procedures, and data analysis methods is therefore essential to properly represent soil behaviour across space and time and to ensure the comparability of results among different studies and sites. Within this perspective, specific research activities were carried out with the aim of improving the optimization and reproducibility of laboratory methodologies, which represent a fundamental prerequisite for the correct characterization of soil hydrodynamic responses. Refining laboratory procedures contributes not only to reducing experimental uncertainty, but also to strengthening the reliability of infiltration measurements and their interpretation.

Building a solid, data-based framework for soil hydrology thus becomes a key objective. Such a framework enables the integration of experimental observations with modelling and mapping tools, supporting informed decisions in land use planning, irrigation management, and ecosystem

restoration. In this way, methodological advances play a crucial role in translating scientific research into effective and operational solutions for sustainable soil and water management.

1.1 Thesis Structure

The thesis is structured into three main sections and an appendix, each addressing a specific stage of this research path. The first three sections present work that have been published to international peer-reviewed journals, while the appendix includes ongoing works that have not yet been completed or published.

- **The Infiltration Measurements with the Mini Disk Infiltrometer section** focuses on evaluating different column packing methods for laboratory analyses, aiming to improve the accuracy and repeatability of infiltration measurements under controlled conditions together with the development and testing of a 3D-printed Mini Disk Infiltrometer (MDI).
- **The Infiltration Processes in Layered Soils section** analyses the effects of soil stratification on infiltration dynamics, focusing on how textural discontinuities influence water flow through the soil profile.
- **The Hydrological Behaviour of Amended Soils section** investigates the hydraulic response of soils modified by the presence of anthropogenic materials such as microplastics or agronomic amendments including compost, zeolite, and biochar, with the goal of assessing how these additions alter soil hydrodynamic properties and water flow processes.
- **The Appendix** includes two completed experiments under analysis: the first follows the previous laboratory investigation on amended soils, transferring the laboratory experience to field conditions, in ordet to evaluate how the effects of compost and zeolite evolve over the medium term after exposure to atmospheric agents. The second examines the development of soil water repellency after wildfires. Both studies are based on completed experimental activities and include preliminary analyses of the collected data. They are presented here because they document a significant part of the research conducted during the PhD programme, and the completion of data processing and interpretation is expected to lead to the preparation of manuscripts for submission to peer-reviewed journals.

Figure 1 provides a schematic overview of the conceptual framework and structure of the PhD research. It summarizes the main research objectives and illustrates how the different thematic areas are integrated and logically connected within the overall research pathway.

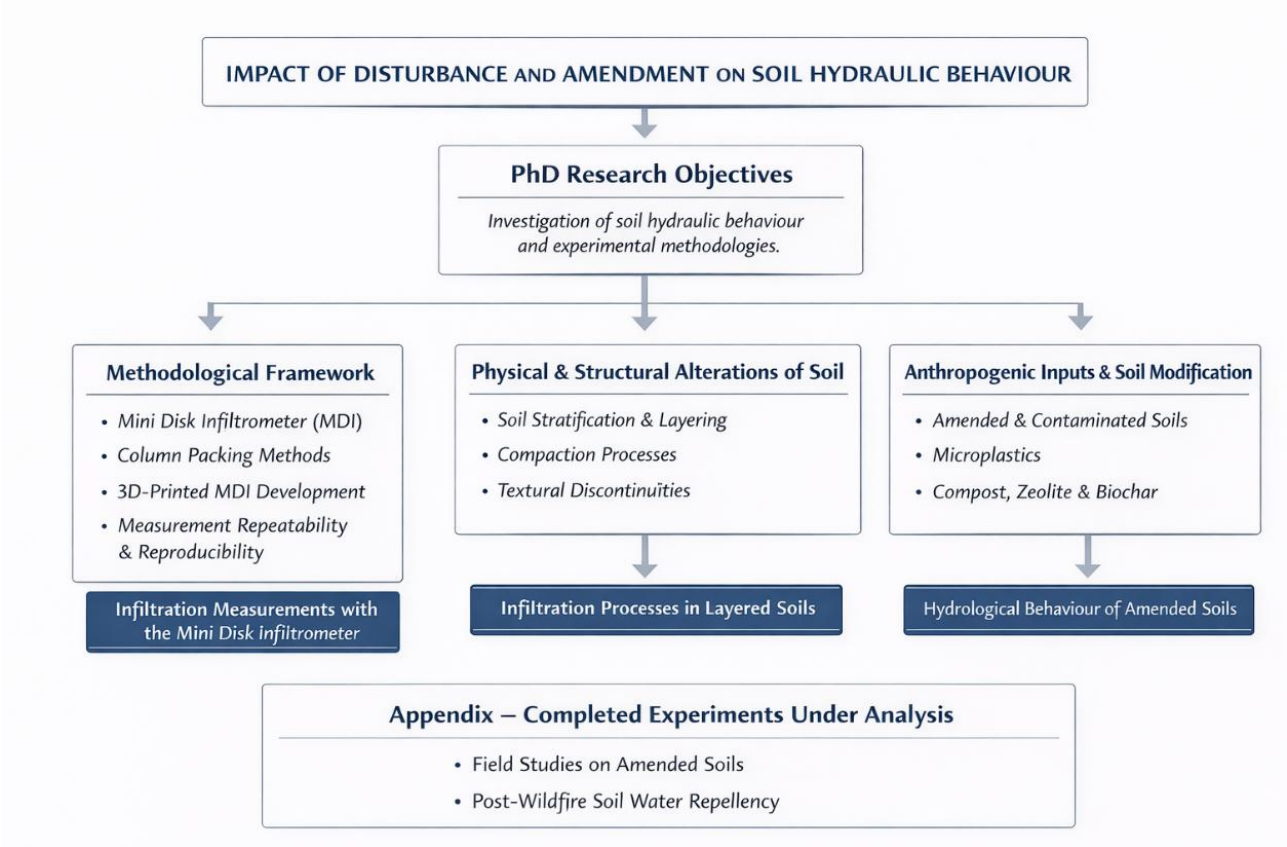

Figure 1. Schematic overview of the thesis structure, illustrating the research objectives and the main thematic sections addressing methodological aspects, soil alterations, and the hydraulic behaviour of amended and disturbed soils.

References:

Bauke, S. L., Amelung, W., Bol, R., Brandt, L., Brüggemann, N., Kandeler, E., ... & Vereecken, H. (2022). Soil water status shapes nutrient cycling in agroecosystems from micrometer to landscape scales. Journal of plant nutrition and soil science, 185(6), 773-792.

Biddoccu, M., Ferraris, S., Pitacco, A., & Cavallo, E. (2017). Temporal variability of soil management effects on soil hydrological properties, runoff and erosion at the field scale in a hillslope vineyard, North-West Italy. Soil and Tillage Research, 165, 46-58.

Caloiero, T., Caloiero, P., & Frustaci, F. (2018). Long-term precipitation trend analysis in Europe and in the Mediterranean basin. Water and Environment Journal, 32(3), 433-445.

Eswaran, H., Lal, R., & Reich, P. F. (2019). Land degradation: an overview. Response to land degradation, 20-35.

Evans, R. G., & Sadler, E. J. (2008). Methods and technologies to improve efficiency of water use. Water resources research, 44(7).

FAO (2015). Status of the World's Soil Resource.

Giordano, L., Giordano, F., Grauso, S., Iannetta, M., Sciortino, M., Rossi, L., & Bonati, G. (2007). Identification of areas sensitive to desertification in Sicily Region. Identifi cation of areas sensitive to desertifi cation in Sicily Region, ENEA, Rome, Italy, 1-16.

Lionello, P., Abrantes, F., Gacic, M., Planton, S., Trigo, R., & Ulbrich, U. (2014). The climate of the Mediterranean region: research progress and climate change impacts. Regional Environmental Change, 14(5), 1679-1684.

Martínez-Mena, M., Carrillo-López, E., Boix-Fayos, C., Almagro, M., Franco, N. G., Díaz-Pereira, E., ... & de Vente, J. (2020). Long-term effectiveness of sustainable land management practices to control runoff, soil erosion, and nutrient loss and the role of rainfall intensity in Mediterranean rainfed agroecosystems. *Catena*, *187*, 104352.

Schneider, U. A., Havlík, P., Schmid, E., Valin, H., Mosnier, A., Obersteiner, M., ... & Fritz, S. (2011). Impacts of population growth, economic development, and technical change on global food production and consumption. *Agricultural Systems*, *104*(2), 204-215.

Seneviratne, S. I., Corti, T., Davin, E. L., Hirschi, M., Jaeger, E. B., Lehner, I., ... & Teuling, A. J. (2010). Investigating soil moisture–climate interactions in a changing climate: A review. Earth-Science Reviews, 99(3-4), 125-161.

Smith, P., House, J. I., Bustamante, M., Sobocká, J., Harper, R., Pan, G., ... & Pugh, T. A. (2016). Global change pressures on soils from land use and management. Global change biology, 22(3), 1008-1028.

Tramblay, Y., Llasat, M. C., Randin, C., & Coppola, E. (2020). Climate change impacts on water resources in the Mediterranean. Regional Environmental Change, 20(3), 83.

Vallebona, C., Pellegrino, E., Frumento, P., & Bonari, E. (2015). Temporal trends in extreme rainfall intensity and erosivity in the Mediterranean region: a case study in southern Tuscany, Italy. Climatic Change, 128(1), 139-151.

Vereecken, H., Amelung, W., Bauke, S. L., Bogena, H., Brüggemann, N., Montzka, C., ... & Zhang, Y. (2022). Soil hydrology in the Earth system. Nature Reviews Earth & Environment, 3(9), 573-587.

Chapter 2 – Instruments and Measurement Methods

2.1 Soil Water Retention Curve Measurement methods

The relationship between soil volumetric water content (θ) and matric potential (ψ_m) is a key hydraulic property of soils and is typically determined through laboratory measurements. The experimental procedure involves subjecting a moist soil sample to a sequence of imposed matric potentials and allowing the system to reach equilibrium at each step. Since the $\theta(h)$ relationship exhibits hysteresis, its shape depends on the direction of the applied pressure head sequence. For most practical and agronomic purposes, attention is focused on the drying or drainage branch of the retention curve. Consequently, measurements are commonly performed following a monotonically decreasing sequence of matric potentials.

In practical applications, one of the most commonly employed techniques for determining the soil water retention curve is the tensiometric method. In this approach, the saturated sample is placed inside a funnel (Fig. 1) equipped with a saturated porous ceramic plate at its base, which is connected to a water reservoir. The imposed pressure induces water to drain from the soil until hydraulic equilibrium is reached, meaning that the matric potential at the base of the sample equals the applied pressure head from the reservoir.

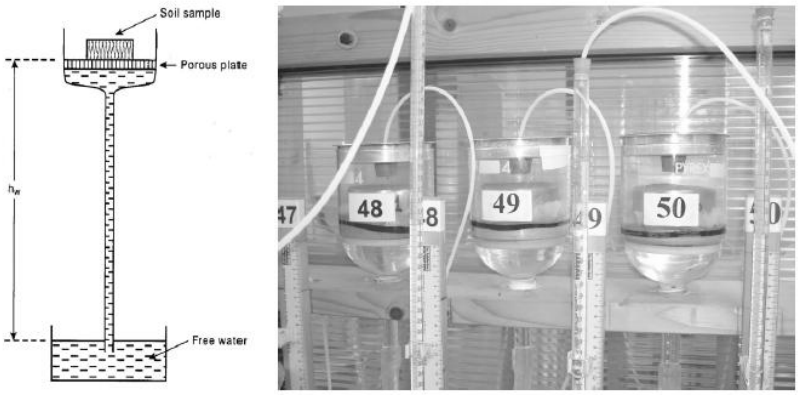

Fig. 1 Hanging water column system in Hydrology Laoratory of University of Palermo

In the *hanging water column* system (Burke et al., 1986), a funnel equipped with a saturated porous ceramic plate is hydraulically connected to a 50 cm^3 graduated burette mounted on a vertical meter stick, with the zero corresponding to the top surface of the ceramic plate (Fig. 1). The soil sample,

previously saturated on the porous plate, is subjected to a monotonically decreasing sequence of matric potentials by progressively lowering the burette along the graduated rod and allowing equilibrium to be reached at each step. As water drains from the sample, the water level in the burette rises, and the burette must be adjusted continuously to maintain the imposed potential. Once equilibrium is established at the lowest potential in the sequence, the sample is removed, and its volumetric water content is determined by termo-gravimetric analysis. The water contents corresponding to the preceding potentials are then calculated retroactively by adding the volumes of water drained at each previous step to the final water content. During the experimental activities conducted throughout the PhD, this method was systematically employed to determine soil water retention up to a matric potential of −0.1 bar (or −1 m), a value typically associated with field capacity. For more negative potentials, the pressure plate method was applied (Dane and Hopmans, 2002). In this case, moist soil samples were placed inside a pressure chamber, with a saturated porous membrane installed at the chamber base (Fig 2). The chamber was then pressurized with pressurised air to a selected value above atmospheric pressure, forcing water to flow through the porous plate until the sample equilibrated at a matric potential equal in absolute value to the applied pneumatic pressure. Using this method, soil water contents were determined for five pressure steps: −0.1 bar (final step of the tensiometric sequence), −0.33 bar, −1 bar, −3 bar, and −15 bar, the latter representing the wilting point.

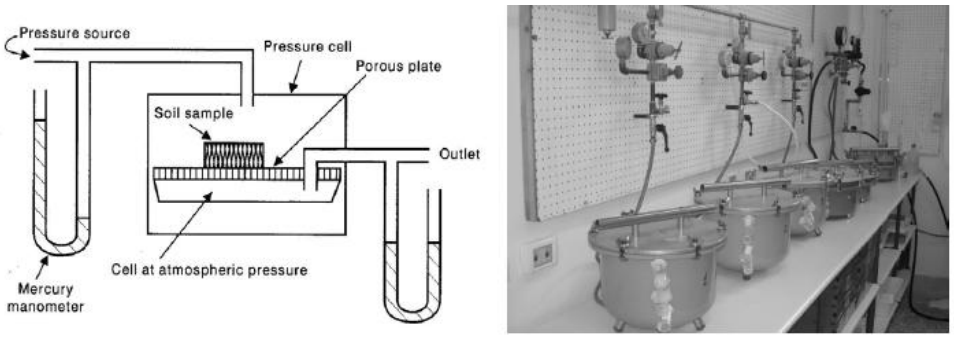

Fig. 2 Pressure plate method in Hydrology Laoratory of University of Palermo

In the range of higher matric potentials (approximately > –1 m), soil water retention is strongly influenced by the structural porosity, the pore space between aggregates (Dexter et al., 2008). In this case, it is preferable to use undisturbed soil samples that preserve the natural pore network as found in situ. For pressure head values lower than approximately –1 m, laboratory-prepared samples can be employed. These are typically obtained by packing air-dried and 2-mm sieved soil into small cylindrical rings. In this samples, water retention is mainly governed by matrix porosity, which includes pores formed within aggregates and between individual soil particles (Dexter et al., 2008).

Empirical functions are often adopted to describe the soil water retention curve by fitting experimental θ–h data pairs. Among the most widely used models are those proposed by Brooks and Corey (1966) and van Genuchten (1980). In particular, the van Genuchten (1980) model is expressed as:

$$S_e = \frac{1}{[1+(a_{vg}|h|^n)]^m} \quad (1)$$

where α (L^{-1}), n, and m are empirical fitting parameters, typically with m defined as $m = 1 - 1/n$ or $m = 1 - 2/n$ (van Genuchten et al., 1991). S_e is the effective saturation, defined as:

$$S_e = \frac{\theta - \theta_r}{\theta_s - \theta_r} \quad (2)$$

where θ_r (v/v) is the residual water content and θ_s (v/v) is the water content at saturation. According to the capillary rise equation, a relationship exists between the matric potential and pore size: a decrease in matric potential from ψ_{m1} to ψ_{m2} causes the drainage of water from pores whose radii lie between r_1 and r_2. Therefore, the water retention curve also provides indirect information about the pore size distribution of the soil sample (Hillel, 1998).

2.2 Hydrodinamic parameters under unsaturated conditions: Mini Disk Infiltrometer (MDI)

2.2.1 Physical principles of MDI experimental trials

The Mini Disk Infiltrometer (MDI), manufactured by Meter Group (Pullman, WA, United States), is a widely used field and laboratory instrument designed to estimate key hydraulic properties of the soil under unsaturated conditions. The instrument consists of a plexiglass tube divided into two chambers: the upper chamber, or Mariotte reservoir, sets the pressure head (typically between h_0 =-6 cm and -0.5 cm), and the lower chamber, or water reservoir, contains approximately 95 ml of water that infiltrates the soil through a porous sintered stainless-steel disk (45 mm in diameter and 3 mm thick), preventing free drainage into the air (Fig. 3). The MDI is especially valued in hydrological, agronomic, and environmental studies due to its portability, ease of use, and ability to generate data rapidly in both natural and managed soils. Two key hydraulic parameters can be derived from MDI infiltration data under a given imposed pressure head (h), each reflecting a distinct physical

mechanism driving water movement in unsaturated soils: sorptivity (S) and unsaturated hydraulic conductivity (K).

Sorptivity (S) quantifies the soil's capacity to absorb water. It is driven by capillary forces and is predominant in the early stage of infiltration, when the soil is initially dry and water is rapidly drawn into the matrix. During this phase, gravitational forces are relatively less important, and the infiltration rate is primarily controlled by the microstructure of the soil matrix. Thus, sorptivity provides an integrated measure of the soil's near-surface capillary behaviour and is a key descriptor of initial infiltration dynamics.

Unsaturated hydraulic conductivity K(h), by contrast, describes the soil's ability to transmit water once the initial capillary intake has declined and gravity-driven flow becomes dominant. K represents the capacity to sustain water movement through the pore network under an applied hydraulic gradient: as the soil becomes wetter, flow occurs through continuous macropores, yielding higher conductivity; as it dries, the loss of hydraulic continuity restricts flow to thin films and micropores, causing a sharp decrease in K.

Together, S and K(h) provide complementary insights into the hydrodynamic behaviour of soils under a given imposed pressure head (h). For a specific h, they jointly describe the infiltration process: S captures the initial, capillary-dominated response that governs the early stage of water entry into the soil matrix, while K(h) characterizes the subsequent quasi-steady, gravity-driven phase of flow through the pore network. Quantifying both parameters at defined pressure heads allows a more comprehensive understanding of soil–water interactions, particularly when assessing the effects of amendments or pollutants that modify soil structure, pore connectivity, or surface properties.

During an MDI test, the operator records the volume of water infiltrated from the reservoir at set time intervals. These data are used to construct the cumulative infiltration curve, which expresses the total volume of infiltrated water as a function of time.

The procedure begins with the preparation of the instrument: the MDI is filled with water, ensuring the reservoir and the porous disk are free of air bubbles. The pressure head is set using the adjustable suction tube, depending on the objective of the test and the soil type. Before starting the measurement, the base of the infiltrometer is gently placed in contact with a leveled and smoothed soil surface, taking care not to compact the soil or cause leakage around the disk. Once positioned, infiltration starts through the steel porous disk at the base of the infiltrometer, allowing water to enter the soil under a known and controlled pressure head. At regular time intervals (e.g., every 30 seconds or 1

minute), the operator manually records the drop in the water level within the graduated reservoir. These volume readings are then converted into cumulative infiltration values over time. The shape of the infiltration curve reflects two dominant processes. Initially, a rapid infiltration occurs due to capillary uptake, producing a steep slope; later, the infiltration rate diminishes and stabilizes as gravity takes over. Analyzing both these phases enables accurate extraction of sorptivity and unsaturated hydraulic conductivity from the early and late parts of the curve, respectively.

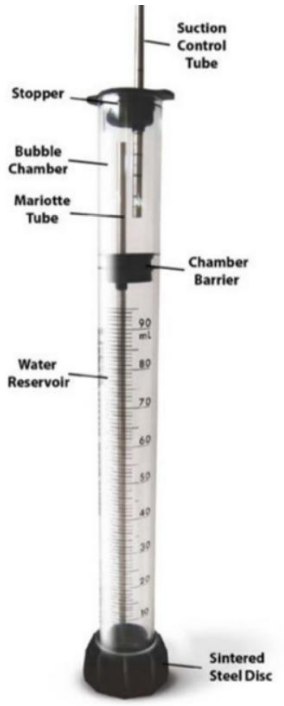

Fig. 3 Mini Disk Infiltrometer by Meter

2.2.2 Methods for the estimation of K(h) and S

Several analytical models have been proposed to estimate soil hydraulic parameters from cumulative infiltration data, including those by Warrick (1992), Haverkamp et al. (1994), and Zhang (1997a, b). These models commonly rely on a two-term cumulative infiltration equation that can rappresent both a 1-dimensional and 3-dimensional process:

$$\boldsymbol{I(t) = C_1 t^{1/2} + C_2 t} \qquad (3)$$

where I(t) [L] is the cumulative infiltration over time t [T], and C_1 [L $T^{-1/2}$] and C_2 [L T^{-1}] are empirical parameters; C_1 represents the influence of capillary forces, whereas C_2 reflects the gravitational component of the infiltration process (Zhang, 1997a, b).

Among these analytical models, the method proposed by Zhang (1997a) has gained widespread application due to its simplicity and effectiveness, particularly under dry initial conditions where capillary forces dominate the infiltration process. For this reason, it has also been recommended by Decagon Devices Inc. (2012) as a standard approach for interpreting infiltration data collected with the MDI.

According to this model, assuming homogeneous and isotropic soil conditions with a uniform initial water content profile, the infiltration process beneath the infiltrometer disk can be effectively described using the same two-term equation, where the parameters C_1 and C_2, are directly related to two key hydraulic properties:

$$\boldsymbol{C_1 = A_1 S_0} \quad \text{and} \quad \boldsymbol{C_2 = A_2 K_0} \tag{4}$$

Here, $\boldsymbol{S_0}$ [L $T^{-1/2}$] is the soil sorptivity and $\boldsymbol{K_0}$ [L T^{-1}] is the unsaturated hydraulic conductivity at the imposed pressure head h_0 [L]. The dimensionless coefficients A_1 and A_2 depend on the soil water retention characteristics and the geometrical and operational parameters of the infiltrometer. For soils characterized by a van Genuchten (1980) type retention function, Zhang (1997a) derived these coefficients through numerical simulations of the infiltration process:

$$\boldsymbol{A_1 = \frac{1.4 b^{0.5} (\theta_0 - \theta_i)^{0.25} \exp[3(n-1.9) a_{vG} h_0]}{(a_{vG} r)^{0.15}}} \tag{5}$$

$$\boldsymbol{A_2 = \frac{11.65 (n^{0.1}-1)^{0.25} \exp[2.92(n-1.9) a_{vG} h_0]}{(a_{vG} r)^{0.91}}} \quad \text{for } n \geq 1.9 \tag{6}$$

$$\boldsymbol{A_2 = \frac{11.65 (n^{0.1}-1)^{0.25} \exp[7.5(n-1.9) a_{vG} h_0]}{(a_{vG} r)^{0.91}}} \quad \text{for } n \leq 1.9 \tag{7}$$

where h_0 (cm) is the applied pressure head during the infiltration process (h_0 is negative for unsaturated conditions), n and α_{vG} (cm^{-1}) are the water retention parameters, r (cm) is the radius of the infiltrometer, θ_0 (cm^3 cm^{-3}) is the soil water content at h0, θ_i (cm^3 cm^{-3}) is the initial soil water

content, and b is a parameter set at 0.55 (Warrick and Broadbridge 1992). The van Genuchten parameters, required by the procedure, can be estimated from soil texture or they can be obtained by fitting laboratory determined soil water retention data. Using numerically simulated MDI data for 12 soils with varying textures, Dohnal et al. (2010) found that Zhang's (1997a) method tends to overestimate unsaturated hydraulic conductivity, with absolute relative errors in K_0 reaching up to 70%. The largest discrepancies were observed in soils with n≤1.35. To address this limitation, an alternative formulation was proposed to estimate the A_2 parameter more accurately for such cases.

$$A_2 = \frac{11.65\left(n^{0.82}-1\right)^{0.25}\exp[34.65(n-1.9)a_{vG}h_0]}{(a_{vG}r)^{0.6}} \quad \text{for } n \leq 1.35 \qquad (8)$$

2.3 Water repellency measurement: Water Drop Penetration Time Method

The Water Drop Penetration Time (WDPT) test (Bisdom &Dekker, 1993; Doerr, 1998; Letey et al., 2000) is one of the most widely used techniques for assessing Soil Water Repellency (SWR). The test quantifies the time required for a water droplet placed on the soil surface to infiltrate, providing an indirect but effective measure of hydrophobicity. The method can be performed both in the field and in the laboratory; however, field measurements are generally preferred because they preserve the natural structure and composition of the soil, avoiding disturbances that could alter the results (Dekker et al., 2009). The procedure is relatively simple and quick: a fixed drop of water is gently placed on the soil surface, and the infiltration time is measured using a stopwatch.

The classification of Soil Water Repellency (SWR) based on the Water Drop Penetration Time (WDPT) provides a standardized framework for interpreting the degree and persistence of hydrophobic behavior in soils; according to the commonly used classification (Dekker and Ristema, 1994), soils can be grouped into discrete classes depending on the time required for a water droplet to infiltrate the surface. Soils with a WDPT shorter than 5 seconds are considered wettable and do not exhibit any significant hydrophobicity. When the WDPT ranges between 5 and 60 seconds, soils are described as slightly water-repellent, typically representing conditions of temporary repellency that may disappear with increasing soil moisture. Values between 60 and 600 seconds define strong water repellency, where infiltration begins to be significantly delayed. WDPT values from 600 to 3600 seconds correspond to severe water repellency, indicating the presence of persistent hydrophobic

coatings on soil particles that strongly hinder water entry. Finally, when the WDPT exceeds 3600 seconds (1 hour), soils are classified as extremely water-repellent.

References:

Bisdom, E. B. A., Dekker, L. W., & Schoute, J. T. (1993). Water repellency of sieve fractions from sandy soils and relationships with organic material and soil structure. In *Soil structure/soil biota interrelationships* (pp. 105-118). Elsevier.

Dane J.H., Hopmans J.W. (2002), *Water retention and storage: laboratory*, Methods of soil analysis, Physical Methods, 3rd ed., Part 4, eds. J. H. Dane e G. C. Topp, Soil Science Society of America Journal, Madison, WI, 2002, pp. 688-692.

Dekker, L. W., & Ritsema, C. J. (1994). How water moves in a water repellent sandy soil: 1. Potential and actual water repellency. *Water Resources Research*, *30*(9), 2507-2517.

Dekker, L. W., Ritsema, C. J., Oostindie, K., Moore, D., & Wesseling, J. G. (2009). Methods for determining soil water repellency on field-moist samples. *Water resources research*, *45*(4).

Doerr, S. H. (1998). On standardizing the 'water drop penetration time'and the 'molarity of an ethanol droplet'techniques to classify soil hydrophobicity: a case study using medium textured soils. *Earth Surface Processes and Landforms: The Journal of the British Geomorphological Group*, *23*(7), 663-668.

Dohnal, M., Dusek, J., & Vogel, T. (2010). Improving hydraulic conductivity estimates from minidisk infiltrometer measurements for soils with wide pore-size distributions. Soil Science Society of America Journal, 74, 804–811.

Haverkamp, R., Ross, P. J., Smettem, K. R. J., & Parlange, J. Y. (1994). Three-dimensional analysis of infiltration from the disc infiltrometer. 2. Physically based infiltration equation. Water Resources Research, 30, 2931–2935.

Hillel D. (1998), *Environmental soil physics*, Academic Press, San Diego, 771 pp.

Van Genuchten, M. T. (1980). A closed-form equation for predicting the hydraulic conductivity of unsaturated soils. *Soil science society of America journal*, *44*(5), 892-898ù

Letey, J., Carrillo, M. L. K., & Pang, X. P. (2000). Approaches to characterize the degree of water repellency. *Journal of Hydrology*, *231*, 61-65.

Van Genuchten M.T., Leij F.J., Yates S.R. (1991), *The RETC code for quantifying the hydraulic functions of unsaturated soils*, Version 1.0. EPAReport 600/2-91/065. U.S. Salinity Laboratory, USDA, ARS, Riverside, CA.

Warrick, A. W. (1992). Models for disc infiltrometers. Water Resources Research, 28(5), 1319–1327.

Warrick, A. W., & Broadbridge, P. (1992). Sorptivity and macroscopic capillary length relationships. Water Resources Research, 28, 427–431.

Zhang, R. (1997a). Determination of soil sorptivity and hydraulic conductivity from the disk infiltrometer. Soil Science Society of America Journal, 61, 1024–1030.

Zhang, R. (1997b). Infiltration models for the disk infiltrometer. Soil Science Society of America Journal, 61, 1597–1603.

.

Chapter 3 – Infiltration Measurements with the Mini Disk Infiltrometer

3.1 Introduction

Soil–water interactions are governed by multiple, interrelated physical mechanisms strongly influenced by both the intrinsic properties of the porous medium and the external conditions during experimental activities. Infiltration processes are strongly affected by soil heterogeneity as a result of variability in particle size and composition, the presence of rock fragments, the distribution and connectivity of macropores, and the spatial arrangement of fine and coarse materials (Sharma et al., 1980). Beyond structural variability, soils also exhibit considerable heterogeneity in hydraulic behaviour. Under dynamic flow conditions, differences in the rigidity of the soil matrix, meaning its resistance to deformation, together with the connectivity of the pore network, influence how the matrix responds to wetting and thereby affect water flow paths and the soil's capacity to transmit and retain moisture (Assouline et al., 2002). Moreover, differences in soil compaction, the presence of organic matter, and stratification or layering within the profile increase the complexity of the system.

Beyond soil-related factors, additional considerations concern the measurement procedure itself. For instance, when focusing on unsaturated infiltration, even under identical soil conditions, different instruments (e.g., mini-disk, tension infiltrometers), or experimental setups (e.g., disc size, applied pressure head) can yield markedly different results (Fusco et al., 2024). Together, these factors create a system in which infiltration is highly sensitive to both intrinsic soil properties and experimental conditions, making accurate and reproducible measurement particularly challenging (Ruggenthaler et al., 2016); therefore, infiltration measurements require selecting methods that achieve a favourable trade-off between realistic conditions and experimental control.

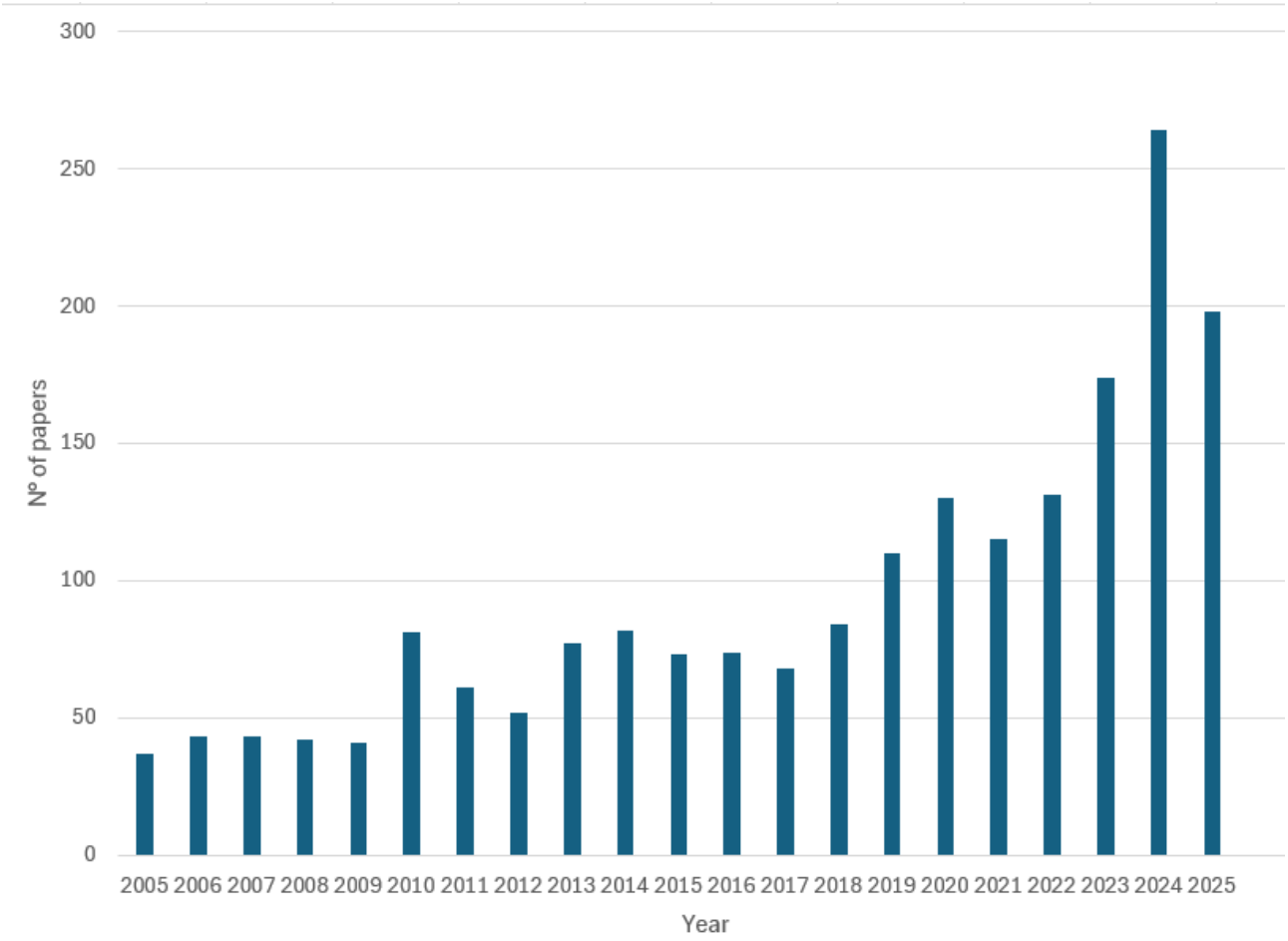

Fig. 1: papers with “mini disk” or “mini disc” in title, abstract and keywords in the last 20 years

Generally, investigations with the MDI can be divided by the nature of the soil sample:

- Experiments on undisturbed soil aim to characterize the hydrological properties of agricultural and forest systems under natural conditions (Basset et al., 2023), maintaining the original pore structure and the prevailing boundary conditions, such as the natural soil layering; this represents the most direct approach for characterizing the hydrological behaviour of soil under natural conditions. This kind of experiments are conducted both in the field and in the laboratory. Applying field experiments, it is possible to obtain direct and realistic information on infiltration dynamics, without the risk of altering the pore structure through sampling or manipulation. However, these clear strengths are associated with important limitations as spatial variability, amplified by rock fragments; moreover, achieving consistent contact between the instrument and the soil can be challenging due to uneven surfaces, potentially affecting measurement accuracy. Laboratory tests on undisturbed soil cores offer a compromise between experimental control and the preservation of natural soil characteristics. By transferring intact samples to a controlled environment, researchers can standardize key

factors such as temperature, initial water content or water content, and boundary conditions, which helps reduce unwanted variability and facilitates reproducible measurements. At the same time, these cores retain the intrinsic spatial heterogeneity of the field, including natural layering and aggregate distribution; maintaining this variability is crucial, as it allows a realistic representation of water flow and retention processes, which are essential for interpreting soil hydraulic behaviour. Moreover, even with careful sampling and handling, minor disturbances to macropore networks and other structural features are unavoidable (Gilbert, 1992).

- Experiments on repacked soil samples have been developed to achieve a greater degree of control over initial conditions (Lewis et al. 2010; Bagarello et al. 2022): through sieving and repacking, key parameters, as bulk density, initial water content, and compaction, can be imposed and systematically varied. This high level of control permits the isolation of singular factors and reduces the background variability that often complicates the interpretation of field data. Moreover, repacked soil columns or cylinders can be designed to reproduce specific configurations, such as layered profiles or the inclusion of contrasting materials (Snehota et al. 2015). The main drawback of these experiments, however, is their limited representativeness: by reconstructing the pore network, macropore continuity and preferential flow pathways are inevitably affected, which limits the applicability of the results to natural conditions (Lewis et al. 2010).

In this context, the Mini Disk Infiltrometer (MDI) is one of the most widely adopted instruments for quantifying soil hydraulic behaviour, with relevance to infiltration processes under both natural and controlled conditions. The MDI is commonly used in the field to measure three-dimensional (3D) infiltration processes (Gonzalez-Sosa et al., 2010; Fodor et al., 2011; Alagna et al., 2013), offering an experimental setup that replicates the natural movement of water through the soil. Alternatively, the MDI can also be used for one-dimensional (1D) infiltration measurements in soil columns (Ghosh & Pekkat, 2019; Naik et al., 2019; Bagarello et al., 2022), which allows more controlled experiments where single factors can be isolated and their effects on infiltration more easily evaluated. Its extensive use is reflected in the scientific literature, where a search on major databases yields dozens of studies employing this device across a wide range of soils and experimental contexts.

The table below provides a summary of selected studies published between 2021 and 2025 in scientific journals, in which the Mini-Disk Infiltrometer (MDI) was employed to investigate soil infiltration processes.

Tab.1 Summary of recent works involving MDI

Authors	Year	Objectives	Experiments
Libutti et al.	2021	Effects of biochar on soil properties, specifically in clay loam soil.	Repacked soil columns
Naik e Pekkat	2022	Indirectly determining wetting water retention characteristics and saturated hydraulic conductivity in soils.	Repacked soil columns
Cleophas et al.	2022	Understanding how soil physical properties influence infiltration rates in a logged-over tropical rainforest in Malaysia	Undisturbed soil (field)
Murta et al.	2022	Investigates the infiltration capacity and soil penetration resistance of plinthic soil under a riparian forest in Central Brazil	Undisturbed soil (field)
Revell et al.	2022	How tree planting affects soil infiltration in a clay-textured area in Warwickshire	Undisturbed soil (field)
Bondì et al.	2023	Investigates the changes in water infiltration rates of an extensive Mediterranean green roof over time	Undisturbed and repacked substrate (field and laboratory)
Wang et al.	2023	How different land uses affect soil macropore characteristics and hydraulic conductivity in a dry-hot valley region of Southwest China	Undisturbed soil (laboratory)
Fattah et al.	2023	To compare hydraulic conductivity estimates using falling head and Mini Disk Infiltrometer methods in gypsiferous soil	Undisturbed soil (laboratory)
Jobbágy et al.	2023	Investigates soil hydraulic conductivity on a plot in Slovakia comparing compacted and uncompacted areas	Undisturbed soil (field)

Svetina et al.	2023	Highlighting the significance of evaluating site-specific infiltration rates for effective stormwater management.	Undisturbed soil (field)
Defterdarovi´c et al.	2024	How agricultural management affects soil compaction, infiltration, and water dynamics on hillslopes in a vineyard	Undisturbed soil (field)
Peng et al.	2024	Investigates the impact of long-term cultivation on soil properties, focusing on infiltration characteristics and pore structure	Undisturbed soil (field)
Pereira et al.	2024	Investigates the physical properties of soil in both rows and inter-rows of a syntropic agroforestry system,	Undisturbed soil (field)
Rathnayake et al.	2025	How shallow-depth hardpans affect soil hydraulic properties, revealing significant reductions in infiltration rates and hydraulic conductivity.	Repacked soil columns
Muhammed et al.	2025	The estimation of hydraulic properties of soilless growing media using a Mini Disk Infiltrometer.	Repacked substrate columns
Zhao et al.	2025	Evaluates three infiltration models—Horton, Kostiakov, and Philip—to determine the best fit for simulating matrix infiltration processes in biocrusts.	Undisturbed soil (field)

All the experimental activities with the MDI reported in Tab.1 are inevitably associated with practical challenges, in addition to the intrinsic limitations already discussed. Laboratory measurements on repacked soil columns with the MDI are typically undertaken with the expectation that, under identical conditions, repeated experiments would yield consistent and reproducible results. In practice, however, this idea is rarely achieved. Even in carefully prepared repacked column, variability can arise from the specific methods used for sample preparation and compaction (Ghosh et al., 2019; Bagarello et al., 2022), as well as from subtle differences introduced by the operator during soil column preparation. Moreover, many studies reported in the literature are based on a limited number of replicates (Assouline and Narkis, 2011; Kargas et al., 2018; Tanner et al., 2021), which further constrains the ability to distinguish between true soil responses and experimental noise. On the other hand, in the field, logistical difficulties, such as transporting water to the experimental

site (a problem partially solved with MDI), and the overall duration of measurements represent the main practical challenges. A further common issue in both contexts is the need for manual readings of the MDI, a task that makes the experimental process time-consuming and less reproducible, particularly in the field, where the instrument sits at ground level and measuring requires working in an awkward position.

The contributions presented in this chapter were specifically designed to address these challenges. Regarding the first study, it is aimed to investigate the sources of variability in laboratory experiments with repacked columns, with particular attention to the impact of manual compaction procedures and the operator-driven variability. The second study, carried out during my research stay at the Czech Technical University in Prague, focused on developing an innovative 3D-printed MDI prototype equipped with an automatic data-acquisition system designed to simplify measurements and enhance reproducibility. This experimental tool embodies an effort to combine the portability and practicality required for field applications with the precision and standardization typical of laboratory experiments, offering new perspectives for the use of the MDI in hydrological research and practical settings thanks to its automatic reading system, particularly useful in field experiments, and its general lower price respect to the commercial MDI.

References:

Alagna, V., Bagarello, V., Di Prima, S., Giordano, G., & Iovino, M. (2013). A simple field method to measure the hydrodynamic properties of soil surface crust. *Journal of Agricultural Engineering*, *44*(s2).

Assouline, S., & Mualem, Y. (2002). Infiltration during soil sealing: The effect of areal heterogeneity of soil hydraulic properties. *Water Resources Research*, *38*(12), 22-1.

Assouline, S.; Narkis, K. (2011). Effects of Long-Term Irrigation with TreatedWastewater on the Hydraulic Properties of a Clayey Soil. Water Resour. Res. 47, 1–13.

Bagarello, V., Caltabellotta, G., & Iovino, M. (2022). Manual packing and soil reuse effects on determination of saturated hydraulic conductivity of a loam soil. *Geoderma*, *405*, 115465.

Basset, C., Abou Najm, M., Ghezzehei, T., Hao, X., & Daccache, A. (2023). How does soil structure affect water infiltration? A meta-data systematic review. *Soil and Tillage Research*, *226*, 105577.

Belanger, N.; Van Rees, K.C.J. Sampling Forest Soils. In Soil Sampling and Methods of Analysis; Carter, M.R., Gregorich, E.G., Eds.; CRC Press and Taylor & Francis Group.: Boca Raton, FL, USA, 2008; pp. 15–24

Cleophas, F., Isidore, F., Musta, B., Ali, B. M., Mahali, M., Zahari, N. Z., & Bidin, K. (2022, August). Effect of soil physical properties on soil infiltration rates. In *Journal of physics: conference series* (Vol. 2314, No. 1, p. 012020). IOP Publishing.

Defterdarović, J., Filipović, L., Ondrašek, G., Bogunović, I., Dugan, I., Phogat, V., ... & Filipović, V. (2024). Impact of Hillslope Agriculture on Soil Compaction and Seasonal Water Dynamics in a Temperate Vineyard. *Land*, *13*(5), 588.

Fattah, A. A., & Shihab, R. M. (2023, November). Comparison of Hydraulic Conductivity Estimation using Falling Head and Mini Disk Infiltrometer in Gypsiferous Soil. In *IOP Conference Series: Earth and Environmental Science* (Vol. 1259, No. 1, p. 012017). IOP Publishing.

Fodor, N., Sándor, R., Orfanus, T., Lichner, L., & Rajkai, K. (2011). Evaluation method dependency of measured saturated hydraulic conductivity. *Geoderma*, *165*(1), 60-68.

Fusco, M., Alagna, V., Autovino, D., Caltabellotta, G., Iovino, M., Vaccaro, G., & Bagarello, V. (2024). Comparing mini-disk infiltrometer, BEST method and soil core estimates of hydraulic conductivity of a sandy-loam soil. *Soil and Tillage Research*, *244*, 106263.

Gilbert, P. A. (1992). *Effect of sampling disturbance on laboratory-measured soil properties* (No. WESMPGL9235).

Gonzalez-Sosa, E., Braud, I., Dehotin, J., Lassabatère, L., Angulo-Jaramillo, R., Lagouy, M., ... & Michel, K. (2010). Impact of land use on the hydraulic properties of the topsoil in a small French catchment. *Hydrological processes*, *24*(17), 2382-2399.

Ghosh, B., & Pekkat, S. (2019). Effect of initial compaction state on near-saturated hydraulic conductivity. *Journal of Irrigation and Drainage Engineering*, *145*(12), 04019028.

Kargas, G.; Londra, P.; Anastasiou, K.; Kerkides, P. (2018). A Note on One- and Three-Dimensional Infiltration Analysis from a Mini Disc Infiltrometer. Water, 10, 1783.

Klute, A., & Dirksen, C. (1986). Hydraulic conductivity and diffusivity: Laboratory methods. *Methods of soil analysis: Part 1 physical and mineralogical methods*, *5*, 687-734.

Lewis, J., & Sjöstrom, J. (2010). Optimizing the experimental design of soil columns in saturated and unsaturated transport experiments. *Journal of contaminant hydrology*, *115*(1-4), 1-13.

Libutti, A., Francavilla, M., & Monteleone, M. (2021). Hydrological properties of a clay loam soil as affected by biochar application in a pot experiment. *Agronomy*, *11*(3), 489.

Muhammed, H. H., Anlauf, R., & Daum, D. (2025). Estimation of Hydraulic Properties of Growing Media from Numerical Inversion of Mini Disk Infiltrometer Data. *Hydrology*, *12*(5), 100.

Naik, A. P., Ghosh, B., & Pekkat, S. (2019). Estimating soil hydraulic properties using mini disk infiltrometer. *ISH Journal of Hydraulic Engineering*, *25*(1), 62-70.

Naik, A. P., & Pekkat, S. (2023). An appraisal on the soil wetting water retention characteristic curve determined from mini disk infiltrometer and sensor measurements. *Acta Geophysica*, *71*(2), 961-982.

Rathnayake, N. R. R. W. S., Leelamanie, D. A. L., & Maeda, M. (2025). Shallow-depth hardpan attributes influence soil surface and subsurface hydraulic properties. *CATENA*, *259*, 109405.

Revell, N., Lashford, C., Rubinato, M., & Blackett, M. (2022). The impact of tree planting on infiltration dependent on tree proximity and maturity at a clay site in Warwickshire, England. *Water*, *14*(6), 892.

Ruggenthaler, R., Meißl, G., Geitner, C., Leitinger, G., Endstrasser, N., & Schöberl, F. (2016). Investigating the impact of initial soil moisture conditions on total infiltration by using an adapted double-ring infiltrometer. *Hydrological Sciences Journal*, *61*(7), 1263-1279.

Sharma, M. L., Gander, G. A., & Hunt, C. G. (1980). Spatial variability of infiltration in a watershed. *Journal of Hydrology*, *45*(1-2), 101-122.

Snehota, M., Jelinkova, V., Sobotkova, M., Sacha, J., Vontobel, P., & Hovind, J. (2015). Water and entrapped air redistribution in heterogeneous sand sample: Quantitative neutron imaging of the process. *Water Resources Research*, *51*(2), 1359-1371.

Svetina, J., Prestor, J., & Šraj, M. (2023). Infiltration measurements during dry conditions in an urban park in Ljubljana, Slovenia. *Water*, *15*(20), 3635.

Tanner, S., Katra, I., Argaman, E., & Ben-Hur, M. (2021). Mechanisms and processes affecting aggregate stability and saturated hydraulic conductivity of top and sublayers in semi-arid soils. *Geoderma*, *404*, 115304.

Wang, Y., Ruan, J., Li, Y., Kong, Y., Cao, L., & He, W. (2023). Soil Macropore and Hydraulic Conductivity Dynamics of Different Land Uses in the Dry–Hot Valley Region of China. *Water*, *15*(17), 3036.

3.2 A Test of Factors Influencing One-Dimensional Mini-Disk Infiltrometer Experiments on Repacked Loam Soil Columnsù

Published on Hydrology 2025, 12, 85. https://doi.org/10.3390/hydrology12040085

Vincenzo Bagarello, Stefano Barone, Gaetano Caltabellotta, Florina Kati Varadi, Francesco Zanna and Dario Autovino

Department of Agricultural, Food and Forest Sciences, University of Palermo,

ABSTRACT

Performing infiltration experiments on sieved and repacked soil columns seems a generally underrated topic from a methodological point of view. This study assessed how the descriptive parameters of the infiltration process were influenced by (i) the operator; (ii) the number of replicated runs; and (iii) the soil sample preparation method. A total of 135 loam soil columns, each 20 cm high were prepared by two operators. Four packing methods, differing by the number of steps required to prepare the sample, were applied. One-dimensional infiltration runs were carried out on each soil column using a Mini-Disk Infiltrometer set at a pressure head of −3 cm. A statistical, or at least practical, similarity of the infiltration parameters obtained by the two operators was detected. Six replicated runs were found to be enough to obtain an acceptable description of the entire infiltration process. Differences between the packing methods were noticeable since infiltration parameters differed by up to 2.7 times, probably because soil compaction energy varied with the applied packing method. Two operators can achieve consistent and reproducible results using the same equipment and packing method since the number of steps in which the soil column is prepared has an appreciable effect on its hydrodynamic response.

INTRODUTION

Laboratory infiltration experiments on sieved and repacked soil columns are carried out for many purposes, including studying soil sealing under controlled rainfall events [1], establishing the effects of water quality [2,3] or amendments of various nature [4–7] on the soil hydrodynamic response. Performing experiments on sieved and repacked soil columns seems a generally underrated topic [8], even if it presents several critical issues [9–11]. Factors to be considered include the following: (i)

the operator preparing the soil column and performing the infiltration run; (ii) the number of replicated runs; and (iii) the method applied to prepare the soil sample. An experiment can be carried out by a single operator or by two or more operators, who may have different abilities in applying experimental methods. The operator-to operator variation is a common aspect of all experimental methods [12,13]. Such variation affects replicability of the experiment and hence its scientific robustness. Variation induced during the sample preparation stage and the subsequent measurement phase can stem from several factors, including the level of experience of the operator. In particular, more experienced operators can be expected to prepare the sample with higher precision and consistency than less experienced operators. However, even duly trained operators can prepare a soil sample in a different manner due to their physical prowess or perhaps fatigue. Although the literature occasionally mentions operator-induced variability [12,14,15], it does not seem that the impact of this type of variability has been extensively tested in relation to measurement of soil hydrodynamic properties. Notably, a sample has to be representative of the target population. Larger sample sizes are expected to better represent the population, but too large sample sizes lead to a loss of time, human resources and money. On the other hand, the risk with too small sample sizes is that they do not satisfactorily represent the sampled population [16,17]. Choosing an appropriate sample size requires considering the actual data variability [18]. Hydrodynamic properties of field or undisturbed soil generally show a noticeable variability, and this circumstance implies that the measurement has to be replicated many times [18,19]. Instead, working in the laboratory with sieved and repacked soil can be expected to require less replications of the measurement since a more homogeneous porous medium is used in this case [20]. To the best of our knowledge, however, large datasets providing realistic estimates of the actual data variability have not been developed with reference to hydrodynamic properties of repacked soil columns. Therefore, the usability of small sample sizes for these types of investigations still needs support. When working with repacked soil samples, it is necessary to choose an appropriate packing method. This choice depends on the purpose of the investigation, but also on several practical constraints, such as the equipment available to researchers and the size of the sample that can be prepared in a laboratory. Several methodologies are, in principle, usable, such as vibrating devices [21] or press pistons [22]. In other cases, soil columns are prepared by manual methods involving a step-by-step procedure [7,23,24]. At each step, a mass of soil is poured into the cylinder, and this mass is then compacted by a pestle or by repeatedly dropping the soil column from a certain height. Packing method effects on measurement of soil hydrodynamic properties can be significant [25], and hence, they should be taken into account when the experiment is planned. The Mini-Disk Infiltrometer, MDI [26], is a compact tension infiltrometer, designed for

quick and straightforward measurement of the infiltration process under unsaturated conditions. In particular, pressure head values, h_0, ranging from −0.5 cm to −7 cm can be established at the infiltration surface. Typically, this device is employed in the field for measuring three-dimensional (3D) infiltration processes for a specific h_0 value [27,28]. However, the MDI is also usable for measuring one-dimensional (1D) infiltration on smalldiameter repacked soil columns [3,29]. Many investigations, some of which are mentioned in Table 1 as an example, have been carried out in the laboratory by applying the MDI on sieved and repacked soil samples. In general, the number of operators performing the experiment is not indicated, the number of replicates varies with the experiment—settling, however, on rather small values—and soil packing methods change from one investigation to another or they are not described. The fact that experimental methods differ with the investigation, or they are not described at all, makes the interpretation of the data difficult and hinders comparison between different investigations [30]. The general objective of this investigation was to test factors influencing 1D infiltration experiments with the MDI on sieved and repacked soil columns. The specific objectives were to establish—for loam soil and a given pressure head on the soil surface—the dependence of the measured infiltration parameters on (i) the operator performing the experiment; (ii) the considered sample size; and (iii) the applied packing method to prepare the soil column.

Table 1. Examples of experiments performed with the Mini-Disk Infiltrometer (MDI) on repacked soil columns.

Reference	Soils	Aims of the MDI Application	Size of the Columns	Soil Column Preparation	N *
Assouline and Narkis [3]	Clayey	Evaluating the impact of 15 years of irrigation with treated wastewater on soil hydraulic properties and flow processes compared to the use of freshwater	10 cm long × 5.2 cm in diameter	Air-dried, crushed and sieved soil. The <2 mm fraction of the aggregates was kept for the study. Packing method not described	2
Fatehnia et al. [31]	Poorly graded sand	Comparing methods to determine soil hydraulic conductivity from infiltration data	Not described	Not described	3
Bordoloi et al. [32]	Inorganic low plastic silt	Determining infiltration rates in compacted natural fiber-reinforced soil composite	17 cm long × 15.5 cm in diameter	Static compaction of the soil at a fixed moisture content. Compaction in three equal layers along the longitudinal axis of the mold at established densities	3
Alghamdi et al. [33]	Sandy	Testing the impact of biochar, bentonite and compost on soil physical characteristics	30 cm long × 5 cm in diameter	Soil hand-mixed, air-dried and sieved at 2 mm. Columns filled to obtain a given bulk density value. Packing method not described	3
Kargas et al. [29]	Sandy-loam; Loam; Silty-clay-loam	Investigating differences between three- (3D) and one-(1D) dimensional infiltration and determining the γ parameter of the Haverkamp et al.'s [34] infiltration model	30 cm long × 30 cm in diameter (3D experiment) and 50 cm long × 4.5 cm in diameter (1D experiment)	Air-dried soil, passed through a 2 mm sieve. Packing method not described	1
Ghosh et al. [35]	Sand; Clay-loam	Testing the effect of the initial compaction state on near-saturated soil hydraulic conductivity	30 cm long × 20 cm in diameter	Mass of air-dried soil mixed with a given amount of water to obtain the desired soil water content. Soil packed in three layers by an equal number of blows with a 1.7 kg rammer on each layer. Number of blows varying with the state of compaction for a particular soil	4
Roy et al. [36]	Silty-clay-loam; Silty-clay; Sandy-loam	Determining hydraulic conductivity of three types of soil in both frozen and unfrozen conditions with five initial soil water contents	17.8 cm long × 20.3 cm in diameter	Use of fixed amounts of soil and water to obtain a given initial water content. Soil columns prepared layer by layer to attain a pre-established bulk density value	3
Naik and Pekkat [37]	Loam; Silt-loam	Using the MDI for estimating water retention characteristic curve parameters	25 cm long × 30 cm in diameter	Nearly dry soil. Soil compacted in three layers by maintaining a uniform bulk density	6
Autovino et al. [38]	Loam; Clay	Determining the impact of soil layering on 1D infiltration processes established with the MDI	20–23 cm long × 5.3 cm in diameter	Air-dried and passed through a 2 mm sieve. Partition of the soil mass into three equal parts. First third poured in the cylinder and soil compacted by a wood pestle. Then, the rotation of the pestle around its vertical axis. Application of the same procedure with the second and third parts	9

* Number of replicates for a given treatment.

Materials and Methods

Soil

The investigation was carried out on a soil collected in Sicily (Italy), in an orchard of the Department of Agricultural, Food and Forest Sciences of the Palermo University (38◦06′24′ ′ N, 13◦21′06′ ′ E). The soil (Typic Rhodoxeralf) has a relatively high gravel content, an organic carbon content of 27 g/kg [39] and it is mostly sandy-loam or loam down to a depth of at least 0.30 m. Average values of saturated soil hydraulic conductivity determined in the field using the so-called BEST procedure [40] vary during the year between 16 and 194 mm/h [41]. For this investigation, an area where the texture was loam (clay = 19.0%, silt = 30.3%, sand = 50.7%; USDA classification system) was sampled [39]. The soil, collected from approximately the upper 10 cm of the profile, was transported to the laboratory and spread on plastic sheets for natural drying at room temperature. This process lasted about 40 days, during which the soil was manually stirred every 2–3 days to facilitate drying. Once the soil was air-dry, it was sieved for 5 min through a 2 mm mesh sieve and the fine fraction was retained for the experiment.

Experimental Methods

Soil columns were prepared in 25 cm long Plexiglas cylinders having an inner diameter, d, of 5.3 cm. Two different operators (V and Z) prepared the soil columns and performed the infiltration runs. The V operator was a master student whereas the Z operator was a PhD student. Soil columns were prepared by pouring the soil into the cylinder and manually pressing the poured soil using a wood pestle with a circular disc with a diameter of 5.0 cm at its bottom. The diameter of the disc was a little smaller (by 3 mm) than that of the cylinder to make it easier to slide the pestle into the cylinder. After concluding pressing, the pestle was rotated clockwise and counter-clockwise around its vertical axis for a few times. Different packing methods (P1, P2, P3 and P4) were applied in this investigation to prepare soil columns with a final length of 20 cm using 537 g of air-dry soil. For P1, all the air-dry soil was poured into the cylinder at once and pressed 200–220 times. For P2, 268.5 g of soil was poured and pressed 80–100 times. Then, another 268.5 g of soil was added and compacted another 80–100 times. For P3, the soil was added in three steps (179 g of air-dry soil at each step), and it was pressed 30 times at each step. For P4, the soil was added in four steps (134.25 g of soil at each step) and pressed 10–15 times after each soil addition. The fact that an operator manually compacted the soil impeded the determination of the dissipated energy for preparing the sample. However, assuming that the pressing action did not vary appreciably between two pestle applications, it can be suggested that 3.3–5.5 times higher energy was required to prepare the soil column using the P1 method than

the P4 method. A direct measurement of the dry bulk density, ρ_b (g/cm3), of a soil column was not available since the soil used to fill the cylinder was air-dry and not oven-dry. Therefore, ρb was determined by the following relationship [20]:

$$\rho_b = \frac{m_s}{V_t} = \frac{m_{ad}}{V_t \times (1 + w_{ad})} \quad (1)$$

where m_s (g) is the mass of the dry soil, Vt (cm3) is the bulk volume of the soil sample, m_{ad} (g) is the mass of the air-dry soil and wad (g/g) is the gravimetric soil water content of the air-dry soil that was measured each working day. Each operator (V and Z) prepared N = 45 soil columns using the P3 packing method. A single operator (Z) prepared N = 15 columns with each of the four packing methods, namely P1, P2, P3 and P4. On average, ρ_b was equal to 1.17 g/cm3 (coefficient of variation, CV = 0.8%; N = 135), and the volumetric air-dry soil water content, θ_{ad}, obtained by ρ_b and wad, was equal to 0.051 m3/m3 (CV = 5.4%). Therefore, the soil columns were overall homogeneous with reference to both ρ_b and θ_{ad}. A Mini-Disk Infiltrometer, MDI, was used to measure 1D infiltration in a laboratory where approximately constant temperature and humidity conditions are maintained. For each run, the MDI was filled with tap water at room temperature. A pressure head, h0, equal to −3 cm, was established at the base of the device. This choice was made to avoid flow along pores with an equivalent diameter > 1.0 mm [42] and, hence, to only consider flow through the soil matrix. Before each test, the soil column was placed on a perforated support that allowed air to easily escape from the bottom of the sample. For each run, the infiltrated volumes were measured every 10 s for the first minute, 15 s for the subsequent minute, 30 s for another two minutes and then every minute until the complete emptying of the MDI reservoir occurred. Cumulative infiltration, I (mm), at a given time, t (h), was obtained by dividing the cumulative infiltrated volume by the cross-sectional area of the soil column. A risk of obtaining inaccurate data with the MDI, as with all tension infiltrometers, is linked to poor hydraulic contact between the rough soil surface and the base of the device [43]. This risk was likely minimal in this investigation since using the pestle implied preparing the smoothest possible infiltration surface. The depth of the wetting front, d_{wf} (cm), with respect to the soil surface, was also measured at the end of the infiltration run. These measurements were performed along four verticals established at a radial distance of 90◦ and the four values were averaged to characterize the soil sample.

Infiltration Parameters

The mean infiltration rate, ir_{med} (mm/h), was calculated for each run as the ratio between cumulative infiltration by the end of the run and its total duration. In addition, the empirical Horton [44] infiltration model was fitted to the I vs. t data by minimizing the sum of the squared residuals between the measured and the predicted I values [45]:

$$I = i_{fH}t + \frac{i_{0H} - i_{fH}}{k_H}\left(1 - e^{-k_H t}\right) \quad (2)$$

where i_{0H} (mm/h) is the initial infiltration rate (t = 0), i_{fH} (mm/h) is the final infiltration rate and the constant k_H (1/h) describes the rate at which i_{0H} approaches i_{fH}. For given i_{0H} and i_{fH} values, the smaller the k_H, the more gradual the transition from the initial to the final conditions [46]. The quality of the fitting was evaluated by calculating the relative error, Er (%), in agreement with Lassabatere et al. [45]. The Er values varied from 1.2% to 5.2%, with a mean value of 3.2%. According to Lassabatere et al. [45] a relative error that does not exceed 5.5% denotes an acceptable fitting of an infiltration model to the data. Therefore, the fitting of the model to the infiltration data was satisfactory for all individual runs. The model developed by Horton was chosen since it describes the infiltration curve in some detail, that is by three different parameters expressive of the initial and the final stages of the process and also of the transition between these two stages.

Data Analysis

Five response variables, that is ir_{med}, i_{0H}, i_{fH}, k_H and d_{wf}, were considered in this investigation. Initially, a comparison was established between the experiments performed by the two operators. Taking into account that the operators V and Z yielded similar results, a single dataset of ir_{med}, i_{0H}, i_{fH}, k_H and dwf, values (N = 90 for each variable) was developed by pooling the data obtained by these two operators. The number of samples, Nr, required to estimate the mean of a variable with a given tolerance, d, for a given confidence level (95% in this investigation) was then calculated according to Warrick [19]:

$$N_r = \frac{z_{0.5\alpha}^2 SD^2}{d^2} = \frac{z_{0.5\alpha}^2 CV^2}{a^2} \quad (3)$$

where $z0.5\alpha$ is the normalized difference from the mean, SD is the standard deviation, CV is the coefficient of variation and a is a fraction of the mean, Me, such that $d = a \times Me$. According to Warrick [19], the sample coefficient of variation was used in the calculations. Using large sample sizes (i.e., N = 90) for estimating CV was considered advantageous in the perspective to obtaining reliable Nr values. Using Equation (3) with a (fraction of the mean) values ranging between 0.05 and 0.25 to estimate appropriate sample sizes is common in investigations on soil hydrodynamic parameters (e.g., [47–50]). Finally, a comparison was performed between the four packing methods. Variability of the data was considered low, medium and high for $CV \leq 15\%$, $15\% < CV \leq 50\%$ and $CV > 50\%$, respectively [19]. All comparisons were carried out by using F and t tests at $p = 0.05$. Percentage differences between two means, Δ, were also calculated as

$$\Delta = 100 \times \frac{highest\ mean - lowest\ mean}{lowest\ mean} \quad (4)$$

Results and Discussion

Operator

With reference to irmed, the means obtained by the two operators differed by a not statistically significant Δ value of 8.8% (Table 2). Considering the fitted parameters of the Horton model, Δ = 8.1% was obtained for i_{0H}, Δ = 5.5% for i_{fH} and Δ = 1.9% for k_H, and no difference between two corresponding means was significant. For d_{wf}, Δ was equal to 1.4% and differences were statistically significant in this case. Following Warrick [19], variability of ir_{med}, i_{0H}, i_{fH} and k_H was medium. A low variability was instead detected for d_{wf}.

Table 2. Statistics of the ir_{med}, i_{0H}, i_{fH}, k_H and d_{wf} values obtained by the two operators (V and Z) (sample size, N = 45 for each operator).

Parameter	Operator	Min	Max	Mean	CV (%)
ir_{med} (mm/h)	V	68.4	169.0	109.9 a	21.0
	Z	89.3	180.6	119.6 a	19.5
i_{0H} (mm/h)	V	381.5	1304.3	685.6 a	29.1
	Z	342.0	1398.4	741.3 a	33.0
i_{fH} (mm/h)	V	56.0	122.8	81.1 a	20.6
	Z	63.9	128.5	85.6 a	18.5
k_H (1/h)	V	21.0	85.8	48.1 a	29.5
	Z	21.7	97.1	49.1 a	34.6
d_{wf} (cm)	V	10.5	11.6	11.0 a	2.6
	Z	10.5	11.3	10.9 b	2.1

ir_{med} = mean infiltration rate; i_{0H} = initial infiltration rate; i_{fH} = final infiltration rate; k_H = decay constant; d_{wf} = depth of the wetting front; *Min* = minimum value; *Max* = maximum value; *CV* = coefficient of variation. For a given parameter, two means in a column followed by the same lowercase letter were not significantly different according to an F test and a two-tailed *t* test at $p = 0.05$. Means followed by a different lowercase letter were significantly different.

According to Wells et al. [51], differences of 0.4 cm in wetting front depths of approximately 2 to 6 cm can be considered small and nearly negligible. Adapting the conclusion by Wells et al. [51] to this investigation, the difference between the two means of dwf obtained by the V and Z operators (Table 2) was significant but negligible in practice, since it was <0.2 cm. Therefore, differences between the two corresponding means were small and not significant or small and practically negligible. Consequently, the results of the experiment did not depend on the operator, or they differed only marginally. In other words, two different operators repeating the same experiment with exactly the same equipment and applying the same manual packing method yielded results that were consistent with each other.

Sample Size

Table 3 summarizes the ir_{med}, i_{0H}, i_{fH}, k_H and d_{wf} values obtained by pooling the data by the V and Z operators (N = 90) and it lists the sample sizes, Nr, required to estimate the mean value of each considered parameter within +5%, +10%, +15% and +25% at the 95% confidence level.

Table 3. Statistics of the ir_{med}, i_{0H}, i_{fH}, k_H and d_{wf} values overall obtained by the V and Z operators (sample size, N = 90) and required sample size, Nr, to obtain sample means differing at the most by a fraction, a, from the true mean with a 95% confidence level.

Parameter	Min	Max	Mean	CV (%)	N_r			
					a = 0.05	a = 0.1	a = 0.15	a = 0.25
ir_{med} (mm/h)	68.4	180.6	114.8	20.5	64.6	16.1	7.2	2.6
i_{0H} (mm/h)	342.0	1398.4	713.5	31.4	151.4	37.8	16.8	6.1
i_{fH} (mm/h)	56.0	128.5	83.4	19.6	59.0	14.8	6.6	2.4
k_H (1/h)	21.0	97.1	48.6	32.0	157.7	39.4	17.5	6.3
d_{wf} (cm)	10.5	11.6	10.9	2.5	0.9	0.2	0.1	0.04

ir_{med} = mean infiltration rate; i_{0H} = initial infiltration rate; i_{fH} = final infiltration rate; k_H = decay constant; d_{wf} = depth of the wetting front; *Min* = minimum value; *Max* = maximum value; *CV* = coefficient of variation.

For a given a value, the required number of replicates was minimal, and also very small (<1 regardless of a), for d_{wf}, intermediate for ir_{med} and i_{fH} and largest for i_{0H} and k_H. Therefore, a very limited experimental information was enough to reliably determine the depth of the wetting front. For a given sample size, the mean and the final infiltration rates were generally more reliable than the initial infiltration rate and the decay constant. In other words, the infiltration process was one, but it was easier to characterize this process in terms of ir_{med} and i_{fH} than i_{0H} and i_{fH}. Taking into account that the actual sample size was N = 90, the means of ir_{med}, i_{fH} and d_{wf} reported in Table 3 differed by even less than 5% from the true mean with a 95% confidence level. Instead, the estimates of i_{0H} and k_H differed a little more, that is by 5% to 10%. This investigation contributed to giving an answer to two different questions. One question was whether a small number of replicates can be used in practice, as is common (Table 1). Another question was if the experiment could be improved to substantially reduce uncertainties of the estimated means for all parameters. Working with numerically simulated data, Reynolds [52] suggested that an individualestimate of saturated soil hydraulic conductivity is accurate if it differs from the true value by no more than 25%. Reynolds [52] suggested such a stringent accuracy criterion since, in his analysis, the data were free of the perturbations embedded in field and laboratory measurements. If a criterion of this type can be accepted under ideal conditions, it can be even more so with reference to experimental data. Therefore, assuming that a difference of 25% can be considered practically negligible for other soil hydrodynamic parameters and with reference to the mean value of a soil hydrodynamic parameter, this investigation supported the usability of small sample sizes in experiments on repacked soil columns with the MDI. The reason was that Nr = 6 was enough to obtain sample means differing at the most by +25% from the true mean with a 95% confidence level for all considered parameters (Table 3). Therefore, the answer to the first

question was that small sample sizes can indeed be used. The uncertainties are larger for the parameters expressive of the transient stage of the infiltration process but practically acceptable. With reference to the second question, the analysis suggested that 150–160 individual determinations of i0H and kH should be carried out to obtain an accurate estimate of the mean (i.e., a = 0.05 in Equation (3)). This is likely an impractically large number. Therefore, the answer in this case was that there is a practical limit to the reliability of a given parameter. The reason is that substantially improving the quality of the estimated mean of this parameter would imply an experiment that cannot be carried out in practice.

Packing Method

Infiltration rates (ir_{med}, i_{0H} and i_{fH}) decreased monotonically from the P4 to the P1 packing methods (Table 4). The ir_{med} and i_{fH} values decreased according to the P4 = P3 > P2 > P1 sequence. The largest difference, detected between the P1 and P4 methods, was by a factor of 2.7 for ir_{med} and 2.4 for i_{fH}. The i_{0H} values differed according to the P4 = P3 > P2 = P1 sequence and the largest difference, also detected between the P1 and P4 methods, was by 1.8 times. Variability was medium in ten of the twelve cases considered (three parameters × four packing methods) and low in the other two cases. The lowest CV values were obtained with the P4 method for ir_{med} and i_{fH} and with the P2 method for i_{0H}, yielding, however, a very similar result to that obtained with the P4 method. The means of k_H decreased according to the P4 = P1 = P3 > P2 sequence since the only significant difference (Δ = 27.6%) was detected between the P2 and P4 methods. Even in this case, the variability of the data was medium regardless of the packing method, and the lowest CV value was obtained with the P4 method. Finally, dwf decreased according to the P2 > P1 > P3 > P4 sequence. Two means differed by 2.3% to 15.6%, depending on the established comparison. The variability of the data was low for all packing methods, and the highest CV value was obtained for the P4 method.

Table 4. Statistics of the ir_{med}, i_{0H}, i_{fH}, k_H and d_{wf} values obtained by four different packing methods (P1, P2, P3, P4).

Parameter	Statistic	Packing Method			
		P1	P2	P3	P4
ir_{med} (mm/h)	Min	31.2	36.4	93.5	104.8
	Max	70.8	113.9	180.6	154.1
	Mean	48.5 a	81.8 b	123.9 c	132.4 c
	CV (%)	27.0	31.2	20.8	9.7
i_{0H} (mm/h)	Min	277.7	435.7	408.6	556.8
	Max	957.4	856.3	1398.4	1280.2
	Mean	519.9 a	590.9 a	805.1 b	939.5 b
	CV (%)	31.9	21.0	36.5	21.9
i_{fH} (mm/h)	Min	30.3	33.0	63.9	83.1
	Max	55.1	89.0	128.5	109.8
	Mean	40.9 a	64.4 b	88.4 c	97.8 c
	CV (%)	20.1	30.2	20.9	8.2
k_H (1/h)	Min	28.1	28.9	23.3	36.0
	Max	108.4	76.2	97.1	86.5
	Mean	54.8 ab	52.6 a	53.7 ab	67.1 b
	CV (%)	39.9	24.1	40.6	22.0
d_{wf} (cm)	Min	10.7	11.6	10.5	8.3
	Max	11.4	13.1	11.3	11.0
	Mean	11.1 a	12.0 b	10.9 c	10.4 d
	CV (%)	1.6	3.1	1.8	5.8

ir_{med} = mean infiltration rate; i_{0H} = initial infiltration rate; i_{fH} = final infiltration rate; k_H = decay constant; d_{wf} = depth of the wetting front; *Min* = minimum value; *Max* = maximum value; *CV* = coefficient of variation. For a given parameter, the means followed by the same lowercase letter were not significantly different according to an F test and a two-tailed *t* test at $p = 0.05$. Means followed by a different lowercase letter were significantly different.

Overall, the effect of the used packing method was noticeable for the infiltration rates and the depth of the wetting front, and it was relatively small with reference to the decay constant of the infiltration model. As reported by Lewis and Sjostrom [10], homogeneous packing requires adding soil in very small increments, at least in case of sand [9], but relatively large increments are commonly used [53,54]. According to this investigation, the greater the number of layers, the higher the infiltration rates. This result likely occurred because, as the number of layers increased, the efforts made to compact the soil were overall smaller and more evenly distributed along the soil column. Reducing and distributing these efforts along the vertical axis of the column gave rise to the formation of a more permeable and homogeneous soil sample than that obtained when these efforts were concentrated on a single or a few exposed soil surfaces. In other words, it seems that the infiltration data obtained on a soil column prepared with a multi-layering method tends to be expressive of an infiltration process that occurs in an overall rather homogeneous soil column. Instead, if the soil is poured into the cylinder only once, the upper soil layer is appreciably more compacted than the subsoil, and this

circumstance makes the infiltration process slower. In particular, infiltration is mainly controlled by the upper soil layer. In this investigation, the applied packing procedure did not appreciably influence the decay constant, k_H. Therefore, not all parameters that describe the dynamics of the infiltration process show the same sensitivity to the applied packing method. In particular, this sensitivity is appreciable for the parameters expressive of the rate at which infiltration occurs (ir_{med}, i_{0H}, i_{fH}), but it is smaller with reference to the rate at which i_{0H} approaches i_{fH}. Using a relatively large number of layers to prepare the soil column appears advantageous for improving reproducibility of the infiltration experiment. This suggestion was based on the fact that the CV values for ir_{med}, i_{0H}, i_{fH} and k_H were lowest, or almost so, with the P4 packing method. However, some word of caution is necessary with reference to this finding since CV did not decrease monotonically from the P1 to the P4 methods. In other words, other investigations should be performed to verify the suggestion that more layers imply less variability in the data. It also seems that the larger the number of layers, the smaller the thickness of the wetted soil volume tends to be, although the decrease in d_{wf} from the P1 to P4 methods was not monotonic either. Perhaps this was a consequence of the fact that, with a multi-layering packing method, pores were overall larger, as also suggested by the higher infiltration rates. Filling these pores required relatively large amounts of water. Consequently, there was not enough water to also fill the pores of the deepest zone of the soil column. To improve the interpretation of packing effects on infiltration, future investigations could also include an accurate characterization of the pore structure in soil samples prepared with different methods. The expectation could be to better understand the link between soil hydrodynamic response and pore system characteristics, including pore volume, size and tortuosity (e.g., [55,56]). Moreover, simple packing devices, such as the one recently developed by Bagarello et al. [57], could be used with a double potential advantage: (i) the dissipated energy to compact the soil could be expressed quantitatively, and (ii) exactly the same experimental method could be applied in different laboratories.

Conclusions

This investigation tested factors influencing 1D infiltration experiments with the MDI on columns of a sieved and repacked loam soil. According to this investigation, it appears reasonable to believe that two operators who apply the same manual method to prepare a soil column and perform an experiment with the Mini-Disk Infiltrometer can collect comparable infiltration data. Obtaining a mean value differing from the true mean by no more than a fixed percentage at a given confidence level requires less replicates of the run for mean and final infiltration rates than for the parameters describing the initial stage of the process. In general, however, a relatively small number of replicated runs is enough to obtain an acceptable description of the entire infiltration process. With a manual packing method

to prepare a soil column, the number of steps in which soil is added from time to time has an appreciable effect on the hydrodynamic response of the tested soil column. Therefore, an experiment carried out by one or two operators applying a given packing method could be considered replicable in other circumstances. In particular, preparing a soil column in subsequent steps is recommended since this choice seems appropriate for reducing variability of the individual measurements of the infiltration parameters. This conclusion is valid for this experiment, and therefore it cannot be considered general unless, perhaps, with reference to other loam soils and an infiltration process that excludes the largest pores, i.e., one that only occurs through the soil matrix. The experiment should be repeated with other soils and other established pressure heads at the infiltration surface, with the goal of collecting experimental information that can be used to reach general conclusions. The methodology applied in this investigation, using simple devices and laboratory methods, could easily be extended to other scenarios.

Author Contributions: Conceptualization, V.B. and D.A.; methodology, V.B. and S.B.; validation, V.B. and D.A.; formal analysis, V.B. and D.A.; investigation, G.C., F.K.V. and F.Z.; data curation, V.B. and D.A.; writing—original draft preparation, V.B.; Writing—review and editing, V.B., S.B. and D.A.; visualization, V.B. and D.A.; supervision, V.B.; project administration, V.B.; funding acquisition, V.B.

All authors have read and agreed to the published version of the manuscript.

Funding: This research was funded by (i) RETURN Extended Partnership, European Union NextGenerationEU (National Recovery and Resilience Plan—NRRP, Mission 4, Component 2, Investment 1.3-D.D. 1243 2/8/2022, PE0000005) and (ii) ASCAN “Indagine di laboratorio e di pieno campo sull’uso di Ammendanti naturali dei Suoli per strategie di Conservazione dell’Acqua e dei Nutrienti”—National Research Centre for Agricultural Technologies, Codice progetto CN00000022, Bando a Cascata Spoke n. 6, CUP D13C22001330005.

Data Availability Statement: The raw data supporting the conclusions of this article will be made available by the authors on request.

Conflicts of Interest: The authors declare no conflicts of interest.

References

1. Armenise, E.; Simmons, R.W.; Ahn, S.; Garbout, A.; Doerr, S.H.; Mooney, S.J.; Sturrock, C.J.; Ritz, K. Soil Seal Development under Simulated Rainfall: Structural, Physical and Hydrological Dynamics. J. Hydrol. 2018, 556, 211–219. [CrossRef] [PubMed]

2. Viviani, G.; Iovino, M.Wastewater Reuse Effects on Soil Hydraulic Conductivity. J. Irrig. Drain. Eng. 2004, 130, 476–484. [CrossRef]

3. Assouline, S.; Narkis, K. Effects of Long-Term Irrigation with TreatedWastewater on the Hydraulic Properties of a Clayey Soil. Water Resour. Res. 2011, 47, 1–13. [CrossRef]

4. Xiubin, H.; Zhanbin, H. Zeolite Application for Enhancing Water Infiltration and Retention in Loess Soil. Resour. Conserv. Recycl. 2001, 34, 45. [CrossRef]

5. Blanco-Canqui, H. Biochar and Soil Physical Properties. Soil Sci. Soc. Am. J. 2017, 81, 687–711. [CrossRef]

6. Bond., C.; Castellini, M.; Iovino, M. Compost Amendment Impact on Soil Physical Quality Estimated from Hysteretic Water Retention Curve. Water 2022, 14, 1002. [CrossRef]

7. Bond., C.; Castellini, M.; Iovino, M. Temporal Variability of Physical Quality of a Sandy Loam Soil Amended with Compost. Biologia 2024. [CrossRef]

8. Gibert, O.; Hernandez, M.; Vilanova, E.; Cornellà, O. Guidelining Protocol for Soil-Column Experiments Assessing Fate and Transport of Trace Organics; European Union: Brussels, Belgium, 2014; Volume 3.

9. Oliviera, I.B.; Demond, A.H.; Salehzadeh, A. Packing of Sands for the Production of Homogeneous Porous Media. Soil Sci. Soc. Am. J. 1996, 60, 49–53. [CrossRef]

10. Lewis, J.; Sjostrom, J. Optimizing the Experimental Design of Soil Columns in Saturated and Unsaturated Transport Experiments. J. Contam. Hydrol. 2010, 115, 1–13. [CrossRef]

11. Nakhli, S.A.A.; Tian, J.; Imhoff, P.T. Preparing and Characterizing Repacked Columns for Experiments in Biochar-Amended Soils. MethodsX 2021, 8, 101205. [CrossRef]

12. Griffiths, J.C.; Rosenfeld, M.A. Operator Variation in Experimental Research. J. Geol. 1954, 62, 74–91. [CrossRef]

13. Zobisch, M.A.; Klingspor, P.; Oduor, A.R. The Accuracy of Manual Runoff and Sediment Sampling from Erosion Plots. J. Soil. Water Conserv. 1996, 51, 231–233.

14. Black, C.A. Operator Variation. In Methods of Soil Analysis, Part 1: Physical and Mineralogical Properties, Including Statistics of Measurement and Sampling; Inc. Book Series: Agronomy Monographs; John Wiley & Sons, Inc.: Hoboken, NJ, USA, 2015; pp. 50–53.

15. Bagarello, V.; Di Piazza, G.V.; Ferro, V. Manual Sampling and Tank Size Effects on the Calibration Curve of Plot Sediment Storage Tanks. Trans. Am. Soc. Agric. Eng. 2004, 47, 1105–1112. [CrossRef]

16. Belanger, N.; Van Rees, K.C.J. Sampling Forest Soils. In Soil Sampling and Methods of Analysis; Carter, M.R., Gregorich, E.G., Eds.; CRC Press and Taylor & Francis Group.: Boca Raton, FL, USA, 2008; pp. 15–24.

17. Pennock, D.; Yates, T.; Braidek, J. Soil Sampling Design. In Soil Sampling and Methods of Analysis; Carter, M.R., Gregorich, E.G., Eds.; CRC Press and Taylor & Francis Group: Boca Raton, FL, USA, 2008; pp. 1–14.

18. Reynolds, W.D.; Elrick, D.E.; Youngs, E.G. Single-Ring and Double- or Concentric-Ring Infiltrometers. In Methods of Soil Analysis, Part 4, Physical Methods; Dane, J.H., Topp, G.C., Eds.; Soil Science Society of America: Madison, WI, USA, 2002; pp. 821–826.

19. Warrick, A.W. Appendix 1: Spatial Variability. In Enviromental Soil Physics; Hillel, D., Ed.; Academic Press: San Diego, CA, USA, 1998; pp. 655–675.

20. Bagarello, V.; Caltabellotta, G.; Iovino, M. Manual Packing and Soil Reuse Effects on Determination of Saturated Hydraulic Conductivity of a Loam Soil. Geoderma 2022, 405, 115465. [CrossRef]

21. Anat, A.; Duke, H.R.; Corey, A.T. Steady Upward Flow from Water Tables Steady Upward Flow from Water Tables; Colorado State University: Fort Collins, CO, USA, 1965; Volume 7, Hydrology Papers.

22. Reicosky, D.C.; Voorhees, W.B.; Radke, J.K. Unsaturated Water Flow Through a Simulated Wheel Track. Soil Sci. Soc. Am. J. 1981, 45, 3–8. [CrossRef]

23. Bagarello, V.; Iovino, M.; Elrick, D. A Simplified Falling-Head Technique for Rapid Determination of Field-Saturated Hydraulic Conductivity. Soil Sci. Soc. Am. J. 2004, 68, 66–73. [CrossRef]

24. Zhang, J.; Lei, T.; Yin, Z.; Hu, Y.; Yang, X. Effects of Time Step Length and Positioning Location on Ring-Measured Infiltration Rate. Catena 2017, 157, 344–356. [CrossRef]

25. Teng, J.; Kou, J.; Zhang, S.; Sheng, D. Evaluating the Influence of Specimen Preparation on Saturated Hydraulic Conductivity Using Nuclear Magnetic Resonance Technology. Vadose Zone J. 2019, 18, 1–7. [CrossRef]

26. METER Group. Mini Disk Infiltrometer Manual; METER Group: Pullman, WA, USA, 2021.

27. Gonzalez-Sosa, E.; Braud, I.; Dehotin, J.; Lassabatère, L.; Angulo-Jaramillo, R.; Lagouy, M.; Branger, F.; Jacqueminet, C.; Kermadi,

S.; Michel, K. Impact of Land Use on the Hydraulic Properties of the Topsoil in a Small French Catchment. Hydrol. Process 2010, 24, 2382–2399. [CrossRef]

28. Fodor, N.; Sandor, R.; Orfanus, T.; Lichner, L.; Rajkai, K. Evaluation Method Dependency of Measured Saturated Hydraulic Conductivity. Geoderma 2011, 165, 60–68. [CrossRef]

29. Kargas, G.; Londra, P.; Anastasiou, K.; Kerkides, P. A Note on One- and Three-Dimensional Infiltration Analysis from a Mini Disc Infiltrometer. Water 2018, 10, 1783. [CrossRef]

30. Bromly, M.; Hinz, C.; Aylmore, L.A.G. Relation of Dispersivity to Properties of Homogeneous Saturated Repacked Soil Columns. Eur. J. Soil. Sci. 2007, 58, 293–301. [CrossRef]

31. Fatehnia, M.; Tawfiq, K.; Abichou, T. Comparison of the Methods of Hydraulic Conductivity Estimation from Mini Disk Infiltrometer. Electron. J. Geotech. Eng. 2014, 19 E, 1047–1063.

32. Bordoloi, S.; Hussain, R.; Garg, A.; Sreedeep, S.; Zhou, W.H. Infiltration Characteristics of Natural Fiber Reinforced Soil. Transp. Geotech. 2017, 12, 37–44. [CrossRef]

33. Alghamdi, A.G.; Aly, A.A.; Al-Omran, A.M.; Alkhasha, A. Impact of Biochar, Bentonite, and Compost on Physical and Chemical Characteristics of a Sandy Soil. Arab. J. Geosci. 2018, 11, 670. [CrossRef]

34. Haverkamp, R.; Ross, P.J.; Smettem, K.R.J.; Parlange, J.Y. Three-dimensional Analysis of Infiltration from the Disc Infiltrometer: 2. Physically Based Infiltration Equation. Water Resour. Res. 1994, 30, 2931–2935. [CrossRef]

35. Ghosh, B.; Pekkat, S. Effect of Initial Compaction State on Near-Saturated Hydraulic Conductivity. J. Irrig. Drain. Eng. 2019, 145, 04019028. [CrossRef]

36. Roy, D.; Jia, X.; Chu, X.; Jacobs, J.M. Hydraulic Conductivity Measurement for Three Frozen and Unfrozen Soils in the Red River of the North Basin. Trans. ASABE 2021, 64, 761–770. [CrossRef]

37. Naik, A.P.; Pekkat, S. An Appraisal on the Soil Wetting Water Retention Characteristic Curve Determined from Mini Disk Infiltrometer and Sensor Measurements. Acta Geophys. 2023, 71, 961–982. [CrossRef]

38. Autovino, D.; Bagarello, V.; Caltabellotta, G.; Varadi, F.K.; Zanna, F. One-Dimensional Infiltration in a Layered Soil Measured in the Laboratory with the Mini-Disk Infiltrometer. J. Hydrol. Hydromech. 2024, 72, 149–157. [CrossRef]

39. Bagarello, V.; Caltabellotta, G.; Iovino, M. Soil Reuse Effects on Determination of Saturated Hydraulic Conductivity of Different Loamy Soils. Eur. J. Soil. Sci. 2024, 75, e13454. [CrossRef]

40. Angulo-Jaramillo, R.; Bagarello, V.; Iovino, M.; Lassabatère, L. Infiltration Measurements for Soil Hydraulic Characterization; Springer International Publishing: Cham, Switzerland, 2016; ISBN 978-3-319-31786-1.

41. Bagarello, V.; Caltabellotta, G.; Concialdi, P.; Iovino, M. Comparing Two Methods to Perform a Beerkan Infiltration Run in a Loam Soil at Different Dates. J. Hydrol. 2023, 617, 129095. [CrossRef]

42. Reynolds, W.D.; Drury, C.F.; Tan, C.S.; Fox, C.A.; Yang, X.M. Use of Indicators and Pore Volume-Function Characteristics to Quantify Soil Physical Quality. Geoderma 2009, 152, 252–263. [CrossRef]

43. Close, K.R.; Frasier, G.; Dunn, G.H.; Loftis, J.C. Tension Infiltrometer Contact Interface Evaluation by Use of a Potassium Iodide Tracer. Trans. Am. Soc. Agric. Eng. 1998, 41, 995–1004. [CrossRef]

44. Horton, R.E. An Approach Toward a Physical Interpretation of Infiltration-Capacity. Soil Sci. Soc. Am. J. 1940, 5, 399–417. [CrossRef]

45. Lassabatère, L.; Angulo-Jaramillo, R.; Soria Ugalde, J.M.; Cuenca, R.; Braud, I.; Haverkamp, R. Beerkan Estimation of Soil Transfer Parameters through Infiltration Experiments-BEST. Soil Sci. Soc. Am. J. 2006, 70, 521–532. [CrossRef]

46. Tindall, J.A.; Kunkel, J.R.; Anderson, D.E. Unsaturated Zone Hydrology for Scientists and Engineers; Prentice Hall: Upper Saddle River, NJ, USA, 1999.

47. Mallants, D.; Mohanty, B.P.; Jacques, D.; Feyen, J. Spatial Variability of Hydraulic Properties in a Multi-Layered Soil Profile. Soil. Sci. 1996, 161, 167–181. [CrossRef]

48. Tsegaye, T.; Hill, R.L. Intensive Tillage Effects on Spatial Variability of Soil Physical Properties. Soil. Sci. 1998, 163, 143–154. [CrossRef]

49. Munoz-Carpena, R.; Regalado, C.M.; Alvarez-Benedi, J.; Bartoli, F. Field Evaluation of the New Philip-Dunne Permeameter for Measuring Saturated Hydraulic Conductivity. Soil. Sci. 2002, 167, 9–24. [CrossRef]

50. Bagarello, V.; Castellini, M.; Iovino, M.; Sgroi, A. Testing the Concentric-Disk Tension Infiltrometer for Field Measurement of Soil Hydraulic Conductivity. Geoderma 2010, 158, 427–435. [CrossRef]

51. Wells, R.R.; Romkens, M.J.M.; Parlange, J.-Y.; DiCarlo, D.A.; Steenhuis, T.S.; Prasad, S.N. A Simple Technique for Measuring Wetting Front Depths for Selected Soils. Soil Sci. Soc. Am. J. 2007, 71, 669–673. [CrossRef]

52. Reynolds,W.D. An Assessment of Borehole Infiltration Analyses for Measuring Field-Saturated Hydraulic Conductivity in the Vadose Zone. Eng. Geol. 2013, 159, 119–130. [CrossRef]

53. Communar, G.; Keren, R.; Li, F. Deriving Boron Adsorption Isotherms from Soil Column Displacement Experiments. Soil Sci. Soc. Am. J. 2004, 68, 481–488. [CrossRef]

54. Plummer, M.A.; Hull, L.C.; Fox, D.T. Transport of Carbon-14 in a Large Unsaturated Soil Column. Vadose Zone J. 2004, 3, 109–121. [CrossRef]

55. Shan, J.; Zhang, Y.;Wu, S.; Lin, Z.; Li, L.;Wu, Q. Pore Characteristics of Pervious Concrete and Their Influence on Permeability Attributes. Constr. Build. Mater. 2022, 327, 126874. [CrossRef]

56. Luo, Y.;Wen, T.; Lin, X.; Chen, X.; Shao, L. Quantitative Analysis of Pore-Size Influence on Granite Residual Soil Permeability Using CT Scanning. J. Hydrol. 2024, 645, 132133. [CrossRef]

57. Bagarello, V.; Caltabellotta, G.; Fusco, M.; Vaccaro, G.; Autovino, D. Investigating Soil Compaction and Its Impact on Physical and Hydraulic Properties Using a Simple Testing Apparatus. Water 2025, 17, 723. [CrossRef]

3.3 Low-Cost Autonomous 3D-Printed Mini Disk Infiltrometer

Published on Journal of Hydrology, 2025, 134212.

Jan-František Kubát, Francesco Zanna, Martin Mildner, Michal Sněhota

ABSTRACT

Hydraulic conductivity on the surface of the soil is crucial to address many hydrological and environmental issues. This study presents the development and validation of a low-cost Autonomous Mini Disk Infiltrometer (AMDI), fabricated using fused deposition modeling (FDM) 3D printing. AMDI integrates a transparent PET-G Mariotte chamber and a TDT-based TMS-4 sensor to allow automated measurement of cumulative infiltration under controlled pressure head levels. Calibration was performed using polynomial regression (cubic) to relate the readings of the TDT sensor to changes in water volume. Laboratory infiltration experiments on loamy Chernozem soil compared AMDI with a commercially available, manually operated minidisk infiltrometer (MDI) at pressure head levels of h0 = -6, -3 and -1 cm. The results of ANOVA did not show significant differences between AMDI and MDI in higher pressure heads ($p < 0.05$), with notable discrepancies at -1 cm ($p > 0.05$) likely attributed to differences in the porous sintered stainless-steel disks, despite the hydraulic conductivity of the CTU disk being significantly higher than that of the soil. The influence of the porous disk was tested using MDI alone, which clearly demonstrated its effect on infiltration. This aspect should be further investigated to better define the impact of the disk on infiltration measurements. Moreover, despite the inherent porosity of FDM prints, air leakage was minimized through optimized printing parameters, allowing for reliable operation without post-processing or specialized equipment. The AMDI offers a functional, cost-effective (approximately € 218), and customizable alternative to traditional MDIs, with potential for broader adoption, including in citizen science applications. Further field testing is needed in diverse soil types and environmental conditions.

INTRODUCTION

Infiltration of water into the soil is a key component of hydrological modeling (Chow and Maidment, 1998). Theoretical developments, from Darcy's law (1856) to Richards' (1931) equation, emphasize the importance of accurately measuring saturated and unsaturated hydraulic conductivity (K) under various soil conditions. Other process-based models used in hydrology to describe infiltration also incorporate K (Green and Ampt, 1911; Philip, 1969, 1957). Therefore, determining K is essential for accurate hydrological modeling. K vary significantly between soils, and substantial variability may also occur within the same soil type due to factors such as soil management practices, crops, edaphon, topography, groundwater, freeze-thaw cycles, and meteorological conditions (Angulo-Jaramillo et al., 2000; Elkateb et al., 2003; Green et al., 2003; Klöffel et al., 2024; Kool et al., 2019; Leuther and Schlüter, 2021; Meurer et al., 2020; Rosenbaum et al., 2012; Severino et al., 2003; Teng et al., 2023), making infiltration one of the most complex components of the hydrological cycle (Mein et al., 1971).

Unsaturated hydraulic conductivity can be measured directly in the laboratory or in the field, or it can be estimated indirectly using related soil properties through water retention curves (Brooks and Corey, 1964; Burdine, 1953; Morel-Seytoux et al., 1996; Mualem, 1976; van Genuchten, 1980; Van Genuchten, 1978; Vogel et al., 2000) or pedotransfer functions (Deb and Shukla, 2012; Kubát et al., 2024; Wosten et al., 1999). Nimmo (2009) reviewed various methods to determine both saturated and unsaturated K. Laboratory steady-state methods using constant pressure or flux (through Darcy's law) are best suited for wet soils, while centrifugal methods are effective in drier conditions. Unsteady methods, such as instantaneous or evaporation-driven profile approaches, estimate K by monitoring changes in soil water content and hydraulic head over time. Field-based indirect methods involve fitting infiltration data to simulated water flow models. A widely used field and laboratory method is the tension infiltrometer (Ankeny et al., 1991; Jarvis et al., 1987; Nestingen et al., 2018; Perroux and White, 1988; Šimůnek and Van Genuchten, 1996; Sněhota and Cislerova, 2002), which estimates K from infiltration rates under controlled pressure heads.

A miniaturized version of the tension infiltrometer, the Mini Disk Infiltrometer (MDI) manufactured by Meter Group (Pullman, WA, United States), is commonly used to assess soil hydrodynamic properties, particularly hydraulic conductivity near saturation (Meter Group, 2021). The instrument consists of a transparent (polycarbonate) tube divided into two chambers: the upper chamber, or Mariotte reservoir, sets the pressure head (typically between h_0 = -6 cm and -0.5 cm), and the lower chamber, or water reservoir, contains approximately 95 ml of water that infiltrates the soil through a porous sintered stainless-steel disk (45 mm in diameter and 3 mm thick), preventing free drainage into the air. During an MDI test, the operator measures the water volume leaving the reservoir at

specific time intervals to construct a cumulative infiltration curve, which allows estimation of the unsaturated hydraulic conductivity (K, in mm h^{-1}) corresponding to the applied pressure head. The MDI is commonly used in the field to measure three-dimensional (3D) infiltration processes (Alagna et al., 2013; Fodor et al., 2011; Gonzalez-Sosa et al., 2010), it is also suitable for one-dimensional (1D) infiltration measurements in repackage soil columns (Autovino et al., 2024; Bagarello et al., 2022; Ghosh and Pekkat, 2019; Naik et al., 2019).

Despite its advantages, manual use of tension infiltrometers is labor intensive. Automation of infiltrometer measurements generally involves monitoring changes in water level. In early work, Ankeny et al. (1988) used a pair of pressure transducers to determine the hydrostatic pressure in the Mariotte column and thereby the actual water volume. The advent of microcontrollers, such as Arduino, has facilitated infiltrometer automation. Di Prima (2015) developed a compact automated single-ring infiltrometer using Arduino and a differential pressure transducer, significantly reducing costs and enabling faster and more precise data collection. Similarly, Madsen and Chandler (2007) automated the mini disk infiltrometer. Recently, Morales-Ortega et al. (2023) utilized a Time-of-Flight (ToF) sensor in combination with an Arduino microcontroller to automate tension infiltrometer. Klípa et al. (2015) automated multiple mini disk infiltrometers by measuring the buoyancy force of the water in the Mariotte bottle on a miniature load cell, with the system validated in a long-term field study (Zumr et al., 2019). An innovative method for measuring very low infiltration rates was presented by Hallett and Gordon (2014), who detected bubble formation by measuring changes in electrical resistivity in the bubbling tower of the infiltrometer. In another approach Moret-Fernández et al. (2012) developed a complex setup with a micro flowmeter and solenoid valves to automate multipotential tension infiltrometry trials. Moret et al. (2004) advocated for the registration using a time domain reflectometry (TDR) probe in the reservoir tube. Alternatively, Jara et al. (2012) proposed a method involving sequential imaging of water levels in the reservoir using an automatic or smartphone camera, with images analyzed through particle tracking image analysis. A similar approach was recently adopted by Latorre et al. (2021), although it requires dyeing of the infiltrating water to enhance image contrast.

Focusing on the development of autonomous MDIs through prototyping and customization, we adopted additive manufacturing (AM) techniques as a method suitable for fabrication of complex three-dimensional geometries. AM, commonly known as 3D printing, constructs objects by layering materials (Ngo et al., 2018), which is expected to revolutionize the manufacturing sector (Mitchell et al., 2018; Patwardhan, 2018). Fused deposition modeling (FDM) and stereolithography (SLA) are the most widely used 3D printing techniques (Ngo et al., 2018; Patel et al., 2022; Percoco et al., 2012).

SLA, one of the earliest methods developed in 1986 by Charles Hull, uses UV light (or an electron beam) to initiate a chain reaction on a layer of resin or monomer solution (Melchels et al., 2010). SLA prints high-quality parts at fine resolutions as low as 10 μm (Gibson et al., 2015). However, SLA is relatively slow and costly, with limited material options and complex curing kinetics (Ngo et al., 2018). FDM, on the contrary, is inexpensive, fast, and simple but suffers from weaker mechanical properties, visible layer lines, poor surface quality, and limited material choices (Chohan et al., 2017; Mohamed et al., 2015). Despite these limitations, FDM is suitable for prototyping due to its affordability and simplicity. A common issue in both techniques is porosity, which compromises fluid containment, which is critical for MDI function. Achieving watertight, and even more airtight FDM prints remains a challenge (Wu et al., 2024). However, successful leak prevention has been achieved by adjusting the printing parameters (AL-Hasni and Santori, 2020; Leite et al., 2018; Romanov et al., 2018), including layer height, extrusion flow, print speed and temperature, shell thickness, and seam positioning. Therefore, it is achievable to limit liquid leakage.

The availability of low-cost, user-friendly instruments can support citizen science initiatives. For example, the Parrot Flower Power soil moisture sensor has been used successfully in citizen science projects, providing valuable environmental monitoring data (Xaver et al., 2020). Affordable scientific instruments can also support research and education in developing countries and disadvantaged regions.

To reduce costs of tension infiltration measurement, lower the labor cost and improve adaptability, our objective was to develop and validate an Autonomous Mini Disk Infiltrometer (AMDI) by integrating commercially available autonomous low-cost sensor (Time Domain Transition) for automation of infiltration measurement process and 3D printing for fabrication. The aim was to provide AMDI design in the form of an open-source platform to be further developed in the scientific community.

Materials and Methods

Design of the AMDI

AMDI consists of an interconnected infiltrometer body with bottom lid, Mariotte bottle, and TDT sensor. The 3D printed were designed in Fusion 360 (Autodesk, United Kingdom). To assemble a functioning AMDI, the following components are required: five O-rings (one piece 45 × 3.6 mm, one piece 5 × 2.0 mm, and three pieces 20 × 3.6 mm), one TMS-4 sensor, sintered stainless steel disk (45 mm in diameter and 3 mm in thickness), and 3D-printed parts A, B, and C (Figure 1). The fully

assembled AMDI is 29.5 cm high and 5 cm in diameter (22.5 cm without the sensor). The Mariotte chamber consists of part B1 (the chamber itself) and part B2 (the suction tube). The suction tube is fixed and the desired pressure head is adjusted by setting the water level in the Mariotte chamber. The chamber has an imprinted scale from 0 to 6 cm, marked in increments of -0.5 cm, and is connected to the Mariotte tube using part A2 (a nozzle-shaped connector). Regarding the pressure head, the offset of the AMDI; the distance between the Mariotte tube and the sintered disk; is -9 mm. This offset must be considered in the calculation of hydraulic conductivity (K), as is also required for the Meter MDI. Parts B1 and B2 are printed separately and then glued together using ethyl 2-cyanoacrylate glue (Henkel CEE GmbH, Germany) and rest for at least 24 hours. A similar procedure is applied to bond parts A1 and A2, as well as part C and the sintered stainless-steel disk (similar to one used in the study by Klípa et al., 2015; Zumr et al., 2019), which must also be glued into place. The porous disk was manufactured from SIKA-R 80 AX sinter metal filter disk (GKN GmbH, Germany) with a nominal pore size of 80 microns. Before inserting the TDT sensor, the O-rings (20 × 3.6 mm) should be placed in the openings and a non-silicone lubricant (preferably a lubricant used for plastic sewerage tubes or similar) should be applied to minimize the risk of damaging the sensor or AMDI. AMDI. When the TDT sensor is placed, the status diode should face the Martiotte chamber. Once the TDT sensor is inserted and all components are glued together, the AMDI can be assembled. The Mariotte chamber features sliders that match the rails in part A1, keeping the chamber in place and facilitating its positioning. Before sliding the Mariotte chamber into place, it should be filled with the desired water level (using a syringe), and the connector should be fitted with the O-ring (5 × 2.0 mm). The infiltrometer should be filled with 150 ml of water, which represents an increase compared to the 90 ml capacity of the conventional MDI. Lastly, the lid (part C), equipped with the O-ring (45 × 3.6 mm), should be screwed into place and tightened to prevent undesirable leakage. All printable parts and 3D printer settings are available at the GitHub repository (Kubát and Sněhota, 2025).

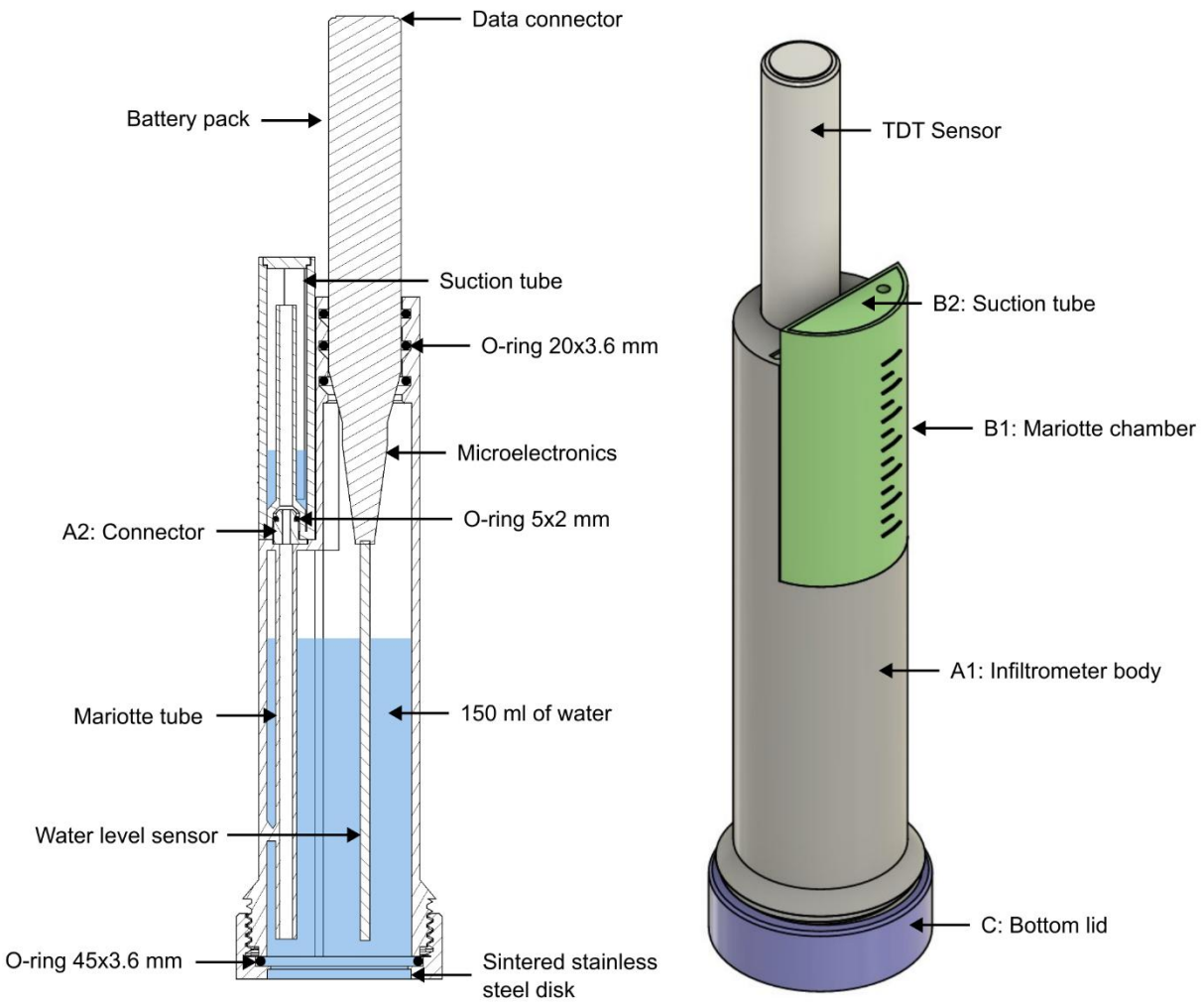

Figure 1: Cross section and visualization of the 3D printed AMDI, parts denoted A, B, and C are 3D printed using FDM technology.

3D Printing

We utilized fused deposition modeling (FDM) technology for 3D printing (Patel et al., 2022; Percoco et al., 2012). All parts of the AMDI were manufactured using polyethylene terephthalate glycol (PET-G) filament produced by Prusa a.s. (Czechia). We employed clear filament (color: E4E7E5) with a diameter of 1.75 ± 0.02 mm. Since the pressure head is set by adjusting the water level in the Mariotte chamber, the transparency of the material is crucial. To prepare the parts for printing, we used the open-source software PrusaSlicer version 2.9. The printing was performed using three different printers: Prusa MINI+, Prusa i3 MK3S+, and Prusa XL, all produced by Prusa a.s. (Czechia), with the same slicer settings applied to all parts across the different printers. To simulate a realistic printing scenario, no enclosure was used, with ambient temperatures fluctuating

between 22 and 28 °C. Each part was treated with a 400 °C heat gun to remove strings (for approximately 30 s), which resulted from the set parameters.

Given the nature of the measurements for which the device is intended, watertightness and airtightness are essential properties. Achieving liquid tightness of the prints is challenging, however, it is possible to minimize the leakage rate by adjusting the printer parameters (AL-Hasni and Santori, 2020; Wu et al., 2024). Therefore, we minimize the porosity (pore connectivity) of the printed objects. Since the number of adjustable printer parameters can easily exceed 300, here is only a brief summary of key parameters (Table 1). The complete MK3S+ configuration is available in the supplementary material (see SP1). In general, we significantly reduced the print speed, increased the temperature and extrusion rate, and lowered the cooling.

Table 1: Key parameters adjusted of the 3D printer to achieve minimal liquid leakage through the printed object.

Parameter	Value
Layer height	0.1 to 0.15 mm
Extrusion multiplier	1.1
Max print speed	15 mm s^{-1}
Printing temperature	260 °C
Wall thickness	2.5 mm
Infill	100%
Cooler speed	15 to 20%
Retraction length	disabled
Infill/perimeters overlap	20%

Airtightness of 3D printed parts

Sufficient air tightness of the mini disk infiltrometer assembly is critical for successful infiltration tests. To determine the air leakage of the material in relation to infiltration, we used a procedure similar to the Darcy falling head experiment, assuming laminar flow through the material. A simple U-shaped glass tube with a valve was used to set the pressure head; the tube was marked with a scale

in centimeters and had an inner diameter of 22.7 mm. We 3D-printed an enclosed Mariotte chamber with a wall thickness of 2.5 mm and a surface area of 103.6 cm², featuring a single opening. This opening was connected to the instrument inlet using silicon tubing. Before measurement, a pressure head of -10 cm was applied. After connecting the Mariotte chamber, the valve was opened to link it to the U-tube. Because the air leakage was very low, we set up a camera to record a time-lapse at 30-second intervals until the water level in the tube equilibrates. The change in water level was manually recorded from the time-lapse at 10-minute intervals. From these readings, the volume of leaked air was calculated, assuming no compression of the air in the tube and isothermal conditions. The mean air conductivity (K_a) was then calculated from the incremental time steps using the following expression:

$$\boldsymbol{K_{a,i} = \frac{\Delta V_i \cdot L}{A \cdot \Delta h_i \cdot \Delta t_i}} \quad (1)$$

where:

- $K_{a,i}$ is the air conductivity for a given time step (mm h^{-1}),
- ΔV_i is the change in volume between time steps (mm^3),
- L is the wall thickness (mm),
- A is the cross-sectional area of the Mariotte chamber (mm^2),
- Δh_i is the pressure head gradient for the given time step (mm),
- Δt_i is the duration of the time step (h).

Maximum air leakage was calculated using the K_a obtained, considering the worst-case scenario: a simple empty tube with a wall thickness of 2.5 mm and a surface area of 362.09 cm^2. The result was then interpreted as the minimum water infiltration rate that can still be measured using AMDI at a pressure head of -6 cm. Below this infiltration rate threshold, water infiltration would be slower than air inflow through the body of the AMDI which would lead to false measurement of K, namely, poorly defined pressure head. It is important to note that as long as air bubbles are observed during infiltration, the instrument is functioning correctly.

Water Level Change Sensing

Following the proposition by Moret et al. (2004) to measure water level changes using Time Domain Reflectometry (TDR), we adopted a similar approach but replaced the sensing technology with Time

Domain Transmission (TDT). Similarly to TDR, TDT measures the propagation speed of high-frequency electromagnetic pulses; however, it does so through transmission along a closed circuit rather than reflection of a pulse. Due to their less demanding electronic requirements, TDT sensors are significantly more cost-effective than TDR systems. To monitor changes in water level, we employ commercially available autonomous soil moisture sensors, TMS-4 'Lollipop' (TOMST sro., Czechia). Detailed sensor specifications are described by Wild et al. (2019). In the TMS logger, high-frequency shaped pulses (approximately 2.5 GHz) are transmitted through a printed circuit approximately 30 cm in length. Upon arrival of a pulse at the counting unit, another pulse is emitted, a process repeated within a 640-microsecond timeframe. These pulses are quantified as a raw moisture signal (ranging from 50 to 200 MHz). The number of pulses counted is inversely proportional to the moisture content; as the moisture increases, the number of pulses received decreases. After inversion, the counts are scaled to a numeric range of 1–4095 (raw TDT data). The recorded values typically range from 100 (ambient air) to 3500 (distilled water). The sensor includes integrated flash memory and a built-in battery for long-term operation. Configuration and data retrieval were performed using the manufacturer's Lolly Manager software (version 1.18.6.6), which supports conditional data recording mode. In this mode, measurements were taken every second, while the data were stored only when a change in the inverted raw count value of the water level was detected between two subsequent readings. The resulting data were saved in CSV format.

AMDI Calibration and Validation

To establish a relationship between the raw TMS-4 signal and the actual change in water volume within the reservoir, we conducted a calibration test for each AMDI unit. The reservoir was first filled with water and the instrument was placed on a holder attached to a precision balance. The Mariotte chamber was then removed to allow air to enter and initiate water outflow through the sintered disk. Weight loss was recorded every 5 seconds as water exited the reservoir. The balance data were later matched with the sensor data and a third-degree polynomial (i.e., cubic) regression model was derived to describe the relationship between the raw TDT signal and the change in water volume. Through trial and error, we identified two key issues: (i) the plastic-covered portion of the sensor continues to provide readings, but with a different response ratio due to its varying thickness, and (ii) as the water level approaches the temperature sensor, the signal no longer follows a monotonic decline, which may compromise measurement reliability. To address these anomalies, we calculated the optimal initial water volume so that the water level would cover only the active sensing portion of the sensor at the start of the test and reach the temperature sensor only after 90–95 ml of water had infiltrated, equivalent to the maximum volume that the Meter MDI reservoir can contain. The calibration models

used to process the infiltration data were derived from trials that account for these two issues: Each calibration trial used 150 ml of water, and readings from the temperature sensor zone were excluded. In the infiltration trials, we utilized two AMDI units to assess potential differences between them and further strengthen the reliability of our results. The calibration process produced individual calibration equations for each AMDI. Upon comparison, it became evident that the relationship between the raw signal and the change in water volume differed significantly for each AMDI (Figure 2). Therefore, it is necessary to calibrate each AMDI individually prior to measurement. To evaluate the accuracy of the cubic approximation used for calibration, we calculated the root mean square error (RMSE) and the normalized RMSE (NRMSE). For AMDI Mark 1, the RMSE was 0.77 and the NRMSE was 1.12%, while for Mark 2, the RMSE was 0.52 and the NRMSE was 0.64%, indicating a good fit to the measured data.

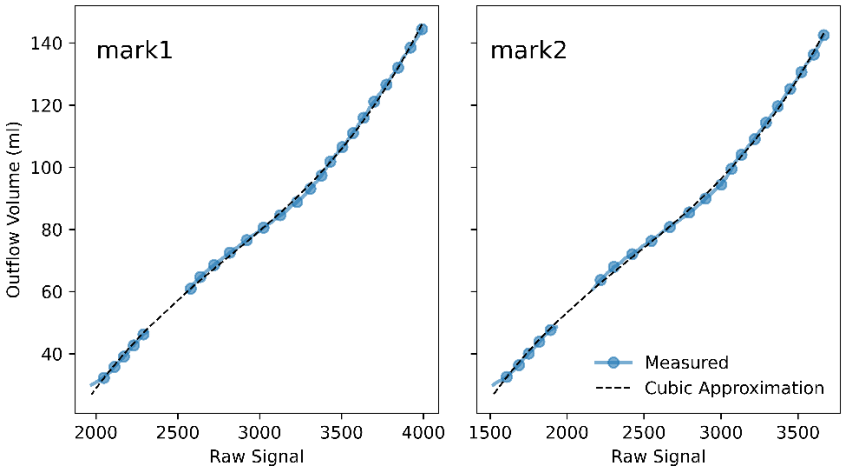

Figure 2: Cumulative outflow measured, and raw signal fitted with cubic model. The zone without data corresponds to the temperature sensor zone.

The constants and models are reported with high precision because reducing the precision could negatively impact the estimation of infiltrated volume. The calibration equation for AMDI Mark 1 is as follows:

$$y = 0.00000001394024182x^3 - 0.00011716285275x^2 + 0.37165278918x - 357.35312208 \quad (2)$$

where:

- y is the water volume (ml)
- x is the raw TDT signal (count)

And similarly, the calibration equation for AMDI Mark 2 is:

$$y = 0.000000011587655934x^3 - 0.000084056506359x^2 + 0.24301347335x - 189.13442161 \quad (3)$$

Experimental Setup

To carry out the infiltration trials, we prepared a soil box under controlled laboratory conditions. The box was first lined with a 2 cm layer of expanded clay at the bottom, followed by a permeable material sheet (geotextile), and then filled with sieved soil (<1 cm). The soil was collected from Ledce (50°12'22.4"N, 14°01'01.6"E) and is classified as Chernozem (Batjes, 2016) with a loam texture class according to the USDA classification system. The partial contents of clay (13%), silt (49%), and sand (38%) were determined using a laser diffractometer, Mastersizer 3000 (Malvern Panalytical, UK), with measurement parameters set according to (Bieganowski et al., 2018; Vrána et al., 2024). The soil was gently compacted and subjected to a wetting–drainage cycle to promote structural development. After drying, the surface crust was broken, the top few centimeters were mixed, and the surface was compacted using a pestle. This procedure was designed to replicate field conditions, minimize variability within the box, and ensure proper contact between the soil surface and the infiltrometer (Bagarello et al., 2022).

In total, we conducted 27 infiltration trials using three instruments: two AMDI units (referred to as Auto1 and Auto2) and one Meter MDI. The trials were carried out at three pressure heads (h_0 = -6 cm, -3 cm and -1 cm), with three replicates for each combination (3 instruments × 3 pressure heads × 3 replicates = 27 trials). The experiments were conducted between February and March under controlled laboratory conditions. Before each trial, a thin layer of air-dried, sieved soil (<2 mm) was applied directly to the surface at the trial location. This layer was then spread and gently compacted to ensure optimal contact between the infiltration disk and the soil surface. To avoid any interaction between wet zones of adjacent tests, each test cycle was limited to six infiltration trials. After each cycle, the upper soil layer was homogenized, reconsolidated, and allowed to dry for 48 to 72 hours to ensure uniform initial conditions across all experiments. For the Meter MDI, an operator manually recorded infiltration data at regular intervals, whereas the AMDI units used TMS-4 sensors to

autonomously record signal changes within the reservoir. These signals were subsequently converted to water volumes using the calibration equations described earlier (Eq. 2 and Eq. 3).

Moreover, although the disk should theoretically not affect infiltration as long as water continuity is maintained for the set pressure heads and its hydraulic conductivity is significantly higher than that of the soil being measured, we also determined the hydraulic conductivity of the disk to ensure the rigor of the study. This aspect had not been previously addressed in the study by Klípa et al. (2015). To measure the saturated hydraulic conductivity of the sintered disk, we employed a variation of the falling head experiment described earlier (Section 2.3). Since the Meter disk and CTU disk have identical dimensions, we used the Meter MDI body to conduct infiltration into a free water level. The MDI was positioned so that its outflow was directed into a metal cylinder with a sharp edge, which was filled with water to maintain continuous contact between the sintered disk and the water surface. The MDI was filled with 90 ml of water, and an empty Mariotte chamber was attached. The suction tube was sealed with a finger to prevent water flow. When the finger was released, the infiltration trial began. This procedure was repeated three times for each type of disk. The saturated hydraulic conductivity for each trial was then calculated using the following equation:

$$\boldsymbol{K_{s,i} = \frac{Q_i L}{A \Delta h_i}} \tag{4}$$

where:

- $K_{s,i}$ is the saturated hydraulic conductivity for given time step (mm h^{-1})
- Q_i is the outflow forms the MDI (mm^3 h^{-1})
- L is the wall thickness (mm)
- A is the cross-sectional area of the Mariotte chamber (mm^2)
- Δh_i is the pressure head gradient for the given time step (mm).

Following the determination of each disk's saturated hydraulic conductivity (K_s), additional trials were conducted using only the Meter mini disk infiltrometer (MDI) to further investigate the influence of the disk on the infiltration process. A total of six trials were performed, three at an initial pressure head (h_0) of -3 cm and three at h_0 of -1 cm. These trials were carried out on a soil different from that used in the infiltration measurements described above. The soil was collected from another agricultural site in Nucice (Li et al., 2023; Zumr et al., 2019) and is classified as Cambisol (Batjes, 2016), with a silty loam texture class according to the USDA classification system. The soil

composition included 3% clay, 61% silt, and 36% sand. Sample preparation and infiltration trials were carried out as previously described.

Scanning Electron Microscopy of Parts

To inspect the morphology of the 3D-printed parts and sintered disk, we used a Phenom XL scanning electron microscope (SEM) (Thermo Fisher Scientific, United States). Since the analysis required small samples, we specifically designed and printed three types of samples; a cube with a hollow middle part, a wall, and a closing top layer; using the settings given in Section 2.2. Prior to analysis, the samples were dried at 40 °C for 48 hours, which should not alter the properties of PET-G. Then they were mounted on 12.5 mm diameter pin stubs using carbon adhesive tape. Loose particles were gently removed with compressed air, and the specimens were coated with a thin conductive metal layer (Pd:Au = 80:20) using a SC7620 sputter coater (Quorum). SEM imaging was performed under high vacuum conditions (1 Pa) a secondary electron detector (SED) at 5 kV.

Data Analysis

To estimate the unsaturated hydraulic conductivity, $K(h)$, we used model proposed by Zhang (1997) which was later modified by Dohnal et al. (2010) and as described in METER Group Mini Disk manual adapting their macro and van Genuchten parameters (Meter Group, 2021). To analyze the differences between the Zhang model and the measured data, we used the Root Mean Square Error (RMSE) and normalized RMSE (NRMSE). After calculating the K values, we divided the data into three groups based on pressure heads (-1, -3, and -6 cm) and instrument type (AMDI Mark 1, Mark 2, and Meter MDI). Each group was tested for normality at confidence level of 0.05 using the Shapiro-Wilk test, which is suitable for small datasets (Shapiro and Wilk, 1965). Since all groups yielded p-values greater than 0.05 we applied a one-way analysis of variance (ANOVA) to assess the significance of differences. If the ANOVA produced a p-value less than 0.05, a Tukey post-hoc test was performed to identify the source of the significant difference. All statistical tests were performed using the SciPy library for Python (Virtanen et al., 2020).

Results

Properties of 3D printed parts

Air leakage due to imperfections in 3D printed parts was determined in three repetitions; the water levels inside the glass tube equilibrated on average after three hours at a pressure head of -10 cm, as

described in Section 2.3. We successfully measured the air conductivity (K_a) of the 3D-printed parts, which, for the modified version of the Mariotte chamber, yielded $8.0 \cdot 10^{-4} \pm 2 \cdot 10^{-4}$ mm h^{-1}. Using this K_a value, we estimate the minimum infiltration rate measurable for pressure head between -0.5 and -6 cm (see Appendix A). For h_0 = -6 cm, and considering that the AMDI is almost empty, the minimum measurable infiltration rate is 0.42 ± 0.11 mm h^{-1}. Given the assumptions used in the estimation method, the minimal measurable infiltration rate can be considered conservative. To closely inspect imperfections in 3D prints that can cause air leakage, we used SEM imaging (Figure 3). It should be noted that the images show an intentionally selected location on the surface prone to imperfections to trace the sources of air leakage. Using the XYZ coordinates, where Z is the vertical axis in Figure 3a and b a corner in the XY plane depicts the adhesion in two cases: good corner adhesion (Figure 3a) and poor adhesion (Figure 3b). The corner gap in Figure 3b may indicate a potential source of air leakage. Figure 3c and d depict the top layer infill in the XY plane. Both images reveal prevalent over-extrusion due to the printer settings. Finally, Figure 3e and Figure 3f show vertical wall layer adhesion in the XZ plane. Figure 3e demonstrates good adhesion and layer overflow from over extrusion, while Figure 3f reveals slightly reduced vertical adhesion, with visible isolated openings between layers. These gaps are not interconnected and are therefore considered isolated pores. The white artifacts circled in red in all images are air bubbles trapped within the material structure formed during printing, which are also not interconnected. Air leakage due to the imperfection in the 3D printed parts was determined in 3 repetitions; the water levels equilibrated on average after 3 hours.

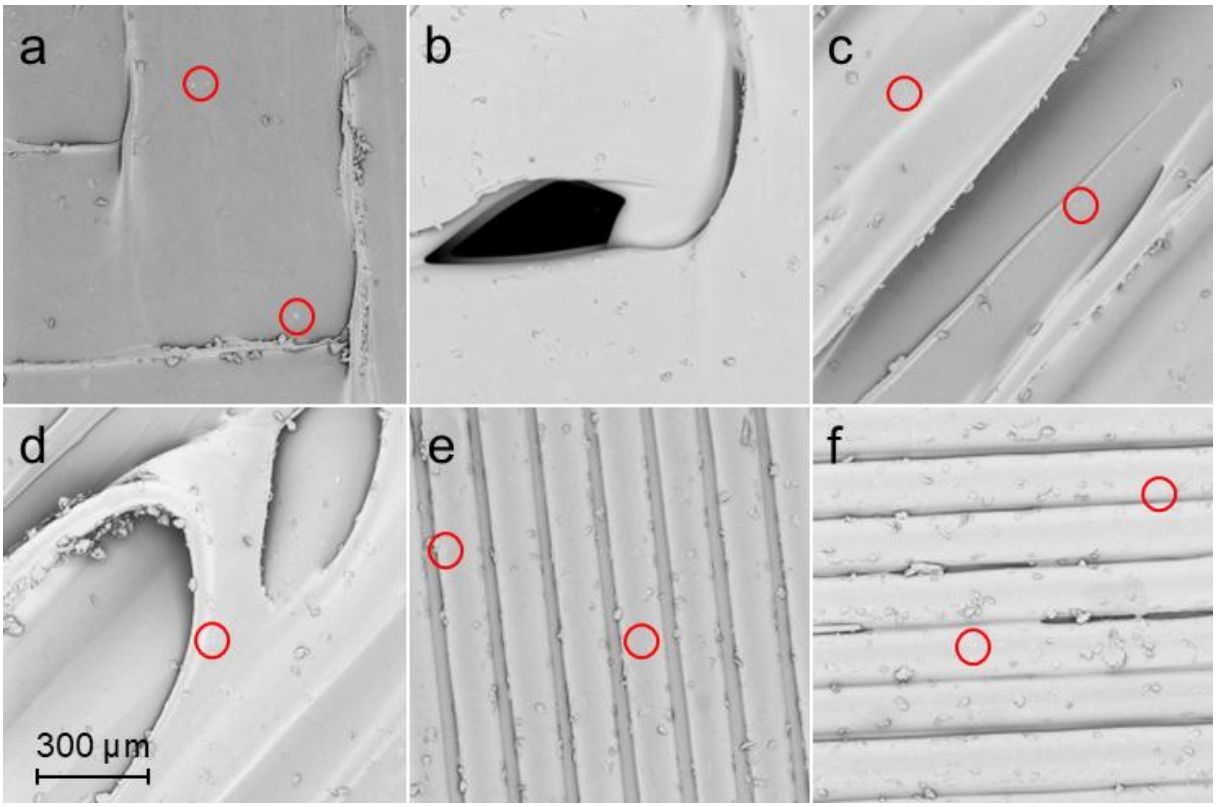

Figure 3: SEM images obtained using a BSD sensor at 250x magnification, illustrating key 3D printing features and defects related to adhesion and extrusion quality. (a) Corner perimeters with good adhesion. (b) Corner perimeters with poor adhesion, indicating a possible source of leakage. (c) Infill of the top layer exhibiting overextrusion. (d) Artifact resulting from the infill of the top layer on the extrusion. (e) Vertical wall layer showing good adhesion to overflow due to overextrusion. (f) Vertical layer of the wall showing slightly reduced adhesion, with visible openings between layers. The coarse particles observed in the images are predominantly dust.

Infiltration Curves

In total, we conducted 27 soil infiltration trials. Cumulative infiltration was calculated according to Eq. 2 and Eq. 3 for each AMDI. The resulting infiltration curves obtained from the automatic instruments generally exhibited a well-defined shape, comparable to those recorded with the METER MDI (Figure 4). The minor noise observed in the AMDI data may be attributed to occasional reading inaccuracies or to limitations in the approximation of the calibration equations. The slight deviation of AMDI compared to MDI at a pressure head of -3 cm (Figure 6B) and the greater deviation at a pressure head of -1 cm (Figure 6C) are likely due to differences in the porous disk.

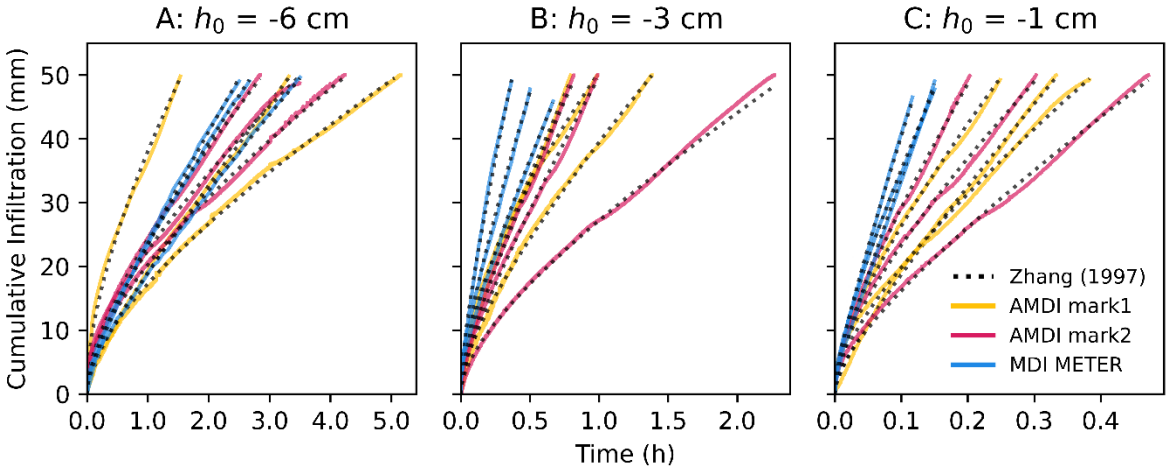

Figure 4: Cumulative infiltration curves for Soil Ledce under three pressure head conditions: (A) -6 cm, (B) -3 cm, and (C) -1 cm. The curves show the difference between infiltrometer types: AMDI Mark 1 (yellow), AMDI Mark 2 (magenta) and Meter MDI (blue) with the fitted infiltration data from the Zhang (1997) model (dotted lines).

The application of the Zhang model to the infiltration curves revealed similar fit performance for both AMDI and the METER infiltrometer with low (< 4%) and nearly identical NRMSE values between the two devices (Appendix B). The resulting fitted curves were similar in shape and trend, showing no substantial differences between the two measurement systems. Using the Zhang model and measured infiltration curves, we calculated hydraulic conductivity (K) for all trials (Table 2). Each device was treated separately to determine whether the two AMDI results were comparable. The *K* values were grouped according to the pressure head levels of h_0 = - 6, -3 and -1 cm, and ANOVA was used to assess the differences. For the pressure head h_0 = -6 cm, ANOVA yielded p = 0.096, indicating that there were no significant differences between the groups, with the F statistic = 3.56. Similarly, for the pressure head h_0 = -3 cm, p = 0.1 with the F statistic = 3.46, again indicating that there is no significant difference. However, for the pressure head h_0 = -1 cm, p = 0.005 with F-statistic = 14.26. Given the significant difference observed, the post hoc Tukey HSD test was used to further investigate the group differences. The Tukey HSD test revealed that AMDI Mark 1 and AMDI Mark 2 did not show significant differences, with p = 1.0. On the other hand, Mark 1 and Mark 2 exhibited a significant difference compared to the MDI of the Meter, with p = 0.009 in both cases.

Table 2: Hydraulic conductivity (K) obtained for all measurements.

h_0 (cm)	K (mm h^{-1})		
	AMDI mark1	AMDI mark2	MDI Meter
-6	1.12	0.81	0.94
-6	0.91	0.41	1.18
-6	0.42	0.54	1.47
-3	2.51	4.49	7.45
-3	1.92	1.39	10.37
-3	5.41	5.50	5.16
-1	17.97	9.66	45.01
-1	15.30	21.77	29.98
-1	9.92	11.70	46.93

Influence of the Sintered Stainless-Steel Disk on Infiltration

In contrast to the previous section, where both the AMDI and MDI meters were used, only the MDI meter was used to conduct the experimental runs in this section. The saturated hydraulic conductivity revealed significant differences between the Meter and CTU disks at lower pressure heads. Measurements were performed in triplicate for each disk (Figure 5C) as described in Section 2.6. The Meter disk produced a K_s of 540.9 ± 101.1 mm h^{-1}, which is, on average, 50% higher than the K_s measured with the CTU disk (275.2 ± 200.3 mm h^{-1}). This difference also results from soil infiltration measurements, especially at the lower pressure head (Figures 4a and b). Furthermore, it can be observed that the higher standard deviation of the CTU disk also propagates to infiltration measurements on the soil. Since the nominal pore size of the Meter disk is not disclosed, we utilized SEM imaging (Figure 6) to further investigate the difference between the Meter and CTU disks, which clearly shows that the Meter disk has larger pores (300 microns).

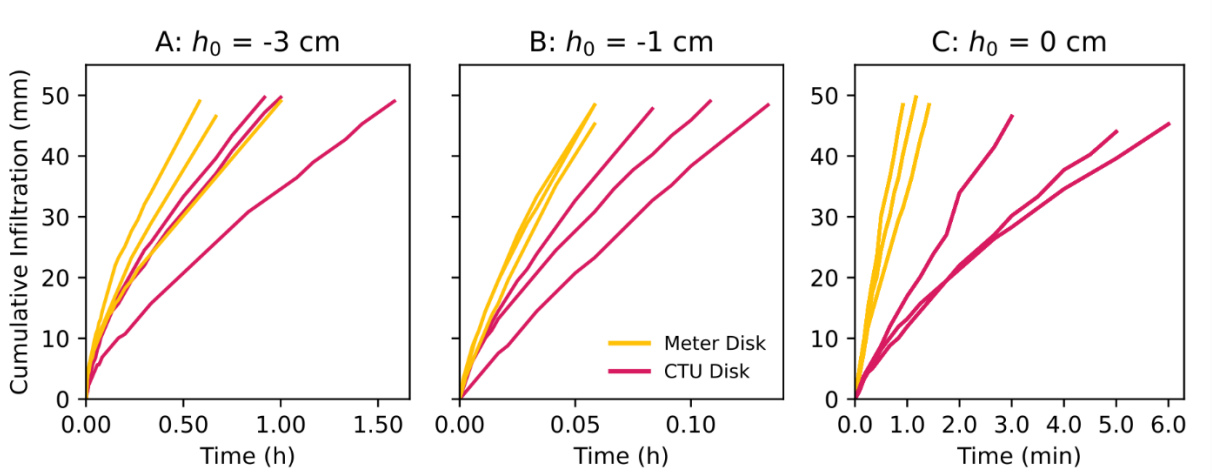

Figure 5: Cumulative infiltration curves comparing meters and CTU disks at two pressure head levels: (A) -3 cm, (B) -1 cm and outflow (C) 0 cm (free water level).

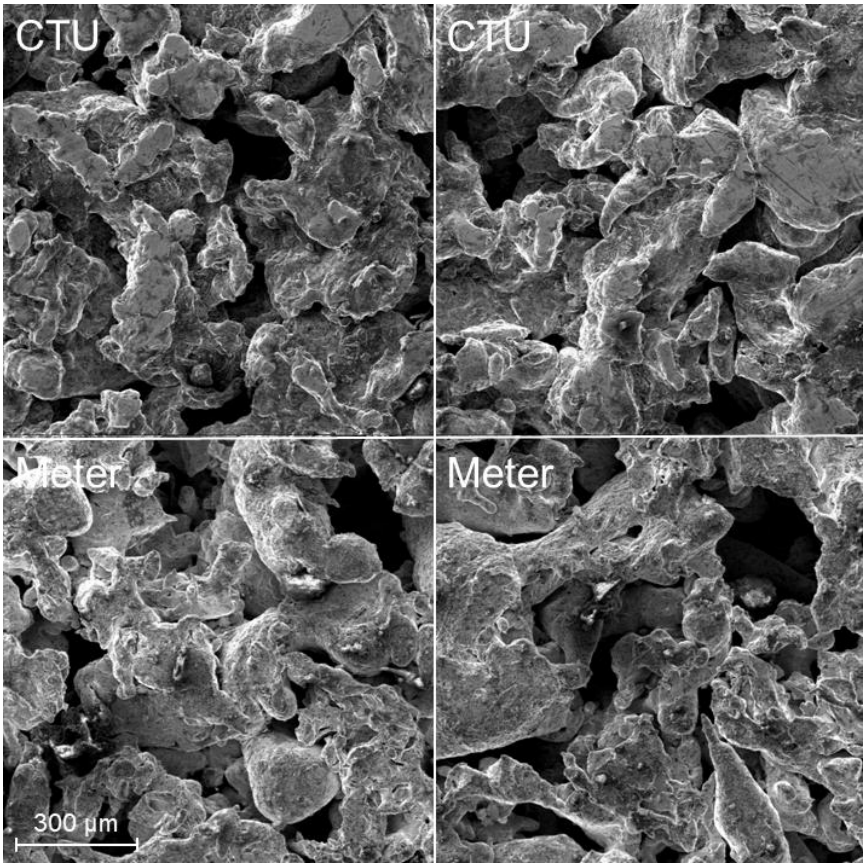

Figure 6: SEM images captured at 250× magnification using a BSD sensor, comparing the pore morphology of sintered stainless-steel disks from Meter (bottom row) and CTU (top row).

Discussion

Considering the shape of the infiltration curves, we can confirm that the AMDI operates effectively and produces reproducible and reliable results, accurately representing the infiltration process under laboratory conditions. Both AMDI mark 1 and mark 2 exhibited a good fit to the Zhang (1997) model, with NRMSE values below 4%, comparable to Meter MDI (NRMSE < 4%). As no significant differences in the majority of hydraulic conductivities (K) were found between the two AMDI versions, it can be inferred that the instruments perform similarly, supporting the reproducibility of the AMDI design. The only significant differences ($p < 0.05$) in K between AMDI and Meter MDI were observed at a pressure head level of h_0 = -1 cm. However, if these discrepancies had resulted from the nonuniformity of the pressure heads within the porous disk or from poor contact between the soil and the porous disk, the measurement deviations would be expected to increase with higher pressure head levels. Because this trend was not observed, we attributed the differences to the intrinsic properties of the sintered porous disk.

The CTU disk used in the AMDI features a denser and more compact morphology, whereas the observed differences are more likely attributed to the characteristics of the Meter disk, which has visibly smaller and less interconnected pore structures. This contrast in porosity appears to influence the infiltration. The 50% higher K_s average for the Meter disk compared to the CTU disk, along with consistent infiltration measurements using the Meter MDI with both disk types, demonstrates that while the infiltration rate of the CTU disk remains significantly higher than that of the in soil, it still affects the infiltration process enough to cause significant differences in the results. This opens the general question of the influence of the properties of porous disks on the infiltration and the resulting K. In the future, the differences in the sintered disks might be added to the Zhang (1997) model using the numerical approach, similar to Dohnal et al. (2010), who however neglected any effect of the disk. Previous studies have focused on the effect of contact between the disk and the soil on the diameter of the disk, but we are not aware of a study dealing with the hydraulic conductivity of the porous disk itself. Although the observed differences between AMDI and Meter MDI at low pressure heads are most likely caused by the characteristics of the porous disks, a detailed investigation of the hydraulic properties of the disks under varying conditions is beyond the scope of this study. A dedicated follow-up study would be necessary to quantify and model these effects across different disk types. Given the constraints of the porous disk, determining its air-entry value is the most reliable way to assess its suitability for lower pressure heads before adjusting the pressure head range beyond -6 cm.

Our 3D-printed AMDI offers an open design, cost-effective, and accessible approach to automating mini disk infiltrometers (MDIs) compared to commercially available models. Unlike the infiltrometer developed by Madsen and Chandler (2007) which primarily utilizes differential pressure transducers and various head control methods such as capillary tubes or bubbling chambers, our design integrates a low-cost autonomous TDT sensor and relies on visual adjustment of the water level within a transparent PET-G Mariotte chamber to set the pressure head. Other automated infiltrometers, such as the tension infiltrometer by Morales-Ortega et al. (2023), use distance sensors with an Arduino-based SCADA system, or the disc infiltrometer by Moret-Fernández et al. (2012), which employs micro flowmeters and solenoid valves. These systems require precise manufacturing, in some cases use costly sensors, and require connection to external units to operate and log data. Our AMDI distinguishes itself through the extensive use of FDM 3D printing for most of its components. This manufacturing method, also used by Morales-Ortega et al. (2023), allows low-cost fabrication and easy customization. However, it presents challenges such as achieving sufficient airtightness and optical clarity due to the layered structure of FDM prints, as discussed by Klípa et al. (2015).

The air leakage rate (K_a) through the body of the AMDI was determined using a modified version of the Darcy falling head experiment, assuming incompressible and isothermal conditions. In terms of volume, the amount of leakage through the material for pressure head at -6 cm after 6 hours would be 4 ml, which is negligible (Appendix A). Given the assumptions used in the estimation, this minimal infiltration rate can be considered fairly conservative. However, it is important to note that as long as air bubbles are observed in the reservoir during infiltration, the AMDI is clearly maintaining a pre-set pressure head. For example, AL-Hasni and Santori (2020) reported for vacuum of 8.2 kPa and 24h duration leakage rate 2.36 10^{-6} Pa m^3 s^{-1} for resin infused FDM prints, which according to their classification was categorized as leaky, however, the AMDI operates under only slight underpressure in relation to atmospheric pressure.

Since we utilized established, low-cost, yet reliable TDT sensor (price level as of 2025 approx. 100€), custom made stainless steel sintered disk (various price levels dependent on scale of the order, approx. 100€ as of 2025) and FDM 3D printing utilizing commercially available 3D printers and widely available PET-G filament (8€), simple sealants and glue (10€) we were able to lower the material cost of the device significantly to 218€ without tax, excluding the cost of 3D printer itself. In comparison, the commercially available manual MDI is sold for a multiple of this price. The open-design, low-cost and simplicity of the device may stimulate the scientific community in further development of

the device as well as its use in citizen science projects. Addressing the primary purpose of the AMDI, which is to measure the unsaturated hydraulic conductivity *K(h)*, the device retains all the advantages of manual MDI while significantly expanding its application potential. Given its low cost, the AMDI enables the use of multiple units to measure *K(h)*. For instance, because the AMDI only requires attention during setup, a single operator can manage multiple infiltration trials simultaneously. This greatly reduces data collection costs while enhancing data quality. Additionally, multiple devices can be arranged in a spatial pattern to assess the spatiotemporal variability of *K(h)*, a task that is typically labor-intensive and costly (e.g. study by (Gadi et al., 2017).

In general, disregarding the automation, the main difference between the AMDI and the Meter MDI lies in the body material and manufacturing process, which significantly influence the instruments' properties, for summary refer to Table 3. In terms of size, the AMDI has a wider and shorter body with a lower center of gravity compared to the Meter MDI, making it more stable in windy conditions. However, it is also twice as heavy, which contributes to its stability but slightly reduces its portability when carrying large number of units. AMDI has 60% higher water volume for infiltration, which may be advantageous under certain conditions that require prolonged infiltration. However, AMDI offers a slightly narrower pressure head range, up to -6 cm (potentially extendable with careful modifications), whereas the Meter MDI supports up to -7 cm. The disk dimensions, and thus the contact area, are similar for both devices, and the porous disk can be replaced based on desired properties. The material used for the AMDI (PET-G) imposes limitations for applications such as water repellency assessment, for which polycarbonate is more suitable. While FDM-printed components are typically porous, we successfully adapted the printing method to achieve an almost watertight design and limited air leakage sufficiently to maintain the device in an operable state.

Table 3: General overview of AMDI and Meter MDI materials and features.

Feature	AMDI	Meter MDI
Body height (cm)	22.5	31.8
Maximum height (cm)	29.5	39.8
Body diameter (cm)	5.0	3.1
Weight (empty) (g)	325	150
Water capacity (ml)	150	90
Pressure head range (cm)	–0.5 to -6	–0.5 to –7
Pressure head offset (cm)	–0.9	Variable with tube insertion (usually –2.0)
Disk diameter (cm)	4.5	4.5
Disk thickness (cm)	0.3	0.3
Infiltration water readings	Automatic TDT	Manual visual
Body Material	PET-G	Polycarbonate
Suction tube material	PET-G	Stainless steel
Average disk pore size (µm)	80	not specified by manufacturer, estimated 300
Watertightness	Nearly full	Full
Airtightness	Limited	Nearly full

Although field validation was beyond the scope of this study, the laboratory conditions were carefully designed to simulate field-relevant scenarios (e.g., loam texture, wetting–drying cycles, compaction), making the results applicable for preliminary field research and educational purposes. Future studies should evaluate field performance under diverse conditions. Another disadvantage of AMDI is that it is not suitable for measuring soil water repellency, as such measurements typically involve the use of 95% ethyl alcohol (Lichner et al., 2007). Exposure to ethyl alcohol would cause brittleness in the AMDI due to the use of PET-G (Told et al., 2022). This issue might be mitigated by replacing PET-G with polycarbonate; however, such a modification requires comprehensive testing to ensure that all requirements are met.

Conclusions

This study aimed to develop an Autonomous Mini Disk Infiltrometer (AMDI). We successfully utilized commercially available FDM 3D printers and low-cost TDT sensors, along with a custom sintered stainless-steel disk, to manufacture a low-cost AMDI (218 €). In most cases, the AMDI produced results that were not significantly different from those obtained using the traditional manual Meter MDI, although the characteristics of the porous disk may have negatively influenced the comparison. This makes the AMDI a functional, cost-effective, and convenient alternative to traditional MDI. By integrating 3D printing for manufacturing and TDT sensing for infiltration measurement, the AMDI offers potential advantages over traditional MDI in terms of application flexibility and enhanced adaptability. Although comparable AMDIs have been tested under field conditions, our 3D-printed AMDI demonstrated reproducible and reliable performance in laboratory settings, comparable to the manual Meter MDI. We were unable to achieve a fully airtight 3D print using FDM technology alone, although the leakage rate was sufficiently limited to allow an accurate AMDI function. The proposed procedure effectively minimized air leakage to a level that did not compromise measurement accuracy, and this was achieved without any additional post-treatment. We would like to emphasize that the use of the AMDI in the field should be preceded by proper validation under controlled laboratory conditions. The differences observed at lower pressure head levels may be attributed to the characteristics of the porous disk.

Unexpectedly, the preliminary evaluation of the sintered porous disk in our study led to the conclusion that, although its hydraulic conductivity is significantly higher than that of the soil, the disk can still negatively influence infiltration measurements. Based on our findings, we propose a dedicated study

comparing different disk types using a manual MDI, with the potential to incorporate disk characteristics into the Zhang (1997) model.

Data availability

3D Printing details – refer to SP1 (SupplementaryMaterial_SP1_MK3Splus_settings.ini) which contains full details of 3D printer settings or refer to GitHub repository (Kubát and Sněhota, 2025).

Acknowledgement

We thank Oscar Petterson from Linköping University for designing the early test version of the 3D model of the printed minidisk infiltrometer during his bachelor project at Czech Technical University in Prague. We express our gratitude to Tomas Haase from TOMST s.r.o. for his support in the development of TMS sensors, which facilitated their application in minidisk infiltrometer research. We would also like to express our gratitude to the two anonymous reviewers whose comments led to an improved contribution.

This study was supported by the Grant Agency of the Czech Technical University in Prague, Grant Nos. SGS23/155/OHK1/3T/11 and SGS23/154/OHK1/3T/11. This work was also part of a project funded by the Czech Science Foundation under Grant No. 22-25673S.

Appendix

Appendix A: Minimal measurable hydraulic conductivity (K_{min}) for each pressure head setting of AMDI and estimated volume of air leakage (V_a) over trial duration.

h_0 (cm)	K_{min} (mm h^{-1})	Hours (h) and V_a (ml)						
		1	2	3	4	5	6	24
-0.5	0.04	0.06	0.11	0.17	0.22	0.28	0.34	1.35
-1	0.07	0.11	0.22	0.34	0.45	0.56	0.67	2.69
-1.5	0.11	0.17	0.34	0.51	0.67	0.84	1.01	4.04
-2	0.14	0.22	0.45	0.67	0.90	1.12	1.35	5.39
-2.5	0.18	0.28	0.56	0.84	1.12	1.40	1.68	6.73
-3	0.21	0.34	0.67	1.01	1.35	1.68	2.02	8.08
-3.5	0.25	0.39	0.79	1.18	1.57	1.96	2.36	9.43
-4	0.28	0.45	0.90	1.35	1.80	2.24	2.69	10.78
-4.5	0.32	0.51	1.01	1.52	2.02	2.53	3.03	12.12
-5	0.35	0.56	1.12	1.68	2.24	2.81	3.37	13.47
-5.5	0.39	0.62	1.23	1.85	2.47	3.09	3.70	14.82
-6	0.42	0.67	1.35	2.02	2.69	3.37	4.04	16.16

Appendix B: RMSE and NRMSE for measured infiltration and Zhang model.

h_0 (cm)	AMDI mark1		AMDI mark2		MDI METER	
	RMSE (mm)	NRMSE (%)	RMSE (mm)	NRMSE (%)	RMSE (mm)	NRMSE (%)
-6	0.55	2.01	0.53	1.82	0.46	2.86
-6	1.20	3.9	0.58	1.88	0.28	1.2
-6	0.50	1.68	0.85	2.76	0.57	2.67
-3	0.72	2.51	0.57	1.84	0.47	1.72
-3	0.77	2.79	0.80	2.77	0.65	2.34
-3	0.66	3.81	0.63	3.53	0.52	2.92
-1	0.62	2.23	0.68	2.34	0.92	3.17
-1	0.75	2.62	0.6	2.03	0.84	2.88
-1	0.47	2.93	0.31	1.73	0.35	2.13

References

Alagna, V., Bagarello, V., Di Prima, S., Giordano, G., Iovino, M., 2013. A simple field method to measure the hydrodynamic properties of soil surface crust. Journal of Agricultural Engineering 44. https://doi.org/10.4081/jae.2013.s2.e14

AL-Hasni, S., Santori, G., 2020. 3D printing of vacuum and pressure tight polymer vessels for thermally driven chillers and heat pumps. Vacuum 171. https://doi.org/10.1016/j.vacuum.2019.109017

Angulo-Jaramillo, R., Vandervaere, J.-P., Âphanie Roulier, S., Thony, J.-L., Gaudet, J.-P., Vauclin, M., 2000. Field measurement of soil surface hydraulic properties by disc and ring in®ltrometers A review and recent developments. Soil Tillage Res 55.

Ankeny, M.D., Ahmed, M., Kaspar, T.C., Horton, R., 1991. Simple Field Method For Determining Unsaturated Hydraulic Conductivity. Soil Science Society of America Journal 55, 467–470.

Ankeny, M.D., Kaspar, T.C., Horton, R., 1988. Design for an Automated Tension Infiltrometer. Soil Science Society of America Journal 52, 893–896. https://doi.org/10.2136/sssaj1988.03615995005200030054x

Autovino, D., Bagarello, V., Caltabellotta, G., Varadi, F.K., Zanna, F., 2024. One-dimensional infiltration in a layered soil measured in the laboratory with the mini-disk infiltrometer. Journal of Hydrology and Hydromechanics 72, 149–157. https://doi.org/10.2478/johh-2024-0001

Bagarello, V., Caltabellotta, G., Iovino, M., 2022. Manual packing and soil reuse effects on determination of saturated hydraulic conductivity of a loam soil. Geoderma 405. https://doi.org/10.1016/j.geoderma.2021.115465

Batjes, N.H., 2016. Harmonized soil property values for broad-scale modelling (WISE30sec) with estimates of global soil carbon stocks. Geoderma 269, 61–68. https://doi.org/10.1016/j.geoderma.2016.01.034

Bieganowski, A., Ryżak, M., Sochan, A., Barna, G., Hernádi, H., Beczek, M., Polakowski, C., Makó, A., 2018. Laser Diffractometry in the Measurements of Soil and Sediment Particle Size Distribution. Advances in Agronomy 151, 215–279. https://doi.org/10.1016/bs.agron.2018.04.003

Brooks, R.H., Corey, A.T., 1964. Hydraulic Properties of Porous Media.

Burdine, N.T., 1953. Relative permeability calculations from pore size distribution data.

Chohan, J.S., Singh, R., Boparai, K.S., Penna, R., Fraternali, F., 2017. Dimensional accuracy analysis of coupled fused deposition modeling and vapour smoothing operations for biomedical applications. Compos B Eng 117, 138–149. https://doi.org/10.1016/j.compositesb.2017.02.045

Darcy, H., 1856. Fontaines publiques de la ville de Dijon.

Deb, S.K., Shukla, M.K., 2012. Variability of hydraulic conductivity due to multiple factors. Am J Environ Sci 8, 489–502. https://doi.org/10.3844/ajessp.2012.489.502

Di Prima, S., 2015. Automated single ring infiltrometer with a low-cost microcontroller circuit. Comput Electron Agric 118, 390–395. https://doi.org/10.1016/j.compag.2015.09.022

Dohnal, M., Dusek, J., Vogel, T., 2010. Improving Hydraulic Conductivity Estimates from Minidisk Infiltrometer Measurements for Soils with Wide Pore-Size Distributions. Soil Science Society of America Journal 74, 804–811. https://doi.org/10.2136/sssaj2009.0099

Elkateb, T., Chalaturnyk, R., Robertson, P.K., 2003. An overview of soil heterogeneity: Quantification and implications on geotechnical field problems. Canadian Geotechnical Journal 40, 1–15. https://doi.org/10.1139/t02-090

Fodor, N., Sándor, R., Orfanus, T., Lichner, L., Rajkai, K., 2011. Evaluation method dependency of measured saturated hydraulic conductivity. Geoderma 165, 60–68. https://doi.org/10.1016/j.geoderma.2011.07.004

Gadi, V.K., Tang, Y.R., Das, A., Monga, C., Garg, A., Berretta, C., Sahoo, L., 2017. Spatial and temporal variation of hydraulic conductivity and vegetation growth in green infrastructures using

infiltrometer and visual technique. Catena (Amst) 155, 20–29. https://doi.org/10.1016/j.catena.2017.02.024

Ghosh, B., Pekkat, S., 2019. A critical evaluation of the variability induced by different mathematical equations on hydraulic conductivity determination using disc infiltrometer. Acta Geophysica 67, 863–877. https://doi.org/10.1007/s11600-019-00266-6

Gibson, I., Rosen, D., Stucker, B., 2015. Directed Energy Deposition Processes, in: Additive Manufacturing Technologies. Springer New York, pp. 245–268. https://doi.org/10.1007/978-1-4939-2113-3_10

Gonzalez-Sosa, E., Braud, I., Dehotin, J., Lassabatère, L., Angulo-Jaramillo, R., Lagouy, M., Branger, F., Jacqueminet, C., Kermadi, S., Michel, K., 2010. Impact of land use on the hydraulic properties of the topsoil in a small French catchment. Hydrol Process 24, 2382–2399. https://doi.org/10.1002/hyp.7640

Green, T.R., Ahuja, L.R., Benjamin, J.G., 2003. Advances and challenges in predicting agricultural management effects on soil hydraulic properties. Geoderma 116, 3–27. https://doi.org/10.1016/S0016-7061(03)00091-0

Green, W.H., Ampt, G.A., 1911. Studies on soil physics, 1: The flow of air and water through soils. Journal of Agricultural Science 4, 1–24.

Hallett, P.D., Gordon, D.C., 2014. An automated microinfiltrometer to measure small-scale soil water infiltration properties. Journal of Hydrology and Hydromechanics 62, 252–256. https://doi.org/10.2478/johh-2014-0023

Jara, V., Arellano, E., Baker, J., 2012. Using An Automatic Camera Attached to Minidisk Infiltrometer to Improve Measurement in Disturbed Soils.

Jarvis, N.J., Leeds-Harrison, P.B., Dosser, J.M., 1987. The use of tension infiltrometers to assess routes and rates of infiltration in a clay soil, Journal of Soil Science.

Klípa, V., Sněhota, M., Dohnal, M., 2015. New automatic minidisk infiltrometer: Design and testing. Journal of Hydrology and Hydromechanics 63, 110–116. https://doi.org/10.1515/johh-2015-0023

Klöffel, T., Larsbo, M., Jarvis, N., Barron, J., 2024. Freeze-thaw effects on pore space and hydraulic properties of compacted soil and potential consequences with climate change. Soil Tillage Res 239. https://doi.org/10.1016/j.still.2024.106041

Kool, D., Tong, B., Tian, Z., Heitman, J.L., Sauer, T.J., Horton, R., 2019. Soil water retention and hydraulic conductivity dynamics following tillage. Soil Tillage Res 193, 95–100. https://doi.org/10.1016/j.still.2019.05.020

Kubát, J.-F., Sněhota, M., 2025. Autonomous 3D Printed Mini Disk Infiltrometer for Soil Hydraulic Conductivity Determination (https://github.com/kubatjanf/AMDI).

Kubát, J.F., Strouhal, L., Kavka, P., 2024. Estimation of Infiltration Parameters: The Role of Pedotransfer Functions and Initial Moisture Conditions. J Hydrol (Amst) 633. https://doi.org/10.1016/j.jhydrol.2024.130954

Latorre, B., Moret-Fernández, D., Lyons, M.N., Palacio, S., 2021. Smartphone-based tension disc infiltrometer for soil hydraulic characterisation. J Hydrol (Amst) 600. https://doi.org/10.1016/j.jhydrol.2021.126551

Leite, M., Varanda, A., Ribeiro, A.R., Silva, A., Vaz, M.F., 2018. Mechanical properties and water absorption of surface modified ABS 3D printed by fused deposition modelling. Rapid Prototyp J 24, 195–203. https://doi.org/10.1108/RPJ-04-2016-0057

Leuther, F., Schlüter, S., 2021. Impact of freeze-thaw cycles on soil structure and soil hydraulic properties. SOIL 7, 179–191. https://doi.org/10.5194/soil-7-179-2021

Li, T., Schiavo, M., Zumr, D., 2023. Seasonal variations of vegetative indices and their correlation with evapotranspiration and soil water storage in a small agricultural catchment. Soil and Water Research 18, 246–268. https://doi.org/10.17221/60/2023-SWR

Madsen, M.D., Chandler, D.G., 2007. Automation and Use of Mini Disk Infiltrometers. Soil Science Society of America Journal 71, 1469–1472. https://doi.org/10.2136/sssaj2007.0009n

Mein, R.G., Assistant, R., Larson, C.L., School, G., 1971. Modeling the Infiltration Component of the Rainfall-Runoff Process.

Melchels, F.P.W., Feijen, J., Grijpma, D.W., 2010. A review on stereolithography and its applications in biomedical engineering. Biomaterials. https://doi.org/10.1016/j.biomaterials.2010.04.050

Meter Group, Inc.U., 2021. Mini Disk Infiltrometer Manual 14560–11.

Meurer, K., Barron, J., Chenu, C., Coucheney, E., Fielding, M., Hallett, P., Herrmann, A.M., Keller, T., Koestel, J., Larsbo, M., Lewan, E., Or, D., Parsons, D., Parvin, N., Taylor, A., Vereecken, H., Jarvis, N., 2020. A framework for modelling soil structure dynamics induced by biological activity. Glob Chang Biol. https://doi.org/10.1111/gcb.15289

Mitchell, A., Lafont, U., Hołyńska, M., Semprimoschnig, C., 2018. Additive manufacturing — A review of 4D printing and future applications. Addit Manuf. https://doi.org/10.1016/j.addma.2018.10.038

Mohamed, O.A., Masood, S.H., Bhowmik, J.L., 2015. Optimization of fused deposition modeling process parameters: a review of current research and future prospects. Adv Manuf 3, 42–53. https://doi.org/10.1007/s40436-014-0097-7

Morales-Ortega, D.A., Cambrón-Sandoval, V.H., Ruiz-González, I., Luna-Soria, H., Hernández-Guerrero, J.A., García-Guzmán, G., 2023. Design of a Tension Infiltrometer with Automated Data Collection Using a Supervisory Control and Data Acquisition System. Sensors 23. https://doi.org/10.3390/s23239489

Morel-Seytoux, H.J., Meyer, P.D., Nachabe, M., Touma, J., Van Genuchten, M.T., Lenhard, R.J., 1996. Parameter equivalence for the Brooks-Corey and van Genuchten soil characteristics: Preserving the effective capillary drive. Water Resour Res. https://doi.org/10.1029/96WR00069

Moret, D., López, M. V., Arrúe, J.L., 2004. TDR application for automated water level measurement from Mariotte reservoirs in tension disc infiltrometers. J Hydrol (Amst) 297, 229–235. https://doi.org/10.1016/j.jhydrol.2004.04.003

Moret-Fernández, D., González, C., Lampurlanés, J., Vicente, J., 2012. An automated disc infiltrometer for infiltration rate measurements using a microflowmeter. Hydrol Process 26, 240–245. https://doi.org/10.1002/hyp.8184

Mualem, Y., 1976. A new model for predicting the hydraulic conductivity of unsaturated porous media. Water Resour Res 12, 513–522. https://doi.org/10.1029/WR012i003p00513

Naik, A.P., Ghosh, B., Pekkat, S., 2019. Estimating soil hydraulic properties using mini disk infiltrometer. ISH Journal of Hydraulic Engineering 25, 62–70. https://doi.org/10.1080/09715010.2018.1471363

Nestingen, R., Asleson, B.C., Gulliver, J.S., Hozalski, R.M., Nieber, J.L., 2018. Laboratory Comparison of Field Infiltrometers. J Sustain Water Built Environ 4. https://doi.org/10.1061/jswbay.0000857

Ngo, T.D., Kashani, A., Imbalzano, G., Nguyen, K.T.Q., Hui, D., 2018. Additive manufacturing (3D printing): A review of materials, methods, applications and challenges. Compos B Eng. https://doi.org/10.1016/j.compositesb.2018.02.012

Nimmo, J.R., 2009. Vadose Water, in: Encyclopedia of Inland Water. pp. 766–777. https://doi.org/doi:10.1016/b978-012370626-3.00014-4

Patel, R., Desai, C., Kushwah, S., Mangrola, M.H., 2022. A review article on FDM process parameters in 3D printing for composite materials. Mater Today Proc 60, 2162–2166. https://doi.org/10.1016/j.matpr.2022.02.385

Patwardhan, A. 1., 2018. How 3D Printing Will Change the Future of Borrowing Lending and Spending?, in: Handbook of Blockchain, Digital Finance, and Inclusion. Elsevier Inc., pp. 493–520. https://doi.org/10.1016/B978-0-12-812282-2.00022-X

Percoco, G., Lavecchia, F., Galantucci, L.M., 2012. Compressive Properties of FDM Rapid Prototypes Treated with a Low Cost Chemical Finishing, Article in Research Journal of Applied Sciences, Engineering and Technology.

Perroux, K.M., White, I., 1988. Design For Disc Permeameters. Soil Science Society of America Journal 52, 1205–1215.

Philip, J.R., 1969. Theory of Infiltration. pp. 215–296. https://doi.org/10.1016/b978-1-4831-9936-8.50010-6

Philip, J.R., 1957. The theory of infiltration: 1. the infiltration equation and its solution. Soil Sci 83, 345–358.

Richards, L.A., 1931. Capillary conduction of liquids through porous mediums. J Appl Phys 1, 318–333. https://doi.org/10.1063/1.1745010

Romanov, V., Samuel, R., Chaharlang, M., Jafek, A.R., Frost, A., Gale, B.K., 2018. FDM 3D Printing of High-Pressure, Heat-Resistant, Transparent Microfluidic Devices. Anal Chem 90, 10450–10456. https://doi.org/10.1021/acs.analchem.8b02356

Rosenbaum, U., Bogena, H.R., Herbst, M., Huisman, J.A., Peterson, T.J., Weuthen, A., Western, A.W., Vereecken, H., 2012. Seasonal and event dynamics of spatial soil moisture patterns at the small catchment scale. Water Resour Res 48. https://doi.org/10.1029/2011WR011518

Severino, G., Santini, A., Sommella, A., 2003. Determining the soil hydraulic conductivity by means of a field scale internal drainage. J Hydrol (Amst).

Shapiro, S.S., Wilk, M.B., 1965. Biometrika Trust An Analysis of Variance Test for Normality (Complete Samples), Source: Biometrika.

Šimůnek, J., Van Genuchten, M.T., 1996. Estimating unsaturated soil hydraulic properties from tension disc infiltrometer data by numerical inversion. Water Resour Res 32, 2683–2696. https://doi.org/10.1029/96WR01525

Sněhota, M., Cislerova, M., 2002. Automated set-up designed to measure hydraulic parameters in heterogeneous soil close to saturation, Article in Journal of Hydrology and Hydromechanics.

Teng, J., Dong, A., Yan, H., Tong, C., Zhang, S., 2023. Predicting the hydraulic conductivity of frozen coarse-grained soils. J Hydrol (Amst) 617. https://doi.org/10.1016/j.jhydrol.2022.129048

Told, R., Ujfalusi, Z., Pentek, A., Kerenyi, M., Banfai, K., Vizi, A., Szabo, P., Melegh, S., Bovari-Biri, J., Pongracz, J.E., Maroti, P., 2022. A state-of-the-art guide to the sterilization of thermoplastic polymers and resin materials used in the additive manufacturing of medical devices. Mater Des 223. https://doi.org/10.1016/j.matdes.2022.111119

van Genuchten, M.Th., 1980. A Closed-form Equation for Predicting the Hydraulic Conductivity of Unsaturated Soils 1.

Van Genuchten, R., 1978. Calculating the unsaturated hydraulic conductivity with new closed-form analytical model.

Virtanen, P., Gommers, R., Oliphant, T.E., 2020. SciPy 1.0: fundamental algorithms for scientific computing in Python. Nat Methods 17, 261–272. https://doi.org/10.1038/s41592-019-0686-2

Vogel, T., Van Genuchten, M.T., Cislerova, M., Brown, G.E., 2000. Effect of the shape of the soil hydraulic functions near saturation on variably-saturated flow predictions.

Vrána, M., Kubát, J.F., Kavka, P., Zumr, D., 2024. A laser diffractometry technique for determining the soil water stable aggregates index. Geoderma 441. https://doi.org/10.1016/j.geoderma.2023.116756

Wosten, J.H.M., Lilly, A., Nemes, A., Le Bas, C., Hungary´d, H., 1999. Development and use of a database of hydraulic properties of European soils, Geoderma.

Wu, Y., Dai, Z., Liu, H., Wang, L., Nemitz, M.P., 2024. Vision-based FDM Printing for Fabricating Airtight Soft Actuators, in: 2024 IEEE 7th International Conference on Soft Robotics, RoboSoft 2024. Institute of Electrical and Electronics Engineers Inc., pp. 249–254. https://doi.org/10.1109/RoboSoft60065.2024.10521961

Xaver, A., Zappa, L., Rab, G., Pfeil, I., Vreugdenhil, M., Hemment, D., Arnoud Dorigo, W., 2020. Evaluating the suitability of the consumer low-cost Parrot Flower Power soil moisture sensor for scientific environmental applications. Geoscientific Instrumentation, Methods and Data Systems 9, 117–139. https://doi.org/10.5194/gi-9-117-2020

Zhang, R., 1997. Infiltration Models for the Disk Infiltrometer. Soil Science Society of America Journal 61, 1597–1603. https://doi.org/10.2136/sssaj1997.03615995006100060008x

Zumr, D., Jeřábek, J., Klípa, V., Dohnal, M., Sněhota, M., 2019. Estimates of tillage and rainfall effects on unsaturated hydraulic conductivity in a small central European agricultural catchment. Water (Switzerland) 11. https://doi.org/10.3390/w11040740

Chapter 4 – Infiltration Processes in Layered Soils

4.1 Introduction

A perfectly homogeneous soil profile, often assumed in controlled infiltration experiments, and numerical simulation of hydrological processes, is relatively rare in natural settings, because soils are commonly characterized by structural heterogeneity produced by both natural processes and external disturbances. This heterogeneity frequently manifests as soil layering, the vertical configuration of distinct layers that differ in texture, structure, or hydraulic properties.

Layered soil profiles can exhibit markedly different hydraulic behaviours depending on the texture and spatial arrangement of their horizons. When a coarse-textured layer overlies a finer, less permeable one, infiltration initially advances rapidly through the coarse material but slows sharply once the wetting front encounters the finer sublayer, where smaller pores and higher water-holding capacity limit downward flow (Hillel, 1998). Conversely, when a fine-textured horizon occupies the surface, whether of natural origin or caused by disturbance, the infiltration rate is controlled by its lower hydraulic conductivity. A particularly common manifestation of this condition is the formation of thin compacted surface crusts. These crusts may develop through repeated wetting–drying cycles that induce surface sealing (Assouline & Mualem, 1997), through the settling of fine sediments after flooding (Lassabatere et al., 2010), or through biological processes such as organic-matter accumulation and decomposition, including the development of microbial or fungal biocrusts (Belnap et al. 2001). Once established, even a very thin crust can substantially impede water entry, regardless of the permeability of the underlying soil, thereby altering infiltration patterns and subsequent water redistribution.

According to Hillel (1998), soil surface crusts can be distinguished as “depositional crusts” and “structural crusts”. Depositional crusts form when sediment-laden water temporarily covers the soil surface. In these conditions, a muddy suspension rich in dispersed particles settles gradually, and the fine materials infiltrate the surface pores, filling and clogging the larger voids and creating a compact, low-permeability layer. On the other hand, structural crusts form through the breakdown of surface soil aggregates, typically triggered by the direct impact of raindrops, or by external mechanical forces that compact the soil, producing a dense layer with reduced infiltration capacity.

Human activities, even when not aimed at deliberate soil modification, can intensify these same mechanisms, leading to surface conditions that foster the formation of compacted crusts and layered

profiles (Smith et al., 2005; Batey, 2009).These factors collectively lead also to a variety of soil alterations, including changes in aggregate stability, pore connectivity, bulk density, and surface roughness, and may consequently influence water infiltration, retention, and flow paths in ways that are highly variable and site-specific (Lindstrom et al., 1984; dos Santos et al., 2018).

Soil compaction is a primary factor promoting development of layered profiles and surface crusts in both agricultural and forest soils and therefore represents a critical issue in the broader field of soil management. Compaction arises mainly from human and animal activity, although it can also develop under natural conditions and contribute to soil erosion, nutrient depletion, and pollution, challenges frequently highlighted in recent reports by the United Nations and other international bodies (Hartemink, 2008).

In agricultural systems, surface compaction commonly results from the repeated passage of heavy machinery and, in a smaller measure, from animal trampling (Batey, 2009; Rodríguez et al., 2012). The pressure exerted by tires or hooves compresses soil particles, increasing bulk density and reducing porosity in the upper soil layers (0–30 cm) (Batey, 2009). The severity of compaction depends on factors such as soil texture, moisture content at the time of traffic, machinery load, and tire inflation pressure, with fine-textured and wet soils being particularly vulnerable (Hamza & Anderson, 2005). According to Batey (2009), while certain operations, such as seedbed preparation, can be scheduled when the soil is firm and supportive to minimize compaction, other activities, like harvesting root and vegetable crops, often must be carried out when the soil is at or above field capacity, increasing the likelihood of compaction. If the soil is dry and firm throughout the profile, traffic may have little effect; however, when moist and soft surface layers overlie drier subsoil, a common situation in late summer due to the first rains of the season, the upper layers can be strongly compressed. Over time, repeated traffic without sufficient recovery can lead to the formation of a dense soil crust, which restricts root growth and hinders vertical water movement, with long-term implications for soil structure and function.

On the other hand, in forest ecosystems surface compaction is primarily associated with logging operations and the movement of heavy machinery during timber harvesting. Skidding trails, log landings, and haul roads are well-known hotspots where machinery traffic, especially under wet soil conditions, can produce significant topsoil compaction (0–10 cm) and reduce macroporosity (Greacen & Sands, 1980; Ampoorter et al., 2012). Soil susceptibility is further affected by organic matter content and the frequency of harvesting operations; although some natural recovery may occur through freeze–thaw cycles, bioturbation, or root growth, compaction in forest soils can persist for

decades, with long-term consequences for infiltration, aeration, and microbial activity (Kremers & Boosten, 2018).

The outcome of these processes can markedly affect water movement, retention, and root penetration, leading to potential modifications in soil aeration, nutrient distribution, and microbial activity (Horton et al., 1994; Mossadeghi-Björklund et al., 2019). Thus, the compacted top layer may interfere with infiltration during rainfall events, causing increased surface runoff and the risk of erosion, while the contrasting permeability of the subsoil can create complex flow patterns and localized preferential pathways (Chyba et al., 2014).

Despite the clear importance of this phenomenon, the hydraulic behaviour of layered soils remains poorly understood, particularly under varying moisture regimes and in response to repeated mechanical or natural stresses, with only limited experimental data currently available. A better understanding of the interactions between the compacted surface horizon and the more permeable subsoil is therefore critical for predicting infiltration dynamics, optimizing water use efficiency, and maintaining overall soil functionality in both managed and natural ecosystems.

Understanding how a compacted surface layer affects water infiltration is challenging, due to the vastity of soil and environmental factors and their interactions. Laboratory experiments offer a way forward by studying one key factor while all other initial conditions are kept constant. In the research proposed in this chapter, we specifically compared infiltration in a homogeneous soil with that in layered profiles containing a low-permeability surface layer of varying thicknesses, in order to isolate and quantify its direct impact on infiltration. This controlled approach helps answer practical questions such as how surface compaction might change the rate and depth of water movement after irrigation or heavy rainfall, or how it influences the recharge of deeper soil layers. The findings can guide decisions on field traffic management, tillage timing, and strategies to improve water availability and reduce runoff in both agricultural and forest soils.

References:

Assouline, S., & Mualem, Y. (2002). Infiltration during soil sealing: The effect of areal heterogeneity of soil hydraulic properties. *Water Resources Research*, *38*(12), 22-1‑22-9. https://doi.org/10.1029/2001WR001168

Batey, T. (2009). Soil compaction and soil management–a review. *Soil use and management*, *25*(4), 335-345.

Belnap, J., Büdel, B., & Lange, O. L. (2001). Biological soil crusts: characteristics and distribution. In *Biological soil crusts: structure, function, and management* (pp. 3-30). Berlin, Heidelberg: Springer Berlin Heidelberg.

Chyba, J., Kroulík, M., Krištof, K., Misiewicz, P. A., & Chaney, K. J. A. R. (2014). Influence of soil compaction by farm machinery and livestock on water infiltration rate on grassland.

dos Santos, K. F., Barbosa, F. T., Bertol, I., de Souza Werner, R., Wolschick, N. H., & Mota, J. M. (2018). Study of soil physical properties and water infiltration rates in different types of land use. *Semina: Ciências Agrárias*, *39*(1), 87-97.

Greacen, E. L., & Sands, R. (1980). Compaction of forest soils. A review. *Soil Research*, *18*(2), 163-189.

Hartemink, A.E. 2008. Soils are back on the global agenda. Soil Useand Management, 24, 327–330

Hillel, D. (1998) Environmental Soil Physics: Fundamentals, Applications, and Environmental Considerations. Academic Press, Waltham.

Horton, R., Ankeny, M. D., & Allmaras, R. R. (1994). Effects of compaction on soil hydraulic properties. *Developments in agricultural engineering*, *11*, 141-165.

Kremers, J., & Boosten, M. (2018). Soil compaction and deformation in forest exploitation. *American Journal for Alternative Agriculture*, *7*(1-2), 25-31.

Laigle, I., Moretti, M., Rousseau, L., Gravel, D., Venier, L., Handa, I. T., ... & Aubin, I. (2021). Direct and indirect effects of forest anthropogenic disturbance on above and below ground communities and litter decomposition. *Ecosystems*, *24*(7), 1716-1737.

Lassabatere, L., Angulo-Jaramillo, R., Goutaland, D., Letellier, L., Gaudet, J. P., Winiarski, T., & Delolme, C. (2010). Effect of the settlement of sediments on water infiltration in two urban infiltration basins. *Geoderma*, *156*, 316‑325. https://doi.org/10.1016/j.geoderma.2010.02.031

Lindstrom, M. J., & Onstad, C. A. (1984). Influence of tillage systems on soil physical parameters and infiltration after planting. *Journal of soil and water conservation*, *39*(2), 149-152.

Mossadeghi-Björklund, M., Jarvis, N., Larsbo, M., Forkman, J., & Keller, T. (2019). Effects of compaction on soil hydraulic properties, penetration resistance and water flow patterns at the soil profile scale. *Soil Use and Management*, *35*(3), 367-377.

Rodríguez, L. A., Valencia, J. J., & Urbano, J. A. (2012). Soil compaction and tires for harvesting and transporting sugarcane. *Journal of Terramechanics*, *49*(3-4), 183-189.

Smith, R. G., Ryan, M. R., & Menalled, F. D. (2011). Direct and indirect impacts of weed management practices on soil quality. *Soil management: Building a stable base for agriculture*, 275-286

4.2 One-dimensional infiltration in a layered soil measured in the laboratory with the mini-disk infiltrometer

Published on Journal of Hydrology and Hydromechanic., 72, 2024, 2, 149–157 https://doi.org/10.2478/johh-2024-0001

Dario Autovino, Vincenzo Bagarello, Gaetano Caltabellotta, Florina Kati Varadi, Francesco Zanna

ABSTRACT

Layered soils can consist of a thin little permeable upper layer over a more permeable subsoil. There are not many experimental data on the influence of this upper layer on infiltration. The mini-disk infiltrometer set at a pressure head of –3 cm was used to compare infiltration of nearly 40 mm of water in homogeneous loam and clay soil columns with that in columns made by a thin layer (1 and 3 cm) of clay soil over the loam soil. For each run, the Horton infiltration model was fitted to the data and the soil sorptivity was also estimated by considering the complete infiltration run. For the two layered soils, the estimates of initial infiltration rate and decay constant were similar but a thicker upper layer induced 2.4 times smaller final infiltration rates. Depending on the infiltration parameter and the thickness of the upper layer, the layered soils were characterized by 2.2–6.3 times smaller values than the loam soil and 2.2–6.6 higher values than the clay soil. Sorptivity did not differ between the homogeneous clay soil and the layered soil with a thick upper layer and a thin layer was enough to induce a decrease of this hydrodynamic parameter by 2.5 times as compared with that of the homogeneous loam soil. Even a thin upper layer influences appreciably infiltration and hydrodynamic parameters. Layering effects vary with the thickness of the upper layer and the considered parameter. The applied experimental methodology could be used with other soils and soil combinations.

INTRDUCTION

Infiltration in layered soils, that are frequent in different environments and situations (Wang et al., 2014; Yang et al., 2006), can differ appreciably from infiltration in non-layered soils (Hillel, 1998). A special case of layered soil is when a seal layer is formed at the surface, yielding a less permeable upper layer as compared with the subsoil (Assouline, 2013). The thickness of this upper layer can be very variable but in a rather narrow range since it should not exceed a few centimeters at the most (Armenise et al., 2018; Assouline, 2004). Even such a thin layer can have a large impact on the hydrological response of a field or a watershed (Assouline and Mualem, 2002, 2006). According to some investigations, when the soil is layered and the upper layer is the less permeable, water

infiltration should be more representative of the upper layer (Bagarello et al., 2023; da Silva Ribas et al., 2021; Lassabatere et al., 2010; Yilmaz et al., 2013). To our knowledge, however, there are not many experimental investigations on the actual correspondence between homogeneous and layered soils (Di Prima et al., 2018). Testing the similarity between these two kinds of soils is advisable to improve our ability to interpret soil hydrologic processes and also in the perspective to use the infiltration data for estimating soil hydrodynamic properties (Assouline and Mualem, 2002; Moret-Fernández et al., 2021).

These experiments should preferably be performed on layered soils with thin or relatively thin little permeable upper layers given that, with large thicknesses, a similarity between the homogeneous and layered soils is expected more since infiltration occurs in porous media with similar characteristics for relatively long times. Performing these checks with as simple as possible experimental methods is advisable to make the experiment easily reproducible and also considering that the experiment is inherently complex even if a single layered soil is considered. The reason is that replicated experiments have to be performed on soil columns made with this layered soil but also with each of the two homogeneous soils that are combined with each other to form the layered porous medium. An infiltration model, such as that by Horton (1940), could be fitted to the data to characterize a run by a limited number of relevant parameters. Performing laboratory infiltration experiments on layered soil columns made with sieved and repacked soil is rather common for a variety of purposes such as improving knowledge of the process in particular situations (Wang et al., 2014), establishing if the data allow to recognize the presence of layering (Moret Fernández et al., 2021), testing predictive infiltration models for these non-homogeneous porous media (Chen et al., 2019; Mohammadzadeh-Habili and Heidarpour, 2015; Moore and Eigel, 1981). Investigations differ by several factors, depending on their specific objectives. For example, simulated rainfall was used in some cases (Yang et al., 2006) whereas a ponded depth of water was established on the infiltration surface in other cases (Wang et al., 2014). The total length of the soil column and the thickness of the tested soil layers also change, even if investigations considering layers of at least a few tens of centimeters seem to be more frequent. For example, total length was 21 cm (Al-Maktoumi et al., 2015), 100 cm (Yang et al., 2006) or 300 cm (Ma et al., 2011). The columns by Yang et al. (2006) were made of 60–65 cm of an upper layer over 35–40 cm of a subsoil. The experiment by Ma et al. (2011) was performed on a soil column filled with five layers of 120, 20, 30, 30 and 120 cm. A 20 cm thick upper layer over a 40 cm thick subsoil was considered by Chen and Hsu (2012). The columns by Wang et al. (2014) and Chen et al. (2019) were made by layers of 22.5–25, 20 and 20–22.5 cm. In the experiment by Batsilas et al. (2023), the height of the upper and lower layers was 45 and 48 cm, respectively. However,

experiments with thinner upper layers have also been performed. For example, Young et al. (2002) considered a two layered soil made of 7.5 cm thick layers. In the experiment by Al-Maktoumi et al. (2015), 15 cm of a soil were overlaid with 6 cm of another soil. A rather simple and cheap method to obtain infiltration data in layered soils with thin little permeable upper layers is performing one-dimensional (1D) experiments with the mini-disk infiltrometer (MDI) on relatively small soil columns, that is on the order of 20‑25 cm in length by 5 cm in diameter. With the MDI, a negative but close to zero pressure head is established on the soil surface. The infiltration data are therefore representative of a nearly saturated soil matrix (Assouline and Narkis, 2011). The device has already been used in the laboratory to perform different 1D experiments on repacked soil, such as those testing the effects of treated wastewater on the hydraulic properties of a clayey soil (Assouline and Narkis, 2011) or performing comparisons with three-dimensional infiltration (Kargas et al., 2018). The general objective of this investigation was to determine the impact of soil layering on one-dimensional infiltration processes established with the mini-disk infiltrometer. The specific objectives were to i) compare infiltration in homogeneous loam and clay soil columns with that measured in columns made by a thin layer of clay soil over the loam soil; ii) test the effect of the thickness of the upper clay soil on infiltration in a rather narrow range of small thickness values; and iii) establish layering effects on the fitted parameters of a three-parameter infiltration model and also on the estimated soil sorptivity.

MATERIALS AND METHODS

Experiment

The infiltration experiment was carried out with two soils differing by texture collected in Sicily (Italy). In particular, a site was the orchard of the Department of Agricultural, Food and Forest Sciences of the Palermo University (38° 06’ 24’’ N, 13° 21’ 06’’ E). The other site was the experimental station for soil erosion measurement Sparacia (37° 38’ 46’’ N, 13° 45’ 43’’ E), located approximately 100 km south of Palermo. The soil at the Palermo site (Typic Rhodoxeralf) has a relatively high gravel content and it is mostly sandy-loam or loam down to a depth of at least 0.30 m. For this investigation, the soil was collected in an area where the texture was loam (clay = 15.4%, silt = 36.2%, sand = 48.4%; USDA classification system) (Agosta et al.,2023). The soil of Sparacia (Vertic Xerocrept) has a clay texture (clay = 62% silt = 33%, sand = 5%) and a negligible gravel content (Pampalone et al., 2022). The soil collected from approximately the upper 10 cm of the profile

(nearly 100 kg for each soil) was transported to the laboratory and it was spread on plastic sheets for natural drying at room temperature. This process lasted about 40 days, during which the soil was shuffled every 2‑3 days to facilitate drying.

Once the condition of air-dry soil was reached, the soil was sieved through a 2 mm mesh sieve and the fine fraction was retained for the experiment. Soil columns were prepared in 25 cm long plexiglass cylinders having an inner diameter of 5.3 cm, equipped with a nylon guard cloth and a thin wire mesh at the base to support the weight of the soil. A total of 36 soil columns were used in this experiments. In particular, nine columns were prepared with the homogeneous loam soil (AO soil) and nine columns were prepared with the homogeneous clay soil (SO). The final length of these soil columns was 20 cm. A layered soil with a little permeable upper layer and a more permeable subsoil was prepared using these fine clay and coarser loam soils. In particular, nine columns were composed of 1 cm of clay soil over 20 cm of the loam soil (L1 soil). The other nine columns were prepared by placing 3 cm of clay soil on 20 cm of the loam soil (L3 soil). Each soil column was prepared with a soil mass that was never used before. The so-called P3 packing method by Bagarello et al. (2022) was used to prepare the homogeneous soil columns and also the subsoil layer of the layered soil columns. This packing method is based on the partition of the air-dry soil mass used to fill the cylinder into three equal parts. One third is poured in the cylinder and the soil is compacted manually by a wood pestle that is pressed downward repeatedly. After concluding pressing, the pestle is rotated clockwise and counter-clockwise around its vertical axis for a few times. The second part is then added and the same compaction procedure is applied again. Finally, the last part of soil is poured and compacted. In this investigation, all interfaces in packing were gently scarified after compaction and before adding another increment to improve the hydraulic contact between the layers (Wang et al., 2014). The AO soil columns were packed in order to obtain a nearly constant dry soil bulk density, ρb, equal to 1.18 g/cm3. For each step of the packing procedure, 179 g of air-dry soil were poured into the cylinder and this soil was pressed 30 times. Therefore, a total of 537 g of air-dry soil was used. The final length of the soil column and the number of compactions for each layer did not change for the homogeneous SO soil columns. In this case, a total of 600 g of air-dry soil was used and the ρb value was equal to 1.25 g/cm3. With reference to the layered soils, an established amount of air-dry clay soil (nearly 30 g for the L1 soil and 90 g for the L3 soil) was placed on the top of the sample and it was pressed with the pestle 10 times to obtain for these upper layers the same dry soil bulk density of the homogeneous SO soil columns (1.25 g/cm3). A direct measurement of ρb was not available since the soil used to fill the cylinder was air-dry. Therefore, ρb was determined by the following relationship (Bagarello et al., 2022):

$$\rho_b = \frac{m_s}{V_t} = \frac{m_{ad}}{V_t(1 + w_{ad})} \quad (1)$$

where *ms* (g) is the mass of the dry soil, *Vt* (cm3) is the bulk volume of the soil sample, *mad* (g) is the mass of the air-dry soil and *wad* (g/g) is the gravimetric soil water content of the air-dry soil, that was measured on six samples during the experiment. The volumetric air-dry soil water content, obtained by ρ*b* and *wad*, was equal to 0.05 m3/m3 for the loam soil and 0.12 m3/m3 for the clay soil. A mini-disk infiltrometer, MDI (manufactured by Decagon Devices, Pullman, WA, USA, Infiltrometer User's Manual, Decagon Devices Inc., 2014), was used to measure infiltration. For each infiltration run, the MDI was filled with tap water at room temperature. A pressure head equal to −3 cm was established at the base of the device. A slightly negative pressure head was used in this investigation to avoid flow along possible large voids resulting from packing or at the contact between the soil and the wall of the column (Assouline and Narkis, 2011). Before each 1D test, the soil column was placed on a perforated support that allowed air to easily escape from the bottom of the sample. For each run, the infiltrated volumes were measured every 10 s for the first minute, 15 s for the subsequent minute, 30 s for another two minutes and then every minute until the complete emptying of the MDI reservoir (95 mL for the A0, L1 and L3 soil runs and 90 mL for the SO soil runs, with differences related to the used device). For the SO soil, the run lasted long and infiltrated water volumes were measured every 5 min after the first 4 hours of infiltration. Cumulative infiltration, *I* (mm), at a given time, *t* (h), was obtained by dividing the cumulative infiltrated volume by the cross-sectional area of the soil column. A check of the laboratory data was first performed by visually examining the *I* vs. *t* curves to verify if they were initially concave and then smoothly described a linear relationship, as expected (Pachepsky and Karahan, 2022). The mean infiltration rate, *irmed* (mm/h), was then calculated for each run. In addition, the empirical Horton (1940) infiltration model was fitted to the *I* vs. *t* data by minimizing the sum of the squared residuals between the measured and the predicted *I* values (Lassabatere et al., 2006):

$$I = i_{fH}t + \frac{i_{0H} - i_{fH}}{k_H}(1 - e^{-k_H t}) \quad (2)$$

where *i*0H (mm/h) is the initial infiltration rate (*t* = 0), *if*H (mm/h) is the final infiltration rate and the constant *k*H (1/h) describes the rate at which *i*0H approaches *if* H. For given *i*0H and *if*H values, the

smaller *k*H the more gradual the transition from the initial to the final conditions (Tindall et al., 1999). The quality of the fitting was evaluated by the relative error, *Er* (%), in agreement with Lassabatere et al. (2006). The model by Horton was chosen since it describes the infiltration curve by three different parameters expressive of the initial and the final stages of the process and also of the transition between these two stages. Another reason was that this model gave a good representation of the experimentally determined *I* v. *t* relationships in other investigations (Agosta et al., 2023; Iovino et al., 2021; Shukla et al., 2003). According to Ndiaye et al. (2005), infiltration measured by a one-dimensional tension infiltrometer experiment can be used to estimate the sorptivity, *S* (mm/h0.5), and the soil hydraulic conductivity, *K* (mm/h), corresponding to the imposed pressure head at the soil surface. In particular, the two-term infiltration equation (Philip, 1957) is fitted to the data to obtain *S* and the *A* (mm/h) parameter:

$$I = St^{0.5} + At \qquad (3)$$

Hydraulic conductivity is then calculated from *A*. For each infiltration run, *S* and *A* were also estimated by fitting a quadratic equation with a null constant coefficient to the (*I*, *t*

0.5) data (Minasny and McBratney, 2000). Each soil column was characterized by a value of *S* but not of *K*. The reason was that *S* was directly obtained by fitting Eq. (3) to the data collected during the entire duration of the run. Therefore, the estimates of *S* were usable to detect differences between the two homogeneous soils and also to verify how layering influenced the sorptivity estimates. Calculation of *K* was not performed for a twofold reason: i) the procedure by Ndiaye et al. (2005) is based on the infiltration model by Haverkamp et al. (1994) that is valid for homogeneous soils and hence is not usable for layered soils; ii) even considering, perhaps forcedly, a sort of equivalent conductivity for the layered soil, calculating *K* was not possible since these calculations require an estimate of the so-called β parameter that, according to recent investigations on three-dimensional infiltration, is soil-dependent (Yilmaz et al., 2023). This circumstance precluded defining a single β value for a soil column made by two texturally different layers. A comparison was then performed between the AO, SO, L1 and L3 soils. Initially, all the experimental infiltration rate, *ir* (mm/h) vs. *I* and *I* vs. *t* relationships for these soils were reported on a single *ir* vs. *I* plot and a single *I* vs. *t* plot and they were visually examined to recognize clear differences among the four soils. The *ir* vs. *I* plot was considered, also according to other investigations (Morin and Benyamini, 1977), since durations changed from run to run, making representation of all data on a single *ir* vs. *t* plot confuse. Then, a statistical comparison between the infiltration (*irmed*, *i*0H, *if*H, *k*H) and hydrodynamic (*S*) parameters

for the four soils was carried out. A pairwise approach was applied to compare two datasets at a time. In particular, F and unpaired, two-tailed t tests were used. The statistical tests were carried out at $P = 0.05$.

RESULTS

Generally, the experimental infiltration processes appeared consistent with theory since the concavity of the *I* vs. *t* curves was faced downwards, denoting that the infiltration rates initially decreased during the run, and the *I* vs. *t* relationship assumed a nearly linear shape at longer times (Fig. 1). However, some curves obtained in the SO soil exhibited a change in slope in an advanced stage of the run. In particular, they appeared to become flatter, denoting smaller infiltration rates. This shape was relatively similar to one of the possible shapes of cumulative infiltration curves recently described by Pachepsky and Karahan (2022), and particularly to the shape shown in their figure 2J. A possible reason why this shape was detected was that the initially air-dry clay soil swelled during wetting, which lasted several hours (on average, 5.85 h), and the consequence was a decrease of the volume of the largest pores (Kalnin et al., 2021) and hence of infiltration rates. According to Lassabatere et al. (2006), a relative error, *Er*, that does not exceed 5.5% denotes an acceptable fitting of an infiltration model to the data. With reference to the SO soil, adapting the Horton model to the complete infiltration curves yielded a mean value of *Er* equal to 4.4% and the threshold of 5.5% was exceeded in a single case (*Er* = 6.6%; Table 1). Therefore, this check, suggesting that the fitting of the model to the complete infiltration curve was overall satisfactory, did not raise any particular concern regarding the possibility to consider the entire infiltration curve for estimating the infiltration parameters. In order to make comparison between homogeneous and layered soils easier to follow, all infiltration rates (AO, SO, L1, L3 soils) were reported on a single *ir* vs. *I* plot (Fig. 2a) but the data were also presented by showing the two homogeneous soils and only one of the two layered soils (Figs. 2b and 2c). The homogeneous AO and SO soils were characterized by the highest and the lowest infiltration rates, respectively, whereas the two layered soils showed intermediate *ir* values, that were generally higher for the L1 soil than the L3 soil. Notwithstanding some data scattering, that was not surprising (e.g., Wang et al., 2014; Xiao et al., 2019), no contact points were recognized between the two homogeneous soils on the *ir* vs. *I* plot. At the beginning of the process, a certain overlap between the infiltration rate curves for the homogeneous SO soil and some curves for the layered soils was evident. This overlap appeared more complete and persisted longer in the case of the L3 soil than for the L1 soil, as logical. In a later stage of the experiment, the difference between

the two layered soils became clearer, with the L1 soil yielding higher *ir* values than the L3 soil. As the applied water volume increased, the infiltration rates of the AO and L1 soils tended to become more similar and the infiltration rates of the SO and L3 soils tended to become more dissimilar on the representation of Fig. 2. The AO vs. L1 soils similarity appeared to be a consequence of decreasing infiltration rates for the former soil and stabilized rates for the latter one. Even the increasing deviation between the SO and L3 soils occurred because infiltration rates for the former soil decreased while those of the latter soil stabilized. Therefore, infiltration rates stabilized after applying a relatively small water volume in the layered soils but not in the homogeneous soils.

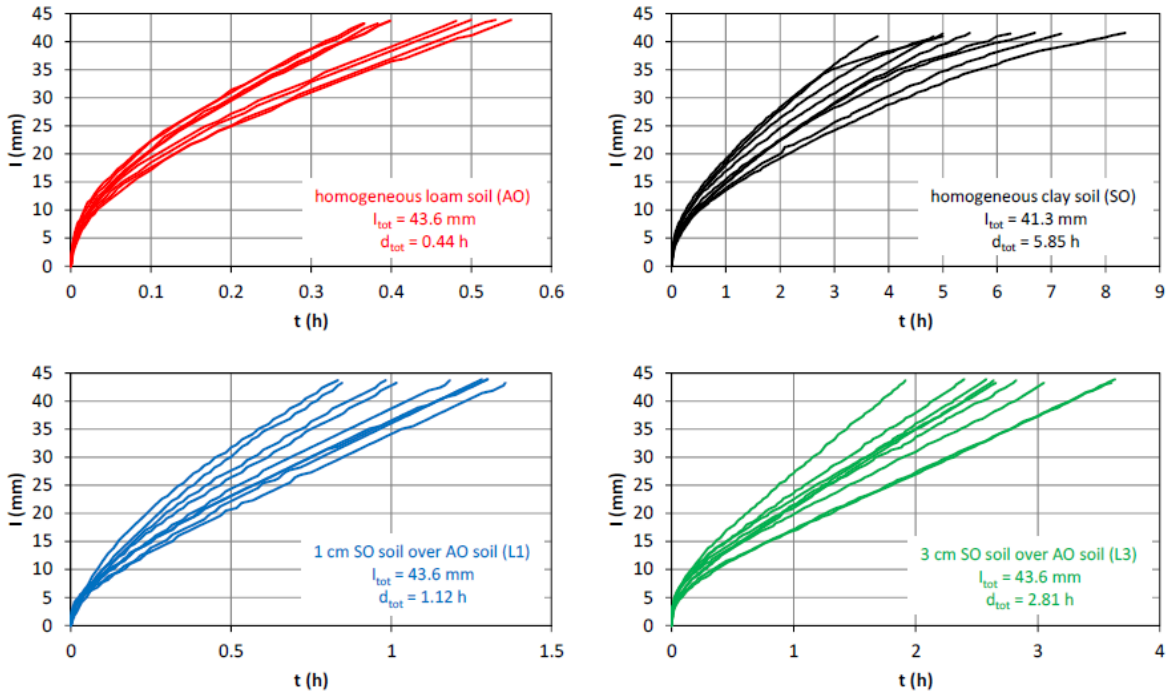

Fig. 1. Cumulative infiltration curves obtained in the four tested soils (*I* = cumulative infiltration; *t* = time; the mean values of the cumulative infiltration by the end of the run, *Itot*, and of the total duration of the run, *dtot*, are reported for each soil).

Table 1. Summary statistics of the mean infiltration rate, *irmed*, the infiltration parameters of the Horton model (i_0H = initial infiltration rate; i_fH = final infiltration rate; kH = decay constant; *Er* = relative error) and the soil sorptivity, *S* (sample size, $N = 9$ for each soil and parameter with the exception of *S* for the AO soil for which *N* was equal to 8).

Parameter	Statistic	SO soil	AO soil	L1 soil	L3 soil
ir_{med} (mm/h)	min	4.97	79.8	31.9	12.0
	max	10.8	118.5	52.5	22.8
	mean	7.43 (a)(c)(e)	101.1 (a)(d)(f)	40.1 (b)(c)(d)	16.1 (b)(e)(f)
	CV (%)	23.6	15.4	19.5	20.6
i_{0H} (mm/h)	min	28.8	476.3	116.6	105.9
	max	72.5	933.0	232.7	261.9
	mean	42.9 (a)(c)(e)	671.5 (a)(d)(f)	166.6 b(c)(d)	171.5 b(e)(f)
	CV (%)	32.8	21.1	22.0	31.7
i_{fH} (mm/h)	min	3.87	59.8	27.2	10.3
	max	8.48	85.1	38.7	18.6
	mean	5.59 (a)(c)(e)	73.4 (a)(d)(f)	31.8 (b)(c)(d)	13.3 (b)(e)(f)
	CV (%)	24.7	14.0	14.4	19.7
k_H (1/h)	min	1.77	34.1	7.24	14.0
	max	6.15	62.9	32.4	31.5
	mean	3.12 (a)(c)(e)	46.1 (a)(d)(f)	16.1 b(c)(d)	20.7 b(e)(f)
	CV (%)	45.9	20.9	51.3	29.6
Er (%)	min	2.36	2.53	0.88	1.25
	max	6.57	3.39	2.85	2.33
	mean	4.40 (a)(c)(e)	3.05 (a)(d)(f)	2.03 b(c)(d)	1.75 b(e)(f)
	CV (%)	27.4	10.2	29.7	22.2
S ($mm/h^{0.5}$)	min	12.8	50.5	18.3	12.0
	max	18.4	69.2	31.5	19.7
	mean	15.0 (a)(c)e	59.8 (a)(d)(f)	23.8 (b)(c)(d)	15.9 (b)e(f)
	CV (%)	13.6	9.7	15.9	19.0

For a given parameter, two means followed by the same letter not enclosed in parenthesis were not significantly different according to an F test and a two-tailed t test at $P = 0.05$. Means followed by the same letter enclosed in parenthesis are significantly different.

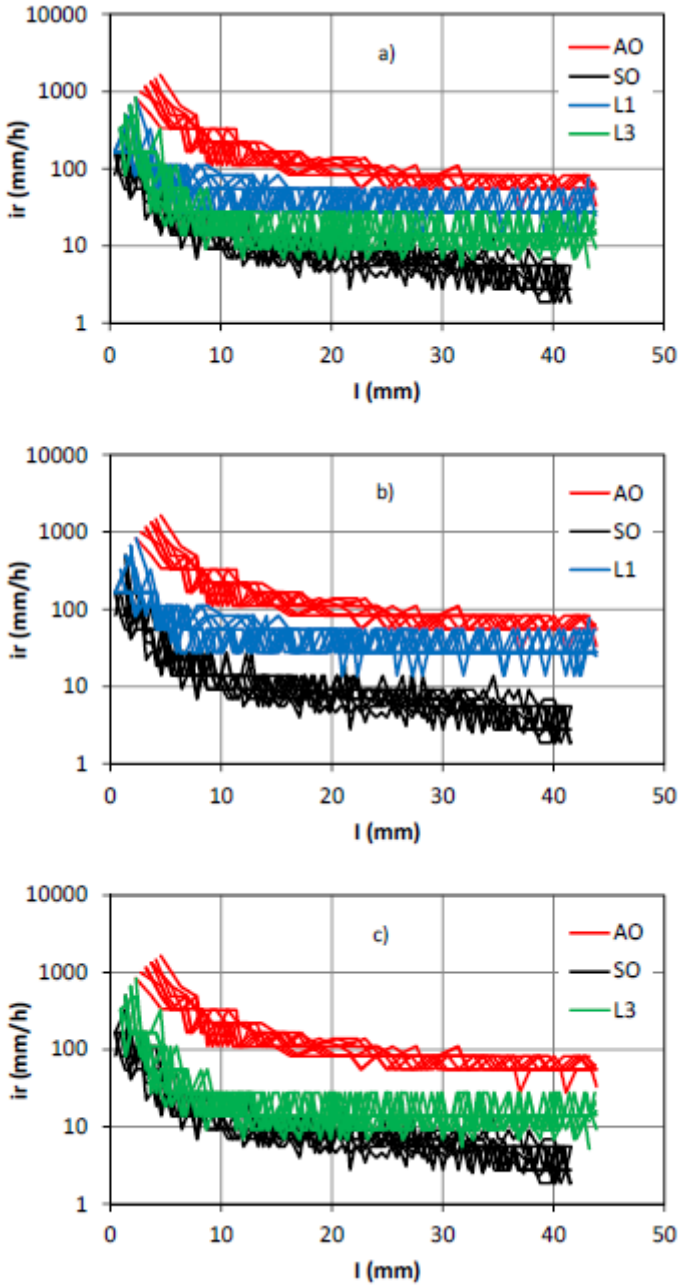

Fig. 2. Infiltration rate, ir, vs. cumulative infiltration, I, relationships for a) the four tested soils (AO: homogeneous loam soil; SO: homogeneous clay soil; L1: 1 cm of SO soil over the AO soil; L3: 3 cm of SO soil over the AO soil), b) the two homogeneous soils and the L1 layered soil, and c) the two homogeneous soils and the L3 layered soil.

On the *I* vs. *t* plot, the results for the two homogeneous soils defined an empty space that was filled by the data for the two layered soils (Fig. 3). The data of the L1 soil were closer to those of the homogeneous loam soil. The data of the L3 soil were closer to those of the homogenous clay soil. The statistical analysis of the data indicated that the mean infiltration rates, *irmed*, varied according to the AO > L1 > L3 > SO sequence (Table 1). The two homogeneous soils differed by more than an

order of magnitude, that is by 13.6 times. Instead, the two layered soils differed by 2.5 times. The L1 soil yielded a 5.4 times higher *irmed* value than the SO soil and a 2.5 times smaller value than the AO soil. The *irmed* value of the L3 soil was 2.2 times greater than that obtained with the SO soil and 6.3 times smaller than the corresponding value for the AO soil. Therefore, with reference to *irmed*, the four soils differed significantly from each other and the layered soils were characterized by intermediate values as compared with those of the two homogeneous soils that were combined one with the other to form the layered system. The L1 soil was more similar to the AO soil than to the SO soil. Instead, the L3 soil was more similar to the SO soil than to the AO soil.

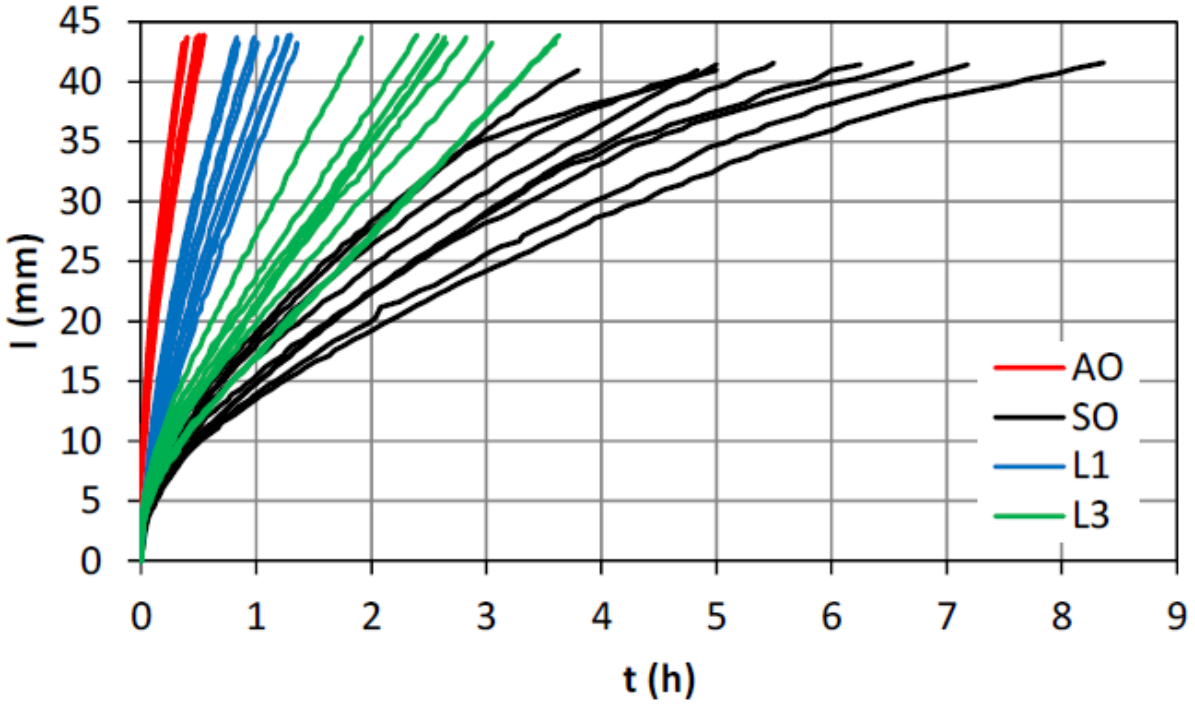

Fig. 3. Cumulative infiltration curves for the four tested soils (I = cumulative infiltration, t = time) for the AO (homogeneous loam soil), SO (homogeneous clay soil), L1 (1 cm of SO soil over the AO soil) and L3 (3 cm of SO soil over the AO soil) soils.

The initial infiltration rates, *i*0H, varied according to the AO > L3 = L1 > SO sequence (Table 1). The two homogeneous soils differed by more than an order of magnitude, that is by 15.7 times. Instead, the two layered soils were characterized by statistically similar values that only differed by 1.03 times. The L1 soil yielded a 3.9 times higher *i*0H value than the SO soil and a 4.0 times smaller value than the AO soil. The *i*0H value of the L3 soil was 4.0 times greater than that obtained with the SO soil and 3.9 times smaller than the corresponding value for the AO soil. Therefore, with reference to *i*0H, the two homogeneous soils differed significantly from each other and also from the two layered soils.

The results of these last two soils were similar to each other and nearly exactly intermediate as compared with those of the two homogeneous soils. In this case, the thickness of the little permeable upper layer did not have any impact on the comparison between the layered and the homogeneous soils.

The final infiltration rates, *if*H, varied according to the AO > L1 > L3 > SO sequence. The two homogeneous soils differed by 13.1 times while the two layered soils differed by 2.4 times. The L1 soil yielded a 5.7 times higher *if*H value than the SO soil and a 2.3 times smaller value than the AO soil. The *if*H value of the L3 soil was 2.4 times greater than that obtained with the SO soil and 5.5 times smaller than the corresponding value for the AO soil. Therefore, even with reference to *if*H, the four soils differed significantly from each other and the results for the layered soils were intermediate as compared with those of the two homogeneous soils. The L1 soil was more similar to the AO soil than to the SO soil. Instead, the L3 soil was more similar to the SO soil than to the AO soil. In both cases, more similar meant that means differed by 2.3‑2.4 times instead of 5.5‑5.7 times. The decay constant, *k*H, decreased according to the AO > L3 = L1 > SO sequence. The two homogeneous soils differed by 14.8 times while the two layered soils differed by 1.3 times. The L1 soil yielded a 5.2 times higher *k*H value than the SO soil and a 2.9 times smaller value than the AO soil. The *k*H value of the L3 soil was 6.6 times greater than that obtained with the SO soil and 2.2 times smaller than the corresponding value for the AO soil. Therefore, with reference to *k*H, the two homogeneous soils differed significantly from each other and also from the two layered soils. However, the results for these last two soils were similar. Regardless of the thickness of the upper layer, the *k*H values of the layered soils were closer to those of the AO soil (differences by 2.2‑2.9 times) than to the *k*H values of the SO soil (differences by 5.2‑6.6 times). The fitting error of the Horton model to the data, *Er*, varied according to the SO > AR > L1 = L3 sequence. Therefore, the quality of the fitting was better for the layered soils than the homogeneous ones but it was satisfactory in general since the means did never exceed the threshold of 5.5% and this threshold was exceeded for only one of the 36 infiltration runs. Finally, an estimate of soil sorptivity, *S*, was obtained for 35 of the 36 infiltration runs (Table 1). The single failure occurred for a run with the AO soil that gave a negative estimate of *A*. The estimates of *S* obtained in the homogeneous soil columns (coefficient of variation, *CV* = 9.7 ‑ 13.6%) were a little less variable than those obtained in the layered soil columns (*CV* = 15.9 ‑ 19.0%). The statistical analysis of the data indicated that *S* varied according to the AO > L1 > L3 > SO sequence. Sorptivity differed by 4.0 times between the two homogeneous soils and by 1.5 times between the two layered soils. The L1 soil was closer to the SO soil than the AO one since the layered soil had a

1.6 times higher *S* value than the SO soil and a 2.5 times smaller value than the AO soil. The *S* value of the L3 soil was 3.8 times smaller than that obtained with the AO soil and it was statistically equal to the sorptivity determined for the SO soil. In particular, the two estimates of *S* differed by 6.3% in this last case. Therefore, with reference to *S*, the two homogeneous soils differed significantly. The L1 soil differed significantly from the two homogeneous soils but it was more similar to the SO soil than the AO soil. The L3 soil was significantly less sorptive than the AO soil but it had the same sorptivity as the SO soil.

DISCUSSION

Infiltration in a layered soil can be qualitatively similar to that of non-layered soils since infiltration rates decrease with time and then tend to stabilize (Bagarello et al., 2023; Wu et al., 1997). However, infiltration in a layered soil with a less permeable upper layer is expected to be more representative of the upper layer (da Silva Ribas et al., 2021; Lassabatere et al., 2010). This investigation contributed to better establish what is meant in practice when one speaks of an infiltration curve being more representative of the upper layer in a context of qualitative similarity of infiltration rate curves for homogeneous and layered soils. In particular, the investigation tested soil layering effects on one-dimensional infiltration when the upper soil layer is relatively thin and has a finer texture than the subsoil. The check performed in this study was strictly valid for i) a layered soil in which the infiltration parameters of the upper layer, 1 to 3 cm thick, were a little more than an order of magnitude smaller than those of the subsoil (by 13.1‑15.7 times, depending on the parameter), ii) a 1D infiltration process under a negative but close to zero pressure head (‑3 cm), and iii) an experiment performed by supplying nearly the same total amount of water to each sampled soil column (41.3‑43.6 mm), that is infiltration runs having a different duration depending on the sampled porous medium. The data suggested that, at the beginning of the process, the layered soils actually show some similarity with the homogeneous clay soil, the more clearly the thicker this upper layer (Fig. 2). The presence of a loam subsoil then determines higher infiltration rates for the layered soil than the homogeneous clay soil, the sooner and the more appreciably the thinner the upper layer. Moreover, infiltration rates appear to stabilize earlier in the layered soils than in the homogeneous ones, in accordance with other findings (Wang et al., 2014). Therefore, with reference to this specific experiment, the similarity between the homogeneous and the layered soils (da Silva Ribas et al., 2021; Lassabetere et al., 2010) appears to depend on the thickness of the upper layer, being more appreciable with thick upper layers, and also on the characteristics of the infiltration run, being stronger for relatively small applied water volumes. In any case, even an upper layer of only 1 cm determines an

appreciable slowdown of the process as compared with that occurring in the homogeneous loam soil (Fig. 2). According to the data of this investigation (Figs. 1 and 3), in this case the total water volume supplied with the MDI will take 2.5 times longer to infiltrate completely. With an upper layer of 3 cm, it will take 6.4 times longer for its full infiltration to occur as compared with the homogeneous loam soil. These slowdowns will effectively make the infiltration process more and more similar to that occurring in the homogeneous clay soil (Lassabatere et al., 2010).

The investigation also allowed to establish the impact of the detected differences between the tested soils in terms of the three fitted parameters of the Horton infiltration model, that summarize the entire infiltration process, and of the estimated soil sorptivity (Table 1). In particular, two layered soils differing by the thickness of the upper layer can be expected not to differ by the estimated values of both the initial infiltration rate and the decay constant. The presence of a thicker layer at the soil surface is only signalled by a lower final infiltration rate. Regardless of the thickness of the upper layer, each infiltration parameter for the layered soil will be smaller than that obtained in the homogeneous coarser soil and higher than the one for the homogeneous fine soil. Soil sorptivity of the layered soil can be expected to be similar or also statistically identical to that of the homogeneous fine soil, depending on the thickness of the upper layer, even if the used data for estimating S are not limited to the early stage of the infiltration process (Minasny and McBratney, 2000). To summarize, a relatively thick upper layer determines an equality between the layered and the fine homogeneous soils limited to sorptivity. Some parameters (*irmed*, *if*H) are closer to the fine soil than the coarse one. Other parameters (*i*0H) are intermediate between the two homogeneous soils. Still other parameters (*k*H) are closer to the coarse soil than the fine one. The thinning of the upper layer maintains a greater similarity between layered and fine soils only with reference to sorptivity. Evidently, trying to obtain general conclusions requires testing soil layering effects by considering different soils, initial soil water conditions and established pressure heads and, hence, water conducting pore sizes (Reynolds et al., 1995). A way to obtain an extensive information without necessarily performing extremely long and demanding laboratory experiments could consist of using numerical simulation of the processes of interest (e.g., Dohnal et al., 2016). Infiltration experiments performed in the laboratory on homogeneous soil columns could be used to derive the hydraulic parameters of the tested soils necessary for the simulations (Wang et al., 2014). In addition, some of the numerically considered scenarios for a layered soil system could be reproduced experimentally to also establish a comparison between numerical and experimental results. However, a homogeneous soil column and the upper layer of a layered soil column differ by their length and they have likely to be prepared with packing methods that differ to some extent. Packing method effects on the soil sample characteristics are

expected (Bagarello et al., 2022; Lewis and Sjöstrom, 2010; Nimmo and Akstin, 1988; Oliviera et al., 1996). For example, a relatively long soil column could be less uniform than a relatively thin layer of the same soil since the soil compacting force decays gradually from the top to the base of any layer (Gao et al., 2018). Therefore, before performing extensive numerical simulations with laboratory determined soil hydraulic functions, it seems advisable to verify if the hydraulic functions obtained experimentally in a column of a homogeneous fine-textured soil are representative for the upper layer of a layered soil.

CONCLUSIONS

In this investigation, a MDI set at -3 cm and columns of sieved and repacked soil were used in the laboratory to measure one-dimensional infiltration in a layered soil with a clay upper layer and a loam subsoil. Even a thin layer of a little permeable soil at the surface should be expected to appreciably increase the time required by a given water volume to infiltrate. In the early stages of the process, some overlap can actually be detected between infiltration rates in the layered and the homogeneous clay soils but not between the layered and the homogeneous loam soils, regardless of the thickness of the upper layer. The presence of a coarser subsoil makes the infiltration process in the layered soil more rapid than that of the homogeneous fine soil. Two layered soils differing by the thickness of the upper layer can be expected not to differ by both the initial infiltration rate and the decay constant of the Horton infiltration model. Instead, the presence of a thicker layer at the soil surface is signalled by a lower final infiltration rate. Regardless of the thickness of the upper layer, the layered soil is expected to yield smaller infiltration parameters as compared with the homogeneous coarser soil and higher as compared with the homogeneous finer soil. If the upper layer is relatively thick, the sorptivity of the layered soil estimated by considering the complete infiltration run can be expected to coincide with that of the homogeneous fine-textured soil. A single investigation is incompatible with any general conclusion but it can be viewed as a step towards developments of an extensive experimental information that will make general conclusions possible. Other experiments should be carried out, by also considering soils that differ more from each other as compared with those of this investigation, different pressure heads established at the infiltration surface, and also including small positive pressure heads. The same experimental setup used in this investigation could be used to perform most of these additional experiments since combining the MDI with relatively small soil columns guarantees a certain cost-effectiveness of the experiment. Methodological improvements can be suggested, such as i) automatically recording the infiltration data, that could reduce the experimental efforts and the noise in the data, and ii) monitoring wetting front advancement during the run and soil water pressure head at different depths of the column, that could make physical

interpretation of the process easier and stronger. The experimental data could be used to numerically simulate infiltration and also to establish comparisons between numerical and laboratory experiments.

Funding. This study was carried out within the RETURN Extended Partnership and received funding from the European Union Next-GenerationEU (National Recovery and Resilience Plan – NRRP, Mission 4, Component 2, Investment 1.3 – D.D. 1243 2/8/2022, PE0000005).

REFERENCES

Agosta, M., Alagna, V., Bagarello, V., Caltabellotta, G., Iovino, M., Vaccaro, G., 2023. Hydrodynamic response of a loam soil after wetting with different methods. Journal of Hydrology, 623, 129770. https://doi.org/10.1016/j.jhydrol.2023.129770

Al-Maktoumi, A., Kacimov, A., Al-Ismaily, S., Al-Busaidi, H., Al-Saqri, S., 2015. Infiltration into two-layered soil: The Green–Ampt and Averyanov models revisited. Transport in Porous Media, 109, 169–193. https://doi.org/10.1007/s11242-015-0507-8

Armenise, E., Simmons, R.W., Ahn, S., Garbout, A., Doerr, S.H., Mooney, S.J., Sturrock, C.J., Ritz, K., 2018. Soil seal development under simulated rainfall: Structural, physical and hydrological dynamics. Journal of Hydrology, 556, 211–219. https://doi.org/10.1016/j.jhydrol.2017.10.073

Assouline, S., 2004. Rainfall-induced soil surface sealing: A critical review of observations, conceptual models, and solutions. Vadose Zone Journal, 3, 2, 570–591.

Assouline, S., 2013. Infiltration into soils: Conceptual approaches and solutions. Water Resources Research, 49, 1755–1772. DOI: 10.1002/wrcr.20155

Assouline, S., Mualem, Y., 2002. Infiltration during soil sealing: The effect of areal heterogeneity of soil hydraulic properties. Water Resources Research, 38, 12, 1286. https://doi.org/10.1029/2001WR001168

Assouline, S., Mualem, Y., 2006. Runoff from heterogeneous small bare catchments during soil surface sealing. Water Resources Research, 42, 12. https://doi.org/10.1029/2005WR004592

Assouline S., Narkis K., 2011. Effects of long-term irrigation with treated wastewater on the hydraulic properties of a clayey soil. Water Resources Research, 47, 8, W08530. https://doi.org/10.1029/2011WR010498

Bagarello, V., Caltabellotta, G., Iovino, M., 2022. Manual packing and soil reuse effects on determination of saturated hydraulic conductivity of a loam soil. Geoderma, 405, 115465. https://doi.org/10.1016/j.geoderma.2021.115465

Bagarello, V., Iovino, M., Lai, J., 2023. A numerical test of soil layering effects on theoretical and practical Beerkan infiltration runs. Vadose Zone Journal, 22, 6, e20283. https://doi.org/10.1002/vzj2.20283

Batsilas, I., Angelaki, A., Chalkidis, I., 2023. Hydrodynamics of the vadose zone of a layered soil column. Water, 15, 221. https://doi.org/10.3390/w15020221

Chen, C.-T., Hsu, K.-C., 2012. Use of falling-head infiltration to estimate hydraulic conductivity at various depths. Soil Science, 177, 9, 543–553.

Chen, S., Mao, X., Wang, C., 2019. A modified Green-Ampt model and parameter determination for water infiltration in fine-textured soil with coarse interlayer. Water, 11, 787. https://doi.org/10.3390/w11040787

da Silva Ribas, L.V., Coutinho, A.P., Lassabatere, L., dos Santos Neto, S.M., Lima Montenegro, S.M.G., Carvalho de Gusmão da Cunha Rabelo, A.E., Angulo-Jaramillo, R., Ribeiro Neto A., 2021. Effect of the choice of different methods on the permeable pavement hydraulic characterization and hydrological classification. Journal of Hydrology and Hydromechanics, 69, 3, 332–346. https://doi.org/10.2478/johh-2021-0018

Decagon, 2014. Minidisk Infiltrometer User's Manual. Decagon Devices, Inc., Pullman, USA, 24 p.

Di Prima, S., Concialdi P., Lassabatere, L., Angulo-Jaramillo, R., Pirastru, M., Cerdà, A., Keesstra, S., 2018. Laboratory testing of Beerkan infiltration experiments for assessing the role of soil sealing on water infiltration. Catena, 167, 373–384. https://doi.org/10.1016/j.catena.2018.05.013

Dohnal, M., Vogel, T., Dusek, J., Votrubova, J., Tesar, M., 2016. Interpretation of ponded infiltration data using numerical experiments. Journal of Hydrology and Hydromechanics, 64, 289–299.

Gao, Y., Qian, H., Li, X., Chen, J., Jia, H., 2018. Effects of lime treatment on the hydraulic conductivity and microstructure of loess. Environmental Earth Sciences, 77, 529. https://doi.org/10.1007/s12665-018-7715-9

Haverkamp, R., Ross, P.J., Smettem, K.R.J., Parlange, J.Y., 1994. Three-dimensional analysis of infiltration from the disc infiltrometer. 2. Physically-based infiltration equation. Water Resources Research, 30, 2931–2935.

Hillel, D., 1998. Environmental Soil Physics. Academic Press, 771 p. ISBN 0-12-348525-8

Horton, R.E., 1940. An approach towards a physical interpretation of infiltration capacity. Soil Science Society of America Proceedings, 5, 399–417.

Iovino, M., Abou Najm, M.R., Angulo-Jaramillo, R., Bagarello, V., Castellini, M., Concialdi, P., Di Prima, S., Lassabatere, L., Stewart, R.D., 2021. Parameterization of a comprehensive explicit model

for single ring infiltration. Journal of Hydrology, 601, 126801. https://doi.org/10.1016/j.jhydrol.2021.126801

Kalnin, T.G., Ivonin, D.A, Abrosimov, K.N., Grachev, E.A., Sorokina, N.V., 2021. Analysis of tomographic images of the soil pore space structure by integral geometry methods. Eurasian Soil Science, 54, 9, 1400–1409.

Kargas, G., Londra, P., Anastasiou, K., Kerkides, P., 2018. A note on one- and three-dimensional infiltration analysis from a mini disc infiltrometer. Water, 10, 1783. https://doi.org/10.3390/w10121783

Lassabatere, L., Angulo-Jaramillo, R., Soria Ugalde, J.M., Cuenca, R., Braud, I., Haverkamp, R., 2006. Beerkan estimation of soil transfer parameters through infiltration experiments – BEST. Soil Science Society of America Journal, 70, 521–532. https://doi.org/10.2136/sssaj2005.0026

Lassabatere, L., Angulo-Jaramillo, R., Goutaland, D., Letellier, L., Gaudet, J.P., Winiarski, T., Delolme, C., 2010. Effect of the settlement of sediments on water infiltration in two urban infiltration basins. Geoderma, 156, 316–325. https://doi.org/10.1016/j.geoderma.2010.02.031

Lewis, J., Sjöstrom, J., 2010. Optimizing the experimental design of soil columns in saturated and unsaturated transport experiments. Journal of Contaminant Hydrology, 115, 1–13.

Ma, Y., Feng, S., Zhan, H., Liu, X., Su, D., Kang, S., Song, X., 2011. Water infiltration in layered soils with air entrapment: Modified Green-Ampt model and experimental validation. Journal of Hydrologic Engineering, 16, 8, 628–638.

Minasny, B., McBratney, A.B., 2000. Estimation of sorptivity from disc-permeameter measurements. Geoderma, 95, 305–324.

Mohammadzadeh-Habili, J., Heidarpour, M., 2015. Application of the Green–Ampt model for infiltration into layered soils. Journal of Hydrology, 527, 824–832. https://doi.org/10.1016/j.jhydrol.2015.05.052

Moore, I.D., Eigel, J.D., 1981. Infiltration into two-layered soil profiles. Transactions of the ASAE, 24, 6, 1496–1503.

Moret-Fernández, D., Latorre, B., Lassabatere, L., Di Prima, S., Castellini, M., Yilmaz, D., Angulo-Jaramillo, R., 2021. Sequential infiltration analysis of infiltration curves with disc infiltrometer in layered soils. Journal of Hydrology, 600, 126542. https://doi.org/10.1016/j.jhydrol.2021.126542

Morin, J., Benyamini, Y., 1977. Rainfall infiltration into bare soils. Water Resources Research, 13, 5, 813–817. https://doi.org/10.1029/WR013i005p00813

Ndiaye, B., Esteves, M., Vandervaere, J.-P., Lapetite, J.-M., Vauclin, M., 2005. Effect of rainfall and tillage direction on the evolution of surface crusts, soil hydraulic properties and runoff generation for a sandy loam soil. Journal of Hydrology, 307, 294–311. https://doi.org/10.1016/j.jhydrol.2004.10.016

Nimmo, J.R., Akstin, K.C., 1988. Hydraulic conductivity of a sandy soil at low water content after compaction by various methods. Soil Science Society of America Journal, 52, 303–310.

Oliviera, I.B., Demond, A.H., Salehzadeh, A., 1996. Packing of sands for the production of homogeneous porous media. Soil Science Society of America Journal, 60, 49–53.

Pachepsky, Y., Karahan, G., 2022. On shapes of cumulative infiltration curves. Geoderma, 412, 115715. https://doi.org/10.1016/j.geoderma.2022.115715

Pampalone, V., Carollo, F.G., Nicosia, A., Palmeri, V., Di Stefano, C., Bagarello, V., Ferro, V., 2022. Measurement of water soil erosion at Sparacia experimental area (southern Italy): a summary of more than twenty years of scientific activity. Water, 14, 1881. https://doi.org/10.3390/w141218817

Philip, J.R., 1957. Theory of infiltration: 4. Sorptivity and algebraic infiltration equation. Soil Science, 84, 257–264.

Reynolds, W.D., Gregorich, E.G., Curnoe, W.E., 1995. Characterization of water transmission properties in tilled and untilled soils using tension infiltrometers. Soil & Tillage Research, 33, 117–131.

Shukla, M.K., Lal, R., Unkefer, P., 2003. Experimental evaluation of infiltration models for different land use and soil management systems. Soil Science, 168, 3, 178–191.

Tindall, J.A., Kunkel, J.R., Anderson, D.E., 1999. Unsaturated Zone Hydrology for Scientists and Engineers. Prentice Hall, Inc., New Jersey.

Wang, C., Mao, X., Hatano, R., 2014. Modeling ponded infiltration in fine textured soils with coarse interlayer. Soil Science Society of America Journal, 78, 745–753. https://doi.org/10.2136/sssaj2013.12.0535

Wu, L., Pan, L., Roberson, J., Shouse, P.J., 1997. Numerical evaluation of ring-infiltrometers under various soil conditions. Soil Science, 162, 11, 771–777.

Xiao, B., Sun, F., Hu, K., Kidron, G.J., 2019. Biocrusts reduce surface soil infiltrability and impede soil water infiltration under tension and ponding conditions in dryland ecosystem. Journal of Hydrology, 568, 792–802. https://doi.org/10.1016/j.jhydrol.2018.11.051

Yang, H., Rahardjo, H., Leong, E.-C., 2006. Behavior of unsaturated layered soil columns during infiltration. Journal of Hydrologic Engineering, 11, 4, 329–337. https://doi.org/10.1061/(ASCE)1084-0699(2006)11:4(329)

Yilmaz, D., Lassabatere, L., Deneele, D., Angulo-Jaramillo, R., Legret, M., 2013. Influence of carbonation on the microstructure and hydraulic properties of a basic oxygen furnace slag. Vadose Zone Journal, 12, 2. https://doi.org/10.2136/vzj2012.0121

Yilmaz, D., Lassabatere, L., Moret-Fernandez, D., Rahmati, M., Angulo-Jaramillo, R., Latorre, B., 2023. Soil-dependent β and γ shape parameters of the Haverkamp infiltration model for 3D infiltration flow. Hydrological Processes, 37, e14928. https://doi.org/10.1002/hyp.14928

Young, M.H., Karagunduz, A., Šimůnek, J., Pennell, K.D., 2002. A modified upward infiltration method for characterizing soil hydraulic properties. Soil Science Society of America Journal, 66, 57–64.

Chapter 5 – Hydrological behaviour of amended soil

5.1 Introduction

Beyond the surface-level physical modifications described in the previous chapter, soils can also undergo internal changes when amended with materials of anthropogenic origin. This phenomenon is widespread and highly variable, embracing a range of particle sizes, chemical compositions, and modes of interaction with the soil, making its understanding essential for interpreting soil structure and hydraulic behaviour (Neubert et al. 2025). Such inclusions, defined here as any solid particles or fragments that would not naturally occur within the soil profile, can significantly affect soil aggregation (Noaman et al., 2022; Sarker et al., 2022), pore connectivity, and water retention (Wang et al., 2019; Shafea et al., 2023), depending on their physical and chemical characteristics.

These foreign materials can be described and classified according to several complementary criteria, each of which provides insight into their potential impact on soil structure and hydraulic behaviour.

- *Origin*: Materials may be intentionally introduced for agronomic purposes or may arrive unintentionally as contaminants such as plastic fragments, industrial residues, or construction debris.
- *Particle size:* Coarse fragments, from gravel-sized inert material (e.g. expanded clay) to large pieces of plastic, tend to behave like structural components of the soil matrix, influencing macroporosity, preferential flow paths, and mechanical stability. Fine particles, including silt-sized industrial dust, microplastic fibers or biochar, are more likely to block pores or interfere with natural aggregation processes, thereby affecting water retention and infiltration.
- *Chemical nature:* Their composition may be predominantly organic (e.g., generic organic matter, organic amendments, plant residues) or mineral (e.g., finely ground construction waste, metal oxides, mineral fertilizers), which governs reactivity with soil minerals and with water.
- *Chemical reactivity*: Some substances are essentially chemically inert, such as many synthetic polymers or coarse mineral aggregates, while others, like compost or certain industrial products, can actively participate in soil chemical reactions, altering pH, nutrient availability, or surface charge.

These categories are not mutually exclusive in the sense that each material can be characterized according to all of them. Together, they provide a structured framework to anticipate how different

inclusions may influence pore connectivity, soil aggregation, water retention and hydraulic conductivity.

Within this framework, the two main topics addressed during the doctoral research concern the effects on soil hydrological properties arising from two contrasting forms of inputs: the unintentional incorporation of microplastics and the deliberate inclusion of organic or mineral amendments.

5.1.1 Microplastic

According to Tian et al. (2022), numerous plastics enter the environment without proper disposal ways, and 79% of total plastic waste has been deposited in landfills. Their durability and resistance to biodegradation lead plastics to persist in the environment. Owing to photodegradation, mechanical abrasion, and bioturbation, plastics can undergo fragmentation into microplastics (MPs): particles smaller than 5 mm (5000 μm), commonly classified by size as small (< 1000 μm), medium (1000–3000 μm), and large (3000–5000 μm) (Liu et al., 2018). Once considered primarily a marine pollutant, microplastic contamination is now recognized as a growing concern for terrestrial environments, including agricultural soils, groundwater, and food-production systems, with potential implications for plant growth and human and animal health (Kumar et al. 2020).

Within soils, microplastics persist because of their chemical stability and can enter through multiple pathways (Tian et al., 2022; Ren et al., 2024) such as the application of contaminated organic amendments, atmospheric deposition, irrigation with treated wastewater, surface runoff or the degradation of plastic mulching film, reported as one of the main sources of MPs in agricultural environments (Huang et al. 2020). Once incorporated, these minute polymeric particles interact with soil aggregates and pore networks, potentially modifying soil structure, water retention, and infiltration dynamics. Their ubiquity, persistence, and capacity to influence key hydraulic properties make microplastics an emerging focus of soil science and environmental research. Fig. 1 schematically illustrates the main pathways and processes governing the entry, transformation, and movement of microplastics within soil systems: microplastics enter agricultural soils through multiple routes and can undergo various physical, chemical, and biological transformations.

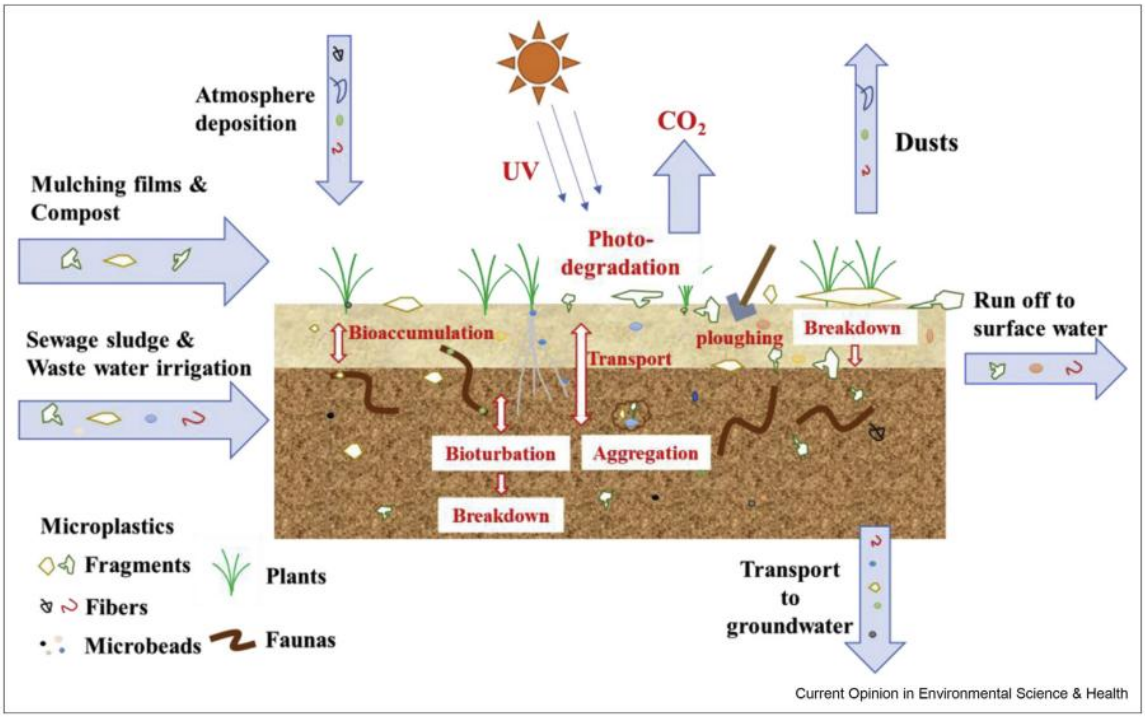

Fig.1 Pathways and processes influencing the introduction, transformation, and transport of microplastics in terrestrial environments. (Tian et al. 2022)

Variety of MPs sources in agricultural soils introduces a wide spectrum of polymer types with distinct physical and chemical characteristics. An important feature to highlight, particularly relevant because of its intrinsic link to soil hydrodynamic properties, is the interaction with water: in general, MPs are hydrophobic (e.g., polyethylene, polypropylene, polyvinyl chloride) (Prajapati et al., 2022), although they can develop hydrophilic characteristics as a result of environmental physicochemical or biological modifications, such as oxidation, exposure to sunlight, or microbial activity (Lozano et al. 2024). Another key variable influencing the interaction between microplastics and soil is particle size and shape. According to Neubert et al. (2025), medium-to-large microplastic fibers can promote the aggregation of soil particles, enhancing structural connectivity, whereas very small particles in dust-like form may instead lead to pore occlusion, potentially reducing soil permeability and altering water flow pathways. The variability of MPs effect on soil is further amplified by the soil environment itself, as the same type of MP can produce different outcomes depending on factors such as texture, mineralogy, and organic matter content. This complexity highlights the importance of investigating specific MP–soil combinations individually, given that current knowledge does not yet encompass the full spectrum of possible interactions.

In recent years, the impact of microplastics on soil hydraulic properties has received considerable attention in the scientific literature, underlining the environmental significance of this emerging issue.

Nevertheless, most existing studies have concentrated on the estimation of saturated hydraulic conductivity (Shafea et al. 2023), providing only a partial understanding of how MPs influence water dynamics in soils; on the other hand, far fewer investigations have examined hydrodynamic properties under near-saturated conditions (Maqbool et al. 2023). Building on these considerations, the study presented in this chapter was specifically designed with the objective of exploring soil–MP interactions by focusing on soils of agronomic relevance in Sicily. Two types of microplastics, each in two different size classes, along with a homogeneous mixture of both, were used to create five treatments compared with a control sample. The objective was to assess the effects of microplastics on unsaturated conductivity in the near-saturated range using the Mini Disk Infiltrometer. (MDI).

5.1.2 Agronomic amendments

In the current context, the agri-food sector faces the dual challenge of increasing productivity per unit of cultivated area while adapting to the environmental constraints imposed by climate change and the growing emphasis on sustainability. To address these challenges, farmers are called to adopt strategies that not only mitigate the adverse effects of climate variability but also ensure economic viability by either reducing production costs or enhancing yield per hectare (Lipper et al., 2014; Makate et al., 2019; Azadi et al., 2021). Among the different approaches, the improvement of soil physico-chemical properties represents a particularly effective pathway, in which the use of soil amendments plays a central role.

Soil amendments include a wide range of materials, whether natural or synthetic, mineral or organic, capable of modifying and enhancing the chemical, physical, biological, and mechanical characteristics of soils. Their application is primarily intended to improve soil structure, increase its resilience, and preserve biological fertility, thereby contributing to both short-term productivity and long-term sustainability. While the positive influence of organic and mineral amendments on soil chemistry and organic matter content is well documented (Lima et al. 2009), current knowledge remains limited regarding their effects on soil hydraulic properties, an aspect that is crucial for understanding water dynamics and optimizing resource management in agricultural systems. Accordingly, the investigations presented in this thesis focused specifically on three widely used and easily available amendments: biochar, compost, and zeolite (Ramesh et al., 2011; Martínez-Blanco et al., 2013; Schmidt et al., 2021).

In the broader framework of global efforts to promote circular economy practices, aimed at minimizing waste generation, recovering valuable resources, and fostering sustainable closed-loop systems, biochar and compost stand out as key examples. They are produced by recycling organic waste materials, such as agricultural residues, food waste, and municipal green waste, into useful products, thereby embodying the core principles of circularity while simultaneously contributing to soil management and agricultural sustainability (Yaashikaa et al., 2020). Biochar is created through pyrolysis (thermal decomposition in low oxygen), while compost is produced via aerobic decomposition (Jakobsen, 1995). These processes divert organic waste from landfills, reduce greenhouse gas emissions, and return nutrients or stable carbon to soils.

On the other hand, zeolite is a naturally occurring volcanic mineral increasingly integrated into sustainable soil management practices. Moreover, synthetic zeolites can be produced from industrial by-products, reinforcing their alignment with circular economy principles by promoting waste valorization and resource efficiency (Yoldi et al., 2019). Their use contributes to more sustainable agriculture by enhancing nutrient retention, reducing fertilizer leaching, and mitigating environmental impacts associated with intensive management. Owing to their crystalline structure, high porosity, and cation exchange capacity, zeolites improve soil chemical balance and provide long-term stability, making them a valuable amendment in both agronomic and environmental applications (Ramesh et al., 2011; Cataldo et al., 2021).

Tab 1: Origin, particle size and main properties of the amendments considered in the following papers

Amendment	Chemical nature	Average particle size	Main physico-chemical properties
Biochar	Organic (pyrolyzed biomass)	10–500 μm (up to mm–cm depending on grinding)	High specific surface area; High CEC (after oxidation/aging); Chemical stability and resistance to decomposition; Reactive surface functional groups
Compost	Organic (plant residues, manure, treated sludge)	<100 μm to >1 mm (highly heterogeneous)	Rich in stabilized organic matter; Increases CEC; Provides nutrients (N, P, K, micronutrients); Enhances soil aggregation and stability
Zeolite	Mineral (natural or synthetic)	1–50 μm (powder) to mm–cm (granules)	Microporous crystalline structure with high surface area; High CEC; Selective ion exchange capacity (e.g., NH_4^+, K^+); High mineral stability

Given their widespread use, amendments such as biochar, compost, and zeolite have been extensively studied, particularly about their physico-chemical structure and their direct beneficial effects on crop performance, as briefly summarized in Tab. 1. From this perspective, it is reasonable to hypothesize that they may also exert a positive influence on soil hydrological properties, as a consequence of the overall improvements they bring to soil structure and chemical composition.

However, such an assumption cannot be taken for granted: any potential hydrological benefit must be demonstrated through targeted research rather than presumed. Moreover, as in the case of microplastics, the magnitude and even the direction of the effects of these materials can vary depending on the specific characteristics of the soil in which they are incorporated.

The studies on amended soils presented in this chapter were developed to address these gaps, each with distinct innovative aspects. The study on microplastics is particularly relevant, being among the first to explore their effects unsaturated hydraulic conductivity. Moreover, it differs from most existing research by adopting a simplified experimental design, with fewer treatments but a larger sampling size, allowing for more robust and statistically reliable evaluation. Regarding agronomic amendments, the biochar study introduces new perspectives by examining the combined effect of the amendment and rill formation on soil hydrodynamics. The experimental design integrates

macroscopic analyses, based on infiltration tests with the MDI and measurements of the soil water retention curve, and microscopic investigations using Nuclear Magnetic Resonance (NMR), enabling a comprehensive evaluation of the processes at different scales. Finally, the work on compost and zeolite focuses on two amendments whose beneficial effects on general soil physicochemical properties are well documented, yet whose specific impact on hydrodynamic properties remains insufficiently studied.

References

Azadi, H., Moghaddam, S. M., Burkart, S., Mahmoudi, H., Van Passel, S., Kurban, A., & Lopez-Carr, D. (2021). Rethinking resilient agriculture: From climate-smart agriculture to vulnerable-smart agriculture. *Journal of Cleaner Production*, *319*, 128602.

Cataldo, E., Salvi, L., Paoli, F., Fucile, M., Masciandaro, G., Manzi, D., ... & Mattii, G. B. (2021). Application of zeolites in agriculture and other potential uses: A review. *Agronomy*, *11*(8), 1547.

Huang, Y., Liu, Q., Jia, W., Yan, C., & Wang, J. (2020). Agricultural plastic mulching as a source of microplastics in the terrestrial environment. Environmental Pollution, 260, 114096.

Jakobsen, S. T. (1995). Aerobic decomposition of organic wastes 2. Value of compost as a fertilizer. *Resources, Conservation and Recycling*, *13*(1), 57-71.

Kumar, M., Xiong, X., He, M., Tsang, D. C., Gupta, J., Khan, E., ... & Bolan, N. S. (2020). Microplastics as pollutants in agricultural soils. *Environmental Pollution*, *265*, 114980.

Lima, D. L., Santos, S. M., Scherer, H. W., Schneider, R. J., Duarte, A. C., Santos, E. B., & Esteves, V. I. (2009). Effects of organic and inorganic amendments on soil organic matter properties. *Geoderma*, *150*(1-2), 38-45.

Lipper, L., Thornton, P., Campbell, B. M., Baedeker, T., Braimoh, A., Bwalya, M., ... & Torquebiau, E. F. (2014). Climate-smart agriculture for food security. *Nature climate change*, *4*(12), 1068-1072.

Liu, M., Lu, S., Song, Y., Lei, L., Hu, J., Lv, W., ... & He, D. (2018). Microplastic and mesoplastic pollution in farmland soils in suburbs of Shanghai, China. *Environmental pollution*, *242*, 855-862.

Lozano, Y. M., Gordillo-Rocha, H., Waldman, W. R., & Rillig, M. C. (2024). Photodegradation modifies microplastic effects on soil properties and plant performance. *Journal of Applied Ecology*, *61*(1), 13-24.

Makate, C., Makate, M., Mango, N., & Siziba, S. (2019). Increasing resilience of smallholder farmers to climate change through multiple adoption of proven climate-smart agriculture innovations. Lessons from Southern Africa. *Journal of environmental management*, *231*, 858-868.

Maqbool, A., Soriano, M. A., & Gómez, J. A. (2023). Macro-and micro-plastics change soil physical properties: a systematic review. *Environmental Research Letters*, *18*(12), 123002.

Martínez-Blanco, J., Lazcano, C., Christensen, T. H., Muñoz, P., Rieradevall, J., Møller, J., ... & Boldrin, A. (2013). Compost benefits for agriculture evaluated by life cycle assessment. A review. *Agronomy for sustainable development*, *33*(4), 721-732.

Neubert, K. J., Weihermüller, L., Vereecken, H., & Brüggemann, N. (2025). Soil texture governs the influence of different microplastics on soil hydraulic properties. *Vadose Zone Journal*, *24*(5), e70044.

Noaman, M. F., Khan, M. A., & Ali, K. (2022). Effect of artificial and natural fibers on behavior of soil. *Materials Today: Proceedings*, *64*, 481-487.

Prajapati, A., Narayan Vaidya, A., & Kumar, A. R. (2022). Microplastic properties and their interaction with hydrophobic organic contaminants: a review. *Environmental Science and Pollution Research*, *29*(33), 49490-49512.

Ramesh, K., & Reddy, D. D. (2011). Zeolites and their potential uses in agriculture. *Advances in agronomy*, *113*, 219-241.

Ren, S., Wang, K., Zhang, J., Li, J., Zhang, H., Qi, R., ... & Chadwick, D. R. (2024). Potential sources and occurrence of macro-plastics and microplastics pollution in farmland soils: A typical case of China. *CritiCal reviews in environmental sCienCe and teChnology*, *54*(7), 533-556.

Sarker, T. C., Zotti, M., Fang, Y., Giannino, F., Mazzoleni, S., Bonanomi, G., ... & Chang, S. X. (2022). Soil aggregation in relation to organic amendment: a synthesis. *Journal of Soil Science and Plant Nutrition*, *22*(2), 2481-2502.

Shafea, L., Felde, V. J., Woche, S. K., Bachmann, J., & Peth, S. (2023). Microplastics effects on wettability, pore sizes and saturated hydraulic conductivity of a loess topsoil. *Geoderma*, *437*, 116566.

Schmidt, H. P., Kammann, C., Hagemann, N., Leifeld, J., Bucheli, T. D., Sánchez Monedero, M. A., & Cayuela, M. L. (2021). Biochar in agriculture–A systematic review of 26 global meta-analyses. *GCB Bioenergy*, *13*(11), 1708-1730.

Tian, L., Jinjin, C., Ji, R., Ma, Y., & Yu, X. (2022). Microplastics in agricultural soils: sources, effects, and their fate. *Current Opinion in Environmental Science & Health*, *25*, 100311.

Wang, D., Li, C., Parikh, S. J., & Scow, K. M. (2019). Impact of biochar on water retention of two. agricultural soils–A multi-scale analysis. *Geoderma*, *340*, 185-191

Yaashikaa, P. R., Kumar, P. S., Varjani, S., & Saravanan, A. J. B. R. (2020). A critical review on the biochar production techniques, characterization, stability and applications for circular bioeconomy. *Biotechnology reports*, *28*, e00570.

Yoldi, M., Fuentes-Ordoñez, E. G., Korili, S. A., & Gil, A. (2019). Zeolite synthesis from industrial wastes. *Microporous and Mesoporous materials*, *287*, 183-191.

5.2 Microplastic contamination effects on hydraulic conductivity of nearly saturated soils

Pubblished on Pedosphere, 2026, https://doi.org/10.1016/j.pedsph.2026.01.007

Ingraffia R., Amato G., Autovino D., Frenda A. S., Giambalvo D., Iovino M., Ruisi P., Zanna F., Bagarello V.

ABSTRACT

Accumulation of microplastics (MPs) in agricultural soils is an increasing environmental concern, with potential effects on soil physical and hydraulic properties. This study investigated the impact of MP contamination (concentration 0.5% w/v; incubation period 15 months) on soil hydraulic conductivity in three soil types (Alfisol, Entisol, and Vertisol). We worked at nearly-saturated conditions by applying three different water pressure heads (−6, −3, and −1 cm) and explored the influence of MP contamination by testing two polymers (low-density polyethylene, PE, and polypropylene, PP) in two shapes (fiber, film), both individually and in combination (MP-mix).

Results indicate that MP fibers, regardless of polymer type, had more pronounced effects on soil physical and hydraulic properties compared to other MP forms, though the extent of these effects varied depending on soil type. Specifically, the presence of MP fibers led to an increase in bulk density in the Vertisol, a slight increase in the Entisol (only with PE fibers), and no change in the Alfisol. Microplastic contamination generally resulted in a decrease in water content, but the intensity of this effect differed among the three soils, being most evident in the Vertisol with PE fibers and in the Alfisol with the MP mix. Additionally, the results revealed a trend of increasing hydraulic conductivity (K) in the Vertisol and Alfisol, whereas the Entisol exhibited a slight reduction, though modest in absolute terms, due to MP contamination.

These findings highlight important agro-ecological implications, as MP contamination may increase nutrient leaching while reducing water availability for crops, a critical issue in water-scarce regions like the Mediterranean.

INTRODUCTION

One of the main challenges in agricultural management is the study of the effect that human activities, directly or indirectly, have on soil physical, chemical, and biological properties (Dexter, 2004). Plastic emerges as a fundamental marker for anthropic activities with mismanagement leading to its accumulation in diverse forms in the marine and terrestrial ecosystems (Kumar et al., 2020).

Microplastic (MP) is the term used to denote small plastic particles, with sizes smaller than 5000 μm, which are further classified as small (<1000 μm), medium (1000–3000 μm) and large (3000–5000 μm) particles (Liu et al., 2018; Qi et al., 2020). Microplastic pollution is of increasing concern and has been described as one of the most important scientific issues in the field of environmental sciences and ecology, also considering that annual plastic release to the land is estimated to be 4-23 times larger than that released to the oceans (Horton et al., 2017). The origin of MP can be attributed to a variety of sources such as degradation of plastic mulch films, abrasion from vehicle tires, discharge from domestic wastewater, fragmentation of macroplastics, atmospheric pollution from urban areas to rural regions induced by wind (Kole et al., 2017; Lohr et al., 2017; Karbalaei et al., 2018). Due to this multitude of sources, MP can be identified as a wide array of polymer types and shapes such as fibers, fragments, films, pellets and flakes.

Inclusion of MP into the soil may induce alterations in its physical and hydraulic properties such as porosity, bulk density, water retention, hydraulic conductivity and water repellency (Zhang et al., 2019; Botyanszká et al., 2022; Ingraffia et al., 2022a,b; Shafea et al., 2023). The general effects of MP addition on soil properties are difficult to establish as they depend on many factors, including chemical composition and concentration of MP, shape and size of the particles, soil type and incubation duration, which often interact with each other in complex ways (Lehmann et al., 2019; Yang et al., 2021; Maqbool et al., 2023).

Soil hydraulic conductivity, K, which reflects the soil's permeability to water, is the primary soil hydrodynamic property governing water infiltration, drainage and redistribution in the soil profile (Topp et al., 1997). Soil hydraulic conductivity is also expected to influence transport of MP particles into the soil (Xing et al., 2021; Yu et al., 2021). Therefore, determining soil hydraulic conductivity in soils treated with MP has a clear hydrological, agronomic, and environmental importance.

Investigating MP addition effects on K is difficult for at least two reasons. The first reason is that K depends on the soil water content, θ, and it changes naturally by several orders of magnitude between saturation and permanent wilting point. The other reason is that the $K(\theta)$ relationship is extremely variable both within and among soil types, depending on many factors including volume, roughness, connectivity, and continuity of soil pores (Topp et al., 1997). In other words, even in the absence of

any MP addition, characterizing a field with a representative K value or a $K(\theta)$ relationship and explaining why that value or relationship was obtained is anything but simple. In this context, the need arises to establish the effects of the addition of MP on K and to explain the reasons for the observed effects.

Most of the investigations currently available provide data on the impact of MP addition on saturated soil hydraulic conductivity, K_s. In general, these investigations were carried out using repacked soil samples, predefined MP concentrations (generally in the range 0.5% to 6% w/w) and measuring K_s by constant- or falling-head laboratory permeameters. The reported results were highly variable, probably demonstrating that the scientific community cannot still draw conclusions of general validity about MP effects on K_s. For example, Xing et al. (2021), using MP particles made of low-density polyethylene, reported that the saturated hydraulic conductivity of both a silt-loam and a loamy-sand soil increased with MP concentration. A similar result was obtained by Guo et al. (2022) for a clay soil. However, these last authors also reported an inverse relationship between K_s and MP concentration for a sandy and a loam soil, particularly for MP particles of 500 μm.

Considering K_s is important since this parameter is measured under saturated conditions and gives the maximum attitude of a porous medium to transmit water. Therefore, MP addition effects are evaluated with reference to all active pores of the sampled soil. However, the size of the actually active pores cannot be specified since the same K_s value can be expressive of the presence, in the soil, of either many small pores or a few large pores (Reynolds et al., 1995).

This problem can be overcome if the unsaturated soil hydraulic conductivity corresponding to a pre-established pressure head value, h_0 (L), is considered. In this case, the Young-Laplace equation can be applied to estimate the diameter, d_{h0} (L), of the largest pores that, for a given value of h_0, are full of water and hence can be expected to participate in the transport process (Hardie et al., 2014). Pores larger than d_{h0} do not participate in water transport. Considering negative but close to zero h_0 values, i.e. in the range from saturation to −15 cm, makes it possible to exclude the effects of macropore and to assess the contribution of the soil matrix saturated hydraulic conductivity (Topp et al., 1997).

Trying to obtain information of general validity, investigations on hydraulic conductivity of unsaturated but close to saturation soils should be carried out on different porous media since, according to several experiments mainly focused on static measurements (i.e. on the experimental determination of the soil water retention curve), the effects of MP addition on soil pore size distribution can vary from soil to soil. For example, Guo et al. (2022) reported that adding MP reduced the water retention capacity more in a clay soil than in a loam and a sandy soil. Ingraffia et al. (2022a) found that polyester MP fiber contamination negatively affected macroporosity of an Alfisol but it

increased that of a Vertisol. Wang et al. (2023) concluded that the soil texture impact on the soil water retention curve was higher than those of the MP concentration and particle sizes. The lack of data on the MP effect on the unsaturated soil hydraulic conductivity is one of the significant research gaps in the list of research needs recently suggested by Maqbool et al. (2023).

The general objective of this investigation was therefore to determine the effects of MP contamination on soil hydraulic conductivity close to saturation. The specific objectives were to determine if and how these effects varied with: i) the soil type; ii) the established pressure head for the hydraulic conductivity determination; and iii) the type of MP for a fixed concentration.

MATERIALS AND METHODS

Soils and microplastic treatments

Three soils (Alfisol, Entisol, and Vertisol), widely spread in the Mediterranean area, were considered in this investigation. The soils were sampled at the beginning of January 2022 from the upper 30 cm of agricultural fields located in Sicily (Italy; Table I). After sampling, the soil was air dried and sieved at 2 mm. During sieving, it was verified that the three soils were not contaminated with meso- and/or macroplastic particles. However, analytical procedures to establish contamination with smaller plastic particles were not applied. Therefore, it cannot be excluded that the control treatments might already contain a certain amount of micro- and/or nanoplastic particles.

Soils were characterized as follows: particle size distribution, that was determined using conventional methods, and soil texture, that was classified according to the United States Department of Agriculture (USDA; Gee and Bauder, 1986); total nitrogen (TN; Kjeldahl method), total organic carbon (TOC; Walkley–Black procedure according to Nelson and Sommers, 1996), pH, saturated electrical conductivity at 25 °C (EC), and cation exchange capacity (CEC). The TOC, silt and clay contents were used to calculate the so-called structural stability index, SSI (%) (Pieri, 1992):

$$SSI = \frac{1.724\,TOC}{(silt+clay)} \times 100 \quad (1)$$

The lower the SSI value the more structurally degraded the soil is (Reynolds et al., 2009). Soil properties were listed in Table I.

Four types of MPs, encompassing two polymer types (polypropylene, PP, and low-density polyethylene, PE) and two shapes (fiber and film), were used. An additional treatment included all the four MP types at equal concentrations, i.e. a quarter of the total concentration for each MP type

(MP-mix). Both fibers were primary MPs. The PP-fiber had a diameter of 21 μm ca. and a length of nearly 3 mm. The PE-fiber had a diameter of 30 μm and a length of 1.65 mm ± 0.35. Both films (PP-film and PE-film) were obtained by manually cutting commercial macroplastics to produce secondary MPs. The obtained MPs particles were sieved through a sieve stack of 1 mm and 53 μm so that all the MPs particles used in the experiment had a size within this range.

MP particles were incorporated into the soil at a concentration of 0.5% weight on soil volume (0.05 g/cm^3). This approach was used since MP contamination in agroecosystems happens at the soil surface. Moreover, as the three soil types had different bulk density, the contamination on a volume basis allowed us to have the same amount of microplastic contamination across the three soils and therefore it allowed comparisons between soils. The MP contamination level was similar to that used in previous studies, which reported noticeable changes in the soil biophysical environment and plant response (de Souza Machado et al., 2018; Lozano et al., 2021; Ingraffia et al., 2022a,b). Moreover, Meizoso-Regueira et al. (2024) recently reported that, by year 2122, MP contamination in agricultural soils can be expected to reach a level similar to that applied in this experiment.

Soil contamination was obtained by adding the MP as a band sandwiched between two layers of soil into a laboratory blender and then mixed following the approach proposed by Ingraffia et al. (2022a,b). Microplastic contamination was determined singularly for each experimental unit. The same treatment was also applied to prepare the control samples (Ctr) for which MP was not used.

Each experimental unit consisted of a cylinder of 254 cm^3 (diameter = 6 cm; height = 9 cm) which was filled according to the dry bulk density, ρ_b, of the considered soil type, equal on average to 1.07 g/cm^3 for the Vertisol, 1.32 g/cm^3 for the Alfisol and 1.36 g/cm^3 for the Entisol. The same amount of soil was used for the Ctr and the five MP treatments within each soil type. A total of 144 experimental units, that is 3 soil types × 6 MP treatments (5 MP contaminations + Ctr) × 8 replicates, were prepared. The experimental units were then watered with distilled water to near field-capacity by capillarity, covered to ensure dark, and incubated outdoors for 15 months (from January 2022 to April 2023) within a sheltered structure that protected them from natural precipitation. Air temperature data collected from a weather station within 200 m of the experimental location are reported in Supplementary Material (Fig. S1). During the incubation period, the experimental units were watered once a week with distilled water to field-capacity by capillarity. The experimental units were re-randomized at each irrigation event.

Laboratory experiment

After incubation, the complete experimental setup was relocated to the laboratory. The hydraulic conductivity, K, for three pre-determined values of the pressure head, h_0 (h_0 = −6, −3, and −1 cm), was determined for each experimental unit by a simplified version of the Unit Hydraulic Gradient (UHG) method (Klute and Dirksen, 1986; Bagarello et al., 2007). With this approach, the same pressure head is established at the top and the base of the unit, resulting in only gravity-driven infiltration. This method requires a preliminary step, during which the experimental unit is equilibrated at the established h_0 followed by an infiltration test.

To establish a given h_0 value at the base of the units, a plastic box of 38 (length) × 17 (width) × 13 (height) cm was filled with a bed of sand and several small holes (diameter = 1 cm) were made on the walls of the box at a downward distance h_0 (L) from the surface of the sand bend. A metal net was glued to each hole to prevent sand from escaping. Water was added to the box to form a saturated zone below the holes and an unsaturated zone above them. At hydrostatic equilibrium, the soil water pressure head at the surface of the sand bed was assumed to be equal to h_0. Different boxes were prepared, depending on the considered h_0 value (h_0 = −6, −3, −1 cm). The first established pressure head was h_0 = −6 cm. The experimental units were placed on the surface of the sand box and left to equilibrate for 24-48 hours. Small volumes of water were periodically added to the box during this period to compensate for water lost due to evaporation and sample wetting, thereby maintaining the h_0 value at the surface of the sand bed constant.

A Mini-Disk Infiltrometer (MDI, METER Group, 2021), set at the same h_0 value of the sand surface, was used to induce a one-dimensional (1D) infiltration process. The MDI is a miniaturized tension infiltrometer that allows simple and rapid determination of the soil hydraulic conductivity corresponding to fixed pressure head, h_0, values in the range from nearly −1 cm to −6 cm. Therefore, the diameter of the largest pores that remain full of water during an infiltration run varies from 3000 (h_0 = −1 cm) to 500 (h_0 = −6 cm) μm. Typically, the device is used in the field to establish a three-dimensional infiltration process (Gonzalez-Sosa et al., 2010; Fodor et al., 2011; Alagna et al., 2013). However, the MDI was also used in the laboratory on soil columns to perform 1D infiltration runs (Assouline and Narkis, 2011; Kargas et al., 2018). Using the UHG method with the MDI, a given soil sample can be equilibrated at fixed, and high (close to zero), h_0 values to obtain points of the hydraulic conductivity curve close to saturation (Bagarello et al., 2007).

For each run, the MDI reservoir was filled with 90 mL of tap water. The run was considered concluded either upon complete depletion of the MDI or after reaching a maximum duration of 2 hours. Readings of the infiltrated water at the MDI reservoir were taken visually at 0.5 to 5 min time intervals,

depending on the imposed pressure head and the stage of the run. Both before and after the run, each experimental unit was weighed to then determine the gravimetric water content, w (g/g), at the considered h_0 value. The soil water content immediately before the MDI run was denoted by the w_i symbol (i = initial) whereas w_f (f = final) was used to indicate the w value at the end of the infiltration run. The samples were then subjected to the subsequent step placing them on another sand box to impose the higher h_0 value of the sequence. After the last run ($h_0 = -1$ cm), the experimental units were placed in an oven at 105°C for 24 hours to determinate the dry weight. Therefore, a total of 432 MDI runs were carried out (144 experimental units × 3 pressure heads). Moreover, for each sample, the bulk density, ρ_b (g/cm^3), of the soil columns was determined at the end of the last infiltration run ($h_0 = -1$ cm).

For each experimental unit and each pressure head value, the cumulative infiltration, I (mm), versus time, t (h), relationship obtained with the MDI was linear or nearly linear from the early stage of the run, suggesting a rapid stabilization of the flow process. Therefore, an estimate of K was obtained by considering the complete infiltration run and determining by linear regression the slope of the I vs. t relationship forced to pass through the origin of the axes. The coefficient of determination, R^2, of these relationships was > 0.99.

The gravimetric soil water content was considered in this investigation since w represents a direct measure of the amount of water in the soil.

Data analysis

Data were first explored to ensure that, according to theory, hydraulic conductivity decreased with decreasing pressure head values (i.e. $-6 < -3 < -1$ cm). Three experimental units were found to have non-conforming data and they were excluded from the dataset (one Ctr in the Alfisol, one MP-mix in the Vertisol and one PP-fiber in the Entisol).

A Tukey fences test was then performed to identify outliers in hydraulic conductivity data, using a criterion of 3 interquartile range beyond the 1st and the 3rd quartiles. The test identified five experimental units with outlier data, which were consequently removed from the dataset (one PP-fiber and one MP-mix in the Alfisol, one PE-film in the Vertisol, and one PE-fiber and one MP-mix in the Entisol). Therefore, the final dataset consisted of 408 data points for w and K (136 soil samples × 3 pressure heads) and 136 ρ_b values.

Due to violations of parametric assumptions, the aligned rank transformation (ART) was applied using the "ARTool" package (Kay et al., 2021).

Initially, the control samples were analyzed to identify possible differences between the soils in the absence of any intentional MP contamination. With this analysis, the effects of the pressure head and soil type factors and of their interaction on the four considered variables (ρ_b, w_i, w_f and K) were tested. Subsequently, a pairwise comparison between soils was carried out to obtain the p-value of the two-sided permutation t-test using the "dabestr" package (Ho et al., 2019). Then, the relationship between K and w_f was tested using the non-parametric Spearman correlation test. Finally, an analysis of the relationship between w_i and w_f was carried out and, for each soil, the regression line was compared with the identity line by calculating the 95% confidence intervals for the intercept and the slope.

To evaluate the effect of MP incorporation on the four considered response variables, a three-way ANOVA was applied by considering the three explanatory variables (pressure head, soil type, MP treatment) and their interactions. To investigate the effects of MP treatment within each soil type and pressure head, effect sizes were calculated as unpaired mean differences. Bias-corrected and accelerated bootstrapped 95% confidence intervals (CIs) between each microplastic treatment and the Ctr were generated using the "dabestr" package (Ho et al., 2019). The p-value of the two-sided permutation t-test was calculated as reported above. This combined approach was applied since there is an increasing awareness of the limitation of using only p-value statistic approach and avoiding dichotomous cutoffs (Halsey, 2019; Ho et al., 2019; Wasserstein and Lazar, 2020).

Data visualization was performed using the "tidyverse" meta-package (Wickham et al., 2019) which includes "ggplot2" (Wickham, 2016). All data analysis were conducted in R (R Core Team, 2024).

RESULTS

Control samples

The bulk density, ρ_b, data suggested a physical similarity between the Alfisol and the Entisol while the Vertisol exhibited significantly smaller values than the other two soils (Table II).

Soil type and pressure head strongly affected initial and final water content ($p < 0.001$; Table III) but their interaction did not show detectable effects ($p = 0.89$ for w_i and 0.75 for w_f). The results for w_i and w_f were quite comparable. All comparisons between the Vertisol and the other two soils revealed very strong differences (Fig. 1 and Table SI). Instead, the Alfisol and the Entisol differed significantly only at $h_0 = -6$ cm. Values of w_f greater than those of w_i were generally obtained (Fig. 2). This was a physically expected result since w_i is the water content of a soil sample in hydrostatic equilibrium, with an imposed pressure head only at the bottom. Instead, w_f is the water content of a soil sample in which both the bottom and the upper side of the sample are maintained at the same pressure head.

For each soil, the correlation between the two variables was statistically significant. According to the calculated 95% confidence intervals for the intercept and the slope (Table SII), the hypothesis that the linear regression line between w_f and w_i coincided with the identity line was rejected for the Entisol and the Alfisol but not for the Vertisol. A way to summarize this result was that, at the hydrostatic equilibrium, the upper zone of Alfisol and Entisol soil samples was perceivably drier than the bottom zone near the sand surface in the sand box. In the Vertisol, instead, vertical distribution of soil water content was more homogeneous.

For soil hydraulic conductivity, soil type and pressure head and their interaction showed a strong effect ($p < 0.001$; Table III). Variation of the mean K values with h_0 (from −1 to −6 cm; Fig. 1) depended on the soil type since it was smallest for the Alfisol (ratio between the highest and the lowest mean of $K = 2.7$), intermediate for the Entisol (ratio = 6.5) and largest for the Vertisol (ratio = 9.1). The smallest K values were obtained for the Entisol regardless of h_0 whereas the largest value was obtained for the Vertisol at the highest pressure head and the Alfisol at the two smaller h_0 values. As expected, K showed a tendency to increase as w_f increased for all soils even if data were rather scattered for all soils (Fig. 3). However, according to the Spearman correlation test this tendency was only hinted for the Alfisol, whereas the correlation between K vs. w_f was statistically significant for the Entisol and the Vertisol (Fig. 3). At $h_0 = -1$ cm the only significant difference was detected for the comparison between the Vertisol and the Entisol, with the former soil being more conductive than the latter one (Table SI). At $h_0 = -3$ cm, the Entisol had smaller values than the Alfisol and the Vertisol. At $h_0 = -6$ cm, the Alfisol had higher values than the other two soils. Differences between soils become more appreciable as h_0 decreased since the ratio between the highest and the lowest mean of K increased monotonically from 1.6 for $h_0 = -1$ cm to 2.7 for $h_0 = -6$ cm. Based on these results, it appeared that this investigation explored three soils with a different hydrodynamic response both in terms of K (Alfisol and Vertisol generally more conductive than the Entisol in the tested range of pressure heads) but also with reference to the shape of the soil hydraulic conductivity curve, that was steep for the Vertisol and became progressively flatter for the Entisol and, particularly, the Alfisol.

Microplastic contaminated soils

The bulk density, ρ_b, was affected by the presence of MP ($p = 0.003$; Table IV) and a marginally significant interaction between soil and MP was also observed ($p = 0.079$). The presence of MP determined a slight increase of ρ_b (between 0.03 and 0.05 g/cm^3) in the Vertisol (with PP fiber and PE fiber) and in the Entisol (with PE fiber) but not in the Alfisol (Fig. 4). Overall, the effect of MP fibers addition (regardless of MP type) on bulk density was more intense (on average, +3.7%

compared to the control) than both the films and the mix (on average, +0.5% and +1.6% compared to the control, respectively).

The gravimetric water content before, w_i, and after, w_f, the infiltration run was affected by all main factors in all soils ($p < 0.001$; Table IV). Moreover, a strong interaction was also observed between soil type and MP treatment ($p < 0.001$). In particular, by exploring the effects of MP within each pressure head and soil type, it was found that, in the Vertisol, only the application of PE-fiber determined a significant decrease of the water content both before and after performing the MDI run at all pressure heads (Figs. S2 and S3). In the Alfisol, a similar decrease was observed with the MP-mix. No significant effects due to MP treatment on gravimetric water content were instead observed in the Entisol.

Soil hydraulic conductivity was strongly affected by all the three main factors and interactions were observed between all factor combinations (p-values always < 0.0001; Table IV and Fig. 5). Overall, at $h_0 = -1$ cm, the presence of MPs led to an increase in hydraulic conductivity in the Alfisol and the Vertisol, compared to their controls. Conversely, in the Entisol, the effects were consistently diminishing. In all three soils, these effects were particularly pronounced in the MP-mix treatment with differences from the controls of +53.9, +23.9, and −8.63 mm h^{-1} for the Vertisol, the Alfisol, and the Entisol, respectively. At smaller pressure heads (−3 and −6 cm), the intensity of the MPs' effect was generally reduced, and the differences from the controls were almost always non-significant.

Soil contamination with MP made the correlation between K and w_f significant even with reference to the Alfisol (Fig. 6) but it did not have any effect on the circumstance, already noticed in the absence of MP (Fig. 3), that the K vs. w_f relationships differed widely between the Vertisol on one side and the Alfisol and the Entisol on the other side. In particular, both in the case of a soil treated with MP and in that of an untreated soil, a given K value was detected in appreciably wetter soil conditions for the Vertisol than the Alfisol and the Entisol.

In the Vertisol, w_i and w_f decreased at all considered pressure heads by adding PE-fiber (Figs. S2 and S3), but K was not affected by PE-fiber addition (Fig. 5). Hydraulic conductivity increased at $h_0 = -1$ cm with the MP-mix treatment and at $h_0 = -6$ cm with the PP-film but neither w_i nor w_f changed as a consequence of MP addition in these two cases. In all the other cases, w_i, w_f and K did not change as a consequence of the MP treatment. Therefore, adding MP determined a decrease of w that did not influence K or it induced an increase of K without influencing w. However, these results were only obtained in a few cases. Instead, the most common result was that w_i, w_f and K did not change with the MP treatment. In particular, an ineffectiveness of the MP treatment was detected for 12 (w_i and w_f) and 13 (K) of the 15 established comparisons.

In the Alfisol, the addition of the mixture of the four types of MP (MP-mix), determined a decrease of both w_i and w_f for all considered pressure heads while the other MP types did not influence either w_i nor w_f. Adding any type of MP did not modify the K values in the more unsaturated soil conditions ($h_0 = -3$ and -6 cm) but it determined an increase of K at $h_0 = -1$ cm with a single exception (PP-film). Even for this soil, the most common result was that MP addition did not influence w_i, w_f and K since a similarity between treated and non-treated soils was detected for 12 (w_i and w_f) and 11 (K) comparisons.

Finally, the Entisol was insensitive to MP addition with reference to all tested variables and pressure heads. In other words, none of the comparisons suggested statistically significant differences between the treated soil and the control.

DISCUSSION

In this experiment, the effects of MP addition were tested in three soils (namely a Vertisol, an Alfisol, and an Entisol) differing for their physical and hydraulic properties, which provides an optimal condition for testing how and to what extent the effects of this treatment may vary depending on the characteristics of the porous medium in which it is applied. Specifically, the Vertisol was less compacted (Table II), exhibited a steeper hydraulic conductivity curve (Fig. 1), and required a higher water content to yield a given K value (Fig. 3) compared to the Alfisol and the Entisol. The Entisol, compared to the Alfisol, generally exhibited lower water content and hydraulic conductivity.

As a preliminary remark, it should be highlighted that the effects of MP contamination on the physical and hydraulic properties of the soils investigated here were generally of a small magnitude in absolute terms. This could have been due, at least in part, to our level of MP contamination (0.5% w/v), which was chosen to represent a plausible future scenario (Meizoso-Regueira et al., 2024), whereas in other studies, much higher contamination levels have been evaluated (Xing et al., 2021; Botyanskzá et al., 2022; Shafea et al., 2023; Wang et al., 2023; Xie et al., 2023). As highlighted by many authors, the magnitude of the MP effects can be expected to be greater as the amount of contaminant in the soil increases (e.g., Maqbool et al., 2023; Wang et al., 2023; Feng et al., 2025).

Although of modest magnitude, some effects, noteworthy for their agro-environmental implications, were however observed because of soil contamination with MPs. In accordance with the results by de Souza Machado et al. (2019) and Lehmann et al. (2021), MP fibers (irrespective of MP type) had more pronounced effects on soil bulk density compared to both MP films and mix (Fig. 4) and the response to MP addition was different for the three studied soils. Specifically, the presence of MP fibers (both PP and PE) determined an increase in the soil bulk density in the Vertisol, a slight increase

in the Entisol (only with PE fiber), and it had no effects in the Alfisol. The available literature on the impact of MP fibers on soil bulk density is limited and often inconsistent. For example, de Souza Machado et al. (2018, 2019) reported a decrease in bulk density in a loamy-sand soil with increasing concentrations of polyester MP fibers, whereas Zhang et al. (2019), in a study conducted on a clay-loam soil under both field and greenhouse conditions, observed no significant differences in soil bulk density. Furthermore, our findings partially differed from those reported by Ingraffia et al. (2022a) who, in a study involving the same soils used in the present experiment contaminated with polyester MPs fibers, observed significant reductions in soil bulk density in Vertisol, modest decreases in Entisol, and no effects in Alfisol. This discrepancy may be attributed to the different types of MPs used (PP and PE in this experiment vs. polyester in Ingraffia et al., 2022a) and the duration of the incubation (15 vs. 6 months). These observations suggest that the effects of MPs on soil are highly context-dependent, with multiple factors influencing the outcomes, acting individually and interacting, including soil, MPs type, concentration, and shape, incubation time, and experimental methodology.

A general decrease in water content (w_i and w_f) occurred due to MPs contamination (Fig. S2 and S3) but the intensity of these effects was different across the three investigated soils and, specifically, more evident in the Vertisol with the PE fibers and in the Alfisol with the MP mix. Furthermore, the results showed a trend toward an increase of K in Vertisol and in Alfisol, while, in contrast, the Entisol experienced a reduction, though modest in absolute terms, due to the presence of MPs (Fig. 5). In theory, the presence of MPs, by partially occupying the macropores and consequently reducing their lumen, should negatively affect soil water movement, as suggested by Guo et al. (2022) and Feng et al. (2025). This should also lead to a reduction in water content at saturation, which seems to be confirmed by the w values (both w_i and w_f) observed in our study. On the other hand, such effects may have been counterbalanced in the present experiment by both a high hydrophobicity of MPs (Xing et al., 2021,2024; Cramer et al., 2023; Yu et al., 2023) and the structural changes they induced in the soil, which could affect the tortuosity of flow paths; both these factors may have contributed to an increase in hydraulic conductivity. The differences observed in K values across the three soils investigated may depend, in some way, on the impact that MPs contamination can have on soil structure, which can vary significantly depending on soil characteristics, as previously highlighted by Ingraffia et al. (2022a). All this reinforces our belief that MPs impact the soil's full functionality, and that the extent of this impact is soil-dependent. Guo et al. (2022) showed that the addition of MPs to three different soils (specifically a loam, a clay, and a sandy soil) resulted in highly diversified effects on saturated soil hydraulic conductivity, depending on the soil type as well as the concentrations and

sizes of the added MPs. The same authors observed great reductions in hydraulic conductivity in the sandy soil (94% sand), while in the loam soil a slight increase in *K* values was found at 0.5% MPs concentration (the same used in the present study). This result further confirms how the type and extent of interactions between soil particles and MPs particles can differently affect various soil properties. In this regard, an important role may be played by the amount and type of clay and the soil organic matter content. Therefore, the greater response in terms of hydraulic conductivity observed in the present study in the Vertisol can be attributed both to its higher clay content (compared to the other two soils investigated) and to the mineralogy of the clay itself. It is in fact well known that montmorillonite, which dominates in Vertisol and is characterized by its expandable nature and high surface area, is considerably more reactive than kaolinite and illite, which instead dominate in the Alfisol and the Entisol, respectively. In support of this hypothesis, Ingraffia et al. (2022a) highlighted that MPs contamination led to a modest increase in newly formed stable aggregates in Vertisol, with no effect observed in Alfisol and Entisol. Additionally, the different content in soil organic matter, which provides essential binding sites for MP particles and influences both the formation and stability of aggregates in MP-contaminated soil (Liang et al., 2021; Ingraffia et al., 2022a), may help to explain the different results obtained in the present study in terms of hydraulic conductivity. In fact, the reactivity to the addition of MPs, different among the three soils investigated, appeared to some extent positively correlated with the soil organic matter content (Vertisol > Alfisol > Entisol).

Finally, it is interesting to highlight that the magnitude of response to MPs contamination appeared to increase with increasing SSI values (Table I). This index, which is calculated based on the soil organic carbon content and soil texture, does not directly relate to the porosity aspects of soil structure, but rather to the "resilience" of the soil structure (Reynolds et al., 2009). A reduction in SSI value indicates an increase in soil degradation. In the present study, SSI values were, in order, Vertisol > Alfisol > Entisol, which therefore seems to indicate that the effects of MP contamination on soil hydraulic properties are more intense in less degraded soils. Over the 15-month incubation, MPs likely exploited the very mechanisms underpinning soil stability, such as organic-mineral interactions and pore networks, revealing that even resilient soils, i.e. those with relatively higher SSI values, remain vulnerable to these emerging contaminants, which directly target soil's structural foundations.

CONCLUSIONS

The results of the present study, conducted on agricultural soils with varying chemical-physical properties and utilizing extended incubation periods (thus allowing for the establishment of stable

interactions between soil particles and MPs), demonstrate that the impact of MP contamination on soil is influenced by the shape of the MPs. Fibers, regardless of MP type, produced more pronounced effects compared to films and MP mixtures, altering water movement by increasing water infiltration and decreasing water retention. Additionally, the intensity of these effects varied across different soil types, being most pronounced in soils with higher clay and organic carbon content. Under these conditions, MP particles probably form stronger bonds with soil particles, leading to more significant alterations in soil water movements. Further research is necessary to elucidate the mechanisms underlying this response since understanding how MPs influence soil processes can help inform sustainable agricultural practices and policies.

These findings have significant agro-ecological implications, suggesting that MP contamination could enhance nutrient loss through leaching while at the same time reduce water availability for crops. This latter aspect is especially critical in the Mediterranean region, where water scarcity is often the primary constraint on crop productivity. Finally, it cannot be ruled out that the effects observed in this study due to soil contamination with MPs at the concentration used (0.5% w/v) may become more pronounced if, as many authors suggest, MP levels in the soil continue to rise in the future.

DECLARATION OF COMPETING INTEREST

The authors declare that they have no known competing financial interests or personal relationships that could have appeared to influence the work reported in this paper

References:

Alagna V, Bagarello V, Di Prima S, Giordano G, Iovino M. 2013. A simple field method to measure the hydrodynamic properties of soil surface crust. *J Agric Eng*. 44: e14.

Assouline S, Narkis K. 2011. Effects of long-term irrigation with treated wastewater on the hydraulic properties of a clayey soil. *Water Resour Res*. 47: W08530.

Bagarello V, Castellini M, Iovino M. 2007. Comparison of unconfined and confined unsaturated hydraulic conductivity. *Geoderma*. 137: 394–400.

Botyanszká L, Šurda P, Vitková J, Lichner L, Igaz D. 2022. Effect of microplastics on silty loam soil properties and radish growth. *J Hydrol Hydromech*. 70: 321–329.

Cramer A, Benard P, Zarebanadkouki M, Kaestner A, Carminati A. 2023. Microplastic induces soil water repellency and limits capillary flow. *Vadose Zone J.* 22(1): e20215.

Dexter AR. 2004. Soil physical quality: Part I. Theory, effects of soil texture, density, and organic matter, and effects on root growth. *Geoderma*. 120: 201–214.

Feng H, Xing X, Du J, Jiao S, Yu M, Wang W. 2025. Concentration- and size-dependent influences of microplastics on soil hydraulic properties and water flow. *Eur J Soil Sci.* 76(1): e70049.

Fodor N, Sándor R, Orfanus T, Lichner L, Rajkai K. 2011. Evaluation method dependency of measured saturated hydraulic conductivity. *Geoderma*. 165: 60–68.

Gee GW, Bauder JW. 1986. Particle-size analysis. *In* Klute A (ed.), Methods of Soil Analysis, Part 1: Physical and Mineralogical Methods. pp. 383–411.

Gonzalez-Sosa E, Braud I, Dehotin J, Lassabatère L, Angulo-Jaramillo R, Lagouy M, Branger F, Jacqueminet C, Kermadi S, Michel K. 2010. Impact of land use on the hydraulic properties of the topsoil in a small French catchment. *Hydrol Process*. 24: 2382–2399.

Guo ZQ, Li P, Yang XM, Wang ZH, Lu BB, Chen WJ, Wu Y, Li GW, Zhao ZW, Liu GB, Ritsema C, Geissen V, Xue S. 2022. Soil texture is an important factor determining how microplastics affect soil hydraulic characteristics. *Environ Int*. 165: 107293.

Halsey LG. 2019. The reign of the *p*-value is over: What alternative analyses could we employ to fill the power vacuum? *Biol Lett*. 15: 20190174.

Hardie M, Clothier B, Bound S, Oliver G, Close D. 2014. Does biochar influence soil physical properties and soil water availability? *Plant Soil*. 376: 347–361.

Ho J, Tumkaya T, Aryal S, Choi H, Claridge-Chang A. 2019. Moving beyond *P* values: data analysis with estimation graphics. *Nat Methods*. 16: 565–566.

Horton AA, Walton A, Spurgeon DJ, Lahive E, Svendsen C. 2017. Microplastics in freshwater and terrestrial environments: Evaluating the current understanding to identify the knowledge gaps and future research priorities. *Sci Total Environ*. 586: 127–141.

Ingraffia R, Amato G, Bagarello V, Carollo FG, Giambalvo D, Iovino M, Lehmann A, Rillig MC, Frenda AS. 2022a. Polyester microplastic fibers affect soil physical properties and erosion as a function of soil type. *SOIL*. 8: 421–435.

Ingraffia R, Amato G, Iovino M, Rillig MC, Giambalvo D, Frenda AS. 2022b. Polyester microplastic fibers in soil increase nitrogen loss via leaching and decrease plant biomass production and N uptake. *Environ Res Lett*. 17: 054012.

Karbalaei S, Hanachi P, Walker TR, Cole M. 2018. Occurrence, sources, human health impacts and mitigation of microplastic pollution. *Environ Sci Pollut Res*. 25: 36046–36063.

Kargas G, Londra P, Anastasiou K, Kerkides P. 2018. A note on one- and three-dimensional infiltration analysis from a mini disc infiltrometer. *Water (Switzerland)*. 10: 1783.

Kay M, Elkin L, Higgins J, Wobbrock J. 2021. ARTool: Aligned Rank Transform for Nonparametric Factorial ANOVAs.

Klute A, Dirksen C. 1986. Hydraulic conductivity and diffusivity: Laboratory methods. Methods of Soil Analysis, Part 1: Physical and Mineralogical Methods, 2nd edn. Madison, WI, American Society of Agronomy. pp. 687–734.

Kole PJ, Löhr AJ, Van Belleghem FGAJ, Ragas AMJ. 2017. Wear and tear of tyres: A stealthy source of microplastics in the environment. *Int J Environ Res Public Health*. 14: 1265.

Kumar M, Xiong X, He M, Tsang DCW, Gupta J, Khan E, Harrad S, Hou D, Ok YS, Bolan NS 2020. Microplastics as pollutants in agricultural soils. *Environ Pollut.* 265: 114980.

Lehmann A, Fitschen K, Rillig MC. 2019. Abiotic and biotic factors influencing the effect of microplastic on soil aggregation. *Soil Syst*. 3: 21.

Löhr A, Savelli H, Beunen R, Kalz M, Ragas A, Van Belleghem F. 2017. Solutions for global marine litter pollution. *Curr Opin Environ Sustain*. 28: 90–99.

Lozano YM, Lehnert T, Linck LT, Lehmann A, Rillig MC. 2021. Microplastic shape, polymer type, and concentration affect soil properties and plant biomass. *Front Plant Sci*. 12: 616645.

de Souza Machado AA, Lau CW, Kloas W, Bergmann J, Bachelier JB, Faltin E, Becker R, Görlich AS, Rillig MC. 2019. Microplastics can change soil properties and affect plant performance. *Environ Sci Technol*. 53: 6044–6052.

de Souza Machado AA, Lau CW, Till J, Kloas W, Lehmann A, Becker R, Rillig MC. 2018. Impacts of microplastics on the soil biophysical environment. *Environ Sci Technol*. 52: 9656–9665.

Maqbool A, Soriano MA, Gómez JA. 2023. Macro- and micro-plastics change soil physical properties: a systematic review. *Environ Res Lett*. 12: 123002.

Meizoso-Regueira T, Fuentes J, Cusworth SJ, Rillig MC. 2024. Prediction of future microplastic accumulation in agricultural soils. *Environ Pollut*. 359: 124587.

METER Group. 2021. Mini Disk Infiltrometer Manual. Pullman, WA, METER Group.

Nelson DW, Sommers LE. 1996. Total Carbon, Organic Carbon, and Organic Matter. *In* Sparks DL, Page AL, Helmke PA, Loeppert RH (eds.), Methods of Soil Analysis. Part 3. Chemical Methods. Madison, WI, SSSA and ASA. pp. 961–1010.

Pieri CJMG. 1992. Fertility of Soils- A Future for Farming in the West African Savannah. Berlin, Springer-Verlag.

R Core Team. 2024. R: A Language and Environment for Statistical Computing. R Foundation for Statistical Computing. Computing. Available online at https://www.R-project.org/ (accessed January 31, 2025).

Reynolds WD, Drury CF, Tan CS, Fox CA, Yang XM. 2009. Use of indicators and pore volume-function characteristics to quantify soil physical quality. *Geoderma*. 152: 252–263.

Reynolds WD, Gregorich EG, Curnoe WE. 1995. Characterisation of water transmission properties in tilled and untilled soils using tension infiltrometers. *Soil Tillage Res*. 33: 117–131.

Shafea L, Yap J, Beriot N, Felde VJMNL, Okoffo ED, Enyoh CE, Peth S. 2023. Microplastics in agroecosystems: A review of effects on soil biota and key soil functions. *J Plant Nutr Soil Sci*. 186: 5–22.

Topp GC, Reynolds WD, Cook FJ, Kirby JM, Carter MR. 1997. Chapter 2 Physical attributes of soil quality. *Developments in Soil Science*. 25: 21–58.

Wang Y, Ma R, Zhu G. 2023. Representation of the influence of soil structure on hydraulic conductivity prediction. *J Hydrol*. 619: 129330.

Wasserstein RL, Lazar NA, Gruber CW. 2020. ASA Statement on Statistical Significance and *p*-Values. *In* Gruber CW (ed.), The Theory of Statistics in Psychology: Applications, Use and Misunderstandings, 16 16. Switzerland, Springer International Publishing AG. pp. 1–10.

Watson KW, Luxmoore RJ. 1986. Estimating macroporosity in a forest watershed by use of a tension infiltrometer. *Soil Sci Soc Am J*. 50: 578–582.

Wickham H, Averick M, Bryan J, Chang W, McGowan L, François R, Grolemund G, Hayes A, Henry L, Hester J, Kuhn M, Pedersen T, Miller E, Bache S, Müller K, Ooms J, Robinson D, Seidel D, Spinu V, Takahashi K, Vaughan D, Wilke C, Woo K, Yutani H. 2019. Welcome to the Tidyverse. *J Open Source Softw*. 4: 1686.

Wickham H, Chang W, Henry L, Lin-Pedersen T. 2016. Package "ggplot2" Elegant Graphics for Data Analysis.

Xie X, Zhou H, Wu L, Man J. 2024. Numerical modeling of double-ring infiltrometers for determining saturated hydraulic conductivity in heterogeneous and anisotropic soils. *Pedosphere*. 34: 1111–1122.

Xing X, Jing X, Zhao F, Jiao S, Su L, Yu M, Zhao L. 2024. Dry-wet alternation and microplastics particle size effects on and contributions to soil water and soil pore properties. *Eur J Soil Sci.* 75(3): e13522.

Xing X, Yu M, Xia T, Ma L. 2021. Interactions between water flow and microplastics in silt loam and loamy sand. *Soil Sci Soc Am J*. 85: 1956–1962.

Yang J, Li R, Zhou Q, Li L, Li Y, Tu C, Zhao X, Xiong K, Christie P, Luo Y. 2021. Abundance and morphology of microplastics in an agricultural soil following long-term repeated application of pig manure. *Environ Pollut*. 272: 116028.

Yu Y, Battu AK, Varga T, Denny AC, Zahid TM, Chowdhury I, Flury M. 2023. Minimal impacts of microplastics on soil physical properties under environmentally relevant concentrations. *Environ Sci Technol.* 57(13): 5296–5304.

Yu Y, Flury M. 2021. Current understanding of subsurface transport of micro- and nanoplastics in soil. *Vadose Zone J.* 20: e20108.

Zhang GS, Zhang FX, Li XT. 2019. Effects of polyester microfibers on soil physical properties: Perception from a field and a pot experiment. *Sci Total Environ*. 670: 1–7.

Table I. Some physical and chemical properties of the three soils used in the experiment.

Soil type	USDA classification	Site coordinates	Clay	Silt	Sand	TN	TOC	pH	EC	CEC	SSI
				g kg^{-1}		g kg^{-1}	g kg^{-1}		dS m^{-1}	cmol kg^{-1}	%
Alfisol	Typic Rhodoxeralf	37.643511° N 12.628327° E	152	431	417	0.77	11.2	7.58	2.01	13.8	3.31
Entisol	Typic Xerorthent	37.561368° N 13.512904° E	209	461	330	1.20	9.3	7.84	1.88	18.4	2.38
Vertisol	Typic Haploxerert	37.556140° N 13.515400° E	415	357	228	1.54	15.8	7.74	1.89	30.0	3.52

Clay, silt, and sand were classified according to the United States Department of Agriculture (USDA; clay < 2 μm, silt 2–50 μm, and sand 50–2000 μm). TN is total nitrogen, TOC is total organic carbon, EC is electrical conductivity, and CEC is cation exchange capacity.

Table II. Mean values ± standard error of soil bulk density (g cm^{-3}) in the three soils used in the experiment with no addition of microplastics (control samples). The *p*-values for pairwise comparisons and estimated 95% confidence intervals (in square brackets) are also reported.

Soil type	Mean ± SE	Comparison	Difference [95% CI]	*p*-value
Alfisol	1.31 ± 0.03	Alfisol *vs.* Entisol	–0.04 [–0.11; 0.00]	0.178
Entisol	1.35 ± 0.01	Alfisol *vs.* Vertisol	0.26 [0.18; 0.33]	<0.001
Vertisol	1.04 ± 0.02	Vertisol *vs.* Entisol	–0.31 [–0.36; –0.27]	<0.001

Table III. Analysis of variance: the *p*-values for the effects of the applied treatments (Soil type, Pressure head, and their interaction) on some traits (w_i, initial soil water content; w_f, final soil water content; K, soil hydraulic conductivity) measured in the three soils used in the experiment with no addition of microplastics (control samples).

Treatment	Traits		
	w_i	w_f	K
Soil type (S)	<0.001	<0.001	<0.001
Pressure head (P)	<0.001	<0.001	<0.001
S × P	0.890	0.750	<0.001

Table IV. Analysis of variance: the F-values and *p*-values for the effects of the applied treatments (Soil type, Pressure head, Microplastic addition, and their interaction) on some traits (bulk density; w_i, initial soil water content; w_f, final soil water content; K, soil hydraulic conductivity) measured in the three soils used in the experiment.

Treatment	Bulk density			w_i			w_f		K	
	df	F-value	*p*-value	df	F-value	*p*-value	F-value	*p*-value	F-value	*p*-value
Soil type (S)	2	177.91	<0.001	2	378.44	<0.001	370.91	<0.001	117.31	<0.001
Pressure head (P)	–	–	–	2	137.56	<0.001	140.38	<0.001	324.69	<0.001
Microplastic (MP)	5	3.82	0.003	5	15.24	<0.001	14.39	<0.001	11.67	<0.001
S × P	–	–	–	4	0.74	0.559	1.78	0.133	44.14	<0.001
S × MP	10	1.74	0.079	10	5.54	<0.001	6.18	<0.001	6.72	<0.001
P × MP	–	–	–	10	0.53	0.866	0.14	0.999	6.00	<0.001
S × P × MP	–	–	–	20	0.25	0.999	0.42	0.986	3.21	<0.001

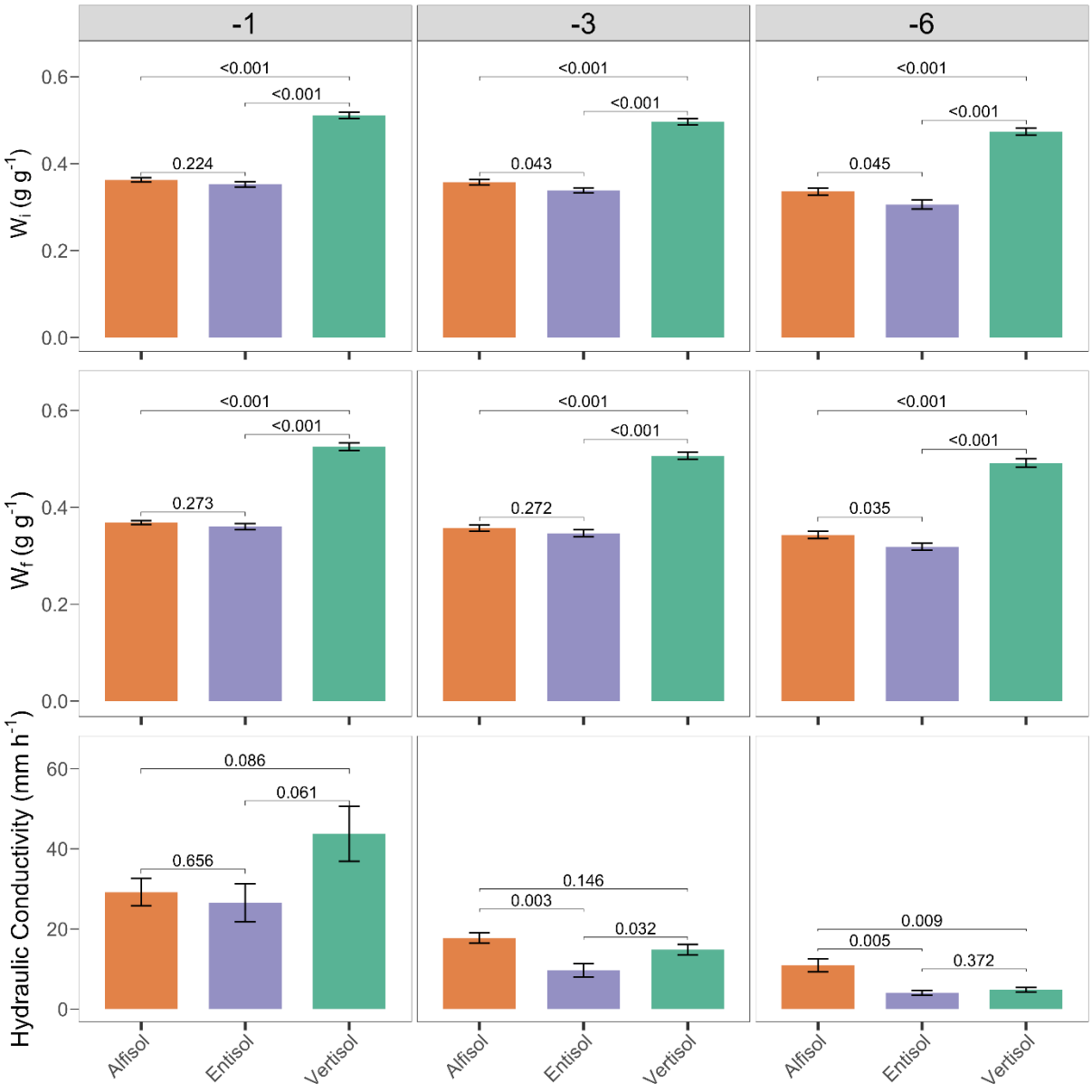

Fig. 1. Initial (w_i) and final (w_f) soil water content, and soil hydraulic conductivity (K) for three pre-established pressure heads (h_0 = −1, −3, and −6 cm) measured in the three soils used in the experiment with no addition of microplastics (control samples). Bars depict the mean values ± standard errors. The p-values for pairwise comparisons are reported in the plots.

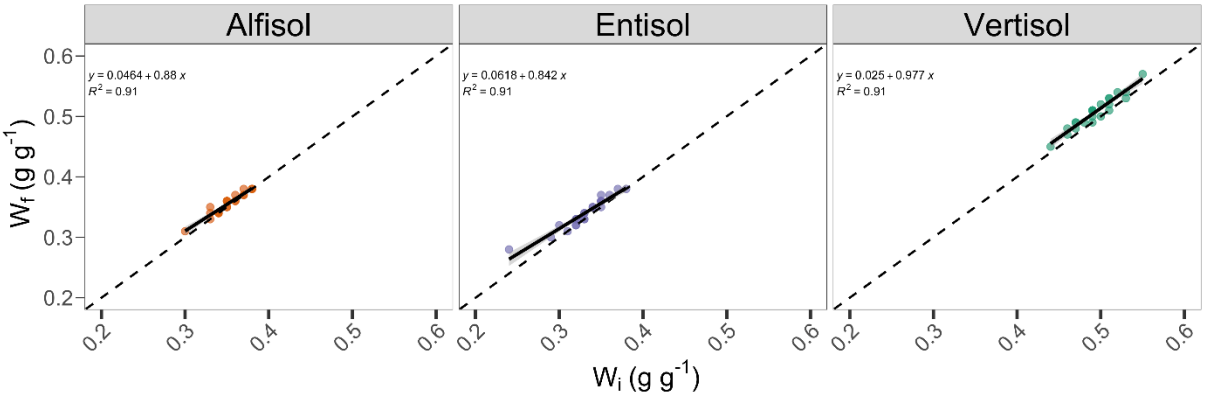

Fig. 2. Relationships between initial (w_i) and final (w_f) soil water content in the three soils used in the experiment with no addition of microplastics (control samples).

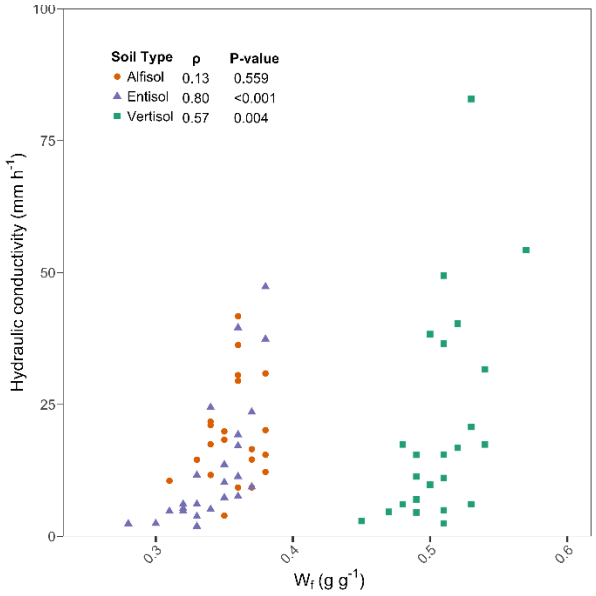

Fig. 3. Relationships between final soil water content (w_f) and soil hydraulic conductivity in the three soils used in the experiment with no addition of microplastics (control samples). The non-parametric Spearman correlation coefficient (ρ) and the *p*-values are reported in the plot.

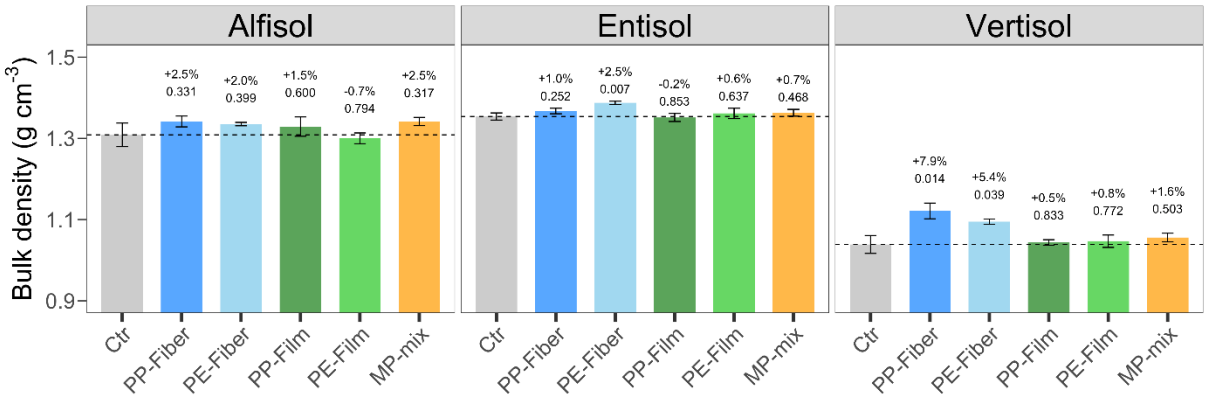

Fig. 4. Soil bulk density measured in the three soils used in the experiment not contaminated (Ctr) and contaminated with microplastics. Bars depict the mean values ± standard errors. PP-Fiber and PP-film are polypropylene fibers and film, respectively; PE-fiber and PE-Film are low-density polyethylene fibers and film, respectively; MP-mix is the mixture of the four types of microplastics. The percentage variation with respect to the Ctr and the *p*-values of two-sided permutation test between each microplastic treatment and the Ctr for each soil type are reported in the plots.

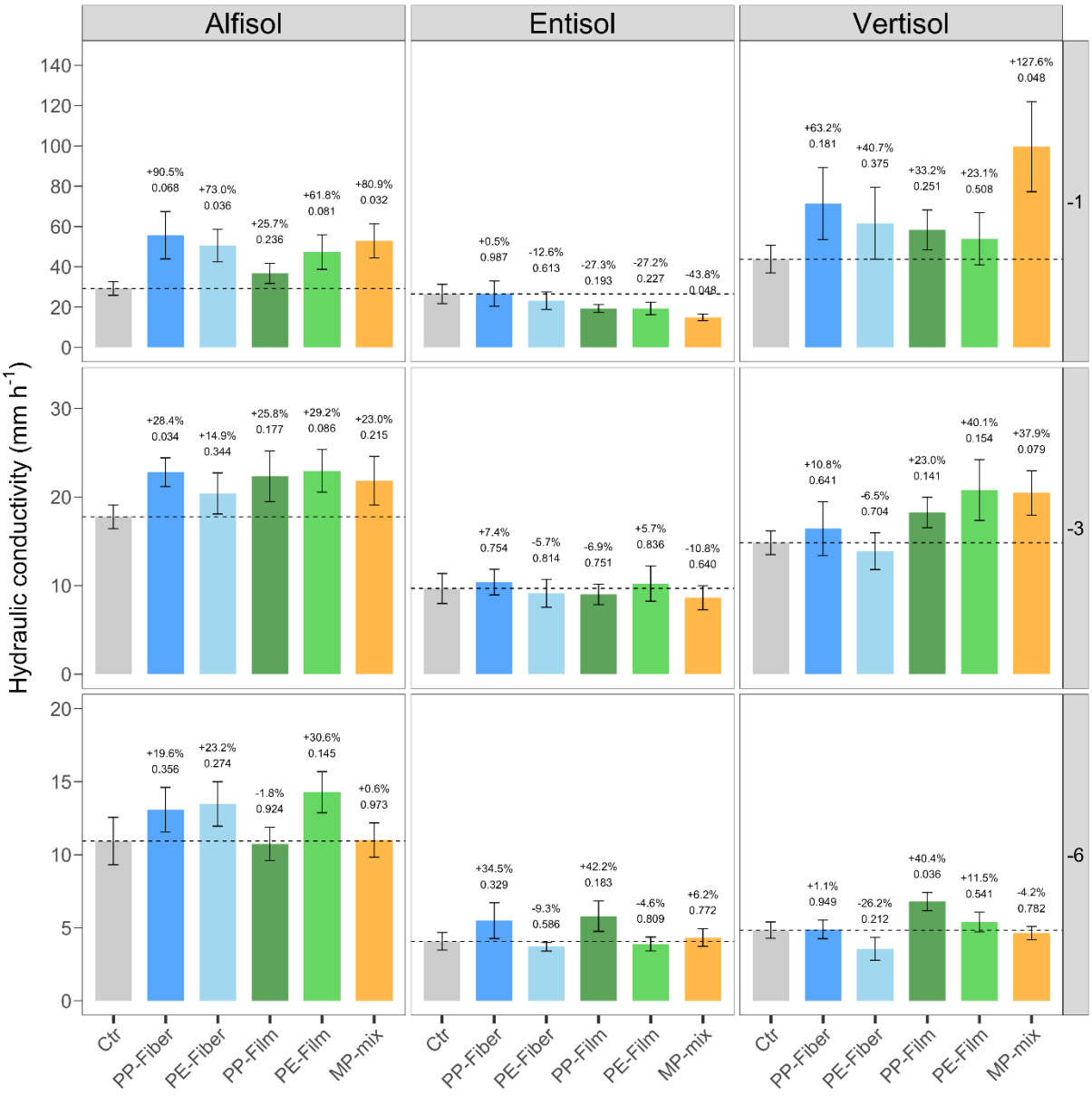

Fig. 5. Soil hydraulic conductivity measured for three pre-established pressure heads ($h_0 = -1$, -3, and -6 cm) in the three soils used in the experiment not contaminated (Ctr) and contaminated with microplastics. Bars depict the mean values ± standard errors. PP-Fiber and PP-film are polypropylene fibers and film, respectively; PE-fiber and PE-Film are low-density polyethylene fibers and film, respectively; MP-mix is the mixture of the four types of microplastics. The percentage variation with respect to the Ctr and the *p*-values of two-sided permutation test between each microplastic treatment and the Ctr for each soil type are reported in the plots.

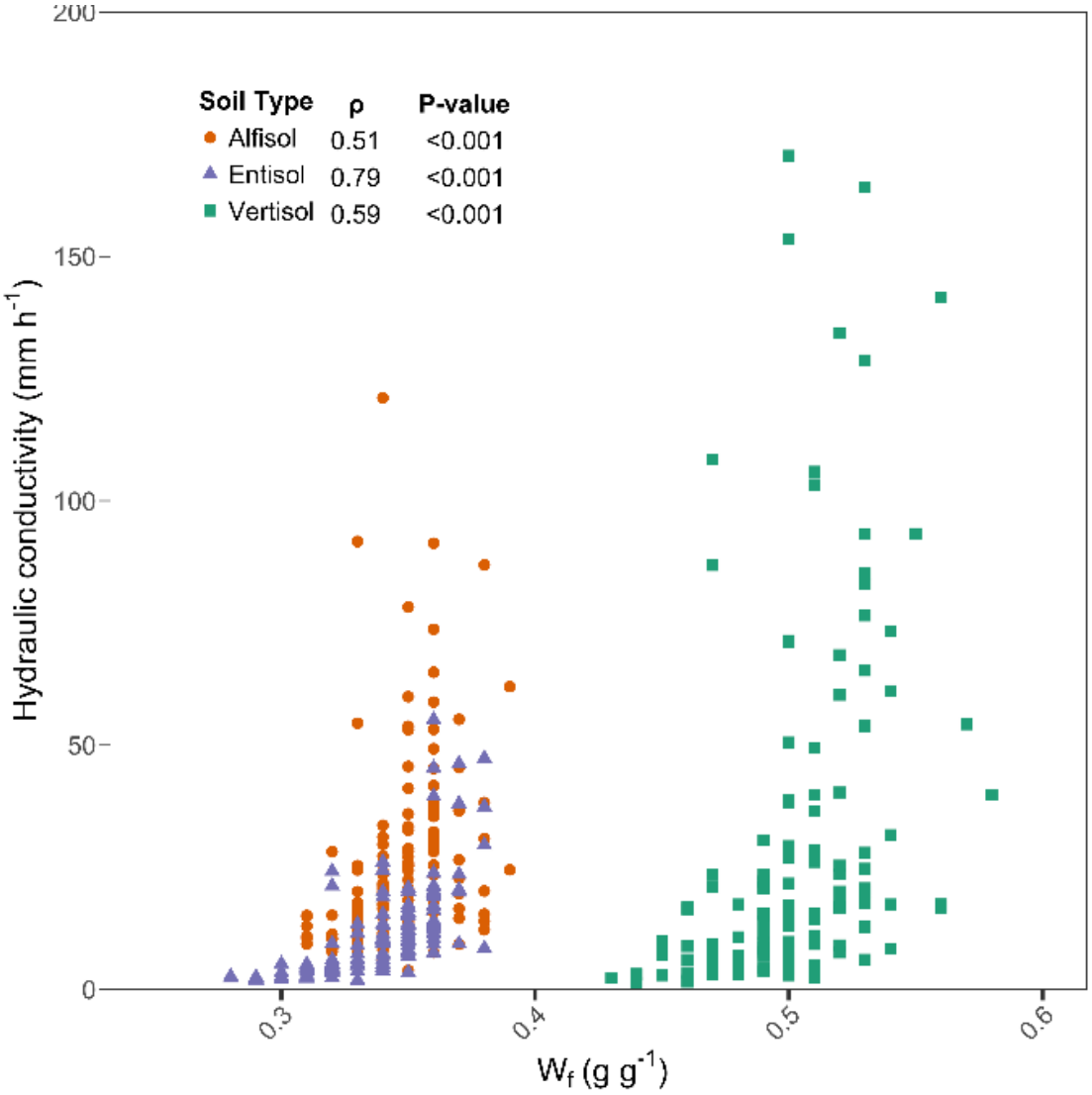

Fig. 6. Relationships between final soil water content (w_f) and soil hydraulic conductivity in the three soils used in the experiment considering all samples (with and without the addition of microplastics). The non-parametric Spearman correlation coefficient (ρ) and the *p*-values are reported in the plot.

SUPPLEMENTARY MATERIAL

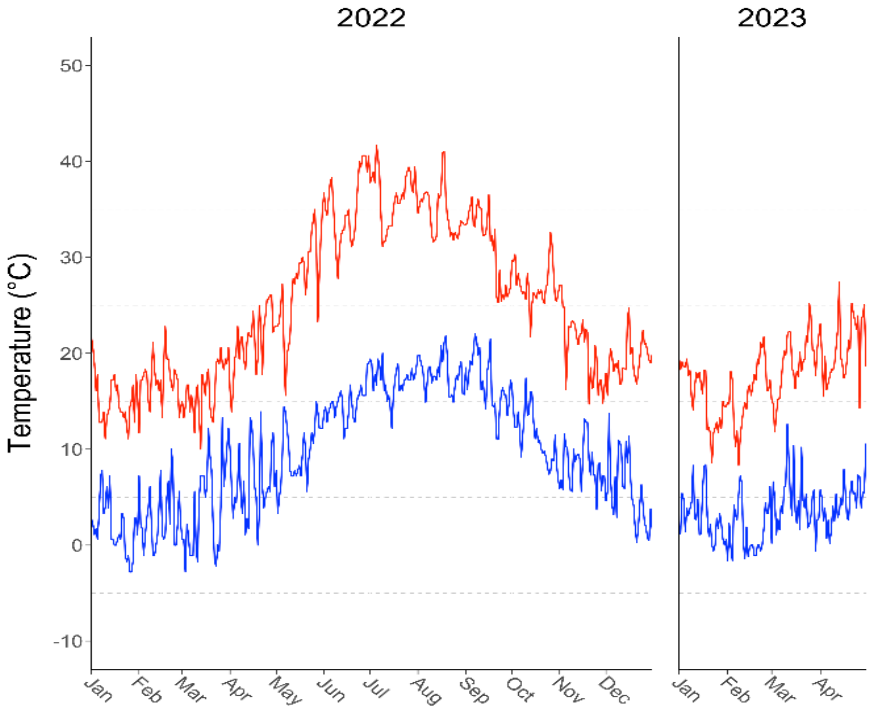

Fig. S1. Minimum (blue line) and maximum (red line) temperatures registered during the incubation period (15 months; from January 2022 to April 2023).

Table SI. Comparison between pairs of soil for initial (w_i) and final (w_f) soil water content, and hydraulic conductivity (K): mean difference, 95% confidence interval (CI) and p-value at three pressure head levels (h_0 = –1, –3, and –6 cm).

	$h_0 = -1$ cm		$h_0 = -3$ cm		$h_0 = -6$ cm	
Comparison	Mean diff. [95% CI]	p-value	Mean diff. [95% CI]	p-value	Mean diff. [95% CI]	p-value
w_i (g g^{-1})						
Alfisol *vs.* Vertisol	−0.14 [−0.16; −0.13]	0.001	−0.13 [−0.15; −0.12]	0.001	−0.13 [−0.16; −0.11]	0.001
Alfisol *vs.* Entisol	0.01 [−0; 0.02]	0.27	0.01 [0; 0.03]	0.102	0.02 [0; 0.02]	0.02
Vertisol *vs.* Entisol	0.15 [0.14; 0.17]	<0.001	0.15 [0.14; 0.17]	<0.001	0.16 [0.14; 0.19]	<0.001
w_f (g g^{-1})						
Alfisol *vs.* Vertisol	−0.15 [−0.17; −0.14]	0.001	−0.14 [−0.16; −0.13]	0.001	−0.14 [−0.17; −0.12]	0.001
Alfisol *vs.* Entisol	0.00 [0; 0]	0.41	0.01 [0; 0.02]	0.51	0.02 [0; 0.04]	0.034
Vertisol *vs.* Entisol	0.16 [0.14; 0.18]	<0.001	0.16 [0.14; 0.18]	<0.001	0.17 [0.15; 0.19]	<0.001
K (mm h^{-1})						
Alfisol *vs.* Vertisol	−14.55 [−29.68; 0.01]	0.054	2.92 [−0.55; 6.62]	0.14	6.09 [2.48; 9.26]	0.012
Alfisol *vs.* Entisol	2.67 [−7.75; 13.69]	0.69	8.08 [3.91; 12.09]	0.005	6.85 [3.52; 10.20]	0.006
Vertisol *vs.* Entisol	17.23 [1.65; 33.56]	0.03	5.16 [0.87; 9.11]	0.03	0.75 [−0.83; 2.27]	0.42

Table SII. The 95% confidence intervals for intercept and slope parameters of linear regressions between initial (w_i) and final (w_f) soil water content in the three soils used in the experiment. Intervals were derived to test whether regression models significantly deviate from the identity line (intercept = 0, slope = 1), which would indicate a departure from a 1:1 relationship. Soil-specific intervals for the intercept and slope (Variable X1) are reported to assess type dependent deviations in water content dynamics.

Soil type		95% confidence intervals	
Alfisol	Intercept	0.0004	0.0923
	Variable X1	0.7501	1.0107
Entisol	Intercept	0.0235	0.1002
	Variable X1	0.7266	0.9565
Vertisol	Intercept	−0.0412	0.0913
	Variable X1	0.8432	1.1111

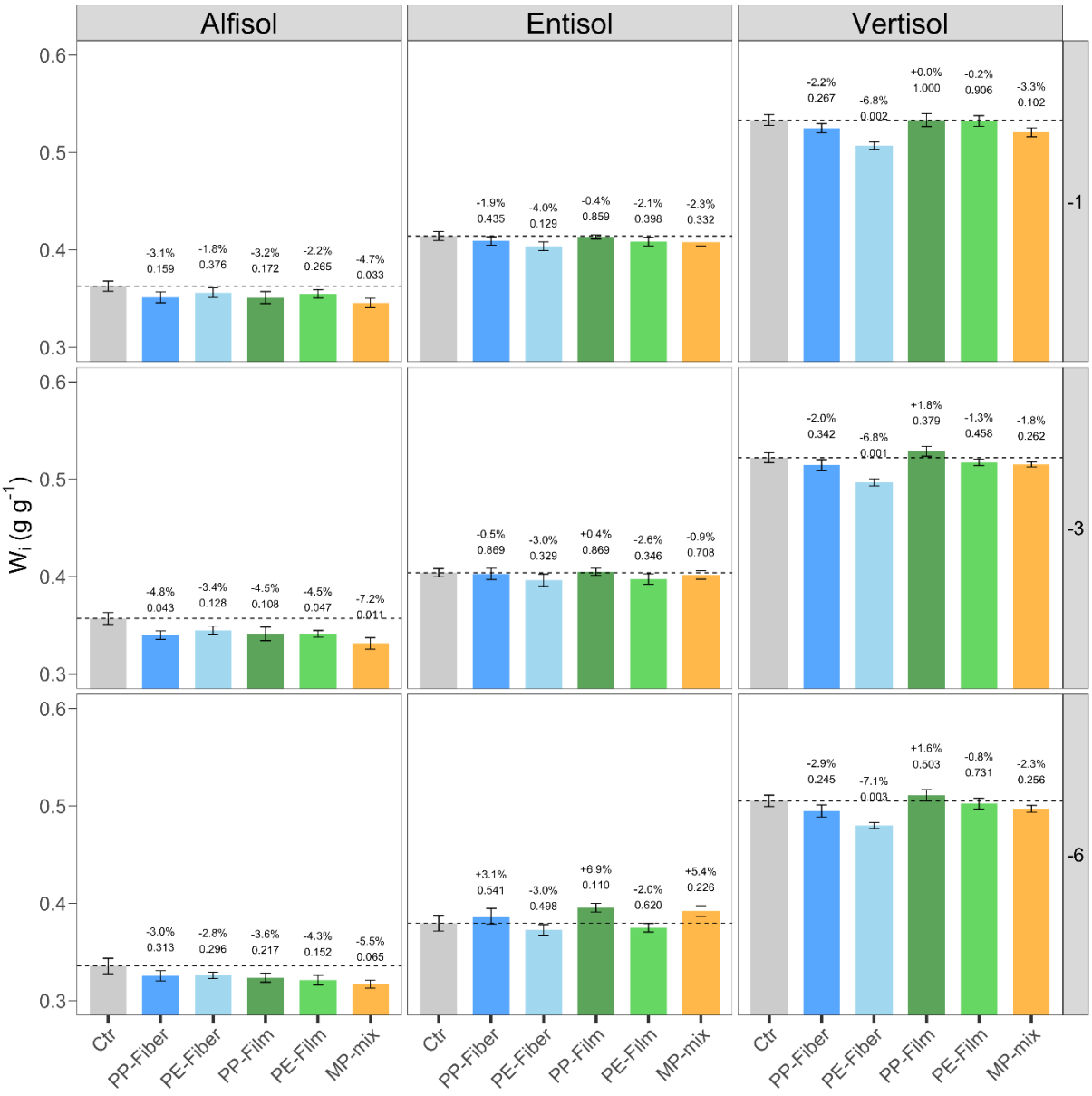

Fig S2. Initial soil water content (w_i) measured for three pre-established pressure heads (h_0 = −1, −3, and −6 cm) in the three soils used in the experiment not contaminated (Ctr) and contaminated with microplastics. Bars depict the mean values ± standard errors. PP-Fiber and PP-film are polypropylene fibers and film, respectively; PE-fiber and PE-Film are low-density polyethylene fibers and film, respectively; MP-mix is the mixture of the four types of microplastics. The percentage variation with respect to the Ctr and the *p*-values of two-sided permutation test between each microplastic treatment and the Ctr for each soil type are reported in the plots.

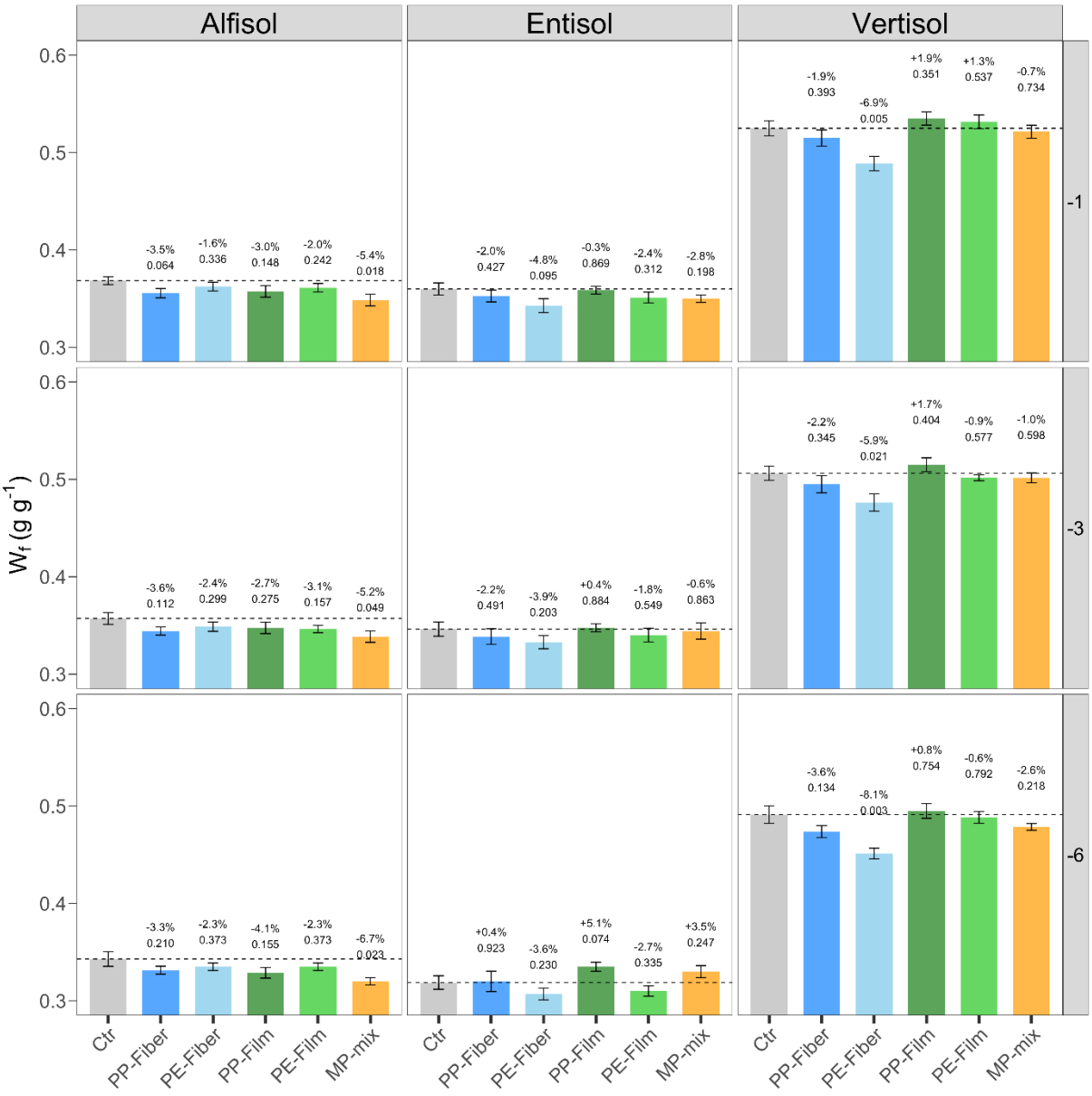

Fig S3. Final soil water content (w_f) measured for three pre-established pressure heads (−1, −3, and −6 cm) in the three soils used in the experiment not contaminated (Ctr) and contaminated with microplastics. Bars depict the mean values ± standard errors. PP-Fiber and PP-film are polypropylene fibers and film, respectively; PE-fiber and PE-Film are low-density polyethylene fibers and film, respectively; MP-mix is the mixture of the four types of microplastics. The percentage variation with respect to the Ctr and the *p*-values of two-sided permutation test between each microplastic treatment and the Ctr for each soil type are reported in the plots.

5.3 How Rilling And Biochar Addition Affect Hydraulic Properties Of A Clay-Loam Soil

Published on European Journal of Soil Science, 2025, 76(1), e70034.

Vincenzo Bagarello, Pellegrino Conte, Vito Ferro, Massimo Iovino, Calogero Librici, Alessio Nicosia, Vincenzo Palmeri, Vincenzo Pampalone, Francesco Zanna.

Abstract

Rill erosion is a significant problem worldwide as it determines relevant amounts of soil loss on hillslopes. Although, in the last few years, many studies have focused on rill erosion and biochar as soil amendment, their influence on soil hydrological properties and relevance on soil conservation strategies is still uncertain. In this paper, the effects of rill formation and biochar addition on the physical and hydraulic properties of a clay-loam soil were assessed by laboratory measurements (water retention, hydraulic conductivity, minidisk infiltrometer data, and ^{1}H Nuclear Magnetic Resonance (NMR) relaxometry with the fast field cycling (FFC) setup) and field tests (rill formation tests at the plot scale). The rilled and non-rilled soils did not show any difference in the volume of pores with a diameter (d) > 300 μm, but the former showed a smaller volume for the pores in the size range between 300 and 0.2 μm. As compared with an untreated rilled soil, the addition of 5% (w w^{-1}) biochar in the soil in which the rill is incised did not change the volume of pores with d > 300 μm, while there were more pores of both 30 ≤ d ≤ 300 μm and 0.2 ≤ d ≤ 30 μm. Moreover, there were less pores with d < 0.2 μm. Shaping the rill did not influence the hydraulic conductivity of the nearly saturated soil (pressure head, h = -1 cm), while it determined a significant decrease of the soil ability to transmit water in more unsaturated conditions (h ≤ -3 cm). The addition of biochar to the soil improved, in general, the soil aptitude to transmit water, regardless of the pore size. However, this improvement was statistically irrelevant in the case of a transport process governed by larger pores. The hydrological measurements also demonstrated that the addition of a large amount of biochar (5%) impedes soil characteristics alteration as the changes due to rilling are balanced by adding biochar in the soil. NMR was also used to measure the structural and functional connectivity of the original soil, the biochar, and a mixture with three biochar concentrations (i.e., BC = 1, 3, and 5 % w w^{-1}) traditionally applied in agronomical activity. These measurements revealed that the mixture of soil and biochar was characterized by longitudinal relaxation time (T_1) values, which are related to pore sizes, longer than those measured for the soil. In addition, the soil empirical cumulative frequency

distribution of T_1 was always skewed towards shorter T_1 values, thereby suggesting that the macro-pore component (that is the largest T_1 values) was never dominant while biochar addition increased the size of mesopores and micropores. Biochar concentrations larger than 3 % (w w^{-1}) did not produce appreciable changes in the pore distribution inside the mixture. The biochar component improved the structural connectivity up to BC = 5 %, while decreased the functional connectivity up to BC = 3%. A relationship between the water volume contained in soil pores and the NMR data was established for the micropores ($d \leq 0.2$ μm). The biochar-amended soil was characterized by fewer small pores, but these micropores were greater than those in non-treated soil.

Introduction

Soil erosion is a relevant environmental problem whose effects are often underestimated although its importance is highlighted in many field investigations (Borrelli et al., 2017). The soil loss rate in agricultural land is estimated as 10-40 times faster than the rate of soil formation, while slope protection is often inadequate, and strategies to mitigate or even prevent hydrogeological risk are rare (Carollo et al., 2023).

The evaluation of the link between soil physical and hydraulic properties and soil erosion process is a complex subject as soil physical and hydraulic properties have to be determined for parameterizing soil erosion prediction models (Risse et al., 1994, 1995; Nearing et al., 1996; Morgan and Duzant, 2008). Moreover, generally, these investigations are experimentally rather complex as intensive soil physical and hydraulic characterization, and the monitoring of surface runoff and soil erosion processes have to be performed at the same time. Perhaps, this is one of the reasons why the direct measurements of the soil hydraulic properties in relevant contexts from a soil erosion point of view are not widely reported in the literature.

Rill erosion is caused by soil particle detachment and transport by channelized flows which are characterized by high flow shear stresses and velocities, which lead to an increased sediment yield. Rills are small-eroded channels, which rapidly change their own morphology, represent a relevant sediment source producing most of the sediment transport on hillslopes (Mutchler and Young, 1975; Zhang et al., 2016), and can have a very appreciable impact on the hydrological response of the field in its entirety. Quite surprisingly, despite the hydrological relevance of the small field portions interested by rills, studies about the differences between the hydraulic properties of the rilled and non-rilled soils are lacking.

In a context in which alternative soil conservation practices aimed at the limitation of soil erodibility appear to be a valid solution to mitigate erosion processes, organic amendments, such as biochar (Mukherjee et al., 2014) or compost (Chia et al., 2020), can be considered as a valid and eco-friendly solution for soil amendment.

Biochar is obtained from the pyrolysis (i.e., thermal degradation) of biomasses in oxygen-starved conditions (Sohi et al., 2010; Conte et al., 2021). It improves soil structure (size, arrangement, and aggregate stability) (Blanco-Canqui, 2017; Conte et al., 2021), increases its organic matter content, and determines an increase in crop yield and quality (Wang and Wang, 2019; Conte et al., 2021). However, contrasting effects of biochar addition on runoff and soil loss have been reported since some authors (Lee et al., 2018; Li et al., 2017; 2019; Zhang et al., 2019) concluded that biochar addition can promote soil loss, while other investigations (Abrol et al., 2016; Baiamonte et al., 2015; Doan et al., 2015; Hseu et al., 2014; Jien and Wang, 2013; Lee et al., 2015; Sadeghi et al., 2016; Smetanova et al., 2013) supported the hypothesis that this addition reduces soil susceptibility to erosion. Moreover, the existing literature pointed out that the biochar effectiveness is influenced by the added concentration. Some authors (Li et al., 2019; 2020) suggested that low (from 1 % to 3 %) and high *BC* (higher than 5 %) values generally inhibited and promoted soil loss, respectively, while the results of the meta-analysis by Gholamahmadi et al. (2023) indicated the limit of 2.5 % w w^{-1} by considering that it seems that larger *BC* have no effect on the reduction of soil loss.

These contrasting results can be justified by several effects: (i) differences due to the biochar type and its particle size; (ii) changes in physical and chemical properties of investigated soils; (iii) the vegetation growth; and (iv) the method used for adding biochar (spread over the soil surface, incorporated into the soil) (Wani et al., 2021). In particular, when biochar was spread on the soil surface (Sadeghi et al., 2016; Smetanova et al., 2013), a biochar surficial layer forms and inhibits seal formation, favors infiltration processes, and reduces runoff and soil loss. Moreover, spreading of biochar on soil surface produces a preferential transport of low-density biochar particles (Sadeghi et al., 2016) and a reduction of soil loss. However, biochar is usually applied in the field inside the arable soil horizon and thoroughly mixed to favor the effects on soil properties.

At present, most of the literature studies deal with interrill erosion processes due to simulated rainfalls, while few investigations on rill erosion are available (Li et al., 2021; Nicosia et al., 2021). Li et al. (2021) carried out some experimental runs on the susceptibility to rill formation, and they observed a decrease in rilling in biochar-amended soil. Nicosia et al. (2021), using the data collected by Li et al. (2021), demonstrated that the biochar addition led to an increase in roughness, which determined the decrease in flow velocity and the increase in water depth. Parhizkar et al. (2023)

studied the effect of rice husk-biochar on rill erosion by flume experiments with both not amended soil and soil with a *BC* of 3 % w w^{-1}. The measurements revealed that biochar reduced rill erodibility and critical shear stress for the investigated soil. Furthermore, Parhizkar et al. (2023) found greater stability of the aggregates and a lower bulk density of the treated soil as compared to the non-amended one.

Biochar application influences soil porosity via direct pore contribution from pores within the biochar, creation of packing or accommodation pores between biochar and the surrounding soil aggregates, improved persistence of soil pores due to increased aggregate stability, increased bioturbation such as earthworm activity (Hardie et al., 2014; Blanco-Canqui, 2017). According to Hardie et al. (2014), who worked on a sandy-loam soil, large macropores (> 1200 μm) can be formed due to a greater earthworm burrowing in the biochar-amended soil. In clayey soils, biochar may favor the formation of mesopores (Lu et al., 2014). For loamy-sand soils, small particles of biochar (< 500 μm) can reduce the volume of small pores (diameter < 0.5 μm) and fissures (> 500 μm) while can increase the volume of pores in the range 0.5-500 μm (Głąb et al., 2016). With reference to coarse soils, biochar addition might convert large pores into smaller pores (Petersen et al., 2016; Villagra-Mendoza and Horn, 2018).

Biochar addition can also be expected to variably influence soil water transmission properties. For example, different biochar treatments could not have any statistically significant effect on saturated soil hydraulic conductivity, K_s, in clay (Castellini et al., 2015) and loamy-sand soils (Głąb et al., 2016). However, the fill in of larger pores due to biochar addition in coarse-textured soils can be expected to decrease K_s and increase the unsaturated soil hydraulic conductivity (Villagra-Mendoza and Horn, 2018).

An increase in field studies on biochar, the need to focus less on the effects and more on the mechanisms by which biochar application alters soil physical properties, and more research on biochar benefits in degraded or problematic soils are some of the research needs on biochar application that were identified only a few years ago (Blanco-Canqui, 2017).

The word “connectivity” states the way in which an environmental system favors matter and energy movement inside or among its elements (Pringle, 2003; Bracken and Crooke, 2007; Marchamalo et al., 2016; Keesstra et al., 2020). This concept highlights the attitude of a vector, such as water, to transport materials at different spatial and temporal scales (Bracken et al., 2013; Reaney et al., 2014; López-Vincente et al., 2017), considering the heterogeneity and complexity of an environmental system.

Wainwright et al. (2011) proposed to characterize an environmental system by *structural* (*SC*) and *functional* (*FC*) connectivity. The first one (*SC*) represents how the investigated process is affected by the interactions among structural characteristics of the environmental system (Belisle, 2005; Turnbull et al., 2008; Baartman et al., 2013; Uezu et al., 2005). For example, this is the case when the focus is to establish how the grain size distribution and arrangement of soil particles affect water movement inside the soil. The second one (*FC*) represents how a specific process (e.g., hydrological) is affected by the interactions among the structural components of the investigated system and the vector (e.g., water) (Wainwright et al., 2011). According to these definitions, structural connectivity provides a time-independent (stationary) response of the examined system, while functional connectivity reflects a dynamic viewpoint.

Conte and Ferro (2018, 2020, 2022) proposed the concept of *hydrological connectivity inside the soil* (*HCS*) to represent how water movement inside the soil is affected by the interaction of soil spatial patterns (i.e., *SC*) with chemical and physical processes (i.e., *FC*). In this system, the structural connectivity represents the spatial distribution of soil particles and considers the spatial arrangement of soil pores and micro-channels, while the functional connectivity complies with the water movement inside soil pores and is related to the physical-chemical interactions of water with the pore edges (Conte et al., 2017).

The scientific gaps to overcome concerns the definition of the threshold value of biochar concentration useful for soil conservation strategies and understanding the connectivity of biochar-amended soils.

In this paper, experimental measurements performed on rills of a clay-loam soil amended with different concentrations of biochar are aimed to: i) investigate how the soil hydrological properties of the rilled soil with different biochar concentrations (*BC* = 0, 3, and 5%) change in comparison with the original soil; ii) assess, by the nuclear magnetic resonance (NMR) relaxometry with the fast field cycling (FFC) layout, the structural and functional connectivity of the original soil, the biochar, and mixtures with different biochar concentrations (*BC* = 1, 3, and 5 % w w^{-1}); iii) test if the increase of *BC* produces appreciable changes in the pore distribution inside the mixture; and iv) combine hydrological and NMR measurements to establish a relation between the water volume contained in different-sized soil pores, and their number and size.

Materials and methods

Experimental setup

The experimental measurements were performed on a plot, which is a large box (Figure 1) 2 m wide and 7 m long, located at the Department of Agricultural, Food, and Forest Sciences (AFFS) of the University of Palermo (38° 06' 25" N, 13° 20' 59" E). The plot is manually filled with a clay-loam soil (32.7 % clay, 30.9 % silt, and 36.4 % sand), which is the same already used by Carollo et al. (2021), Di Stefano et al. (2022), and Nicosia et al. (2022a, b), compacted at the field bulk density and with an average slope of 15%. The soil depth in the plot ranges from 0.45 m (upstream end) to 0.15 m (downstream end). This soil was taken in the area surrounding the Department, which is characterized by a typical Mediterranean climate (*Csa*, according to the Köppen classification (Köppen, 1918) and vegetation. The soil was collected from different points within the area to consider field variation. The abovementioned soil texture was determined by the hydrometer method (Kroetsch and Wang, 2008) for fine size fractions and mechanical dry sieving for coarse fractions, applied to five samples homogeneously distributed on the plot surface. Other five soil samples were collected by steal cylinders of known dimensions (5 cm in height and 5 cm in diameter) to determine bulk density (1.23 g cm-3) (Hao et al., 2008), by oven-drying at 105 °C for 24 h. The organic matter content of the soil, determined by oven-drying the samples in a muffle furnace at 400°C (Skjemstad and Baldock, 2008), is approximately equal to 2%. Two trenches (Figure 1a), 5.7 m long, 0.2 m wide, and 0.1 m deep, were dug in the plot for a total removal of approximately 100 kg of soil for each of them. The soil removed from each trench was distributed on plastic sheets in piles and left to air-dry for a week.

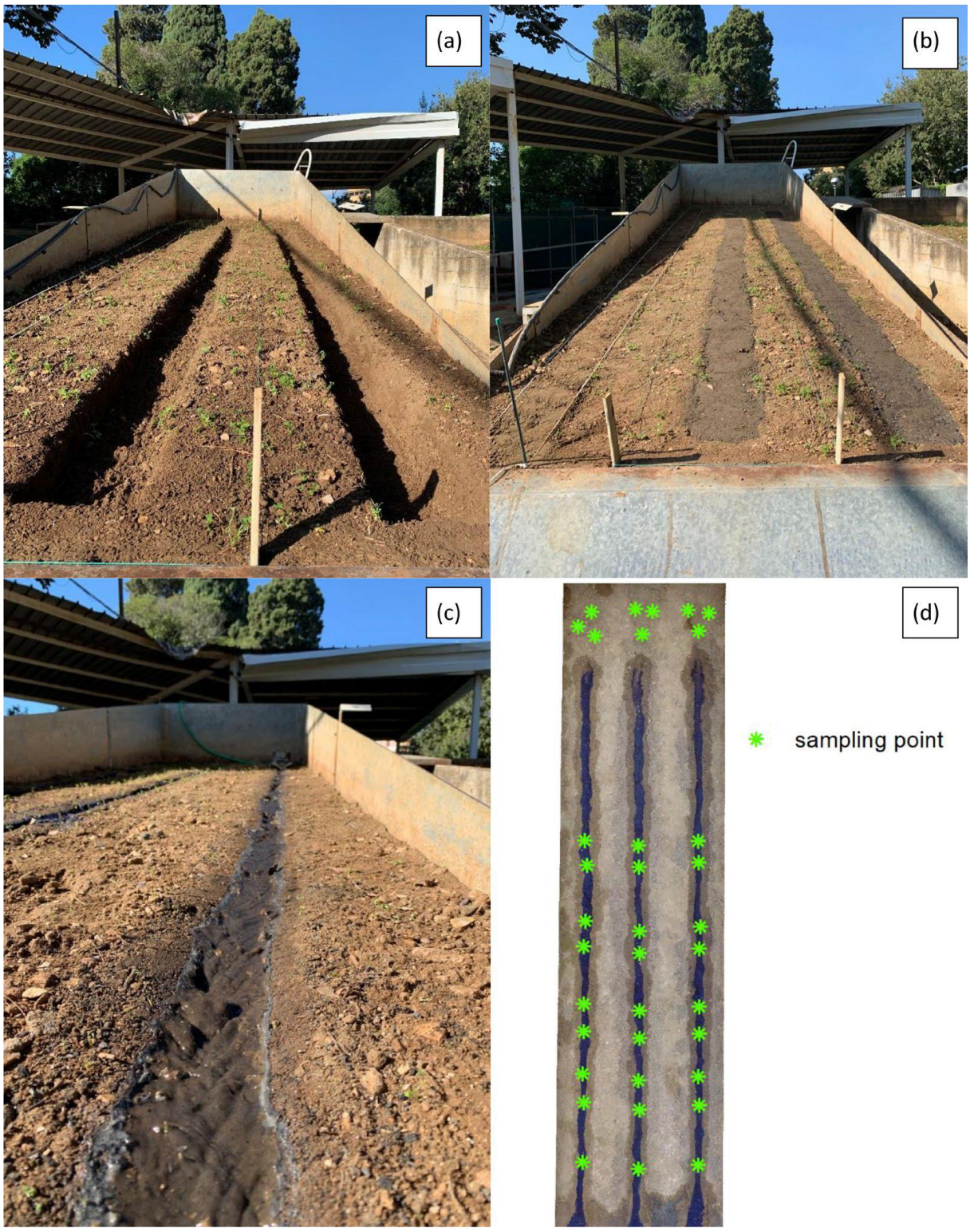

FIGURE 1 | View of the experimental plot with the two empty (a) and filled trenches (b), the preferential paths (c) and scheme of the sampling points (d).

At the end of the week, three samples were taken and weighted from each pile, and they were subsequently oven-dried at 105° for 24 hours to determine soil moisture, which was found to be on average 12.5± 0.004 %. The pre-established *BC* of 3% (B_3 treatment) and 5% (B_5 treatment) was reached by adding 300 and 500 g of biochar to 10 kg of soil in dry weight, corresponding to approximately 11.4 kg in wet weight, due to the measured soil moisture. The mixing phase between soil and biochar was performed for 60 s. Each biochar-soil mixture corresponding to an investigated *BC* (3% and 5%) was used to fill a trench (Figure 1b). The experimental runs were carried out after an incubation period of 30 days to allow biochar incorporation into the soil. Two preferential paths were established on the surface of the two filled trenches (B_3 and B_5 treatment) and modeled by a constant clear inflow discharge of 0.33 L s^{-1} (Figure 1c) applied for 12 min to simulate rilling. A preferential flow path, evolving in a rill during the run, was also established in a zone of the plot in which the soil was not treated with biochar (B_0 treatment) (Figure 1b) as control. The same discharge of 0.33 L s^{-1} was applied for 12 min.

Hydrological measurements

After the rilling, the surface soil was sampled in four zones of the plot (Figure 1d) using stainless steel cylinders (diameter = 0.05 m, height = 0.05 m) to collect undisturbed soil cores. In particular, for each rill (B_0, B_3, and B_5 treatments), a total of nine soil cores were collected along the rill in correspondence of the sampling points shown in Figure 1d. The other nine soil cores were randomly collected in the upper plot area (Figure 1d), in a zone without rills and where biochar was not added (C treatment). Therefore, a total of 36 undisturbed soil cores were collected.

Water retention data were obtained for each undisturbed soil core for pressure head, *h*, values of 0, -0.05, -0.075, -0.10, -0.15, -0.20, -0.25, -0.30, -0.40, -0.50, -0.70, and -1.0 m by a self-made hanging water column apparatus (Bagarello and Iovino, 2012; Bondì et al., 2022). The apparatus consists of an array of 40 glass funnels, each equipped with a sintered porous plate having an air entry value of -2.0 m that is connected to a graduated burette, which can be moved in height to establish a given pressure head value and allows measurement of the drained water from the core. The cores were previously saturated on the porous plate by wetting from below and then equilibrated at decreasing *h* values. The dry soil bulk density, ρ_b, and the volumetric water content corresponding to the last equilibrium pressure head value were determined by oven-drying the core. The volume of water drained into the burette was recorded and used to calculate the volumetric water content corresponding to the equilibrium pressure heads.

The oven-dried soil cores were placed for several days in a large container containing a few small plastic cups with water. For a given (negative) *h* value, the hydraulic conductivity, *K*, of a soil core was then determined by a simplified version of the Unit Hydraulic Gradient (UHG) method (Klute and Dirksen, 1986; Bagarello et al., 2007). In particular, to establish a given *h* value at the base of the core, a plastic box of 38 (length) × 17 (width) × 13 (height) cm^3 was filled with a bed of sand up to a certain height, and several small holes were made on the walls of the box at a downward distance *h* (L) from the surface of the sand bend. A metal screen was glued to each hole to prevent sand from escaping through the hole. Water was added to the box so as to form a saturated zone below the holes and an unsaturated zone above them. At hydrostatic equilibrium, the soil water pressure head at the surface of the sand bed was assumed to be equal to *h*. Different boxes were prepared, depending on the considered *h* value (*h* = -6, -3, and -1 cm in this investigation). The soil core, with an attached nylon guard cloth at its base to prevent soil loss from the bottom, was placed on the surface of the sand box and left to equilibrate for several days. Small volumes of water were periodically added to the box during this period to maintain the *h* value at the surface of the sand bed constant. Then, a Mini-Disk Infiltrometer (MDI), set at the same *h* value of the sand surface, was placed on the top of the soil core, and a one-dimensional infiltration process was activated. When necessary, small amounts of loose soil were applied to the soil surface of the core to improve the contact between the device and the soil. The first established pressure head was *h* = -6 cm. At the end of the run, the soil core was subjected to the subsequent step by imposing the higher *h* value of the sequence. Readings at the MDI reservoir were taken visually at 0.5 to 5 min time intervals, depending on the imposed pressure head and the stage of the run.

After drying, the soil was used to prepare packed soil samples (diameter = 0.05 m, height = 0.01 m) at the same bulk density of the soil core. In particular, a pestle was gently used to crush the soil, which was then passed through a 2 mm sieve. These soil samples were used to determine the soil water content corresponding to *h* values of -10 and -150 m by a pressure plate apparatus (Dane and Hopmans, 2002).

Soil water retention and hydraulic conductivity data

Four points of the water retention curve were considered to establish comparisons between the four treatments (C, B_0, B_3, B_5), in accordance with Reynolds et al. (2009). These points corresponded to pressure heads of 0, -0.1 m, -1 m, and -150 m. Consequently, the saturated soil volumetric water content, θ_s (m^3/m^3), the "saturated" volumetric water content of the soil matrix, $\theta_{-0.1m}$ (m^3/m^3), the field capacity volumetric soil water content, θ_{-1m} (m^3/m^3), and the permanent wilting point volumetric

soil water content, θ_{-150m} (m^3/m^3) were considered. According to Hardie et al. (2014), the Young-Laplace equation can be used to determine the size of the largest pores that are full of water for a given absolute value of the soil water pressure head, h (m):

$$\boldsymbol{d = \frac{30}{|h|}} \quad (1)$$

where d (μm) is the pore diameter. All pores are full of water for $\theta = \theta_s$. The d values are equal to 300, 30, and 0.2 μm for h = -0.1, -1, and -150 m, respectively. Equivalent pore diameters ≤ 300 μm ($h \leq$ -0.1 m) comprise the soil matrix domain, while diameters > 300 μm ($h >$ -0.1 m) form the macropore domain (Topp et al., 1997; Jarvis et al., 2002; Reynolds et al., 2002).

Soil air and water storage capacities were expressed by distinguishing between pore sizes (Reynolds et al., 2002, 2009). In particular, macroporosity, equal to (θ_s - $\theta_{-0.1m}$), gives the total volume of large (macro) pores (i.e., > 300 μm equivalent pore diameter), which indicates, albeit indirectly, the soil's ability to quickly drain excess water and facilitate root proliferation. According to Reynolds et al. (2009), macroporosity is optimal if (θ_s - $\theta_{-0.1m}$) ≥ 0.07 m^3/m^3, intermediate if 0.04 ≤ (θ_s - $\theta_{-0.1m}$) < 0.07 m^3/m^3, and limited if (θ_s - $\theta_{-0.1m}$) < 0.04 m^3/m^3. The ($\theta_{-0.1m}$ - θ_{-1m}) difference ($30 \leq d \leq 300$ μm) is expressive of soil aeration in the soil matrix domain (Reynolds et al., 2002). As suggested by Reynolds et al. (2002), aeration of soil matrix is good if ($\theta_{-0.1m}$ - θ_{-1m}) ≥ 0.10 - 0.15 m^3/m^3 and is limited for smaller values. The ($\theta_{-0.1m}$ - θ_{-1m}) difference was denoted as drainable porosity and corresponds to the -1.0 to -10 kPa matric pressure considered in other investigations in other investigations specifically focused on biochar addition effects on soil water retention (Hardie et al., 2014). The plant-available water capacity, equal to (θ_{-1m} - θ_{-150m}) ($0.2 \leq d \leq 30$ μm), represents the plant available water capacity (Reynolds et al., 2002). According to Reynolds et al. (2009), water availability is ideal if (θ_{-1m} - θ_{-150m}) > 0.20 m^3/m^3, good if 0.15 ≤ (θ_{-1m} - θ_{-150m}) < 0.20 m^3/m^3, limited if 0.10 ≤ (θ_{-1m} - θ_{-150m}) < 0.15 m^3/m^3, and poor if (θ_{-1m} - θ_{-150m}) < 0.10 m^3/m^3.

The S index by Dexter (2004) was also calculated to evaluate the soil physical quality (SPQ) of the sampled soil by considering the soil water retention curve expressed in terms of gravimetric soil water content θ_g (g/g). In particular, the van Genuchten (1980) model was adapted to the measured data:

$$\theta_g(h) = \theta_{gr} + (\theta_{gs} - \theta_{gr})(1 + |\alpha h|^n)^{-m} \quad (2)$$

in which θ_{gs} (g/g) and θ_{gr} (g/g) are respectively the saturated and residual gravimetric water content, α (1/cm) is a scale parameter, and n and m (with $m = 1-1/n$) are shape parameters. Eq. (2) was adapted to the data by optimizing the parameters θ_{gr}, α, and n. The calculation of S was performed according to the following equation (Reynolds et al., 2009):

$$\boldsymbol{S = \left| -n(\theta_{gs} - \theta_{gr}) \left[1 + \frac{1}{m} \right]^{-(m+1)} \right|} \quad (3)$$

The S index represents the magnitude of the slope of the soil water retention curve at the inflection point when the curve is expressed as gravimetric water content vs. natural logarithm of the pore water tension head. According to Dexter and Czyż (2007), $S \geq 0.050$ indicates "very good" soil physical or structural quality, $0.035 \leq S < 0.050$ is indicative of a "good" physical quality, $0.020 \leq S < 0.035$ suggests a "poor" physical quality, and $S < 0.020$ denotes a "very poor" or "degraded" physical quality. This evaluation criterion does not appear to have universal validity since large S values can also be expected to reflect the soil matrix characteristics rather than the soil structural characteristics (Reynolds et al., 2009). For this purpose, Dexter et al. (2008) reported that large apparent values of S, which are not reflected in other physical properties, can be obtained in well-graded sands and sandstones that have a very narrow distribution of pore sizes and can empty over a very narrow range of suctions. Nevertheless, the S index is largely used, probably because it allows for defining the SPQ on the basis of a single value that is expressive of a robust experimental information, given that determining S requires adapting a model to the experimentally determined water retention data. In particular, this index was taken into consideration in several investigations testing the impact on SPQ of various amendments, including biochar (Reynolds et al., 2009; Gląb et al., 2016; Dokoohaki et al., 2017; Fouladidorhani et al., 2023).

For each soil core and each pressure head value, the cumulative infiltration, I (mm), versus time, t (h), relationship obtained with the MDI was linear or nearly linear from the early stage of the run, suggesting a rapid stabilization of the flow process. Therefore, an estimate of K was obtained by considering the complete infiltration run and determining by linear regression the slope of the I vs t relationship forced to pass through the origin of the axes. As an example, Figure 2 shows, for the run no. 7 of the B_0 treatment, the $I(t)$ data points for the three established pressure heads (-6, -3, and -1 cm) and the corresponding estimates of K coinciding with the slopes of the fitted linear regression lines. The coefficient of determination, R^2, of these relationships was ≥ 0.99. The symbols K_{-6cm}, K_{-3cm}, and K_{-1cm} were used to denote the K values corresponding to h = -6, -3, and -1 cm, respectively.

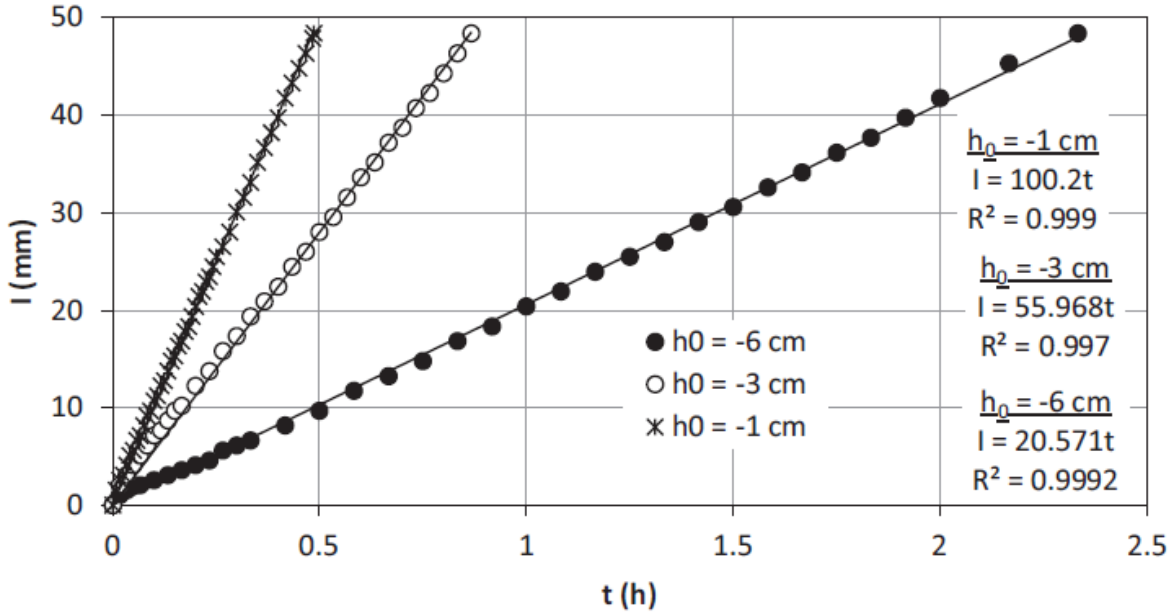

FIGURE 2 | Example of the applied procedure to determine the soil hydraulic conductivity at a given pressure head, $h0$, from the MDI runs (I = cumulative infiltration; t = time).

2.4 Hydrological data analysis

Initially, rilling effects on soil physical and hydraulic properties were tested by comparing the C and B_0 treatments. Then, biochar addition effects on the soil of a rill were tested by comparing the B_0, B_3, and B_5 treatments.

For each tested effect, comparisons were performed by considering the following variables: ρ_b, θ_s, $\theta_{-0.1m}$, θ_{-1m}, θ_{-150m}, $(\theta_s - \theta_{-0.1m})$, $(\theta_{-0.1m} - \theta_{-1m})$, $(\theta_{-1m} - \theta_{-150m})$, S, K_{-6cm}, K_{-3cm}, and K_{-1cm}. An F test and a two-tailed t test at $P = 0.05$ were applied to establish the statistical significance of the differences. At this aim, the statistical functions for data analysis of the Excel® spreadsheet (Microsoft Corporation, Redmond, WA) were used.

Finally, an attempt to describe the combined rilling and biochar addition effects was made by considering four measured points of the water retention curve (θ_s, $\theta_{-0.1m}$, θ_{-1m}, θ_{-150m}), the S index obtained from the complete water retention dataset for a core, and also K for the three pressure heads (K_{-6cm}, K_{-3cm}, K_{-1cm}).

Sample preparation for FFC NMR relaxometry analyses

All the soil samples were weighed (≈ 2 g) in a 10 mm NMR glass-tube. Then, MilliQ grade water (18.2 MΩ cm at 25 °C) was gradually added till saturation occurred. The samples were kept overnight and, finally, analyzed with the NMR machine described below.

FFC NMR relaxometry experiments

A Stelar SmarTracer Fast-Field-Cycling NMR Relaxometer (Stelar s.r.l., Mede, PV–Italy) at a constant temperature of 25 °C was used to carry out the relaxometry experiments. The basics of the FFC NMR relaxometry are reported elsewhere (Conte and Lo Meo, 2020). Briefly, the technique is based on the rapidly switching among three different magnetic fields, that are referred to as polarization (B_{POL}), relaxation (B_{RLX}), and acquisition (B_{ACQ}) field. In the non-polarized (NP) configuration, B_{POL} intensity is kept null. Therefore, only B_{ACQ} and B_{RLX} are used. The former is applied to generate the magnetization whose intensity depends on that of B_{ACQ} which is changed in the proton Larmor frequency (ν_L) interval 0.01 - 10 MHz. The intensity of the latter (i.e., B_{ACQ}) was set at the constant ν_L value of 7.2 MHz. This was needed to keep the magnetization aligned along the +y-axis after the application of a ^1H $90°_{(-x)}$ pulse of 6.6 μs necessary to generate the observable and, hence, to allow signal acquisition. B_{ACQ} duration (usually indicated with the Greek letter τ) was logarithmically changed at least 32 times between a minimum given by $0.01 \cdot T_1^*$ and a maximum given by $4 \cdot T_1^*$. Here, T_1^* represents the supposed longitudinal relaxation time of the system under study (Conte, 2021). The aforementioned 32 τ values were automatically calculated by the software (AcqNMR95, V. 2.20, 2007) provided with the NMR machine. When B_{RLX} Larmor frequency became ≤ 3 MHz, the pre-polarized (PP) configuration was used. In other words, B_{POL} intensity was set to be non-null. The B_{POL} intensity (expressed as proton Larmor frequency) used in the present study was 10 MHz. It was applied for a period of time (also referred to as T_{POL}) given by $4 \cdot T_1^*$, having T_1^* the same meaning reported above. The necessity of the PP configuration lies in the fact that when B_{RLX} $\nu_L \leq 3$ MHz, a lack of NMR sensitivity is achieved. Therefore, the application of a polarization field prior of B_{RLX} allows sensitivity enhancement and amelioration of FFC NMR data quality (Conte, 2021). A recycle delay (RD) of 4 s was applied when either NP or PP configurations have been used. This RD value was long enough to prevent any problem due to signal saturation. Finally, a switching time of 3 ms, an acquisition delay of 8 μs, a receiver inhibit of 15 μs, and a block size of 512 points were used.

FFC NMR relaxometry data analyses

Once the FFC NMR relaxometry data have been acquired, the Uniform PENalty regularization (UPEN) algorithm (Borgia et al., 1998; Conte, 2019) was used to achieve the distribution of the longitudinal relaxation times to assess the hydrological connectivity inside a soil (HCS).

For each soil, following the result by Conte and Ferro (2020), the distribution of T_1 was obtained using a sample-to-water ratio of 1:0.25 (w/w), corresponding to the water holding capacity *WHC*, at a proton Larmor frequency ν_L varying from 0.01 to 10 MHz. In other words, the experimental runs were carried out with a single value of *WHC* and different values of ν_L. Each sample was prepared in a beaker, and then the wet sample was manually transferred in the NMR tubes to obtain a homogeneous packing. The FFC NMR measurements were carried out for the original soil (C treatment), the biochar, and the mixtures with different biochar concentrations (1, 3, and 5%, i.e., B_1, B_3, and B_5 treatments). Three replicates of NMR measurement were carried out for each investigated sample.

Assessing Hydrological Connectivity inside a soil (HCS)

NMR relaxometry measures how quickly the z-component of the nuclear magnetic moment (i.e., the bulk nuclear spin magnetization) changes from a non-equilibrium state to the equilibrium distribution. Fluctuations of local magnetic or electrical fields generate a phenomenon, named relaxation, which is mainly affected by molecular motions. Therefore, measurements of the longitudinal relaxation time, T_1, express the molecular dynamics. The T_1 values provide information about motion frequencies in the range (10^5-10^8 Hz) characteristic of water molecules moving in porous media (Conte, 2021). If the porous medium is the soil, the shortest T_1 values are associated with small-sized pores (i.e., pores bounded by clay primary particles and small aggregates), while the longest T_1 values correspond to pores bounded by sand particles, silt, and large aggregates (Pohlmeier et al., 2009; Conte et al., 2017).

Water molecules moving within the micro-pores have a range of T_1 values (T_A in Figure 3b) near the lower T_1 limit, while molecules moving within the macro-pores are characterized by T_1 values near the upper T_1 limit (range named T_B in Figure 3b) of the measured relaxation time distribution. Water molecules moving within meso-pores are identified by all T_1 values included between the upper T_1 limit of the micro-pores (point A in Figure 3b) and the lower T_1 limit of macro-pores (point B in Figure 3b).

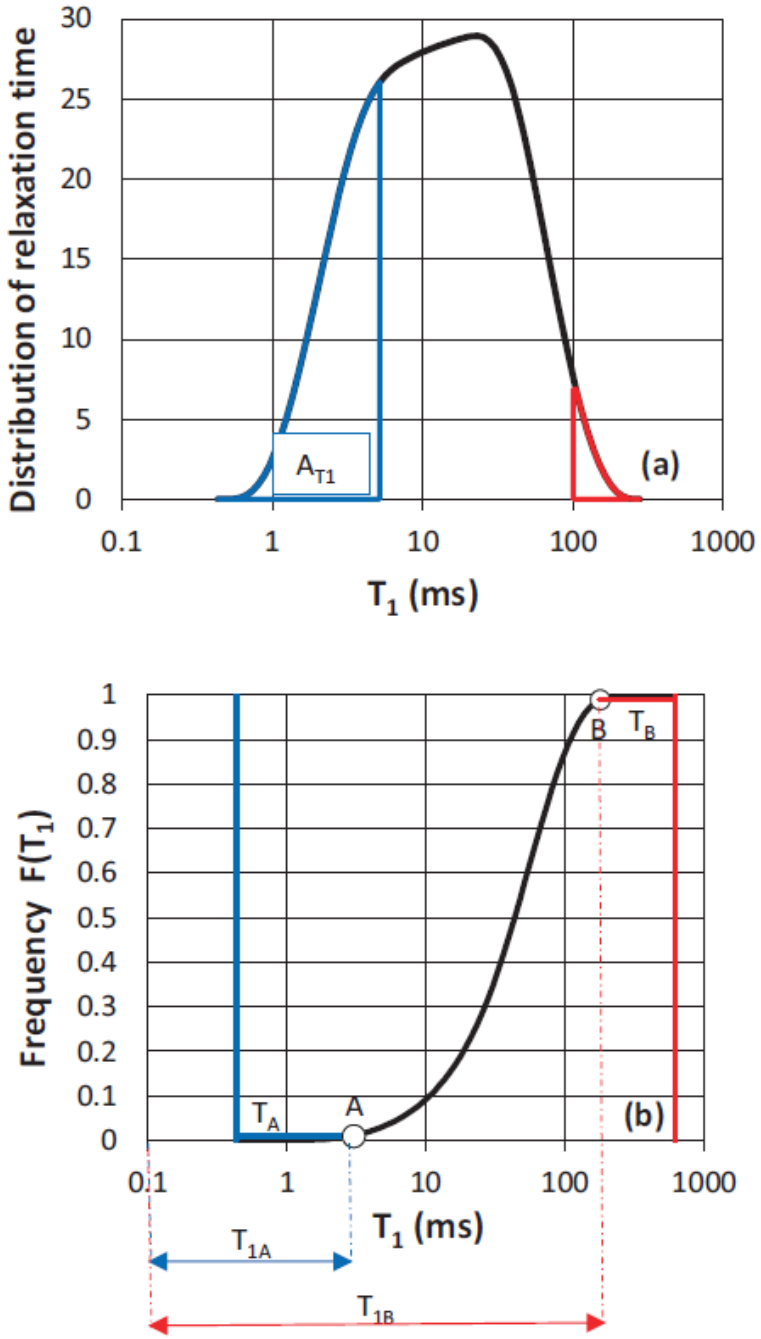

FIGURE 3 | Relaxogram (a) and example of the integral curve of the relaxogram that associates the ratio $AT1/A$ with each $T1$ value (b).

Conte and Ferro (2018, 2020, 2022) presented a method for defining the SC and FC of a given soil by introducing a new mathematical use of the relaxograms obtained by NMR relaxometry. The quantification of structural connectivity and functional connectivity was made by two indexes, *SCI* and *FCI*, calculated by taking into account the NMR relaxogram shapes. In detail, for a given proton Larmor frequency, the distribution of the longitudinal relaxation time T_1 (i.e., the relaxogram in Figure 3a) is integrated, and the area, A_{T1}, bounded by the relaxogram curve, the T_1 axis, and the

ordinate value corresponding to T_1 value, is related to each T_1 value. Figure 3b plots an example of the integral curve of the relaxogram, associating the ratio A_{T1}/A with each T_1 value. This ratio, ranging from 0 to 1, is equal to the non-exceeding empirical cumulative frequency, $F(T_1)$, of each T_1 value. Conte and Ferro (2018, 2020, 2022) demonstrated that $F(T_1)$ is S-shaped and found two points (A and B in Figure 3b) characterized by a sudden change in the curve slope. The A point bounds a part of the curve corresponding to the shortest T_1 values and the time range T_A (Figure 3b), while the B one limits the part characterized by the longest T_1 values obtained in the T_B time range. Conte and Ferro (2018, 2020, 2022) set the A and B points to identify the two extreme components of the S-shaped $F(T_1)$ distribution: point A, with ordinate $F(T_1) = 0.01$, and point B, with ordinate $F(T_1) = 0.99$. The ordinate of point A distinguishes the low component (only 1% of the measured T_1 values are less than the abscissa characterizing the A point), whereas the ordinate of the B point distinguishes the high component (only 1% of the measured relaxation times values are higher than the abscissa characterizing this point).

The water movement in macropores, mesopores, and micropores is considered by the hydrological connectivity inside the soil. Adapting the classification by Reynolds et al. (2009) to this investigation, macropores have a diameter $d > 300$ μm, mesopores vary in size between 300 and 0.2 μm, and micropores have $d \leq 0.2$ μm. Note that this classification is similar to some extent to the one by Russell (1973), distinguishing between coarse (> 200 μm), medium (200-20 μm), fine (20-2 μm) and very fine (< 2 μm) pore width classes. Associating the relaxation times with pore sizes, the low component of the $F(T_1)$ distribution, corresponding to T_1 values lower than the abscissa of the A point (Figure 3b), identifies micro-pores, where limited space causes a reduction of molecular movement. The high component, corresponding to T_1 values higher than the B point abscissa (Figure 3b), is related to macro-pores characterized by wide mobility.

For the NMR analysis, the pore-size ranges suggested by Pagliai and Vignozzi (2002) were applied. In particular, micropores have a diameter less than 50 μm, mesopores range from 0.5 to 50 μm, and macropores have $d \geq 50$ μm. Therefore, according to Conte and Ferro (2018), in Figure 3b, the abscissa of the point A (T_{1A}) corresponds to the micropore limit ($d < 0.5$ μm), while T_{1B} represents the lower limit of the macropore range ($d \geq 50$ μm). The range between T_{1A} and T_{1B} represents the mesopore size interval. The limit of this approach is the unavailability of a direct relationship between the measured T_1 values (relaxogram) and pore diameter sizes. In other words, a calibration of the relaxogram, where the T_1 scale corresponds to the pore diameter size scale has not been attempted yet.

Bulk water movement, characterized by a high sensitivity by the NMR technique (Conte, 2019), is related to the limb of the $F(T_1)$ curve (bounded by the A and B points of Figure 3b), whereas the high and low $F(T_1)$ components refer to water interacting with the soil pore edges.

Conte and Ferro (2018, 2020, 2022) proposed the ratio T_B/T_A as *FCI*. This definition of functional connectivity allows for taking into account that the T_1 values in the range T_A identify water trapped in small pores, whereas those in the range T_B correspond to water contained in large pores. Conte and Ferro (2018, 2020, 2022) proposed to use the AB limb zone of the $F(T_1)$ curve (Figure 3b), falling in the central range of T_1 values, to calculate the *SCI*. In other words, the spatial pattern inside the soil can be represented by the central range of T_1 values, identifying water moving in meso-pores. Considering the relationship between T_1 values and pore size, the *SCI* is the coefficient of variation of T_1 values characterized by $0.01 < F(T_1) < 0.99$.

Results and discussion

Rilling

The ρ_b values did not differ between the C and B_0 treatments (Table 1). The non-rilled soil had significantly higher θ_s and $\theta_{-0.1m}$, equal θ_{-1m} and smaller θ_{-150m} values as compared with the rilled soil. There was not any statistically significant difference between the C and B_0 treatments with reference to (θ_s - $\theta_{-0.1m}$) but the former treatment yielded higher ($\theta_{-0.1m}$ - θ_{-1m}) and (θ_{-1m} - θ_{-150m}) values than the latter one. Regardless of the treatment, data variability was low for ρ_b, θ_s, $\theta_{-0.1m}$, θ_{-1m}, θ_{-150m} and (θ_{-1m} - θ_{-150m}) and medium for ($\theta_{-0.1m}$ - θ_{-1m}) (Warrick, 1998). The variability of (θ_s - $\theta_{-0.1m}$) was high for the C treatment and medium for the B_0 one.

According to the *S* calculations, the soil had a very good physical or structural quality (Dexter and Czyż, 2007), regardless of whether sampling was performed in the control area or in the rill. However, the *S* index differed significantly between the C and B_0 treatments since the former treatment yielded a significantly larger *S* value than the latter one. The relative variability of *S* varied only minimally with the treatment, and it was medium in both cases.

Therefore, rilling did not influence dry soil bulk density. However, as compared with the control, the soil of the rill had a smaller water content at saturation and at -0.1 m, a similar water content at -1 m, and a larger water content at -150 m. Consequently, (θ_s - $\theta_{-0.1m}$) did not vary significantly between the two treatments since both θ_s and $\theta_{-0.1m}$ decreased from the C to the B_0 treatment. A decrease of ($\theta_{-0.1m}$ - θ_{-1m}) occurred in the rilled soil because $\theta_{-0.1m}$ decreased while θ_{-1m} did not vary. The decrease of (θ_{-1m} - θ_{-150m}) from the C to the B_0 treatment was due to the circumstance that the soil of the rill had a higher θ_{-150m} value than the control. As compared with the non-rilled soil, rilling implied that the

volume of pores with $d > 300$ μm did not change. There were fewer pores of both $30 \leq d \leq 300$ μm and $0.2 \leq d \leq 30$ μm and more pores with $d < 0.2$ μm. According to the S calculations, rilling determined a decrease in the SPQ that, however, remained very good.

TABLE 1 | Summary statistics of the ρ_b, θ_s, $\theta_{-0.1m}$, θ_{-1m}, θ_{-150m}, θ_s-$\theta_{-0.1m}$, $\theta_{-0.1m}$-θ_{-1m}, θ_{-1m}-θ_{-150m} and S values obtained in the non-rilled upper area of the plot (control, C) and in the rills treated with biochar at a rate of 0% (B_0), 3% (B_3) and 5% (B_5) (sample size, $N=8$ for the C treatment and $N=9$ for the B_0, B_3 and B_5 treatments; d = pore diameter).

Parameter	Statistic	C	B0	B3	B5
ρ_b (g/cm³)	Min	1.134	1.127	0.920	0.989
	Max	1.298	1.295	1.214	1.186
	Mean	1.235 a	1.207 a A	1.087 B	1.088 B
	CV (%)	4.3	4.7	9.3	6.9
θ_s (m³/m³)	Min	0.482	0.429	0.452	0.489
	Max	0.660	0.528	0.597	0.633
	Mean	0.557 a	0.484 b A	0.503 A	0.561 B
	CV (%)	12.8	7.0	10.4	8.8
$\theta_{-0.1m}$ (m³/m³) $d \leq 300\,\mu m$	Min	0.412	0.341	0.347	0.393
	Max	0.536	0.448	0.475	0.470
	Mean	0.463 a	0.396 b A	0.412 A	0.449 B
	CV (%)	8.8	8.4	9.6	5.5
θ_{-1m} (m³/m³) $d \leq 30\,\mu m$	Min	0.229	0.233	0.218	0.241
	Max	0.260	0.269	0.272	0.305
	Mean	0.248 a	0.249 a A	0.248 A	0.274 B
	CV (%)	4.6	5.7	7.1	7.4
θ_{-150m} (m³/m³) $d \leq 0.2\,\mu m$	Min	0.098	0.109	0.098	0.090
	Max	0.109	0.126	0.122	0.114
	Mean	0.103 a	0.117 b A	0.112 A	0.102 B
	CV (%)	3.4	5.0	7.4	7.7
$\theta_s - \theta_{-0.1m}$ (m³/m³) $d > 300\,\mu m$; macroporosity	Min	0.052	0.062	0.047	0.054
	Max	0.184	0.115	0.141	0.184
	Mean	0.094 a	0.088 a A	0.091 A	0.112 A
	CV (%)	53.2	21.5	31.0	39.3
$\theta_{-0.1m} - \theta_{-1m}$ (m³/m³) $30 \leq d \leq 300\,\mu m$; soil aeration in the soil matrix domain or drainable porosity	Min	0.183	0.108	0.129	0.152
	Max	0.281	0.189	0.203	0.188
	Mean	0.215 a	0.147 b A	0.164 AB	0.175 B
	CV (%)	16.1	17.1	14.2	6.5
$\theta_{-1m} - \theta_{-150m}$ (m³/m³) $0.2 \leq d \leq 30\,\mu m$; plant available water capacity	Min	0.131	0.120	0.120	0.151
	Max	0.155	0.144	0.150	0.191
	Mean	0.144 a	0.132 b A	0.136 A	0.172 B
	CV (%)	5.9	6.8	7.9	8.5
S	Min	0.067	0.045	0.066	0.069
	Max	0.103	0.074	0.084	0.094
	Mean	0.083 a	0.058 b A	0.074 B	0.079 B
	CV (%)	16.1	16.8	9.3	10.3

Note: A comparison was established between the C and B_0 treatments using an F test and a two-tailed t test at $p=0.05$. For a given parameter, means followed by the same lower case letter are not significantly different. Means followed by a different lower case letter are significantly different. A pairwise comparison was established between the B_0, B3 and B5 treatments using an F test and a two-tailed t test at $p=0.05$. For a given parameter, means followed by the same upper case letter are not significantly different. Means followed by a different upper case letter are significantly different.

The ratio between θ_s and the soil porosity, obtained from ρ_b and assuming a soil particle density of 2.65 g cm^{-3}, was equal to 1.04 for the C treatment and 0.89 for the B_0 one. Despite the numerical uncertainty linked to a ratio > 1, likely attributable to the approximations of the experiment, the sign was that soil saturation was more complete in the former soil than the latter one. Therefore, shaping the rill and allowing water to move in this incision did not induce soil compaction in the zone surrounding the channel, probably because the rill was formed by gently excavating and removing soil. However, the repeated passage of water promoted some soil alteration with different mechanisms, such as slaking at the beginning of the experiment or weakening of the bonds between soil particles due to wetting or mechanical solicitations (e.g., Le Bissonnais, 1996). A part of the smallest and most mobile particles penetrated the soil. These particles did not modify the largest pores since they were too small as compared with these pores. However, they partially occluded pores of intermediate sizes and induced the formation of very small pores.

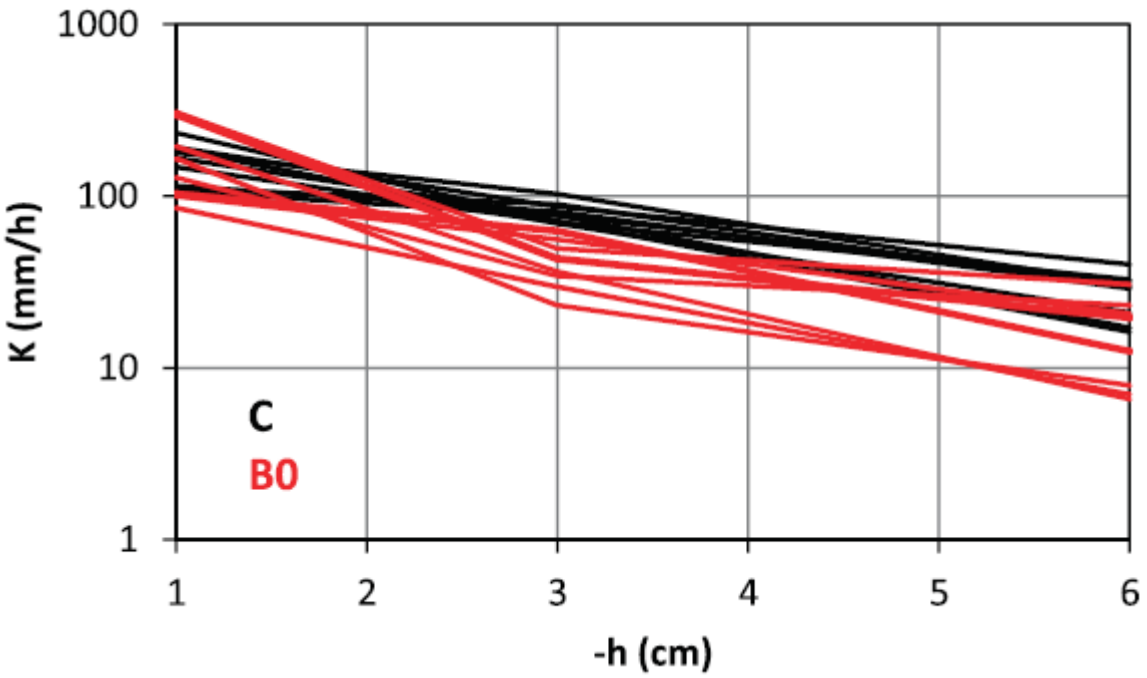

FIGURE 4 | Hydraulic conductivity, *K*, versus pressure head, *h*, relationships determined in the non-rilled plot area (C) and the non-treated rill (B0).

According to the guidelines by Reynolds et al. (2002, 2009), macroporosity and soil aeration in the soil matrix domain were good, but the plant-available water capacity was limited regardless of the treatment. Therefore, the formation of the rill and the establishment of a flow through the incision did not have appreciable effects on the soil's ability to quickly drain excess water and facilitate root

proliferation. However, the soil became less aerated in the soil matrix domain and also less able to retain available water for crop growth.

An overlap of the hydraulic conductivity curves obtained with the C and B_0 treatments was noticed close to saturation (Figure 4). For smaller (more negative) pressure heads, the curves obtained in the C area tended to stay above those obtained in the B_0 rill, particularly with reference to the intermediate pressure head established experimentally (h = -3 cm). The means of K_{-1cm} did not differ significantly between the two treatments (160-173 mm/h) while the K_{-3cm} and K_{-6cm} values obtained in the B_0 rill were smaller by 1.9 and 1.7 times, respectively, than those obtained in the C zone (Table 2). Regardless of h, the relative variability of the data was more appreciable in the rill than in the non-rilled area. In particular, the coefficients of variation, CV, of K denoted consistently a medium variation in the C area, but they signaled a high variation for two of the three established pressure heads in the B_0 rill (Warrick, 1998). In summary, shaping the rill and flow establishment in this rill i) did not influence hydraulic conductivity of the nearly saturated soil (h = -1 cm), ii) determined a significant decrease of the soil ability to transmit water in more unsaturated conditions ($h \leq$ -3 cm), and iii) enhanced spatial variability of K regardless of the considered pressure head.

TABLE 2 | Summary statistics of the soil hydraulic conductivity, K (mm/h), values for different pressure heads, h_0, established in the non-rilled upper area of the plot (control, C) and in the rills treated with biochar at a rate of 0% (B_0), 3% (B_3) and 5% (B_5) (sample size, N=8 for the B_0 treatment and N=9 for the C, B_3 and B_5 treatments).

h_0 (cm)	Statistic	C	B_0	B_3	B_5
−6 $d \leq 0.5$ mm	Min	16.2	6.6	8.6	16.2
	Max	40.0	30.6	39.3	29.5
	Mean	27.5 a	16.0 b A	20.9 AB	24.0 B
	CV (%)	28.6	55.1	46.7	20.1
−3 $d \leq 1$ mm	Min	69.1	23.2	17.6	46.5
	Max	102.6	62.7	99.7	97.8
	Mean	80.6 a	41.9 b A	62.3 B	71.3 B
	CV (%)	13.5	32.3	37.4	27.2
−1 $d \leq 3$ mm	Min	106.5	85.0	119.5	129.6
	Max	234.1	309.1	306.3	560.0
	Mean	159.9 a	173.1 a A	214.3 A	277.7 A
	CV (%)	27.2	51.1	29.7	50.0

Note: A comparison was established between the C and B0 treatments using an F test and a two-tailed t test at p=0.05. For a given pressure head, means followed by the same lower-case letter are not significantly different. Means followed by a different lower-case letter are significantly different. A pairwise comparison was established between the B0, B3 and B5 treatments using an F test and a two-tailed t test at p=0.05. For a given pressure head, means followed by the same upper-case letter are not significantly different. Means followed by a different upper-case letter are significantly different.

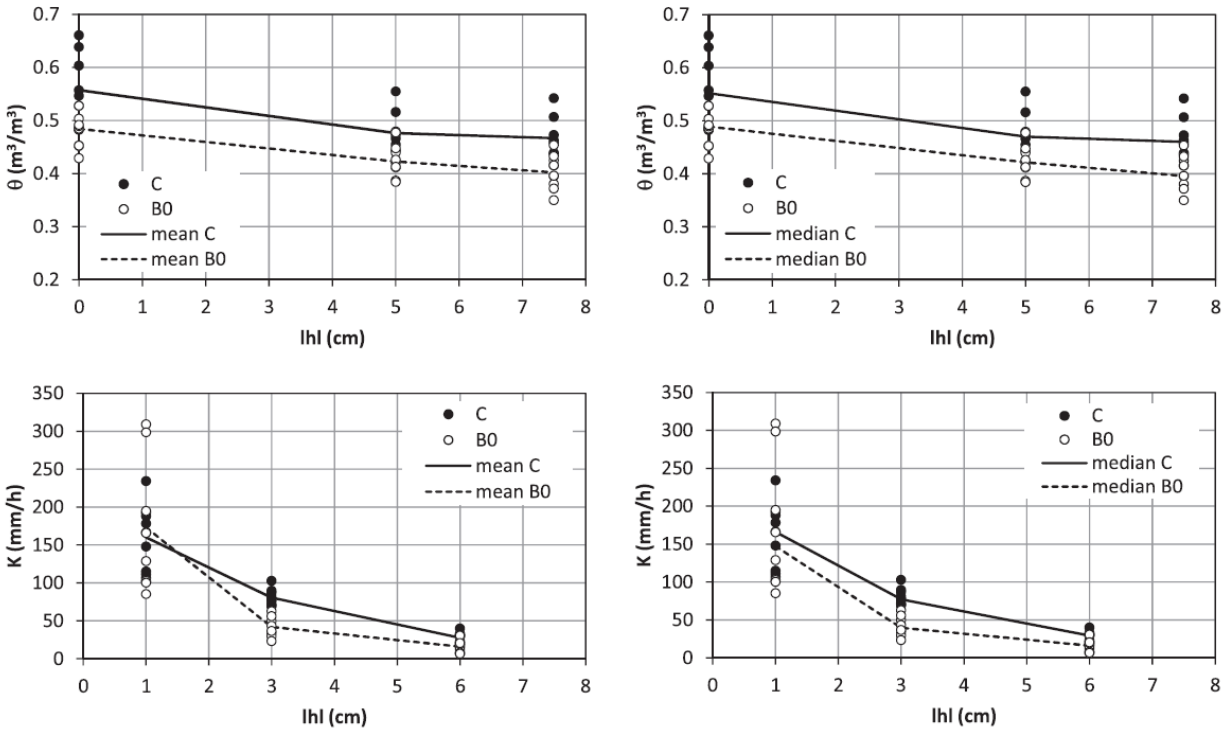

FIGURE 5 | Volumetric soil water content, θ, and soil hydraulic conductivity, K, against the absolute value of the soil water pressure head, h, for the control (C) and the rilled (B_0) soil.

Soil erosion can be expected to induce changes in the hydraulic properties of the exposed soil surface (Li et al., 2021). This investigation supported this expectation and also demonstrated that, with reference to the near-saturated soil hydraulic conductivity (close to zero h values), soil erosion effects can change with the considered pressure head. The smaller the imposed pressure head at the soil surface, the smaller the active soil pores in the soil water transport process. Likely, shaping the rill induced some smearing and compaction of the exposed soil surface, and hence a general decrease of K, but soil particle detachment induced by rill flow determined a reactivation of the largest pores. Another, not necessarily alternative, interpretation could be that some of the transported sediments were trapped at the bottom of the rill as a consequence, for example, of surface soil roughness. According to this investigation, these trapped sediments were particularly effective in occluding the smaller exposed pores.

Figure 5 establishes a comparison between the water retention and the hydraulic conductivity relationships obtained under the C and B_0 treatments in the nearly common pressure head range. The figure is repeated twice since the individual data were summarized by both the mean and the median, and reporting all curves on a single plot was found to make some confusion. At least with reference to the medians, there was consistency between the water retention and hydraulic conductivity curves, given that, notoriously, K decreases for smaller θ values. In particular, for high (little negative)

pressure heads, rilling induced a decrease in the soil's ability to retain water, and therefore the soil became less conductive. A consistency between water retention and hydraulic conductivity curves was also perceived considering the means, even if, in this case, the results were a little less clear (h = -1 cm: C soil was wetter than the B_0 soil but had similar K values).

Biochar addition

Numerically, ρ_b and θ_{-150m} decreased monotonically or almost monotonically in the passage from the B_0 to B_5 treatment. Instead, θ_s, $\theta_{-0.1m}$, θ_{-1m}, $(\theta_s - \theta_{-0.1m})$, $(\theta_{-0.1m} - \theta_{-1m})$ and $(\theta_{-1m} - \theta_{-150m})$ increased more or less monotonically between the two extreme treatments (Table 1). Regardless of the treatment, data variability was low for ρ_b, θ_s, $\theta_{-0.1m}$, θ_{-1m}, θ_{-150m} and $(\theta_{-1m} - \theta_{-150m})$ and medium for $(\theta_s - \theta_{-0.1m})$. The variability of the $(\theta_{-0.1m} - \theta_{-1m})$ values was medium for the B0 treatment and low for the B_3 and B_5 treatments.

The ρ_b values for the B_3 and B_5 treatments were statistically similar and smaller than those obtained with the B_0 treatment. The means of θ_s, $\theta_{-0.1m}$, θ_{-1m} and θ_{-150m} did not differ between the B_0 and B_3 treatments. The B_5 treatment yielded higher θ_s, $\theta_{-0.1m}$ and θ_{-1m} values and smaller θ_{-150m} values than the other two treatments. Macroporosity $(\theta_s - \theta_{-0.1m})$ did not change significantly with the treatment. Soil aeration in the soil matrix domain $(\theta_{-0.1m} - \theta_{-1m})$ varied according to the $B_5 = B_3 \geq B_0$ sequence. The plant available water capacity $(\theta_{-1m} - \theta_{-150m})$ did not differ between the B_0 and B_3 treatments, but it was higher with the B_5 treatment.

The SPQ was very good ($S > 0.05$) regardless of the treatment. However, the B_3 and B_5 treatments yielded statistically similar S values and both these values were significantly higher than that obtained for the B_0 treatment. Adding biochar reduced the variability of S since it was medium for the B_0 treatment and low for both the B_3 and B_5 treatments.

The ratio between θ_s and the soil porosity was not calculated in this case since the assumption that soil particle density was equal to 2.65 g cm^{-3} could not be made due to the presence of biochar.

Therefore, a small amount of biochar (B_3 treatment) was enough to induce a significant decrease in ρ_b that did not decrease further with more biochar (B_5 treatment). Except for θ_{-150m}, the same small amount of biochar tended to generally give larger θ values and θ differences, but not enough to make differences with the untreated soil statistically significant. Instead, these differences became significant with more biochar. With reference to θ_{-150m}, even a small amount of biochar yielded a little smaller value as compared with the non-treated soil, but a large amount of biochar was necessary to make the differences significant.

In summary, as compared with the non-treated soil, a small addition of biochar (3%) did not significantly affect θ_s, $\theta_{-0.1m}$, θ_{-1m}, and θ_{-150m}. When more biochar (5%) was used, the first three parameters significantly increased, while the fourth parameter significantly decreased. Consequently, (θ_s - $\theta_{-0.1m}$) did not change significantly between the B_0 and B_5 treatments since both θ_s and $\theta_{-0.1m}$ increased. An increase of ($\theta_{-0.1m}$ - θ_{-1m}) occurred because $\theta_{-0.1m}$ increased more (by 0.053 m^3 m^{-3}) than θ_{-1m} (by 0.025 m^3 m^{-3}). Finally, (θ_{-1m} - θ_{-150m}) increased because θ_{-1m} increased and θ_{-150m} decreased. As compared with the non-treated soil, adding 5% of biochar implied that the volume of pores with $d > 300$ μm did not change. There were more pores of both $30 \leq d \leq 300$ μm and of $0.2 \leq d \leq 30$ μm and less pores with $d \leq 0.2$ μm. According to guidelines by Reynolds et al. (2002, 2009), macroporosity and soil aeration in the soil matrix domain were good regardless of the treatment. Instead, the plant-available water capacity was limited for the B_0 and B_3 treatments and good for the B_5 treatment.

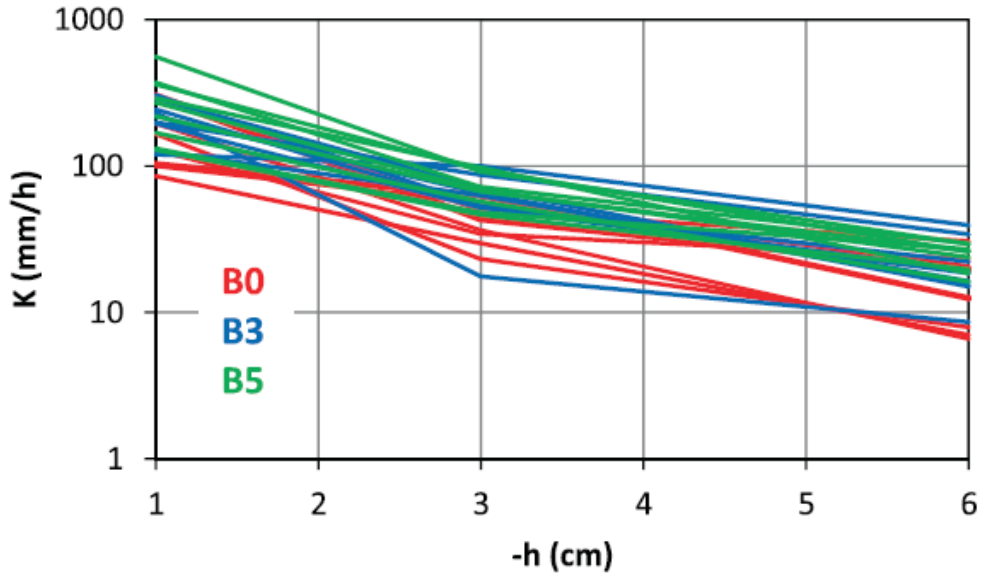

FIGURE 6 | Hydraulic conductivity, *K*, versus pressure head, *h*, relationships determined in the non-treatedrill (B0) and in the treated rills with biochar at a rate of 3% (B3) and 5% (B5).

According to the *S* calculations, even a relatively small addition of biochar (B_3 treatment) was enough to significantly improve the SPQ. With more biochar (B_5 treatment), the differences between the treated and non-treated soils became larger. However, the two treatments with biochar did not differ significantly, suggesting that using 5 % of biochar instead of 3 % had a limited effect on *S*. Adding biochar made *S* calculations less variable, suggesting a homogenizing effect of the treatment, even for a relatively small percentage of biochar.

A partial overlap of the hydraulic conductivity curves obtained with the B_0, B_3, and B_5 treatments was noticed close to saturation (Figure 6). For more negative pressure heads, the curves obtained in the B_3 and B_5 rills appeared to overlap with each other and overall stay above those obtained in the B_0 rill. For all established pressure heads, *K* increased monotonically with the applied amount of biochar. In particular, *K* for the B_5 rill was 1.5-1.7 times greater than *K* for the B_0 rill, depending on *h*. The means of K_{-1cm} did not differ significantly among the three treatments (173-278 mm h^{-1}; Table 2). Those of K_{-3cm} varied between 42 and 71 mm/h according to the $B_5 = B_3 > B_0$ sequence. Finally, the means of K_{-6cm} varied between 16 and 24 mm h^{-1} according to the $B_5 = B_3 \geq B_0$ sequence. Relative variability of *K* decreased monotonically from the B_0 to the B_5 rill with reference to K_{-6cm}, but a similar trend was not detected for the other two pressure heads since the B_3 rill yielded the highest *CV* with reference to K_{-3cm} and the lowest *CV* of K_{-1cm}.

Therefore, regardless of *h*, using 3 % or 5 % of biochar did not induce statistically significant differences between the corresponding *K* values. For the highest pressure head (h = -1 cm), adding biochar did not significantly modify the soil hydraulic conductivity. For the intermediate pressure head (h = -3 cm), even a limited concentration of biochar (3%) determined a significant increase in *K*. For the most negative pressure head (h = -6 cm), a significant increase in *K* as compared with a non-treated soil (B_0) required adding 5% of biochar. In other terms, from a purely numerical point of view, the inclusion of biochar in the soil improved, in general, the soil aptitude to transmit water, regardless of the pore size. This improvement was statistically irrelevant in the case of a transport process governed by the larger pores. Instead, the water transport ability of the smallest pores ($h \leq$ -3 cm) increased with a high percentage of biochar.

A variety of results have been reported for other loamy soils, texturally similar, in a broad sense, to the one considered in this investigation. According to Blanco-Canqui (2017), the addition of biochar can be expected to reduce unsaturated conductivity close to saturation due to the filling or clogging of soil macropores with fine biochar particles. An increase in near-saturated conductivity in biochar-amended soils can instead occur as a consequence of increased earthworm burrowing (Hardie et al., 2014). Biochar may enhance the transport of water under unsaturated conditions by reducing the formation of larger pores (draining pores) and promoting finer inter-particle pore formation (Villagra-Mendoza and Horn, 2018). The results of this investigation were not consistent with the suggestion by Blanco-Canqui (2017), nor were explained by earthworm activity since earthworms were not noticed, and in any case, the experiments were performed after a short incubation period. Instead, the suggestion by Villagra-Mendoza and Horn (2018) appeared approximately adaptable to our data. In particular, biochar addition was statistically ineffective with reference to the largest sampled pores,

but including a relatively high amount of this amendment (5%) favored the formation of smaller pores, that is, those active for pressure heads smaller than or equal to -3 cm.

Another way to summarize the results is to recognize that there is some correspondence between the static porosity, as determined from the water retention measurements, and the dynamic porosity determined by the UHG experiment. Macroporosity does not change but the drainable porosity increases. Taking into account that K is an integral measurement, expressive of flow in all porosity classes from zero to the upper boundary, it is plausible to believe that, for h = -6 cm, the weight of the drainable porosity is greater and this explains the increase of K_{-6}. For h = -1 cm, the contribution of the macroporosity prevails and for this reason significant differences in K_{-1} are not detected even if the mean increases anyway.

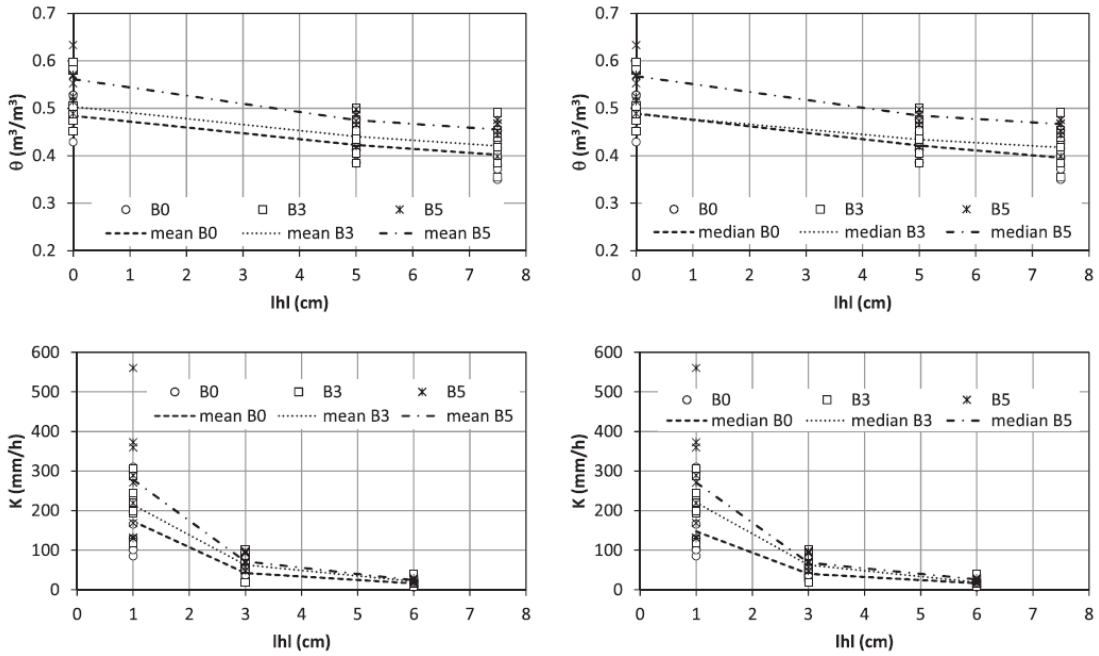

FIGURE 7 | Volumetric soil water content, θ and soil hydraulic conductivity, K, against the absolute value of the soil water pressure head, h, for the rilled soil with different concentrations of biochar (0%: B_0; 3%: B_3; 5%: B_5).

Figure 7 establishes a comparison between the water retention and the hydraulic conductivity relationships corresponding to the B_0, B_3, and B_5 treatments in a common range of high pressure head values. Also in this case, the figure is repeated twice since the individual data were summarized by both the mean and the median. Considering the means, the water retention and hydraulic conductivity curves appeared consistent between them since adding biochar increased the soil's ability to retain water and hence its ability to transmit water. A consistency between water retention and hydraulic conductivity curves was also perceived considering the medians, even if, in this case, the results were

a little less clear (h = -1 cm: similar θ value for the B_0 and B_3 soils but a higher K value in the treated soil).

Combined rilling and biochar addition effects

Figure 8 compares the means of θ_s, $\theta_{-0.1m}$, θ_{-1m}, θ_{-150m}, S, K_{-6cm}, K_{-3cm}, and K_{-1cm} for the four treatments considered in this investigation (C, B_0, B_3, B_5).

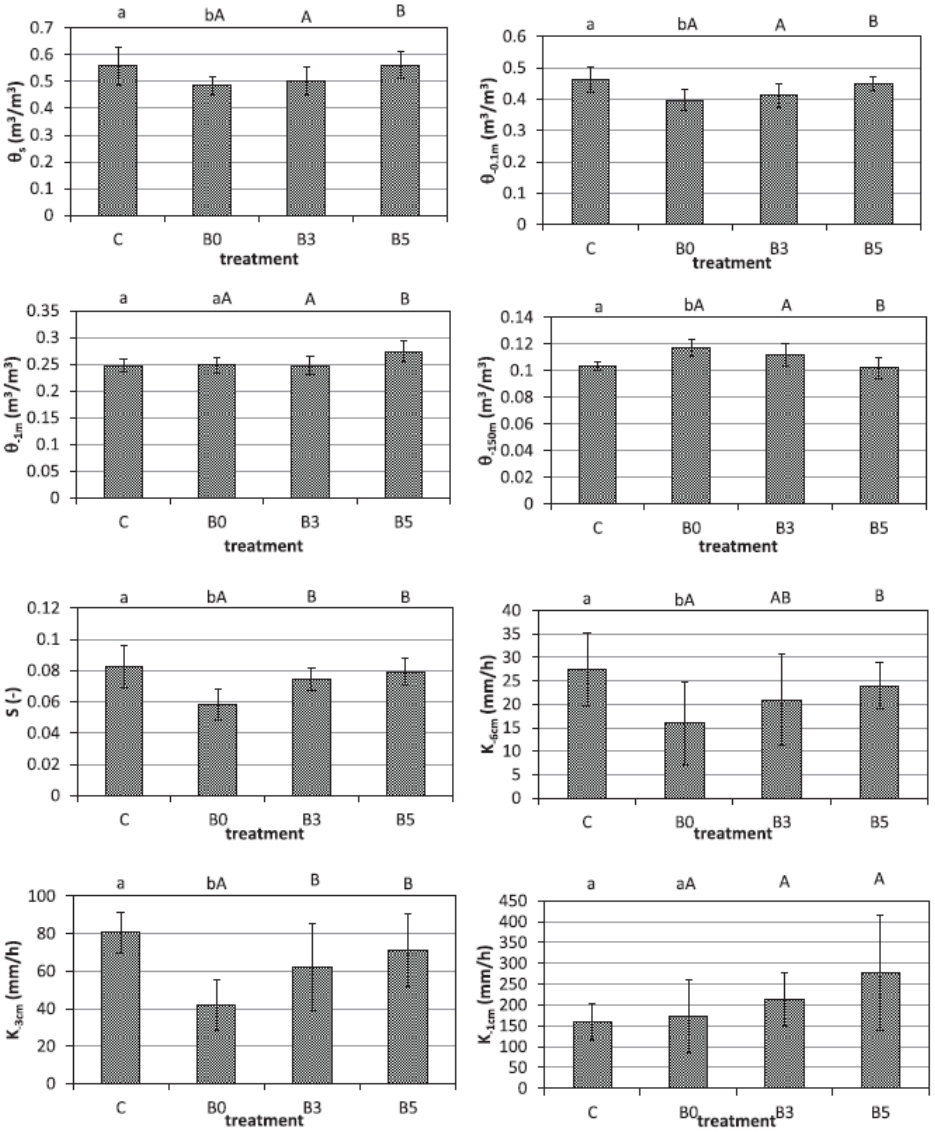

FIGURE 8 | Means of saturated soil volumetric water content, θ_s, volumetric soil water content at a pressure head of -0.1 m ($\theta_{-0.1m}$), -1 m (θ_{-1m}), -150 m (θ_{-150m}), S-index, and soil hydraulic conductivity at a pressure head value of -6 cm (K_{-6cm}), -3 cm (K_{-3cm}) and -1 cm (K_{-1cm}) for four soil treatments (C: control; B_0: rilled soil; B_3: rilled soil with 3% of biochar; B_5: rilled soil with 5% of biochar). Error bars represent $\pm$ one standard deviation. Histograms denoted by the same lower (comparison between the C and B0 treatments) or upper (comparison between the B0, B3 and B5 treatments) case letters indicate that means did not differ significantly at P = 0.05. Histograms denoted by different lower- or upper-case letters indicate that means differed significantly.

Rilling of the non-treated soil (B_0) determined a decrease of θ_s, $\theta_{-0.1m}$, S, K_{-6cm}, and K_{-3cm} and an increase of θ_{-150m} as compared with the control (C). The addition in the rill of a relatively large amount of biochar (B_5) effectively contrasted these rilling effects since θ_s, $\theta_{-0.1m}$, θ_{-150m}, S, K_{-6cm}, and K_{-3cm} did not appear to differ appreciably between the C and B_5 treatments. Rilling effects were also contrasted by adding a relatively small amount of biochar (B_3), but to a more limited extent. Neither rilling alone nor rilling in a soil with a relatively low biochar content (B_3) resulted in appreciable variations in θ_{-1m} compared to the control. Instead, adding relatively high amounts of biochar in the rilled soil (B_5) yielded higher θ_{-1m} values both with respect to the control and with reference to the other two rills (B_0, B_3). Finally, rilling (B_0) did not appear to appreciably alter K_{-1cm} as compared with the control. However, more biochar in the rill implied obtaining higher K_{-1cm} values.

Therefore, six (θ_s, $\theta_{-0.1m}$, θ_{-150m}, S, K_{-6cm}, and K_{-3cm}) of the eight considered parameters consistently indicated that i) in the absence of any treatment with biochar, rilling altered the soil characteristics, and ii) the addition of a large amount of biochar impeded these alterations to occur. In other terms, the changes induced by rilling were compensated by the presence of biochar in the soil. This interpretation is not contradicted by the results obtained with the other two parameters (θ_{-1m} and K_{-1cm}), since in this case the suggestion was that the addition of large amounts of biochar in the rill can make the soil even more able than the non-rilled soil to retain water at field capacity and more conductive in close to saturation conditions.

NMR measurements on soil samples with different biochar concentration

For calculating *FCI* and *SCI* indexes, the empirical cumulative frequency distributions of the longitudinal relaxation time ($F(T_1)$ distribution) for the relaxograms corresponding to the B_1, B_3, B_5, and C treatments, and the applied biochar measured at the different applied magnetic fields were examined.

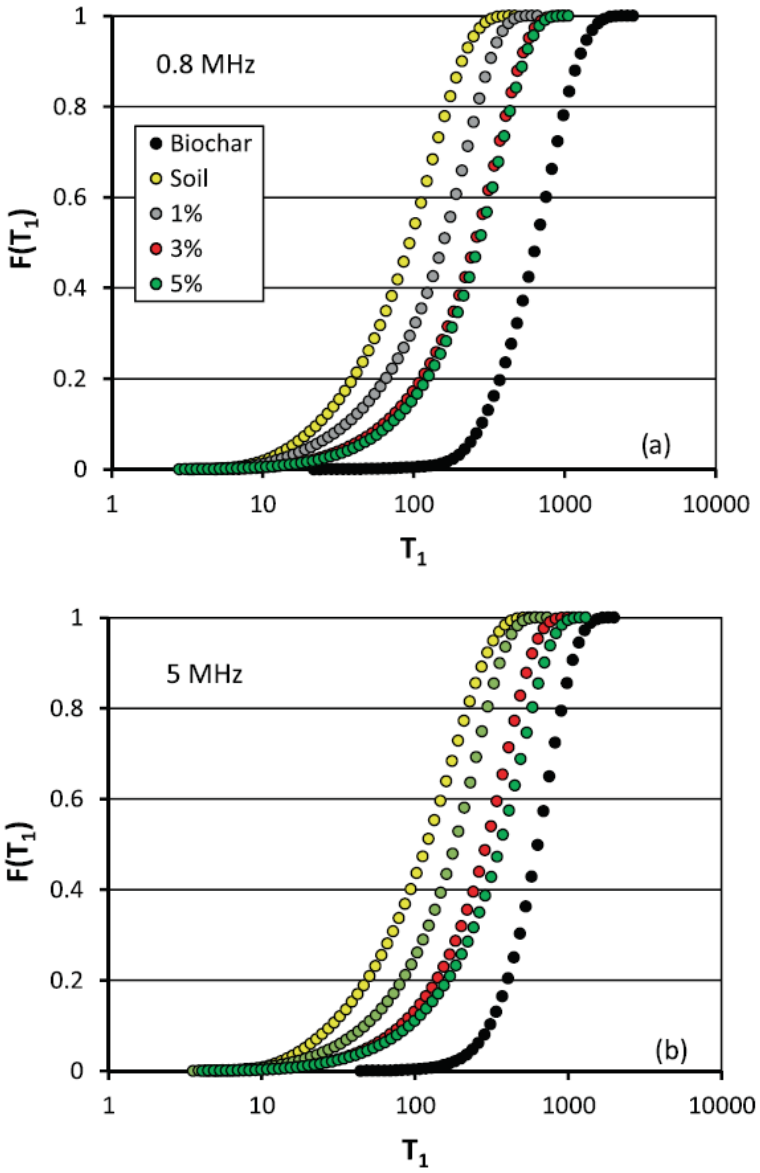

FIGURE 9 Empirical cumulative frequency distributions $F(T_1)$ of the investigated samples (Biochar, C, B_1, B_3, and B_5) for two applied proton Larmor frequencies

Figure 9 shows, as an example for two values of the applied magnetic field (ν_L of 0.8 and 5 MHz), the detected $F(T_1)$ distribution. For each ν_L value, the relaxation time distribution of the investigated soil (C treatment) is always on the left of the $F(T_1)$ corresponding to the other treatments. Therefore, the shortest T_1 values correspond to the soil, while, on the contrary, biochar is characterized by the longest T_1 values. This detected difference between the original soil and the three mixtures of soil and biochar (i.e. B_1, B_3, and B_5 treatments) can be attributed to the increase in size of the pores in the latter due to the biochar component. Figure 9 also highlights that all $F(T_1)$ distributions are S-shaped and skewed towards shorter T_1 values, suggesting that the macro-pore component (largest T_1 values) is not dominant, and the biochar addition increases the size of mesopores and micropores. The

overlapping between the $F(T_1)$ distributions corresponding to BC = 3 and 5% establishes that this increase does not produce appreciable changes in the pore distribution inside the mixture.

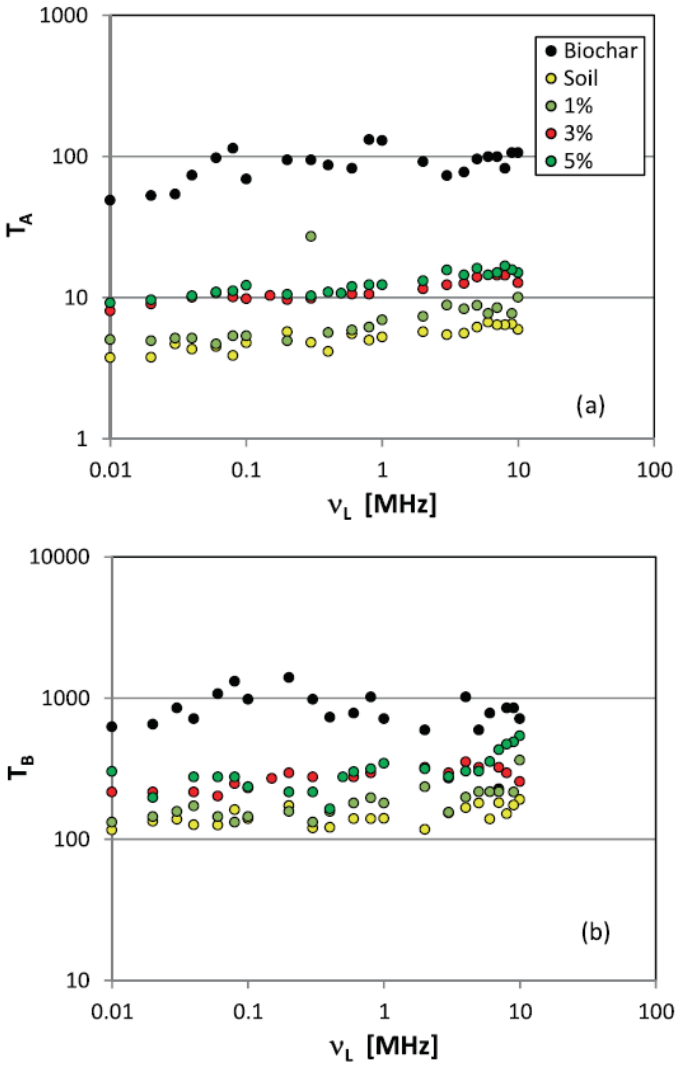

FIGURE 10 | Relationship between the applied proton Larmor frequency νL and *TA* (a) and *TB* (b) for all the investigated samples.

For a given percentage of biochar, Figure 10 shows the variation of T_A, which is indicative of water molecules contained in small pores, and T_B, corresponding to water contained in large pores, with the proton Larmor frequency ν_L. Figure 10 points out that (i) the highest T_A and T_B values are characteristic of soil-biochar mixtures, while the lowest values correspond to the soil; (ii) T_A and T_B are independent of ν_L; (iii) T_A and T_B increase with the biochar percentage. Furthermore, Figure 10 demonstrates that B_3 and B_5 treatments are characterized by similar values of T_A and T_B. In other words, a biochar amount equal to 5% can be considered a limit value to obtain appreciable variations of the micro-pores and macro-pores as compared to the original soil. From a hydrological point of view, the increase of *BC* from 3 % to 5 % does not change the micro-pore and the macro-pore

components. This result agrees with those obtained by Li et al. (2019; 2020) and Gholamahmadi et al. (2023), who found a threshold value of biochar addition effectiveness equal to 3 and 2.5 %, respectively.

According to a previous study (Conte and Ferro, 2020), the *SCI* and *FCI* values of the investigated mixtures measured applying different magnetic fields were merged into a single statistical sample, thereby obtaining the corresponding cumulative frequency distributions plotted in Figure 11. For each index, Figure 11 shows that the empirical cumulative frequency distribution of the biochar is always placed on the left-hand side of that of the original soil, i.e., the *SCI* and *FCI* values for the soil sample are always greater than those of the biochar. Figure 11a also demonstrates that the B_5 treatment has higher *SCI* values than B_1 and B_3, for which, instead, the index distributions overlap. Figure 11b points out that *FCI* distributions for C and B_1 treatments overlap as well as those for the B_3 and B_5 ones, and the latter shift to the left as compared to the former. This result reveals that, with respect to the original soil, *FCI* does not reduce further beyond $BC = 3$ % Therefore, biochar concentrations of 5% and 3% are discriminating values for *SCI* and *FCI*, respectively.

In conclusion, the developed analysis demonstrated that the FFC NMR technique is able to measure the two components, *SCI* and *FCI*, of the hydrological connectivity inside the soil and their variability with the percentage of biochar added to the original soil.

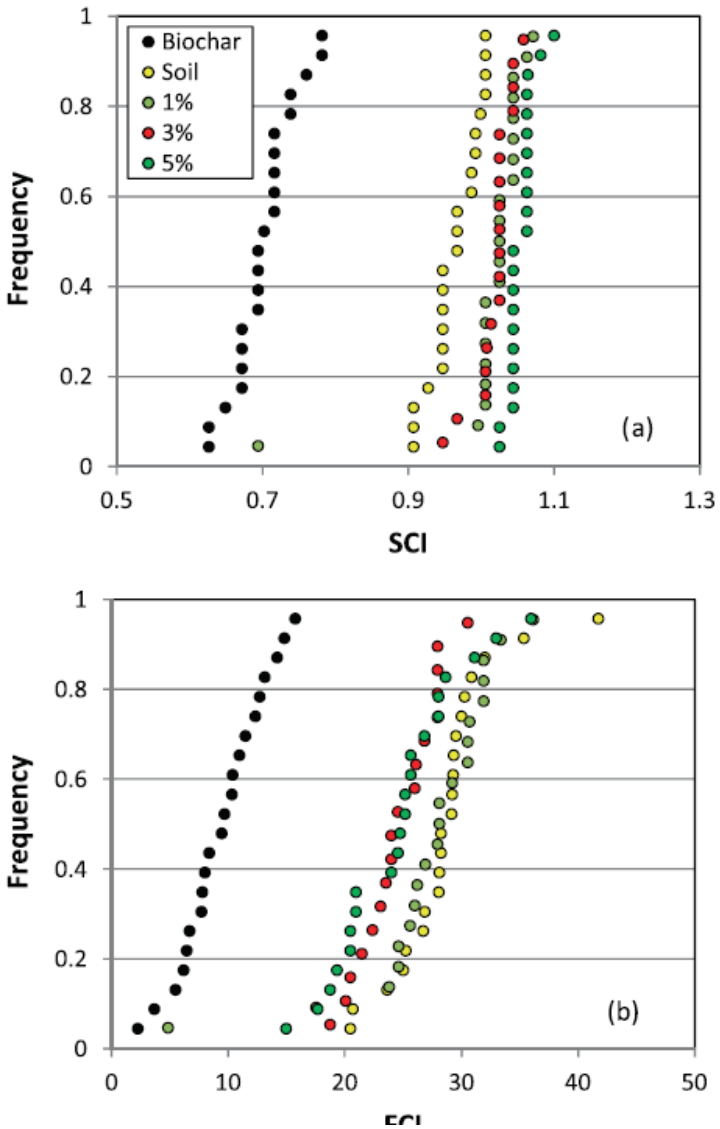

Figure 11 Empirical frequency distributions of SCI (a) and FCI (b) for all the investigated samples

3.5 Combination of hydrological and NMR measurements

One of the innovative aspects of this investigation was the attempt to look at the pore system from two different observation scales: a macroscopic scale by the hydrological measurements and a microscopic or molecular scale by the NMR measurements. In both cases, the pore size distribution, leading to categorization into macropores, mesopores, and micropores, was estimated and not measured directly. In particular, hydrological data were analyzed by the Young-Laplace equation under the assumption that the pores are perfectly cylindrical, uniform, and equally drained (e.g., Hardie et al., 2014). For the NMR data, the correspondence between pore sizes and the measured relaxogram represented an assumption (Conte and Ferro, 2018) still needing testing. A comparison

between the hydrological and the NMR data was made to verify if there was a link between the two approaches.

The water volume contained in the macropores ($d > 300$ μm) did not change significantly between the non-treated rilled soil (B_0 treatment) and the rilled soil treated with 5% of biochar (B_5 treatment) (Table 1). However, the FFC NMR investigations revealed that the size of the largest pores ($d \geq 50$ μm) increased as comparing the untreated soil and the biochar/soil mixture (Figure 9). By considering the hydrological and NMR measurements together, it is possible to suggest that the former investigation can be affected by the larger pore-size scale ($d > 300$ μm) in comparison with the NMR analysis ($d \geq 50$ μm). As a consequence, the amount of free bulk water affecting the hydrological measurements is larger than that present during the NMR investigations. Moreover, the combined results appear to suggest that while the total volume of the largest pores remains constant, the number of pores can decrease. In other words, the addition of biochar did not alter total pore volume but could modify only the total number of pores, determining fewer macropores having larger sizes.

Adding biochar increased the water volume contained in pores of intermediate size ($0.2 \leq d \leq 300$ μm), and the NMR analysis signaled an increase in the size of the mesopores. In this case, it was not possible to draw a conclusion on the number of mesopores since three different combinations (larger and more numerous mesopores, larger but unvaried number of mesopores, and larger but fewer mesopores) can be expected to yield the result that was obtained with the water retention measurements.

Finally, less water was contained in the micropores of ≤ 0.2 μm, but the NMR data suggested an increase in the size of these pores with the addition of biochar. Therefore, the suggestion was that in the treated soil there were fewer small pores, but they were greater than those in the non-treated soil. The scale difference and the uncertainties in the analysis methodologies of the data that are actually collected (soil water content for established pressure heads with the hydrological measurements and relaxogram for the NMR measurements) induce not to exclude that the two types of measurement may be disconnected from each other. However, it cannot even be ruled out that there is some link between the two experimental approaches since soil-water interactions are investigated in both cases. According to the results of this investigation, the latter hypothesis appears to have some support. Consequently, additional efforts should be made to develop a clear relationship between the two different types of measurements.

Conclusions

Contrasting effects of biochar addition on runoff and soil loss have been reported in the literature, and the existence of a threshold value of biochar concentration useful for soil conservation strategies needs further investigations. In this study, the effects of rill formation and biochar addition on the physical and hydraulic properties of a clay-loam soil were assessed by laboratory measurements and field tests.

According to the water retention measurements performed on a clay-loam soil, the formation of the rill and establishment of a flow through the incision can be expected to have no appreciable effect on the soil's ability to quickly drain excess water and facilitate root proliferation. However, the soil could become less aerated in the soil matrix domain and also less able to retain readily available water for crop growth. As compared with a non-treated rilled soil, adding 5% of biochar to the soil surrounding the rill incision can imply that the volume of pores with diameter $d > 300$ μm does not change. More pores of both $30 \leq d \leq 300$ μm and of $0.2 \leq d \leq 30$ μm and fewer pores with $d \leq 0.2$ μm can develop. On the basis of the water transmission parameters determined in this investigation, shaping the rill and flow establishment in this rill could not influence the hydraulic conductivity of the nearly saturated soil (pressure head, $h = -1$ cm), but it could also determine a significant decrease in the soil ability to transmit water in more unsaturated conditions ($h \leq -3$ cm). Inclusion of biochar in the soil can be expected to improve, in general, the soil aptitude to transmit water, regardless of the pore size. This improvement could be statistically irrelevant in the case of a transport process governed by the larger pores. Instead, the water transport ability of the smallest pores ($h \leq -3$ cm) can increase with a high percentage of biochar.

The NMR measurements revealed that the increase of *BC* from 3% to 5% does not change the micro- and macro-pore components, and biochar addition of 5% can be considered a limit value to obtain appreciable variations of the micro-pores and macro-pores as compared to the original soil. Furthermore, the addition of biochar to the original soil improves the structural connectivity component, while the functional connectivity index of the mixtures is similar to that of the original soil only for $BC = 1\%$, it does not change between *BC* contents of 3 and 5 % and lowers as compared to the original soil.

Finally, the combination of hydrological and NMR measurements suggested that a relation between the water volume contained in the pores and the NMR results (distribution of T_1, size of the pores) can be established.

In conclusion, the hydrological measurement demonstrated that the addition of biochar to the soil improved, in general, the soil aptitude to transmit water, regardless of the pore size, and demonstrated

that the addition of a large amount of biochar (5%) impeded soil characteristics alteration as the changes due to rilling were compensating by adding biochar in the soil. NMR measurements revealed that the mixture of soil and biochar was characterized by longitudinal relaxation time T_1 values, which are related to pore sizes, longer than those measured for the soil. The analysis also suggested that the macro-pore component (that is the largest T_1 values) was never dominant, while biochar addition increased the size of mesopores and micropores.

Acknowledgements

All authors set up the research, analyzed and interpreted the results and contributed to write the paper.

FUNDING

This work was supported by the Project "Indagine di laboratorio e di pieno campo sull'uso di Ammendanti naturali dei Suoli per strategie di Conservazione dell'Acqua e dei Nutrienti" (ASCAN) - National Research Centre for Agricultural Technologies, Codice progetto CN00000022, Bando a Cascata Spoke n. 6, CUP D13C22001330005 – PRJ-1815.

REFERENCES

Abrol, V., Ben-Hur, M., Verheijen, F.G.A., Keizer, J.J., Martins, M.A.S., Tenaw, H., Tchehansky, L., Graber, E.R., 2016. Biochar effects on soil water infiltration and erosion under seal formation conditions: Rainfall simulation experiment. J. Soils Sediments, 16, 2709–2719.

Baartman, J.E.M., Masselink, R., Keesstra, S.D., Temme, A.J.A.M., 2013. Linking landscape morphological complexity and sediment connectivity. Earth Surf Process Landforms 38:1457–1471. https://doi.org/10.1002/esp.3434

Bagarello, V., Iovino, M., 2012. Testing the BEST procedure to estimate the soil water retention curve. Geoderma, 187-188: 67-76, doi:10.1016/j.geoderma.2012.04.006.

Bagarello, V., Castellini, M., Iovino, M., 2007. Comparison of unconfined and confined unsaturated hydraulic conductivity. Geoderma, 137: 394-400.

Baiamonte, G., De Pasquale, C., Marsala, V., Cimò, G., Alonzo, G., Crescimanno, G., Conte, P., 2015. Structure alteration of a sandy-clay soil by biochar amendements Journal of Soils and Sediments 15: 816-824

Belisle, M., 2005. Measuring landscape connectivity: the challenge of behavioural landscape ecology. Ecology 86:1988–1995.

Blanco-Canqui, H., 2017. Biochar and soil physical properties. Soil Science Society of America Journal, 81: 687-711, doi: 10.2136/sssaj2017.01.0017.

Bondì, C., Castellini, M., Iovino, M., 2022. Compost amendment impact on soil physical quality estimated from hysteretic water retention curve. Water 14, 1002 doi: 10.3390/w14071002.

Borgia, G.C., Brown, R.J.S., Fantazzini, P., 1998. Uniform-Penalty Inversion of Multiexponential Decay Data. J Magn Reson 132(1), 65–77. https://doi.org/10.1006/jmre.1998.1387.

Borrelli, P., Robinson, D.A., Fleischer, L.R., Lugato, E., Ballabio, C., Alewell, C., Meusburger, K., Modugno, S., Schütt, B., Ferro, V., Bagarello, V., Van Oost, K., Montanarella, L., Panagos, P., 2017. An assessment of the global impact of 21st century land use change on soil erosion. Nature communications, 8(1), 1-13.

Bracken, J., Croke, J., 2007. The concept of hydrological connectivity and its contribution to understanding runoff-dominated geomorphic systems. Hydrol Process 21:1749–1763. https://doi.org/10.1002/hyp.6313

Bracken, L.J., Wainwright, J., Ali, G.A., Tetzlaff, D., Smith, M.W., Reaney, S.M., Roy, A.G., 2013. Concepts of hydrological connectivity: Research approaches, Pathways and future agendas. Earth Science Rev 119:17–34. https://doi.org/10.1016/j.earscirev.2013.02.001

Carollo, F.G., Di Stefano, C., Nicosia, A., Palmeri, V., Pampalone, V., Ferro, V., 2021. Flow resistance in mobile bed rills shaped in soils with different texture. Eur. J. Soil Sci. 72, 2062–2075.

Carollo, F. G., Di Stefano, C., Nicosia, A., Palmeri, V., Pampalone, V., Ferro, V., 2023. A new strategy to assure compliance with soil loss tolerance at a regional scale. Catena, 223, 106945.

Castellini, M., Giglio, L., Niedda, M., Palumbo, A.D., Ventrella, D., 2015. Impact of biochar addition on the physical and hydraulic properties of a clay soil. Soil & Tillage Research, 154: 1–13, http://dx.doi.org/10.1016/j.still.2015.06.016.

Chia, W. Y., Chew, K. W., Le, C. F., Lam, S. S., Chee, C. S. C., Ooi, M. S. L., Show, P. L., 2020. Sustainable utilization of biowaste compost for renewable energy and soil amendments. Environmental pollution, 267, 115662.

Conte, P., 2019. Environmental Applications of Fast Field-cycling NMR Relaxometry. In: Kimmich R. (ed.) Field-Cycling NMR Relaxometry: Instrumentation, Model Theories and Applications. The Royal Society of Chemistry, Croydon CRo 4YY, UK, pp 229–254

Conte, P., 2021. Applications of fast field cycling NMR relaxometry Annual Reports in NMR Spectroscopy 104: 141-188

Conte, P., Bertani, R., Sgarbossa, P., Bambina, P., Schmidt, H.P., Raga, R., Lo Papa, G., Chillura Martino, D.F., Lo Meo, P., 2021. Recent Developments in Understanding Biochar's Physical–Chemistry Agronomy 11: 615

Conte, P., Di Stefano, C., Ferro, V., Laudicina, V.A., Palazzolo, E., 2017. Assessing hydrological connectivity inside a soil by fast-field-cycling nuclear magnetic resonance relaxometry and its link to sediment delivery processes. Environ Earth Sci 76:526. https://doi.org/10.1007/s12665-017-6861-9

Conte, P., Ferro, V., 2018. Measuring hydrological connectivity inside a soil by low field nuclear magnetic resonance relaxometry. Hydrol Process 32:93–101. https://doi.org/10.1002/hyp.11401

Conte, P., Ferro, V., 2020. Standardizing the use of fast-field cycling NMR relaxometry for measuring hydrological connectivity inside the soil. Magn Reson Chem 58:41–50. https://doi.org/10.1002/mrc.4907

Conte, P., Ferro, V., 2022. Measuring hydrological connectivity inside soils with different texture by fast field cycling nuclear magnetic resonance relaxometry. Catena 209:105848, https://doi.org/10.1016/j.catena.2021.105848

Conte, P., Lo Meo, P., 2020. Nuclear Magnetic Resonance with Fast Field-Cycling Setup: A Valid Tool for Soil Quality Investigation Agronomy 10: 1040

Dane, J.H., Hopmans, J.W., 2002. Water retention and storage: laboratory, In: Dane, J.H., Topp, G.C. (Eds.), Methods of Soil Analysis, Physical Methods, Part 4, 3 rd edition. Soil Science Society of America, Madison, WI, pp. 688–692.

De Pasquale, C., Marsala, V., Berns, A.E., Valagussa, M., Pozzi, A., Alonzo, G., Conte, P., 2012. Fast field cycling NMR relaxometry characterization of biochars obtained from an industrial thermochemical process. J Soils Sediments 12: 1211-1221.

Dexter, A.R., 2004. Soil physical quality. Part I: theory, effects of soil texture, density, and organic matter, and effects on root growth. Geoderma 120: 201-214.

Dexter, A.R., Czyż, E.A. 2007. Applications of S-theory in the study of soil physical degradation and its consequences. Land Degradation & Development, 18: 369-381.

Dexter, A.R., Czyż, E.A., Richard, G., Reszkowska, A. 2008. A user-friendly water retention function that takes account of the textural and structural pore spaces in soil. Geoderma, 143: 243–253, doi:10.1016/j.geoderma.2007.11.010.

Di Stefano, C., Nicosia, A., Palmeri, V., Pampalone, V., Ferro, V., 2022. Rill flow resistance law under sediment transport. Journal of Soils and Sediments, 22, 334–347. https://doi.org/10.1007/s11368-021-03083-x.

Doan, T.T., Henry-des-Tureaux, T., Rumpel, C., Janeau, J.L., Jouquet, P., 2015. Impact of compost, vermicompost and biochar on soil fertility, maize yield and soil erosion in Northern Vietnam: A three year mesocosm experiment. Sci. Total Environ., 514,147–154.

Dokoohaki, H., Miguez, F.E., Laird, D., Horton, R., Basso, A.S., 2017. Assessing the biochar effects on selected physical properties of a sandy soil: An analytical approach. Communications in Soil Science and Plant Analysis, doi: 10.1080/00103624.2017.1358742.

Fouladidorhani, M., Shayannejad, M., Mosaddeghi, M.R., Shariatmadari, H., Arthur, E., 2023. Biochar, manure and superabsorbent improve the physical quality of saline-sodic soil under greenhouse conditions. Soil Science Society of America Journal, 87: 1003–1017, doi: 10.1002/saj2.20538.

Gholamahmadi, B., Jeffery, S., Gonzales-Pelayo, O., Prats, S.A., Bastos, A.C., Keizer, J.J., Verheijen, F.G.A., 2023. Biochar impacts on runoff and soil erosion by water: a systematic global scale meta-analysis. Science of the Total Environment, 871, 161860, http://dx.doi.org/10.1016/j.scitotenv.2023.161860

Gląb, T., Palmowska, J., Zaleski, T., Gondek, K., 2016. Effect of biochar application on soil hydrological properties and physical quality of sandy soil. Geoderma, 281: 11–20, http://dx.doi.org/10.1016/j.geoderma.2016.06.028.

Hao X., Ball B.C., Culley J.L.B., Carter M.R., Parkin G.W., 2008. Chapter 57 Soil Density and Porosity. p.743-759 in Soil Sampling and Methods of Analysis, edited by M.R. Carter and E.G. Gregorich, 2nd ed. ISBN-13: 978-0-8493-3586-0.

Hardie, M., Clothier, B., Bound, S., Oliver, G., Close, D., 2014. Does biochar influence soil physical properties and soil water availability? Plant and Soil, 376: 347-361, doi: 10.1007/s11104-013-1980-x.

Hseu, Z.Y., Jien, S.H., Chien, W.H., Liou, R.C., 2014. Impacts of biochar on physical properties and erosion potential of a mudstone slopeland soil. Sci. World J., 2014, 602197.

Jarvis, N. J., Zavattaro, L., Rajkai, K., Reynolds, W.D., Olsen, P.A., McGechan, M., Mecke, M., Mohanty, B., Leeds-Harrison, P.B., Jacques, D., 2002. Indirect estimation of near-saturated hydraulic conductivity from readily available soil information, Geoderma, 108: 1–17.

Jien, S.H., Wang, C.S., 2013. Effects of biochar on soil properties and erosion potential in a highly weathered soil. Catena, 110, 225–233.

Keesstra, S.S., Bagarello, V., Ferro, V., Finger, D., Parsons, A.J., 2020. Connectivity in hydrology and sediment dynamics. Land Degrad Dev 31:2525-2528. https://doi.org/10.1002/ldr.3401

Klute, A., Dirksen, C., 1986. Hydraulic conductivity and diffusivity: Laboratory methods. Methods of soil analysis: Part 1 physical and mineralogical methods, 5, 687-734.

Köppen, W. (1918). Classification of climates according to temperature, precipitation and seasonal cycle. Petermanns Geogr. Mitt, 64(1918), 193-203.

Kroetsch D, Wang C., 2008. Chapter 55 Particle Size Distribution. p.713-725 in Soil Sampling and Methods of Analysis, edited by M.R. Carter and E.G. Gregorich, 2nd ed. ISBN-13: 978-0-8493-3586-0.

Laudicina, V.A., De Pasquale, C., Conte, P., Badalucco, L., Alonzo, G., Palazzolo, E., 2012. Effects of afforestation with four unmixed plant species on the soil–water interactions in a semiarid Mediterranean region (Sicily, Italy). J Soils Sediments 12: 1222-1230.

Le Bissonnais, Y., 1996. Aggregate stability and assessment of soil crustability and erodibility: I. Theory and methodology. European Journal of Soil Science, 47: 425-437.

Lee, C.H., Wang, C.C., Lin, H.H., Lee, S.S., Tsang, D.C.W., Jien, S.H., Ok, Y.S., 2018. In-situ biochar application conserves nutrients while simultaneously mitigating runoff and erosion of an Fe-oxide-enriched tropical soil. Sci. Total Environ., 619–620, 665–671.

Lee, S.S., Shah, H.S., Awad, Y.M., Kumar, S., Ok, Y.S., 2015. Synergy effects of biochar and polyacrylamide on plants growth and soil erosion control. Environ. Earth Sci., 74, 2463–2473.

Li, Q.X., Jin, Z.W., Chen, X.M., Jing, Y., Huang, Q.R., Zhang, J.B., 2017. Effects of biochar on aggregate characteristics of upland red soil in subtropical China. Environ. Earth Sci., 76, 372.

Li, Y., Feng, G., Tewoldec, H., Yang, M., Zhang, F., 2020. Soil, biochar, and nitrogen loss to runoff from loess soil amended with biochar under simulated rainfall. J. Hydrol., 591, 125318.

Li, Y.Y., Zhang, F.B., Yang, M.Y., Zhang, J.Q., Xie, Y.G., 2019. Impacts of biochar application rates and particle sizes on runoff and soil loss in small cultivated loess plots under simulated rainfall. Sci. Total Environ., 649, 1403–1413.

Li, H., Zhu, H., Wei, X., Liu, B., Shao, M., 2021. Soil erosion leads to degradation of hydraulic properties in the agricultural region of Northeast China. Agriculture, Ecosystems and Environment, 314: 107388, 9 pp., doi: 10.1016/j.agee.2021.107388.

López-Vicente, M., Nadal-Romero, E., Cammeraat, E.L.H., 2017. Hydrological Connectivity Does Change Over 70 Years of Abandonment and Afforestation in the Spanish Pyrenees. Land Degrad Dev 28:1298–1310. https://doi.org/10.1002/ldr.2531

Lu, S.-G., Sun, F.-F., Zong, Y.-T., 2014. Effect of rice husk biochar and coal fly ash on some physical properties of expansive clayey soil (Vertisol). Catena, 114: 37–44, http://dx.doi.org/10.1016/j.catena.2013.10.014.

Marchamalo, M., Hooke, J.M., Sandercock, P.J., 2016. Flow and Sediment Connectivity in Semi-arid Landscapes in SE Spain: Patterns and Controls. Land Degrad. Dev. 27:1032–1044. https://doi.org/10.1002/ldr.2352

Morgan, R.P.C., Duzant, J.H., 2008. Modified MMF (Morgan–Morgan–Finney) model for evaluating effects of crops and vegetation cover on soil erosion. Earth Surface Processes and Landforms, 32: 90–106, doi: 10.1002/esp.1530.

Mukherjee, A., Lal, R., Zimmerman, A.R., 2014. Effects of biochar and other amendments on the physical properties and greenhouse gas emissions of an artificially degraded soil. Sci Total Environ 487:26–36. https://doi.org/10.1016/j.scitotenv.2014.03.141

Mutchler, C.K., Young, R.A., 1975. Soil detachment by raindrops. In Present and Prospective Technology for Predicting Sediment Yields and Sources; USDA Sedimentation Laboratory: Oxford, MS, USA, ARS-S-40; pp. 113–117.

Nearing, M. A., Liu, B. Y, Risse, L. M., Zhang, X., 1996. Curve Numbers and Green-Ampt effective hydraulic conductivities. Water Resources Bulletin, 32(1): 125-136.

Nicosia, A., Pampalone, V., Ferro, V., 2021. Effects of biochar addition on rill flow resistance. Water, 13, 3036.

Nicosia, A., Palmeri, V., Pampalone, V., Di Stefano, C., Ferro, V., 2022a. Slope threshold in rill flow resistance. Catena, 208, 105789.

Nicosia, A., Di Stefano, C., Palmeri, V., Pampalone, V., Ferro, V., 2022b. Evaluating the Effects of the Rill Longitudinal Profile on Flow Resistance Law. Water, 14, 326. https://doi.org/10.3390/w14030326.

Pagliai, M., Vignozzi, N., 2002. Soil pore system as an indicator of soil quality. In M. Pagliai, & R. Jones (Eds.), Sustainable land management - environmental protection - a soil physical approach, advances in GeoEcology (Vol. 35) (pp. 71–82). Reiskirchen: catena Verlag.

Parhizkar, M., Shabanpour, M., Lucas-Borja, M.E., Zema, D.A., 2023. Effects of rice husk biochar on rill detachment capacity in deforested hillslopes. Ecological Engineer-ing, 191, 106964.

Petersen, C.T., Hansen, E., Larsen, H.H., Hansen, V., Ahrenfeldt, J., Hauggaard-Nielsen, H., 2016. Pore-size distribution and compressibility of coarse sandy subsoil with added biochar. European Journal of Soil Science, November, 67: 726–736, doi: 10.1111/ejss.12383.

Pohlmeier, A., Haber-Pohlmeier, S., Stapf, S., 2009. A Fast Field Cycling Nuclear Magnetic Resonance Relaxometry Study of Natural Soils. Vadose Zone J 8:735–742. https://doi.org/10.2136/vzj2008.0030

Pringle, C., 2003. What is hydrologic connectivity and why is it ecologically important? Hydrol Process 17:2685–2689. https://doi.org/10.1002/hyp.5145

Reaney, S.M., Bracken, L.J., Kirkby, M.J., 2014. The importance of surface controls on overland flow connectivity in semi-arid environments: Results from a numerical experimental approach. Hydrol Process 28:2116–2128. https://doi.org/10.1002/hyp.9769

Reynolds, W.D., Bowman, B.T., Drury, C.F., Tan, C.S., Lu, X., 2002. Indicators of good soil physical quality: density and storage parameters. Geoderma, 110: 131-146.

Reynolds, W.D., Drury, C.F., Tan, C.S., Fox, C.A., Yang, X.M., 2009. Use of indicators and pore volume-function characteristics to quantify soil physical quality. Geoderma, 152: 252–263, doi:10.1016/j.geoderma.2009.06.009.

Risse, L.M., Nearing, M.A., Savabi, M.R., 1994. Determining the Green-Ampt effective hydraulic conductivity from rainfall-runoff data for the WEPP model. Transactions of the ASAE, 37(2): 411-418.

Risse, L.M., Nearing, M.A., Zhang, X.C., 1995. Variability in Green-Ampt effective hydraulic conductivity under fallow conditions. Journal of Hydrology, 169: 1-24.

Russell, E.W., 1973. Soil conditions and plant growth. 10th ed. Longman, London.

Sadeghi, S.H.R., Hazbavi, Z., Harchegani, M.K., 2016. Controllability of runoff and soil loss from small plots treated by vinasse-produced biochar. Sci. Total Environ., 541, 483–490.

Skjemstad J.O., Baldock J.A., 2008. Total and Organic Carbon. p.225-237 in Soil Sampling and Methods of Analysis, edited by M.R. Carter and E.G. Gregorich, 2nd ed. ISBN-13: 978-0-8493-3586-0.

Smetanová, A., Dotterweich, M., Diehl, D., Ulrich, U., Fohrer, N., 2013. Influence of biochar and terra preta substrates on wettability and erodibility of soils. Z. Geomorphol., 57, 111–134.

Sohi, S.P., Krull, E., Lopezcapel, E., Bol, R., 2010. A review of biochar and its use and function in soil. Adv. Agron., 105, 47–82.

Topp, G.C., Reynolds, W.D., Cook, F.J., Kirby, J.M., Carter, M.R., 1997. Physical attributes of soil quality. In: E.G. Gregorich and M.R. Carter, editors, Soil Quality for Crop Production and Ecosystem Health. Development in Soil Science, vol. 25. Elsevier, New York, NY. p.21-58.

Turnbull, L., Wainwright, J., Brazier, R.E., 2008. A conceptual framework for understanding semi-arid land degradation: ecohydrological interactions across multiple-space and time scales. Ecohydrology 1: 23–34. https://doi.org/10.1002/eco.4

Uezu, A., Metzger, J.P., Vielliard, J.M.E., 2005. Effects of structural and functional connectivity and patch size on the abundance of seven Atlantic Forest bird species. Biological Conservation 123:507–519.

van Genuchten, M.Th., 1980. A closed-form equation for predicting the hydraulic conductivity of unsaturated soil. Soil Science Society of America Journal, 44: 892-898.

Villagra-Mendoza, K., Horn, R., 2018. Effect of biochar on the unsaturated hydraulic conductivity of two amended soils. International Agrophysics, 32: 373-378, doi: 10.1515/intag-2017-0025.

Wainwright, J., Turnbull, L., Ibrahim, T.G., Lexartza-Artza, I., Thornton, S.F., Brazier, R.E., 2011. Linking environmental régimes, space and time: Interpretations of structural and functional connectivity. Geomorphology 126:387–404. https://doi.org/10.1016/j.geomorph.2010.07.027

Wang, J., Wang, S., 2019. Preparation, modification and environmental application of biochar: A review. Journal of Cleaner Production, 227, 1002-1022.

Wani, I., Narde, S.R., Huang, X., Remya, N., Kushvaha, V., Garg, A., 2021. Reviewing role of biochar in controlling soil erosion and considering future aspect of production using microwave pyrolysis process for the same. Biomass Conversion and Biorefinery, 11543–11569 https://doi.org/10.1007/s13399-021-02060-1

Warrick, A.W., 1998. Appendix 1: Spatial Variability. pp. 655-675 in Hillel D., Environmental Soil Physics, Academic Press, CA, USA, 771 pages, ISBN 0-12-348525-8.

Zhang, F., Huang, C., Yang, M., Zhang, J., Shi, W., 2019. Rainfall simulation experiments indicate that biochar addition enhances erosion of loess-derived soils. Land Degradation and Development, 30, 30, 2272–2286.

Zhang, P., Tang, H., Yao, W., Zhang, N., Xizhi, L.V., 2016. Experimental investigation of morphological characteristics of rill evolution on loess slope. Catena, 137, 536–544.

5.4 Hydrodynamic behavior of a near-saturated sandy-loam soil shortly after incorporating compost or zeolite

Pubblished on Soil and Tillage Research, 2026, https://doi.org/10.1016/j.still.2025.107035

D. Autovino, V. Bagarello, C. Bondì, G. Russo, F. Zanna, K. Zhioua

ABSTRACT

Little is known about short-term effects of compost and zeolite addition on hydrodynamic properties of near-saturated coarse-textured soils. These effects were tested for a sandy-loam soil by a Mini-Disk Infiltrometer at three pressure heads (-6, -3 and -1 cm) and a wide range of amendment percentages, pa. Soil hydraulic conductivity was determined on two dates separated by nearly one month whereas soil sorptivity was determined at the end of the sampling period. Overall, the effect of the compost varied from null to appreciable since increasing pa from 0 to 40% did not affect the considered parameter or induced a decrease by up to eight times. Instead, the zeolite was largely ineffective since the tested parameters did not vary with pa. At the end of the experiment, the soil amended with zeolite was up to 70-90% more sorptive and conductive than that amended with the compost. Perhaps the particles of compost represented a physical obstacle to water flow and probably also induced some soil water repellency. Instead, the particles of zeolite were wettable, and they did not appreciably alter the pore size distribution. Adding compost can determine a decrease in the ability of a near-saturated soil to draw and conduct water but this ability does not change with zeolite. Other investigations are required to confirm these results, test the suggested explanation and finally draw general conclusions. The applied methodology in this investigation is easy, cheap and suitable for prolonged monitoring without causing an appreciable alteration of the sampled soil.

INTRODUCTION

Soils with a coarse texture, typically dominated by sand and deficient in organic matter, present several limitations to sustainable land use. Their loose structure, poor water retention, rapid drainage, and high vulnerability to nutrient leaching and erosion reduce both their agronomic potential and ecological stability (Garbowski et al., 2023). To address these constraints, the application of soil

amendments, whether organic (e.g., compost, vermicompost, biochar, peat) or mineral (e.g., lime, volcanic rocks, zeolites, clay minerals), has emerged as a promising strategy for improving the physical, chemical, and biological quality of such soils (Reynolds et al., 2009; Castellini et al., 2024) and can also be used to prepare engineered growing substrates (Autovino et al., 2024).

Composting refers to the process of humification and stabilization of organic wastes including sewage sludge, manure, municipal solid waste and green waste (Huang et al., 2016). Under the action of micro-organisms and enzymes, organic wastes are degraded and transformed into CO2, H2O, mineral ions and humic substances. Compost application to coarse-textured soils can be expected to improve soil organic matter content (Dong et al., 2022), bulk density (Mandal et al., 2013), soil structure (Rivier et al., 2022), total porosity (Arthur et al., 2011), pore size distribution (Bondì et al., 2022) and water holding capacity (Curtis and Claassen, 2009). Applying compost to these soils can determine a decrease (Whelan et al., 2013) or an increase (Kranz et al., 2020) of saturated soil hydraulic conductivity, Ks.

Among the mineral soil amendments, zeolites have assumed an increasingly significant role in recent years. Zeolites are a family of silica polymorphs or crystalline aluminosilicates composed of corner-sharing TO_4 tetrahedra (T = typically Si or Al), forming a three-dimensional, four-connected framework with uniformly sized, molecular-scale pores (Ghasemi et al., 2016). A wide range of natural and synthetic zeolites exists, characterized by differing Si/Al ratios that determine their ion exchange capacity and can differently influence soil behavior and plant responses (Cataldo et al., 2021), also depending on soil texture (Gholizadeh-Sarabi and Sepaskhah, 2012). Adding zeolite in sandy and loamy soils can be expected to improve soil water retention and holding capacity while simultaneously reducing Ks and infiltration rate (Colombani et al., 2015). However, a high application rate of zeolite particles could also induce particle dispersion, structural degradation and an increase of Ks of sandy-loam soils due to the coarseness of the zeolite particles and the addition of Na^+ ions (Ghorbani et al., 2022). According to Ibrahim and Alghamdi (2021), application of natural clinoptilolite zeolite in the ultra-fine nanoparticle size can be expected to increase water-holding capacity and reduce hydraulic conductivity of coarse-textured soils.

The experimental information currently available on soil-water relationships in coarse-textured porous media amended with compost or zeolite seems mainly focused on water retention characteristics and, for the hydrodynamic aspects, on Ks. There is less data regarding soil's hydrodynamic properties in close to saturation conditions. Further, there is almost nothing on

hydrodynamic parameters controlling early-time infiltration. Instead, this information is expected to have a noticeable hydrological relevance for different reasons.

A reason is that full saturation of well permeable soils rarely occurs under natural field conditions (Dohnal et al., 2016). Therefore, Ks data alone are not enough to characterize the soil's hydrodynamic behavior. Moreover, Ks data are expected to be largely influenced by fragile, unstable and often highly variable macropores of different nature (Dohnal et al., 2010; Jarvis et al., 2013). Hence, these data are expressive of the bulk soil, but they could not appropriately describe the effect of the amendment on the soil matrix (Logsdon and Jaynes, 1993). Matrix pores are small enough to remain water-filled at pore water pressure head values varying between -3 cm and -10 cm, depending on the investigation, and the hydraulic conductivity, K, corresponding to these pressure heads represents the saturated hydraulic conductivity of the soil matrix (Topp et al., 1997; Reynolds and Topp, 2008). Therefore, determining this soil hydrodynamic parameter requires collecting data corresponding to little negative pressure heads.

Soil sorptivity, S, should also be determined since this parameter, representing the soil's ability to draw water (Stewart et al., 2013), is dominated by soil capillarity forces (Cook and Broeren, 1994) and it affects estimation of other soil hydraulic properties (Minasny and McBratney, 2000). Sorptivity controls early-time infiltration and both S and K have to be determined for predicting one- and three-dimensional infiltration with physically-based models (Philip, 1957; Haverkamp et al., 1994).

Amendment effects on sorptivity and hydraulic conductivity of near-saturated soils can be tested, both in the laboratory and the field, with the Mini-Disk Infiltrometer (MDI, Meter Group, 2021). This device provides a simple, rapid and cost-effective method for measuring, with a minimal disturbance of the sampled soil volume, three-dimensional infiltration under a fixed negative pressure head, h0 ($-6\ cm < h0 < -0.5\ cm$), established on the infiltration surface. One of the most important features of the MDI, and generally of tension infiltrometer methods, is that the use of a slightly negative h0 value for the run makes it possible to measure the hydrodynamic response of the soil matrix independently of preferential flow effects (Dohnal et al., 2010; Wilson and Luxmoore, 1988). With the device, the sorptivity and hydraulic conductivity values that control infiltration under the established h0 value can be calculated (Zhang, 1997; Dohnal et al., 2010). Therefore, there is a direct correspondence between the soil hydrodynamic parameters and the experimentally measured infiltration process.

The general aim of this investigation was to evaluate short-term effects of two commercial soil amendments, that are an organic compost and a mineral zeolite, on hydraulic conductivity and sorptivity of a near-saturated sandy-loam soil sampled with an MDI. The specific objectives were to:

(i) determine the effects of the two amendments, applied at seven different rates, on the considered soil hydrodynamic parameters; (ii) establish differences between the two treatments; and (iii) assess short-term temporal variation in amendment effects.

THEORY

Transient cumulative infiltration, I (L), measured with the MDI can be described by the following well known relationship (Philip, 1957):

$$\boldsymbol{I = C_1 t^{1/2} + C_2 t} \qquad (1)$$

where t (T) is the time and C1 (L T-1/2) and C2 (L T-1) are coefficients that can be estimated by different methods (Vandervaere et al., 2000), including minimizing the sum of the squared residuals between the measured I(t) values and those predicted by eq.(1) (Lassabatere et al., 2006).

According to Zhang (1997), for a homogeneous and isotropic soil and a uniform initial soil water content, the C1 and C2 values obtained by a three-dimensional infiltration process at a given pressure head, h0 (L) (h0 < 0), on the soil surface can be described as a function of soil sorptivity, S0 (L T-1/2), and hydraulic conductivity, K0 (L T-1), respectively, as:

$$\boldsymbol{C_1 = A_1 S_0} \qquad (2)$$

$$\boldsymbol{C_2 = A_2 K_0} \qquad (3)$$

where A1 and A2 are dimensionless coefficients that depend on soil water content, soil water retention and infiltrometer parameters. For soils with the van Genuchten (1980) water retention function, the expressions of these coefficients were determined using numerically simulated infiltration data (Zhang, 1997):

$$\boldsymbol{A_1 = \frac{1.4 b^{0.5}(\theta_0 - \theta_i)^{0.25}\exp[3(n-1.9)\alpha_{vG} h_0]}{(\alpha_{vG} r)^{0.15}}} \qquad (4)$$

$$\boldsymbol{A_2 = \frac{11.65(n^{0.1}-1)\exp[2.92(n-1.9)\alpha_{vG} h_0]}{(\alpha_{vG} r)^{0.91}}} \quad \text{for } n \geq 1.9 \qquad (5a)$$

$$\boldsymbol{A_2 = \frac{11.65(n^{0.1}-1)\exp[7.5(n-1.9)\alpha_{vG} h_0]}{(\alpha_{vG} r)^{0.91}}} \quad \text{for } n < 1.9 \qquad (5b)$$

where h0 (cm) is the applied pressure head during the infiltration process (h0 is negative for unsaturated conditions), n and □vG (cm□1) are the water retention parameters, r (cm) is the radius of the infiltrometer, □0 (cm3cm□3) is the soil water content at h0, □i (cm3cm□3) is the initial soil water content, and b is a parameter set at 0.55 (Warrick and Broadbridge, 1992). Determination of S0 and K0 consists of using eqs.(2) and (3) once C1 and C2 have been calculated. The van Genuchten parameters required by the procedure can be estimated from soil texture (e.g., Carsel and Parrish, 1988) or they can be obtained by fitting laboratory determined soil water retention data, although in this last case the procedure of soil hydraulic characterization becomes more complicated from an experimental point of view. Dohnal et al. (2010) improved eq.(5b) suggesting, for low n values, the following alternative expression of A2, that was optimized specifically for a small disk size (15.2 cm2) and a range of pressure head values varying between -0.5 and -6 cm:

$$A_2 = \frac{11.65\left(n^{0.82}-1\right)\exp\left[34.65\left(n-1.19\right)\alpha_{vG}h_0\right]}{\left(\alpha_{vG}r\right)^{0.6}} \quad \text{for } n \leq 1.35 \qquad (5c)$$

According to the □vG and n parameters of the van Genuchten water retention curve listed by Dohnal et al. (2010), eq.(5c) should be used for sandy-clay-loam, sandy-clay, silty-clay and clay soils.

Therefore, transient infiltration and both initial and final soil water content values are necessary to determine S0 by eqs.(2) and (4). Instead, only infiltration data are required to obtain K0 by eqs.(3) and (5).

MATERIALS AND METHODS

Soil and amendments

A coarse-textured soil was collected from a citrus orchard located at the Department of Agriculture, Food and Forest Sciences of the University of Palermo, Italy (UTM 33S 355511E - 4218990N). Approximately 200 kg of soil were sampled from the upper 15 cm of the soil profile, sieved through a 1 cm mesh to remove gravel and large vegetation residues and subsequently air-dried under controlled laboratory conditions at approximately 20 °C for nearly three weeks.

The particle size distribution (PSD) of the soil sieved at 2 mm was determined by standard laboratory procedures (Gee and Or, 2002). In particular, 50 g samples were pre-treated with hydrogen peroxide and sodium polyphosphate to remove organic matter and induce colloid deflocculation, respectively.

The fine particle fractions were determined by the hydrometer method whereas the coarse fractions were obtained by mechanical sieving. According to the USDA soil texture classification system, the soil was sandy-loam with clay, silt and sand contents equal to 15.1%, 29.0% and 55.9%, respectively. Based on the IUSS Working Group WRB (2022) guidelines, the soil was classified as a Terric Chromic Cambisol (Loamic).

Two soil amendments of distinct origin were employed in this study. An organic amendment was a commercial compost (C) supplied by GECOS (Italy). This compost was obtained through a controlled process of transformation and stabilization of wastewater and sludge, combined with organic matrices such as untreated wood and pruning residues from ornamental greenery. A mineral amendment was a natural zeolite (Z), manufactured by GECOS (Italy), based on chabazite and free from pollutants. According to the manufacturer, the particles of Z ranged between 0.7 and 2 mm but no information on the particle size range was provided for the C. The main chemical characteristics of the used amendments were reported in Table 1.

To determine the actual size of the fine (< 2 mm) soil, C and Z particles used for the experiment, their PSD was also determined by sieving without performing any pre-treatment. In particular, 50 g of air-dried material were passed through a stack of sieves with decreasing mesh openings (2, 0.85, 0.425, 0.25, 0.106 and 0.074 mm) and vibrated for 5 minutes. The PSD was determined as the percentage by weight of particles within the following six size classes: 2-0.85, 0.85-0.425, 0.425-0.25, 0.25-0.106, 0.106-0.074 and <0.074 mm. All measurements were performed in duplicate. Both amendments were coarser than the soil (Fig. 1). The particles with an equivalent diameter ≥ 0.25 mm represented the 98.3% for the C, the 73.1% for the Z and the 59.4% for the soil. Therefore, as compared with the soil, the percentage of coarse particles was larger by 38.9 percentage units with the C and 13.7 units with the Z. Particles smaller than 0.25 mm were detected for both the soil and the Z but not for the C. Thus, the C was clearly coarser than the soil. Instead, the Z and the soil had a similar PSD.

Loss on ignition (LOI) was also determined for the soil, the C and the Z using 3 g (±0.006 g) samples weighed into porcelain crucibles. The samples were oven-dried at 105 °C for 24 h, cooled in a desiccator for 30 min and the dry weight (w105) was recorded. Subsequently, the samples were combusted in a preheated muffle furnace at 400 °C for 16 h, cooled in a desiccator, and the final weight (w400) was recorded. The LOI was calculated as the percentage difference between w105 and w400 referred to w105. The resulting LOI values were 5.6% for the soil, 31.1% for the C and 8.9% for the Z. These values reflect not only the oxidation of organic matter but also the thermal

decomposition of inorganic soil constituents such as hydrated aluminosilicates, structural water, carbonates, and hydrates (Nelson and Sommers, 1996). In the case of the Z, that is an aluminosilicate, the LOI value primarily indicates the quantity of structural water incorporated within its framework (Luukkonen et al., 2017).

Preparing mixtures and microplots

The two soil amendments, previously air-dried, were mixed with the soil at eight different percentages, pa, by weight: 0% (i.e., control soil without amendment), 5%, 10%, 15%, 20%, 25%, 30%, and 40%. High pa values were included in this investigation even if, due to economic and practical reasons, smaller percentages could be used in the field (Abildayev et al., 2025; Arthur et al., 2011; Eden et al., 2017; Kukowska and Szewczuk-Karpisz, 2025; Mohammadi et al., 2025; Pratt et al; 2025). This choice was made since relatively large amendment percentages could however be used in some circumstances, such as for greenhouse cultivation (Prisa, 2020) or other pot experiments (Chatzistathis et al., 2020). Moreover, considering a wide range of pa values was expected to yield a detailed representation of the effects of the treatment on a considered soil property, in accordance with other recent investigations (Bondì et al., 2022, 2024, 2025; Castellini et al., 2025).

The dry mass of both components was determined using the following equations (Bondì et al., 2022):

$$\boldsymbol{M_s = \frac{V\,\rho_{b,a}\,\rho_{b,s}}{\rho_{b,a}+r\,\rho_{b,s}}} \quad (6a)$$

$$\boldsymbol{M_a = rM_s} \quad (6b)$$

in which Ma (g) and Ms (g) represent the dry masses of amendment (C or Z) and soil, respectively, □b,a (g cm-3) and □b,s (g cm-3) are the dry bulk densities of the two constituents, determined using the core sampling method followed by oven-drying at 105 °C, V (cm3) is the sample volume, and r is the amendment-to-soil ratio. The air-dried masses were corrected to account for the initial volumetric water content of the soil.

The soil was mixed with the amendment until a homogeneous mixture was obtained. A total of sixteen microplots (8 amendment rates × 2 amendments) were established in polypropylene boxes with dimensions of 60 cm × 40 cm and a height of 13 cm. Microplots for control were replicated twice considering that two different controls would be used by two research groups working on the same soil with different amendments and in different laboratories. Each microplot comprised an 8 cm layer

of the soil–amendment mixture placed above a 3 cm drainage layer composed of expanded clay granules supplied by GECOS (Italy). To prevent migration of fine particles from the substrate into the drainage layer, a thin (<1 cm) polypropylene geotextile was placed between the two layers. Two additional boxes were prepared with non-amended soil above the drainage layer to initially perform some checks of the applied experimental method for measuring infiltration.

Mixtures were gradually transferred into the containers using a hand scoop, followed by manual compaction to ensure uniform settling. In particular, to ensure a uniform vertical soil distribution, the mixture was applied in three steps, and each layer was lightly compacted by hands and a shovel. Compaction was light to prevent hydraulic discontinuities between two adjacent layers as far as possible (Autovino et al., 2024). A single operator filled the boxes in order to favour uniformity across the different boxes (Bagarello et al., 2025). Microplots were then left air exposed to ambient laboratory conditions during the two measurement campaigns. After the last infiltration measurements, the boxes were exposed to open air.

Soil sampling experimental methods

Three-dimensional infiltration experiments were performed on the packed soil in a microplot by an MDI having a disk diameter of 4.5 cm. Two sampling campaigns were carried out. The first campaign (I) started immediately after preparing the microplots and its overall duration was four days. The second campaign (II) started nearly 30 days after concluding the first campaign and its overall duration was six days. At the end of the first measurement campaign, 1 L of water was uniformly poured onto each microplot in order to promote a uniform soil wetting and drying process during the time interval between the two measurement campaigns. A 30-day interval between the sampling campaigns was considered appropriate to try capturing short-term variations in amendment effects on the measured soil properties in more or less similar initial soil water content conditions.

For each microplot, that is for a given soil/amendment mixture, infiltration data were collected at three different pressure head, h0, values, equal to -6 cm, -3 cm and -1 cm. Each individual infiltration process for an established h0 value was carried out at a different sampling point, so as to obtain all infiltration curves in a microplot under similar initial soil water content conditions. For a given h0 value and a microplot, the experiment was replicated at two different, randomly chosen, sampling points, for a total of six MDI infiltration runs in a microplot. The soil surface at a sampling point was gently leveled with a trowel and small amounts of loose soil were used when necessary to improve

the contact between the MDI and the infiltration surface. The device was fixed to a support to keep it still during the run and infiltration was measured until the reservoir emptied. Readings were taken visually at time intervals varying from 5 s for the first 30 s to 2 min after the twentieth minute of the run. A cumulative infiltration, I (L), vs. time, t (T), curve was obtained at each sampling point.

A few MDI runs were initially carried out in the two additional boxes with non-amended soil until the reservoir was empty. This initial check of the applied experimental methodology confirmed that every point of the wetting front remained within the soil volume by the end of the run. In other terms, the infiltration data were not noised by edge or bottom effects.

Obtaining K0 data only requires MDI data whereas MDI and soil water content data are necessary for also determining S0 (Zhang, 1997). Especially for the final water content, the destructive thermo-gravimetric method seems an appropriate method to be applied since the actually wetted soil volume under the device can be sampled. In light of these considerations, only K0 was determined in the first sampling campaign so as not to cause alterations to the soil in different positions of the microplot which could have compromised or hindered the second campaign of measurements. In other words, sorptivity was not determined in the first sampling campaign in order not to disturb excessively the soil in an intermediate stage of the experiment.

The soil was sampled immediately before performing the second series of MDI runs to determine the dry soil bulk density, □b (g cm-3), and the initial gravimetric soil water content, wi (g g-1). Two undisturbed soil samples were collected by manually pressing two metal cylinders with a height of 2 cm and a diameter of 5 cm into the soil. The initial volumetric soil water content, □i (m3m-3) was then determined from □b and wi. The two □b, wi and □i values were averaged to characterize the soil in a microplot.

After an MDI run, the wetted soil under the device was sampled with a teaspoon to determine the final gravimetric soil water content, w0 (g g-1). The final volumetric soil water content, □0 (m3m-3), was determined from w0 and the □b value for the considered microplot, determined before the run. The diameter of the wetted bulb at the soil surface, db (cm), was also measured along two orthogonal directions. A representative db value for the run was obtained by averaging these two measurements.

Overall, 192 MDI runs were performed in this investigation, i.e. 2 sampling campaigns × 3 pressure heads × 2 replicated runs per microplot × 8 mixtures per amendment × 2 amendments.

After about a month of exposure of the boxes to open air, soil water repellency data were collected by the widely applied water drop penetration time (WDPT) test (Doerr, 1998; Letey et al., 2000). In particular, 60 drops of deionized water were evenly applied with a medical dropper at the surface of each box from a height of 10 mm and the time for their complete penetration was recorded. Two disturbed soil samples were also collected to determine the gravimetric soil water content, wWDPT (g g-1), immediately before the WDPT experiment. Therefore, a total of 16 wWDPT values were determined for each treatment.

Calculations and data analysis

For each MDI infiltration run, eq.(1) was fitted to the cumulative infiltration, I (mm), vs. time, t (h), data by minimizing the sum of the squared residuals between the measured and the predicted I values (Lassabatere et al., 2006) to simultaneously estimate the C1 (mm h-1/2) and C2 (mm h-1) parameters of the model. In a single case (second campaign with the compost, h0 = -1 cm, pa = 40%) the adaptation of the model to the data failed (C1 = 0). In the other cases, the relative error, Er (%), calculated according to Lassabatere et al. (2006) varied from 0.6% to 4.7% with a mean value of 1.5%. According to Lassabatere et al. (2006), an Er value that does not exceed 5.5% denotes an acceptable fitting of an infiltration model to the data. Therefore, the fitting of the model to the infiltration data was satisfactory for all individual runs. The soil hydraulic conductivity, K0 (mm h-1), and sorptivity, S0 (mm h-1/2), values corresponding to a run with a given pressure head were then calculated according to Zhang (1997) and Dohnal et al. (2010), i.e. using eqs.(2)-(5). The required soil water retention parameters for the calculations were chosen from Table 1 by Dohnal et al. (2010).

With reference to a given soil property, the data were analyzed in order to establish i) the amendment effect; ii) if the effect was similar between the two amendments; and iii) if the effect changed with time.

Amendment effects were tested by performing a linear regression analysis of the considered soil property vs. pa and determining the statistical significance of the correlation coefficient, R, by a two-tailed t test at P = 0.05 (Glantz, 2012). The intercept of a statistically significant relationship represents the value of the considered soil property without any treatment whereas the slope is expressive of the rate at which that property varies by adding the amendment (Bondì et al., 2022, 2024, 2025; Castellini et al., 2025).

To establish similarity between the amendments and to evaluate time effects, two means of a soil property were compared by F and two-tailed t tests at P = 0.05. This choice was made instead of comparing two regression lines (Glantz, 2012) since a statistical significance of both regression lines between a soil parameter and pa was only detected in a few cases.

In this investigation, a given variable (e.g., soil sorptivity or soil hydraulic conductivity at an established pressure head) was determined by using different percentages of amendment, pa (%) (from 0 to 40%) for two reasons: i) making this choice was necessary for testing the relationship between the considered variable and the intensity of the treatment (Bondì et al., 2022, 2024, 2025; Castellini et al., 2025); and ii) for a fixed amount of applied amendment (e.g., given mass per unit surface area and incorporation depth), it is unlikely that every point of a field soil will receive exactly the same treatment. Instead, some heterogeneity in the distribution of the amendment will be more or less unavoidable. An experiment making use of different amendment doses seems therefore appropriate to predict the overall response of the field soil with reference to the variables of interest.

The WDPT data were summarized considering the five soil water repellency classes by Bisdom et al. (1993): wettable (WDPT < 5 s), slightly water repellent (WDPT = 5-60 s); strongly water repellent (WDPT = 60-600 s); severely water repellent (WDPT = 600-3600 s), and extremely water repellent (WDPT > 3600 s). For each microplot, the percentage of WDPT values falling in each class was determined.

RESULTS

For each sampling campaign (I or II), amendment (C = compost; Z = zeolite) and percentage of amendment, pa (%), soil hydraulic conductivity generally increased according to the sequence K-1 (K for h0 = -1 cm) > K-3 (K for h0 = -3 cm) > K-6 (K for h0 = -6 cm) (Fig. 2). For each amendment and pa value, soil sorptivity, that was only determined in the second campaign, generally increased according to the sequence S-1 (S for h0 = -1 cm) > S-3 (S for h0 = -3 cm) > S-6 (S for h0 = -6 cm) (Fig. 3). Larger soil hydraulic conductivity and sorptivity values with greater (less negative) h0 values are physically expected. Therefore, this initial check of the data did not suggest any anomaly in the developed dataset.

First sampling campaign

With the C, the relationship between K-6 and pa was statistically significant (coefficient of determination, R2 = 0.69, R > 0) but pa did not influence significantly either K-3 or K-1 (R2 = 0.11 - 0.13, depending on h0; Fig. 2a). In particular, K-6 decreased by 3.1 times as pa increased from zero to 40%.

With the Z, none of the tested relationships between K and pa was statistically significant (0.0001 < R2 < 0.15; Fig. 2b), indicating that soil hydraulic conductivity did not vary with the amount of Z regardless of the established pressure head.

For each pressure head, a comparison was carried out between the K values obtained with the two amendments. The hydraulic conductivity of the soil treated with the Z was greater than that obtained using the C by 10.0-21.7%, depending on h0 (Table 2), but the differences between the two treatments were not statistically significant. Using the Z instead of the C implied detecting a smaller coefficient of variation, CV, of K for the smallest h0 value (h0 = -6 cm), a little higher CV value for the intermediate pressure head (h0 = -3 cm) and an appreciably higher CV value for the highest pressure head (h0 = -1 cm).

Therefore, signs of a treatment effect on K were weak since they included a significant relationship between K and pa for only one of the six tested relationships and consistently higher values of K with one of the two soil amendments, but only a little and not significantly. Overall, the data suggested that adding an amendment at different rates or using an amendment instead of another did not influence K. Therefore, amending the soil was largely ineffective immediately after performing the treatment.

Second sampling campaign

With both amendments, □b decreased significantly as pa increased (Fig. 4a). On average, the dry soil bulk density differed with the used amendment by 2.2% and the difference between the two treatments was not statistically significant (Table 3).

The antecedent gravimetric soil water content, wi, increased significantly with pa for both amendments even if the wi vs. pa relationships were rather scattered, with R2 values of 0.35 for the C and 0.29 for the Z (Fig. 4b). The mean wi value of the soil treated with the C was larger than that of the soil treated with the Z by 53.1% and the difference between the two treatments was statistically significant (Table 3).

For both treatments, the relationship between □i and pa was not significant (Fig. 4c). The soil treated with the C had a 43.6% larger mean of □i than the soil treated with the Z and the difference between the two treatments was significant (Table 3).

Neglecting from the calculations an apparently anomalous soil water content value for the C treatment (Figs. 4b,c) yielded smaller differences between the treatments, equal to 34.6% for wi and 28.0% for □i. However, even in this case, differences between treatments were significant.

The soil treated with the Z was more homogeneous (smaller CV values) than that treated with the C with reference to □b, wi and □i.

Therefore, before performing the second sampling campaign with the MDI, the soil amended with the C was on average wetter than the soil amended with the Z. The □i values were nearly independent of pa since an increase of pa determined an increase of wi and a decrease of □b.

The final gravimetric soil water content, w0, increased significantly with pa with a single exception since it did not vary significantly with pa for the Z and h0 = -1 cm (Figs. 5a-c). At the end of the MDI runs, the soil treated with the C had a significantly larger w0 value than that treated with the Z (Table 4). In particular, w0 was larger by 18.0-20.3%, depending on h0, in the former case than the latter one.

Instead, the final volumetric soil water content, □0, did not vary significantly with pa in the soil treated with the C, regardless of h0 (Figs. 5d-f). With the Z treatment, the □0 vs. pa relationship was inverse and significant, even if rather weak ($0.28 < R2 < 0.30$) for h0 = -3 and -1 cm and not significant for h0 = -6 cm. The soil treated with the C was significantly wetter than that treated with the Z by a percentage varying with h0 between 13.5% and 15.0% (Table 4).

Therefore, the volumetric soil water content at the end of the run with the MDI did not vary with pa or it decreased as pa increased. Using the C instead of the Z determined larger □0 values regardless of h0.

The slope of the relationship between db and pa was numerically negative in all cases, that is for the two amendments and the three established pressure heads (Fig. 6), but the db vs. pa relationships were not statistically significant with a single exception. This relationship was significant but rather weak

(R2 = 0.39, R > 0) for the C amendment with h0 = -1 cm. Therefore, the analysis generally suggested that, for given amendment and pressure head value, db did not vary with pa.

For both amendments, db decreased monotonically as h0 increased from -6 cm to -1 cm (Table 5). However, the means of db obtained with a given amendment and the three h0 values did not differ significantly one from the other with a single exception. With the C amendment, establishing h0 = -6 cm instead of -1 cm yielded an 8.2% higher db value. Therefore, db generally decreased with larger h0 values but this decrease was statistically significant for only one of the six established comparisons. The most common result was that, with a given amendment, db did not vary significantly with h0.

For a given pressure head, the C treatment yielded larger db values than the Z one and the differences between the two amendments were statistically significant for all h0 values (Table 5). In particular, the percentage differences between the db values for the C and Z treatments varied in the 9.5-12.9% range depending on h0.

Overall, there were some signs that db decreased with larger pa and h0 values but these signs were weak and statistically supported only in a few cases. Instead, the effect of the amendment on db was clearer and also significant. Specifically, using the Z amendment instead of the C one consistently implied measuring smaller wetted bulbs at the soil surface.

With the C, all tested relationships between S and pa were statistically significant and they indicated that S decreased as pa increased (Fig. 3a). In particular, S-6, S-3 and S-1 decreased by 5.0, 5.8 and 7.6 times, respectively, as pa increased from zero to 40%. Therefore, adding more C implied making the soil less sorptive, more appreciably with reference to the highest (less negative) pressure heads.

With the Z, none of the tested relationships between S and pa was statistically significant (Fig. 3b), indicating that soil sorptivity at a given h0 value did not vary with the amount of Z.

For each pressure head, the sorptivity of the soil treated with the Z was significantly greater than that obtained using the C (Table 6). Two corresponding S values differed by 59.2-69.9%, depending on h0. Therefore, treating the soil with the Z made the soil more sorptive as compared with a treatment with the C.

The coefficients of variation, CV, of the data were smaller with the Z as compared with the C and differences between the two treatments were more appreciable for the higher h0 values. Therefore,

the soil treated with the Z was also more homogeneous than that treated with the C with reference to the ability of the soil to draw water.

With the C, all tested relationships between K and pa were statistically significant, indicating that K decreased as pa increased (Fig. 2c). In particular, K-6 decreased by 6.8 times as pa increased from zero to 40%. A smaller decrease was detected for K-3 (by 2.5 times) and K-1 (by 2.9 times).

With the Z, none of the tested relationships between K and pa was statistically significant (Fig. 2d), indicating that soil hydraulic conductivity did not vary with the amount of Z regardless of the considered pressure head. Therefore, using different percentages of Z did not have any effect, to a scale corresponding to that of an MDI run, on the ability of the soil pores to conduct water.

The hydraulic conductivity of the soil amended with the Z was larger by 41.7-88.1%, depending on h0, than that of the soil amended with the C and all differences between the two treatments were statistically significant (Table 2). Therefore, treating the soil with the Z made the soil more conductive as compared with a treatment with the C.

Even with reference to the soil hydraulic conductivity values, the soil treated with the Z was more homogeneous (smaller CV values) than that treated with the C regardless of h0.

Comparing the two sampling campaigns

For each amendment and pressure head, a comparison was carried out between the K values obtained in the two sampling campaigns to verify if a short-term temporal variability of K occurred. In all cases, i.e. for both amendments and the three h0 values, the soil hydraulic conductivity obtained in the second date was numerically smaller than that obtained in the first date (Table 2). However, there was a difference between the amendments.

With the C, the K values obtained in the second date were smaller by 40.2-50.1% than those obtained in the first date, depending on h0, and the differences between the two sampling campaigns were statistically significant in all cases.

With the Z, the K values obtained on the second date were smaller by 21.2-22.9% than those obtained on the first date, depending on h0, and the differences between the two sampling dates were statistically significant for h0 = -6 and -3 cm but not for h0 = -1 cm.

With a single exception (Z, h0 = -1 cm), relative variability of the K data increased from the first to the second sampling date.

Soil water repellency

After the second campaign with the MDI and an additional month of exposure of the soil boxes to open air, the gravimetric soil water content did not differ significantly between the C and Z treatments since the mean and the CV of wWDPT were equal to 0.22 g g-1 and 22.3%, respectively, in the former case and to 0.20 g g-1 and 18.0% in the latter case.

In the absence of any treatment, the 35%-45% of the WDPT tests did not suggest any soil water repellency whereas the remaining 55%-65% of the tests suggested a slight water repellency (Fig. 7). The treatment with the C at different rates i) did not modify soil water repellency as compared with the untreated soil in a case, ii) suggested that the treatment improved a little soil wettability in another case, and iii) determined an increase of the WDPT tests indicating water repellency in five cases. Even in these last cases, water repellency was slight with the exception of a very few tests suggesting a strong water repellency. Instead, the treatment with the Z at different rates suggested that, although not monotonically, larger concentrations of amendment improved soil wettability. In detail, with the largest concentration of Z, all WDPT tests suggested wettable conditions.

Therefore, the data overall indicated that the soil was naturally wettable or slightly water repellent. Addition of C did not modify appreciably soil water repellency or it determined a limited increase, remaining however in a situation of slight water repellency. Instead, addition of Z determined a decrease and also disappearance of any water repellency.

Summary of the amendment effects on the soil hydrodynamic behavior

Overall, the two amendments yielded different results. Using the C induced a decrease of near-saturated soil hydrodynamic parameters with larger amendment rates, pa. Initially, this decrease was limited to some of the tested parameters but then it was detected for all parameters (Figs. 2 and 3). Instead, adding the Z did not influence any of the tested parameters regardless of both pa and the sampling date.

With the C, near-saturated soil hydraulic conductivity decreased appreciably in the relatively short time period between the two sampling campaigns (Table 2). Instead, using the Z made this decrease smaller.

Nearly 1.5 months after preparing the samples, the soil treated with Z was more sorptive (Table 6) and more conductive (Table 2) than the same soil treated with C. Moreover, the former soil was drier than the latter one both before (Table 3) and after (Table 4) the MDI run.

The effect of the amendment was also visually perceivable since, at the end of the MDI runs, the diameter of the wetted bulb at the soil surface was larger with the C treatment than the Z one (Table 5).

Therefore, the hydrodynamic response of the soil treated with the C was more dependent on both the time from the beginning of the experiment and the amount of the amendment used than that of the same soil treated with the Z.

Both sorptivity and hydraulic conductivity are expected to be smaller in finer soils (Moret-Fernández et al., 2020; Yilmaz et al., 2023) and capillary forces, controlling lateral expansion of the wetting front around a near-point source of water, are greater in finer soils with smaller pores. Therefore, the soil treated with the C was functionally finer than that treated with the Z.

Finally, soil water repellency was at the most slight in untreated conditions (Fig. 7). Addition of Z determined disappearance of any water repellency. Adding C did not modify or it induced a limited increase of soil water repellency.

DISCUSSION

Some experimental evidence that a treatment with C or other organic amendments can induce a decrease of the unsaturated soil hydraulic conductivity can be found in the literature (Aggelides and Londra, 2000; Wanniarachchi et al., 2019) and this investigation supported previous findings. However, we did not find data about the Z effects on hydrodynamic properties of near-saturated coarse-textured soils. This investigation suggested that these effects could be negligible.

Trying to explain these results, it was preliminarily recognized that the overall duration of the experiment was short, that is a couple of months. Therefore, the occurrence of relevant soil aggregation processes promoted in some different manner by the two amendments appeared unlikely.

Instead, the following considerations were made: i) the soil was packed manually and some soil settling and compaction phenomena likely occurred during the experimental period due to gravity, wetting and drying (Murphy et al., 1993; Busscher et al., 2002); ii) in coarse soils, some physical pore obstruction due to amendment addition can be expected to occur (Villagra-Mendoza and Horn, 2018; Wanniarachchi et al., 2019); iii) soil pore size distribution depends on the soil particle size distribution (Arya et al., 1999; Arya and Heitman, 2015; Lebron et al., 2002; Nimmo, 2004). With reference to the particles smaller of 2 mm, the soil and the Z had a relatively similar particle size distribution whereas the C was overall coarser than both the soil and the other amendment (Fig. 1); and iv) using the C implied introducing in the soil particles that were essentially non-porous and impermeable to water. Instead, the used Z particles likely had pores and channels within their structure (Nakhli et al., 2017; Satriani et al., 2024). Consequently, all other things being equal, it can be presumed that a particle of C might hinder flow more effectively than a particle of Z.

In light of these considerations, a possible explanation of the results obtained in this investigation was the following. Relatively small sorptivity and hydraulic conductivity values were obtained with the C and with large amounts of this amendment since the large particles of C obstructed the relatively large conductive soil pores and hence, they constituted a physical obstacle to water flow. Instead, with the Z, appreciable obstruction phenomena did not occur, and the pore size distribution did not change appreciably. Hence, the treatment with the Z did not impede water transport and neither S nor K changed substantially after the treatment.

In the first sampling campaign, the C effect was only detected for the smallest (most negative) pressure head since the smaller conductive soil pores were more easily obstructed than the larger pores. Soil settling and compaction phenomena occurring between the two sampling campaigns determined a decrease of pore sizes and also a closer contact between the soil and the particles of amendment. The decrease of K between the two sampling campaigns was more appreciable with the C than with the Z since, in the former case, settling and compaction phenomena also enhanced the ability of the amendment to retard flow. In the latter case, instead, settling and compaction phenomena were not, or were less, associated with an enhanced ability of the amendment to retard flow. Moreover, the Z made perhaps the soil matrix more rigid as compared with the C.

Finally, differences between the two treatments increased from the first to the second sampling campaign because the hydraulic conductivity of the soil treated with the C decreased more than that of the soil treated with the Z.

This explanation shows some similarity with that by Belviso et al. (2022), which suggested that a particle of amendment can limit water transport into the soil by favoring development of a clay-like porous medium due to an increase in meso-micropores combined with macropore loss. The larger □i (Table 3) and □0 (Table 4) values obtained with the C than the Z suggest an improved ability of the soil treated with the organic amendment to retain water. Hence, the data obtained in this investigation are consistent with the interpretation by these authors. However, there are also some differences between this investigation and that by Belviso et al. (2022) since these authors considered a silty-loam soil amended with zeolite but just this amendment did not influence soil hydrodynamic properties in this investigation. In other words, C but not Z addition favored development of a clay-like porous medium.

Another possible reason why soil hydrodynamic parameters became smaller with larger percentages of C but not with more Z was that the former amendment induced some soil water repellency that instead did not occur with the latter amendment.

This explanation, that is not necessarily alternative to the previous one, was considered plausible taking into account that: i) an increase in soil water repellency can determine smaller values of both sorptivity and hydraulic conductivity close to soil saturation (Wahl et al., 2003; Ebel and Moody, 2020); ii) an increase in soil water repellency can occur with more compost (Müller and Deurer, 2011; Głąb, 2014; Leelamanie and Manawardana, 2019) but the zeolite could not have the same effect. For example, Müller and Deurer (2011) listed zeolite as one of the possible surfactants to be used for alleviating soil water repellency and Gholami et al. (2024) recognized that a treatment with zeolite effectively mitigated the adverse hydrological effects of soil water repellency in fire affected soils; and iii) the WDPT data collected a few weeks after the MDI runs suggested more water repellency in the soil treated with C than in that treated with Z (Fig. 7).

However, this explanation is not free from uncertainties since, with the C treatment, the K and S values obtained in the second campaign decreased with more amendment (Figs. 2 and 3), but more C did not suggest a continuous increase of soil water repellency (Fig. 7). Another more general reason is that, according to other investigations, the soil water repellency attributable to organic amendments could overall be negligible under field conditions (Castellini et al., 2024) and zeolite could also exhibit some hydrophobicity, depending on the Si/Al ratio and the surface hydroxyl group content (Tatlier et al., 2022). In other words, it cannot be excluded at all that the soil hydrodynamic response did not depend, or depended only a little, on soil water repellency.

Taking into account that WDPT and MDI data are collected at different scales (point for the WDPT test and small area for the MDI), developments of this investigation should be performed by also considering the need to determine soil water repellency and infiltration at more directly comparable scales.

Numerical simulation of hydrological states and fluxes requires describing appropriately the spatially and temporally variable soil hydraulic parameters (Christiaens and Feyen, 2000; Assouline and Mualem, 2006; Baroni et al., 2017; Šípek et al., 2019). This investigation contributed to understanding how the soil should be described soon after application of a large amount of amendment in the upper zone of a tilled layer.

With the C, the tilled soil should be considered as a two-layered system, with different soil hydrodynamic parameters for the upper amended layer and the non-amended deeper layer. Time changes of soil properties in the amended layer can be appreciable and hence they should also be considered.

Instead, with the Z, the tilled soil could be considered vertically almost homogeneous, regardless of whether the soil contains the amendment or not. Further, time changes of soil hydrodynamic parameters can be expected to be smaller and perhaps it could not be strictly necessary taking these changes into account.

Therefore, soil parameterization for numerical modelling purposes seems simpler if the Z is used as amendment instead of the C. Of course, this suggestion is based on a single experiment, and it is valid for a soil similar to the sampled one and a relatively short time period, that is one or two months after adding the amendment. Considering other soils and performing longer experiments could help to draw general conclusions.

The MDI appears to be a good method for performing these developments for different reasons. The device is simple and cheap, and its application determines a minimal, or even negligible, disturbance of the sampled soil volume. Therefore, the data are expressive of the soil response and not of any soil alteration due to the run.

The non-destructive nature of the run implies that the same sampled soil can also be subjected to subsequent determinations. In other terms, soil monitoring campaigns can easily be realized. This is

an important aspect of the methodology since amendment effects on soil-water relationships can be expected to vary with the elapsed time after the treatment (Bondì et al., 2022).

The operating principle of the MDI is the same as that of the classical tension infiltrometer (Perroux and White, 1988), that can be used in the field to explore larger and more representative areas by a single run. Therefore, performing comparisons between laboratory and field experiments should be easy.

The data obtained under close to zero, but negative pressure heads can be expected to be more representative of common field situations as compared with those obtained by ponding infiltration experiments, taking into account that ponded infiltration is an extreme case which is rarely seen in the field (Dohnal et al., 2016).

Finally, the MDI can also be used for detecting soil water repellency (Lichner et al., 2018; Alagna et al., 2019).

Evidently, tension infiltrometers are not perfect devices since they also have limitations such as, for example, the risk of poor contact between the disc and the soil that could compromise the quality of the data (Close et al., 1998). However, it seems plausible to suggest that the advantages outweigh the disadvantages.

Finally, it has to be acknowledged that the use of two sampling points within each microplot could be expected to introduce pseudo-replication, which may limit the statistical independence of the observations. Likely, future studies should consider replicating entire microplots to improve statistical power and also account for packing-related heterogeneity.

CONCLUSIONS

Understanding soil hydraulic properties changes is essential for sustainable land management, especially in arid and semi-arid regions, where water availability is a limiting factor. The two tested amendments can be expected to have a different short-term impact on the hydrodynamic properties of a near-saturated coarse-textured soil. According to this investigation, the soil sorptivity and hydraulic conductivity values corresponding to high pressure head values (-6 cm $< h0 <$ -1 cm) decrease with larger compost rates whereas they do not vary with different amounts of zeolite. Overall, adding compost makes the soil functionally finer as compared with the soil treated with

zeolite. Moreover, the soil amended with compost experiences more appreciable short-term temporal variations of soil hydrodynamic parameters than that amended with the zeolite.

In summary, the compost can be expected to favor development of a clay-like porous medium if the particles of this amendment act as a physical obstacle to water flow. Development of a clay-like porous medium is not expected with the zeolite if the particles of this amendment do not alter appreciably the pore size distribution.

Characterizing a soil profile for numerical simulation purposes appears easier if the zeolite is used as an amendment instead of the compost.

From a practical point of view, using compost, especially in large percentages, can be expected to induce a slowdown of the water transport processes towards the deeper layers in conditions of near-saturation of the soil, especially a few weeks after the treatment. This circumstance could help to maintain a water reserve usable by plants in the treated soil layer. The same conclusion cannot be drawn for the zeolite since, in this case, hydrodynamic processes in near-saturated soil conditions can be expected not to change appreciably, regardless of the amount of amendment used and the time elapsed since the treatment.

Of course, trying to draw general conclusions requires testing experimentally the suggested interpretations, considering other soils, performing longer measurement campaigns and making use of other amendments.

The experimental methodology applied in this investigation could also be applied by other research groups, as it seems appropriate for developing larger and more complete soil datasets. Exposing some soil boxes to open air for long periods and possibly sowing appropriate plant species could make it possible to also establish if and how the effects of the applied soil amendments vary with meteorological forcing and development of vegetation.

CRediT authorship contribution statement

Dario Autovino: Data curation, Investigation, Validation, Writing – original draft. Vincenzo Bagarello: Conceptualization, Data curation, Formal analysis, Funding acquisition, Investigation, Project administration, Supervision, Validation, Writing – original draft. Cristina Bondì: Data curation, Investigation, Validation, Writing – original draft. Giovanni Russo: Data curation,

Investigation, Validation, Writing – original draft. Francesco Zanna: Validation, Writing – original draft. Khedija Zhioua: Data curation, Investigation, Validation, Writing – original draft.

Declaration of Competing Interest

The authors declare that they have no known competing financial interests or personal relationships that could have appeared to influence the work reported in this paper.

Acknowledgements

This study was partially funded by ASCAN "Indagine di laboratorio e di pieno campo sull'uso di Ammendanti naturali dei Suoli per strategie di Conservazione dell'Acqua e dei Nutrienti" - National Research Centre for Agricultural Technologies, Codice progetto CN00000022, Bando a Cascata Spoke n. 6, CUP D13C22001330005.

Data availability

Data will be made available on request.

REFERENCES

Abildayev Y., Yessenbayeva J., Vassilina T., Yeleuova E., Zhussupova L., Uspabayeva A., Baiseitova N., Azhmoldaeva K., 2025. Natural zeolite enhances tomato yield, reduces nitrate accumulation, and immobilizes heavy metal in fertilized dark chestnut soil. Eurasian Journal of Soil Science, 14(3), 262-269. https://doi.org/10.18393/ejss.1703804

Aggelides S.M., Londra P.A. 2000. Effects of compost produced from town wastes and sewage sludge on the physical properties of a loamy and a clay soil. Bioresource Technology, 71, 253-259. https://doi.org/10.1016/S0960-8524(99)00074-7

Alagna V., Iovino M., Bagarello V., Mataix-Solera J., Lichner L. 2019. Alternative analysis of transient infiltration experiment to estimate soil water repellency. Hydrological Processes, 33, 661-674, doi: 10.1002/hyp.13352. https://doi.org/10.1002/hyp.13352

Arthur E., Cornelis W.M., Vermang J., De Rocker E. 2011. Amending a loamy sand with three compost types: impact on soil quality. Soil Use and Management, 27, 116-123, https://doi.org/10.1111/j.1475-2743.2010.00319.x

Arya L.M., Heitman J.L. 2015. A non-empirical method for computing pore radii and soil water characteristics from particle-size distribution. Soil Science Society of America Journal, 79(6), 1537-1544, https://doi.org/10.2136/sssaj2015.04.0145

Arya L.M., Leij F.J., van Genuchten M.Th, Shouse P.J. 1999. Scaling parameter to predict the soil water characteristic from particle-size distribution data. Soil Science Society of America Journal, 63, 510-519, https://doi.org/10.2136/sssaj1999.03615995006300030013x

Assouline S., Mualem Y. 2006. Runoff from heterogeneous small bare catchments during soil surface sealing. Water Resources Research, 42, W12405, https://doi.org/10.1029/2005WR004592

Autovino D., Alagna V., Bondì C., Iovino M. 2024. Hydraulic characterization of green roof substrates by evaporation experiments. Applied Sciences, 14, 16 pp., https://doi.org/10.3390/app14041617

Autovino D., Bagarello V., Caltabellotta G., Varadi F. K., Zanna F. 2024. One-dimensional infiltration in a layered soil measured in the laboratory with the mini-disk infiltrometer. Journal of Hydrology and Hydromechanics, 72(2), 149–157, https://doi.org/10.2478/johh-2024-0001

Bagarello V., Barone S., Caltabellotta G., Varadi F.K., Zanna F., Autovino D. 2025. A test of factors influencing one-dimensional Mini-Disk Infiltrometer experiments on repacked loam soil columns. Hydrology, 12(4), 85, 13 pp., https://doi.org/10.3390/hydrology12040085

Baroni G., Zink M., Kumar R., SamaniegoL., Attinger S. 2017. Effects of uncertainty in soil properties on simulated hydrological states and fluxes at different spatio-temporal scales. Hydrology and Earth System Sciences, 21, 2301-2320, https://doi.org/10.5194/hess-21-2301-2017

Belviso C., Satriani A., Lovelli S., Comegna A., Coppola A., Dragonetti G., Cavalcante F., Rivelli A.R. 2022. Impact of zeolite from coal fly ash on soil hydrophysical properties and plant growth. Agriculture, 12, 356, 13 pp., https://doi.org/10.3390/agriculture12030356

Bisdom E.B.A., Dekker L.W., Schoute J.F.T. 1993. Water repellency of sieve fractions from sandy soils and relationships with organic material and soil structure. Geoderma, 56(1), 105-118. http://dx.doi.org/10.1016/0016-7061(93)90103-R

Bondì C., Castellini M., Iovino M. 2022. Compost amendment impact on soil physical quality estimated from hysteretic water retention curve. Water, 14, 1002. https://doi.org/10.3390/w14071002

Bondì, C., Auteri, N., Saiano, F., Scalenghe, R., D'Acqui, L.P., Bonetti, A., Iovino, M., 2024. Cactus pear pruning residue in agriculture: Unveiling soil-specific responses to enhance water retention. Environmental Technology & Innovation, 34: 103602. https://doi.org/10.1016/j.eti.2024.103602

Bondì C., Castellini M., Iovino M. 2025. Temporal variability of physical quality of a sandy loam soil amended with compost. Biologia, 12 pp., https://doi.org/10.1007/s11756-024-01637-1

Busscher W.J., Bauer P.J., Frederick J.R. 2002. Recompaction of a coastal loamy sand after deep tillage as a function of subsequent cumulative rainfall. Soil and Tillage Research, 68(1), 49-57, https://doi.org/10.1016/S0167-1987(02)00083-1

Carsel R.F., Parrish R.S. 1988. Developing joint probability distributions of soil water retention characteristics. Water Resources Research, 24(5), https://doi.org/10.1029/WR024i005p00755

Castellini M., Bondì C., Giglio L., Iovino M. 2024. Impact of vermicompost addition on water availability of differently textured soils. Heliyon, 10, e35699, 15 pp., https://doi.org/10.1016/j.heliyon.2024.e35699

Castellini M., Bondì C., Leogrande R., Giglio L., Vitti C., Mastrangelo M., Bagarello V. 2025. Evaluating the effects of compost, vermicompost, and biochar on physical quality of sandy-loam soils. Applied Sciences, 15, 3392, 23 pp., https://doi.org/10.3390/app15063392

Cataldo E., Salvi L., Paoli F., Fucile M., Masciandaro G., Manzi D., Masini C.M., Mattii G.B. 2021. Application of zeolites in agriculture and other potential uses: a review. Agronomy, 11, 1547, 14 pp., https://doi.org/10.3390/agronomy11081547

Chatzistathis T., Tzanakakis V., Giannakoula A., Psoma, P. 2020. Inorganic and Organic Amendments Affect Soil Fertility, Nutrition, Photosystem II Activity, and Fruit Weight and May Enhance the Sustainability of Solanum lycopersicon L. (cv. 'Mountain Fresh') Crop. Sustainability, 12(21), 9028, 20 pp., https://doi.org/10.3390/su12219028

Christiaens K., Feyen J. 2000. The influence of different methods to derive soil hydraulic properties on the uncertainty of various model outputs of a distributed hydrological model. Physics and Chemistry of the Earth, Part B, 25(7-8), 679-683. https://doi.org/10.1016/S1464-1909(00)00084-8

Close K.R., Frasier G., Dunn G.H., Loftis J.C. 1998. Tension infiltrometer contact interface evaluation by use of a potassium iodide tracer. Transactions of the American Society of Agricultural Engineers, 41, 995-1004, doi: 10.13031/2013.17272

Colombani N., Mastrocicco M., Di Giuseppe D., Faccini B., Coltorti M. 2015. Batch and column experiments on nutrient leaching in soils amended with Italian natural zeolitites. Catena, 127, 64-71. https://doi.org/10.1016/j.catena.2014.12.022

Cook F.J., Broeren A. 1994. Six methods for determining sorptivity and hydraulic conductivity with disc permeameters. Soil Science, 157(1), 2-11, https://doi.org/10.1097/00010694-199401000-00002

Curtis M.J., Claassen V.P. 2009. Regenerating topsoil functionality in four drastically disturbed soil types by compost incorporation. Restoration Ecology, 17, 24-32, https://doi.org/10.1111/j.1526-100X.2007.00329.x

Doerr S.H. 1998. On standardizing the 'Water Drop Penetration Time' and the 'Molarity of an Ethanol Droplet' techniques to classify soil hydrophobicity: A case study using medium textured soils. Earth Surface Processes and Landforms, 23(7), 663-668, https://doi.org/10.1002/(SICI)1096-9837(199807)23:7<663::AID-ESP909>3.0.CO;2-6

Dohnal M., Dusek J., Vogel T. 2010. Improving hydraulic conductivity estimates from minidisk infiltrometer measurements for soils with wide pore-size distributions. Soil Science Society of America Journal, 74, 804-811. https://doi.org/10.2136/sssaj2009.0099

Dohnal M., Vogel T., Dusek J., Votrubova J., Tesar M. 2016. Interpretation of ponded infiltration data using numerical experiments. Journal of Hydrology and Hydromechanics, 64(3), 289-299, doi: 10.1515/johh-2016-0020

Dong L., Zhang W., Xiong Y., Zou J., Huang Q., Xu X., Ren P., Huang G. 2022. Impact of short-term organic amendments incorporation on soil structure and hydrology in semiarid agricultural lands. International Soil and Water Conservation Research, 10: 457-469, https://doi.org/10.1016/j.iswcr.2021.10.003

Ebel B.A., Moody J.A. 2020. Parameter estimation for multiple post-wildfire hydrologic models. Hydrological Processes, 34, 4049-4066, https://doi.org/10.1002/hyp.13865

Eden M., Gerke H.H. Houot S. 2017. Organic waste recycling in agriculture and related effects on soil water retention and plant available water: a review. Agronomy for Sustainable Development, 37(11), 21pp., https://doi.org/10.1007/s13593-017-0419-9

Garbowski T., Bar-Michalczyk D., Charazińska S., Grabowska-Polanowska B., Kowalczyk A., Lochyński P. 2023. An overview of natural soil amendments in agriculture. Soil & Tillage Research, 225, 105462, 20 pp., https://doi.org/10.1016/j.still.2022.105462

Gee G.W., Or D. 2002. 2.4 Particle-Size Analysis. In Methods of Soil Analysis (eds J.H. Dane and G. Clarke Topp), https://doi.org/10.2136/sssabookser5.4.c12

Ghasemi Z., Sourinejad I., Kazemian H., Rohani S. 2016. Application of zeolites in aquaculture industry: a review. Reviews in Aquaculture, 10(1), 75-95, https://doi.org/10.1111/raq.12148

Gholami L., Kavian A., Kiani-Harchegani M., Karimi N., Serrano Bernardo F. 2024. Investigating the zeolite performance in soil and water conservation after prescribed fires in degraded rangelands. Trees, Forests and People, 16, 100576, 9 pp., https://doi.org/10.1016/j.tfp.2024.100576

Gholizadeh-Sarabi S., Sepaskhah A.R. 2012. Effect of zeolite and saline water application on saturated hydraulic conductivity and infiltration in different soil textures. Archives of Agronomy and Soil Science, 59(5): 753-764. https://doi.org/10.1080/03650340.2012.675626

Ghorbani M., Amirahmadi E., Konvalina P., Moudrý J., Bárta J., Kopecký M., Teodorescu R.I., Bucur R.D. 2022. Comparative influence of biochar and zeolite on soil hydrological indices and growth characteristics of corn (Zea mays L.). Water, 14(21), 3506, 14 pp., https://doi.org/10.3390/w14213506

Głąb T. 2014. Water retention and repellency of a sandy soil amended with municipal compost. Compost Science & Utilization, 22, 47-56, https://doi.org/10.1080/1065657X.2014.892444

Glantz S.A. 2012. Primer of Biostatistics. 7th edition. The McGraw-Hill Companies.

Haverkamp R., Ross P.J., Smettem K.R.J., Parlange J.Y. 1994. Three-dimensional analysis of infiltration from the disc infiltrometer: 2. Physically based infiltration equation. Water Resources Research, 30(11), 2931-2935 https://doi.org/10.1029/94WR01788

Huang M., Zhu Y., Li Z., Huang B., Luo N., Liu C., Zeng G. 2016. Compost as a soil amendment to remediate heavy metal-contaminated agricultural soil: mechanisms, efficacy, problems, and strategies. Water, Air, & Soil Pollution, 227, 359, 18 pp., DOI 10.1007/s11270-016-3068-8

Ibrahim H.M., Alghamdi A.G. 2021. Effect of the particle size of clinoptilolite zeolite on water content and soil water storage in a loamy sand soil. Water, 13(5), 607, 19 pp., https://doi.org/10.3390/w13050607.

IUSS Working Group WRB, 2022. World Reference Base for Soil Resources. International soil classification system for naming soils and creating legends for soil maps, 4th edition. International Union of Soil Sciences (IUSS), Vienna, Austria, 236 pages.

Jarvis N., Koestel J., Messing I., Moeys J., Lindahl A. 2013. Influence of soil, land use and climatic factors on the hydraulic conductivity of soil. Hydrology and Earth System Sciences, 17(12), 5185–5195, https://doi.org/10.5194/hess-17-5185-2013

Kranz C.N., McLaughlin R.A., Johnson A., Miller G., Heitman J.L. 2020. The effects of compost incorporation on soil physical properties in urban soils – A concise review. Journal of Environmental Management, 261, 110209, 10 pp., https://doi.org/10.1016/j.jenvman.2020.110209

Kukowska S., Szewczuk-Karpisz K. 2025. Management of the soil environment using biochar and zeolite in various combinations: impact on soil condition and economical aspects. Journal of Soils and Sediments, 25, 77-102. https://doi.org/10.1007/s11368-024-03927-2

Lassabatère L., Angulo-Jaramillo R., Soria Ugalde J.M., Cuenca R., Braud I., Haverkamp R. 2006. Beerkan Estimation of Soil Transfer Parameters through Infiltration Experiments-BEST. Soil Science Society of America Journal, 70(2), 521-532, https://doi.org/10.2136/sssaj2005.0026

Lebron I., Suarez D.L., Schaap M.G. 2002. Soil pore size and geometry as a result of aggregate size distribution and chemical composition. Soil Science, 167(3), 165-172, https://doi.org/10.1097/00010694-200203000-00001

Leelamanie D.A.L., Manawardana C.U. 2019. Soil hydrophysical properties as affected by solid waste compost amendments: seasonal and short-term effects in an Ultisol. Journal of Hydrology and Hydromechanics, 67(3), 232-239, https://doi.org/10.2478/johh-2019-0007

Letey J., Carrillo M.L.K., Pang X.P. 2000. Approaches to characterize the degree of water repellency. Journal of Hydrology, 231-232, 61-65, https://doi.org/10.1016/S0022-1694(00)00183-9

Lichner L., Felde V.J.M.N.L., Büdel B., Leue M., Gerke H.H., Ellerbrock R.H., Kollár J., Rodný M., Šurda P., Fodor N., Sándor R. 2018. Effect of vegetation and its succession on water repellency in sandy soils. Ecohydrology, 11, e1991, 12 pp., https://doi.org/10.1002/eco.1991.

Logsdon S.D., Jaynes D.B. 1993. Methodology for determining hydraulic conductivity with tension infiltrometers. Soil Science Society of America Journal, 57, 1426-1431, https://doi.org/10.2136/sssaj1993.03615995005700060005x

Luukkonen T., Tolonen E.-T., Runtti H., Kemppainen K., Perämäki P., Rämö J., Lassi U. 2017. Optimization of the metakaolin geopolymer preparation for maximized ammonium adsorption capacity. Journal of Materials Science, 52, 9363-9376, https://doi.org/10.1007/s10853-017-1156-9.

Mandal M., Chandran R.S., Sencindiver J.C. 2013. Amending subsoil with composted poultry litter. I: Effects on soil physical and chemical properties. Agronomy 3(4), 657-669, https://doi.org/10.3390/agronomy3040657.

METER Group. 2021. Mini Disk Infiltrometer Manual. METER Group, Pullman, WA.

Minasny B., McBratney A.B. 2000. Estimation of sorptivity from disc-permeameter measurements. Geoderma, 95, 305-324. https://doi.org/10.1016/S0016-7061(99)00096-8

Mohammadi H., Rostamzadeh S., Ghorbanpour M. 2025. Exploring the influence of zeolite and nano-zeolite on growth, physiological and phytochemical parameters of Datura stramonium L. in cadmium-contaminated soil. 3 Biotech 15, 266, 15pp., https://doi.org/10.1007/s13205-025-04442-y

Moret-Fernández D., Latorre B., López M.V., Pueyo Y., Lassabatere L., Angulo-Jaramilo R., Rahmati M., Tormo J., Nicolau J.M. 2020. Three- and four-term approximate expansions of the Haverkamp formulation to estimate soil hydraulic properties from disc infiltrometer measurements. Hydrological Processes, 34, 5543–5556, https://doi.org/10.1002/hyp.13966

Müller K., Deurer M. 2011. Review of the remediation strategies for soil water repellency. Agriculture, Ecosystems and Environment, 144, 208-221, https://doi.org/10.1016/j.agee.2011.08.008

Murphy B.W., Koen T.B., Jones B.A., Huxedurp L.M. 1993. Temporal variation of hydraulic properties for some soils with fragile structure. Australian Journal of Soil Research, 31(2), 179-197, https://doi.org/10.1071/SR9930179

Nakhli S.A.A., Delkash M., Bakhshayesh B.E., Kazemian H. 2017. Application of zeolites for sustainable agriculture: a review on water and nutrient retention. Water, Air, & Soil Pollution, 228, 464, 34 pp., https://doi.org/10.1007/s11270-017-3649-1

Nelson D.W., Sommers L.E. 1996. Total carbon, organic carbon, and organic matter. In Methods of Soil Analysis (eds D.L. Sparks, A.L. Page, P.A. Helmke, R.H. Loeppert, P.N. Soltanpour, M.A. Tabatabai, C.T. Johnston and M.E. Sumner). https://doi.org/10.2136/sssabookser5.3.c34

Nimmo J.R. 2004. Porosity and pore size distribution. In Hillel, D., ed. Encyclopedia of Soils in the Environment: London, Elsevier, v. 3, 295-303, http://dx.doi.org/10.1016/B978-0-12-409548-9.05265-9

Perroux K.M., White I. 1988. Designs for disc permeameters. Soil Science Society of America Journal, 52, 1205-1215. https://doi.org/10.2136/sssaj1988.03615995005200050001x

Philip J.R. 1957. The theory of infiltration. 4. Sorptivity and algebraic infiltration equations. Soil Science, 84(3), 257-264, https://doi.org/10.1097/00010694-195709000-00010

Pratt C., Mahdi Z., Chen C., El Hanandeh A., Vogrin J., Zardo P. 2025. Manufactured zeolite application to soil can rapidly increase pH and enhance inorganic carbon sequestration. Soil and Tillage Research, 254, 106736, 9 pp., https://doi.org/10.1016/j.still.2025.106736

Prisa D. 2020. Comparison between sterilized zeolite and natural zeolite in the Cactus Pear (Opuntia Ficus-Indica L. Mill.) growing. GSC Advanced Research and Reviews, 04(03), 7-14, https://doi.org/10.30574/gscarr.2020.5.1.0080

Reynolds W.D., Topp G.C. 2008. Chapter 69 Soil water analyses: Principles and parameters. pp. 913-937 in M.R. Carter and E.G. Gregorich eds., Soil Sampling and Methods of Analysis, Canadian Society of Soil Science, 2nd ed., CRC Press, Taylor & Francis Group, ISBN-13: 978-0-8493-3585-0; ISBN-10: 0-8493-3586-8.

Reynolds W.D., Drury C.F., Tan C.S., Fox C.A., Yang X.M. 2009. Use of indicators and pore volume function characteristics to quantify soil physical quality. Geoderma, 152, 252-263, https://doi.org/10.1016/j.geoderma.2009.06.009

Rivier P.A., Jamniczky D., Nemes A., Makó A., Barna G., Uzinger N., Rékási M., Farkas C. 2022. Short-term effects of compost amendments to soil on soil structure, hydraulic properties, and water regime. Journal of Hydrology and Hydromechanics, 70, 74-88, https://doi.org/10.2478/johh-2022-0004

Satriani A., Belviso C., Lovelli S., Di Prima S., Coppola A., Hassan S.B.M., Rivelli A.R., Comegna A. 2024. Impact of a synthetic zeolite mixed with soils of different pedological characteristics on soil physical quality indices. Geoderma, 451, 117084, 14 pp., https://doi.org/10.1016/j.geoderma.2024.117084

Šípek V., Jačka L., Seyedsadra S., Trakal L. 2019. Manifestation of spatial and temporal variability of soil hydraulic properties in the uncultivated Fluvisol and performance of hydrological model. Catena, 182, 104119, 11 pp., https://doi.org/10.1016/j.catena.2019.104119

Stewart R.D., Rupp D.E., Abou Najm M.R., Selker J.S. 2013. Modeling effect of initial soil moisture on sorptivity and infiltration, Water Resources Research, 49, 7037-7047, https://doi.org/10.1002/wrcr.20508

Tatlier M., Atalay-Oral C., Bayrak A., Maraş T., Erdem A., 2022. Impact of ion exchange on zeolite hydrophilicity/hydrophobicity monitored by water capacity using thermal analysis. Thermochimica Acta, 713, 179240, 8 pp., https://doi.org/10.1016/j.tca.2022.179240

Topp G.C., Reynolds W.D., Cook F.J., Kirby J.M., Carter M.R. 1997. Physical attributes of soil quality. In: Gregorich, E.G., Carter, M.R. (Eds.), Soil Quality for Crop Production and Ecosystem Health. Developments in Soil Science, vol. 25. Elsevier, New York, NY, pp. 21-58. https://doi.org/10.1016/S0166-2481(97)80029-3

Vandervaere J.-P., Vauclin M., Elrick D.E. 2000. Transient flow from tension infiltrometers: I. The two-parameter equation. Soil Science Society of America Journal, 64, 1263-1272, https://doi.org/10.2136/sssaj2000.6441263x

van Genuchten M.Th. 1980. A closed-form equation for predicting the hydraulic conductivity of unsaturated soils. Soil Science Society of America Journal, 44, 892-898, https://doi.org/10.2136/sssaj1980.03615995004400050002x

Villagra-Mendoza K., Horn R. 2018. Effect of biochar on the unsaturated hydraulic conductivity of two amended soils. International Agrophysics, 32, 373-378, https://doi.org/10.1515/intag-2017-0025

Wahl N.A., Bens O., Schäfer B., Hüttl R.F. 2003. Impact of changes in land-use management on soil hydraulic properties: hydraulic conductivity, water repellency and water retention. Physics and Chemistry of the Earth, 28, 1377-1387, https://doi.org/10.1016/j.pce.2003.09.012

Wanniarachchi D., Cheema M., Thomas R., Kavanagh V., Galagedara L. 2019. Impact of soil amendments on the hydraulic conductivity of boreal agricultural podzols. Agriculture, 9, 133, 12 pp., https://doi.org/10.3390/agriculture9060133

Warrick A.W., Broadbridge P. 1992. Sorptivity and macroscopic capillary length relationships. Water Resources Research, 28, 427-431, https://doi.org/10.1029/91WR02599

Whelan A., Kechavarzi C., Coulon F., Sakrabani R., Lord R. 2013. Influence of compost amendments on the hydraulic functioning of brownfield soils. Soil Use and Management, 29, 260-270, https://doi.org/10.1111/sum.12028

Wilson G.V., Luxmoore R.J. 1988. Infiltration, macroporosity, and mesoporosity distributions on two forested watersheds. Soil Science Society of America Journal, 52(2), 329-335, https://doi.org/10.2136/sssaj1988.03615995005200020005x.

Yilmaz D., Lassabatere L., Moret-Fernandez D., Rahmati M., Angulo-Jaramillo R., Latorre B. 2023. Soil-dependent β and γ shape parameters of the Haverkamp infiltration model for 3D infiltration flow. Hydrological Processes, 37(6), https://doi.org/10.1002/hyp.14928

Zhang R. 1997. Determination of soil sorptivity and hydraulic conductivity from the disk infiltrometer. Soil Science Society of America Journal, 61, 1024-1030. https://doi.org/10.2136/sssaj1997.03615995006100040005x

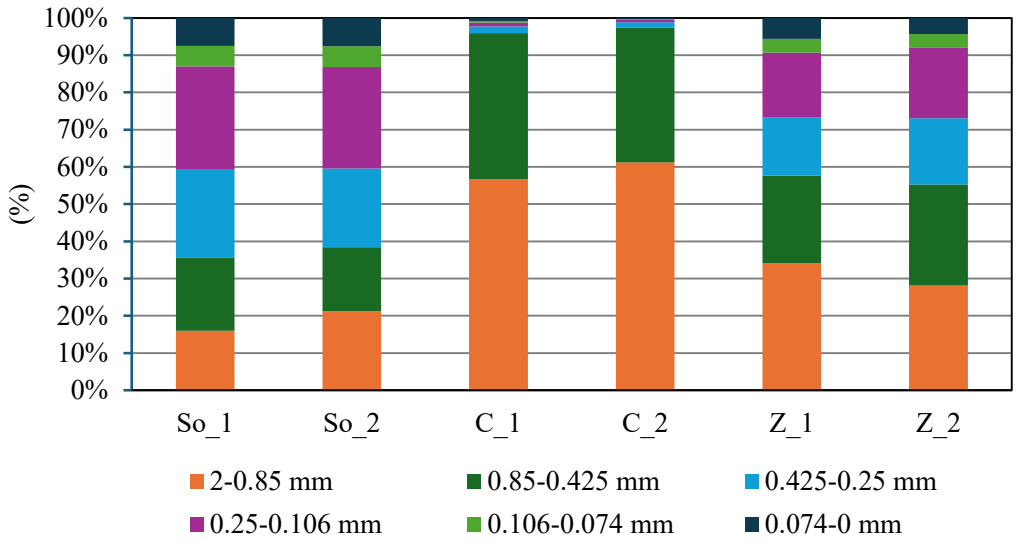

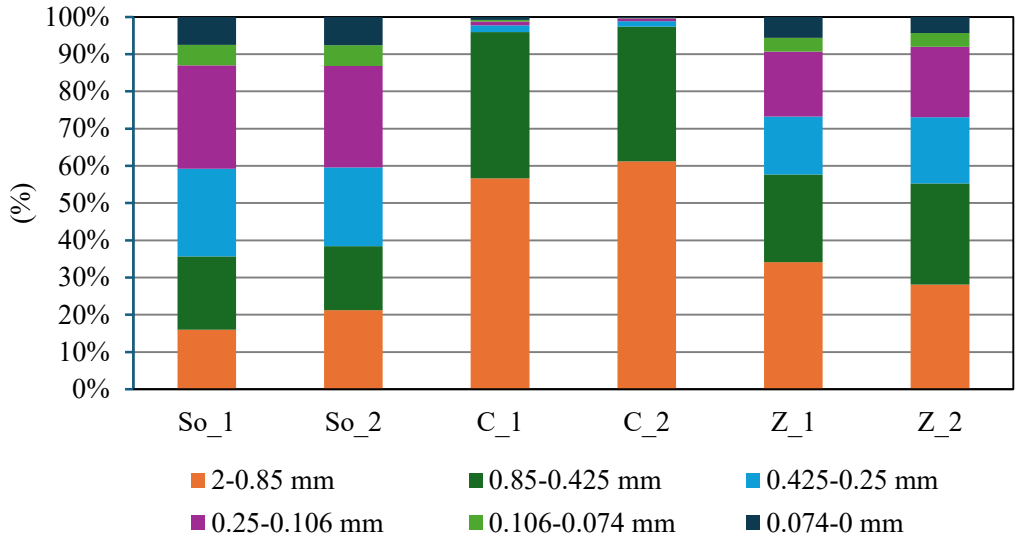

Figure 1. Percentages by weight of soil (So), compost (C) and zeolite (Z) particles of a given size range determined in duplicate (1 and 2) by sieving

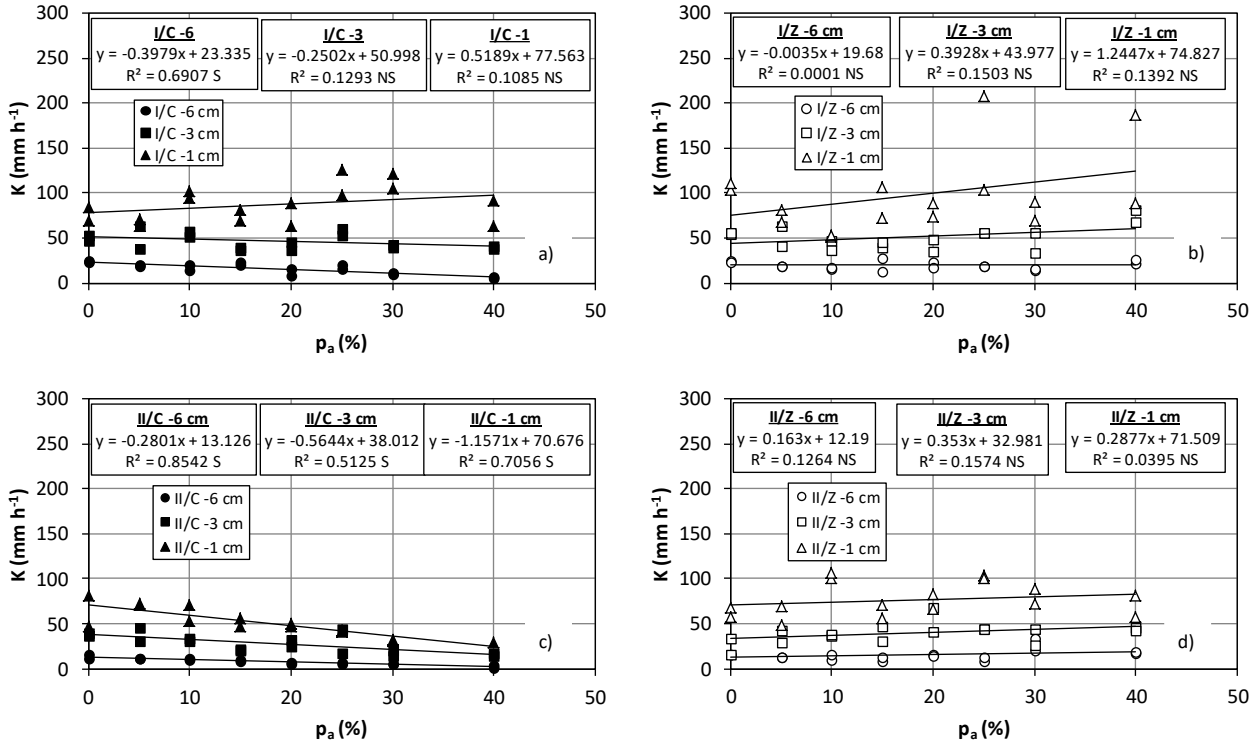

Figure 2. Relationship between the soil hydraulic conductivity, K, and the percentage, p_a, of amendment (C = compost; Z = zeolite) for the three established pressure head, h_0, values (-6, -3 and -1 cm) in the first (I) and second (II) sampling campaigns (soil hydraulic conductivity corresponding to h_0 = -6, -3 and -1 cm denoted as K_{-6}, K_{-3} and K_{-1}, respectively, in the text; S: coefficient of correlation, R, significantly greater than zero at P = 0.05; NS: R not significantly greater than zero)

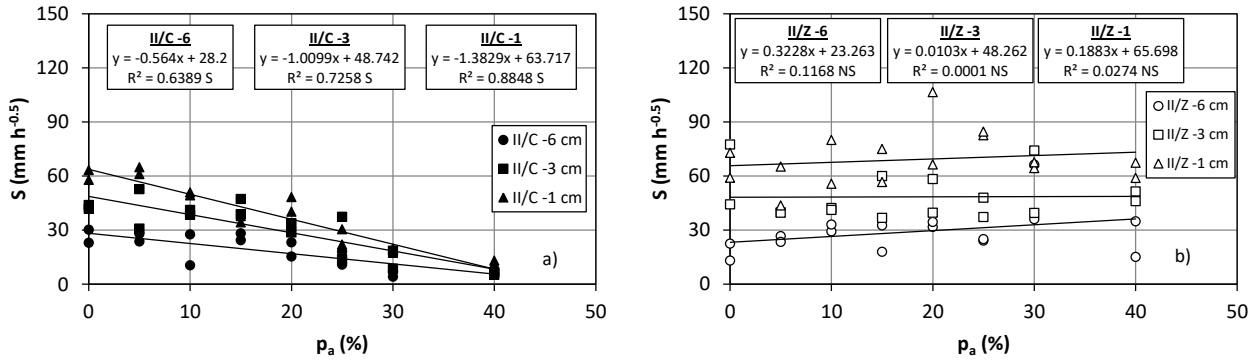

Figure 3. Relationship between the soil sorptivity, S, and the percentage, p_a, of amendment (C = compost; Z = zeolite) for the three established pressure head, h_0, values (-6, -3 and -1 cm) in the second (II) sampling campaign (soil sorptivity corresponding to h_0 = -6, -3 and -1 cm denoted as S_{-6}, S_{-3} and S_{-1}, respectively, in the text; S: coefficient of correlation, R, significantly greater than zero at P = 0.05; NS: R not significantly greater than zero)

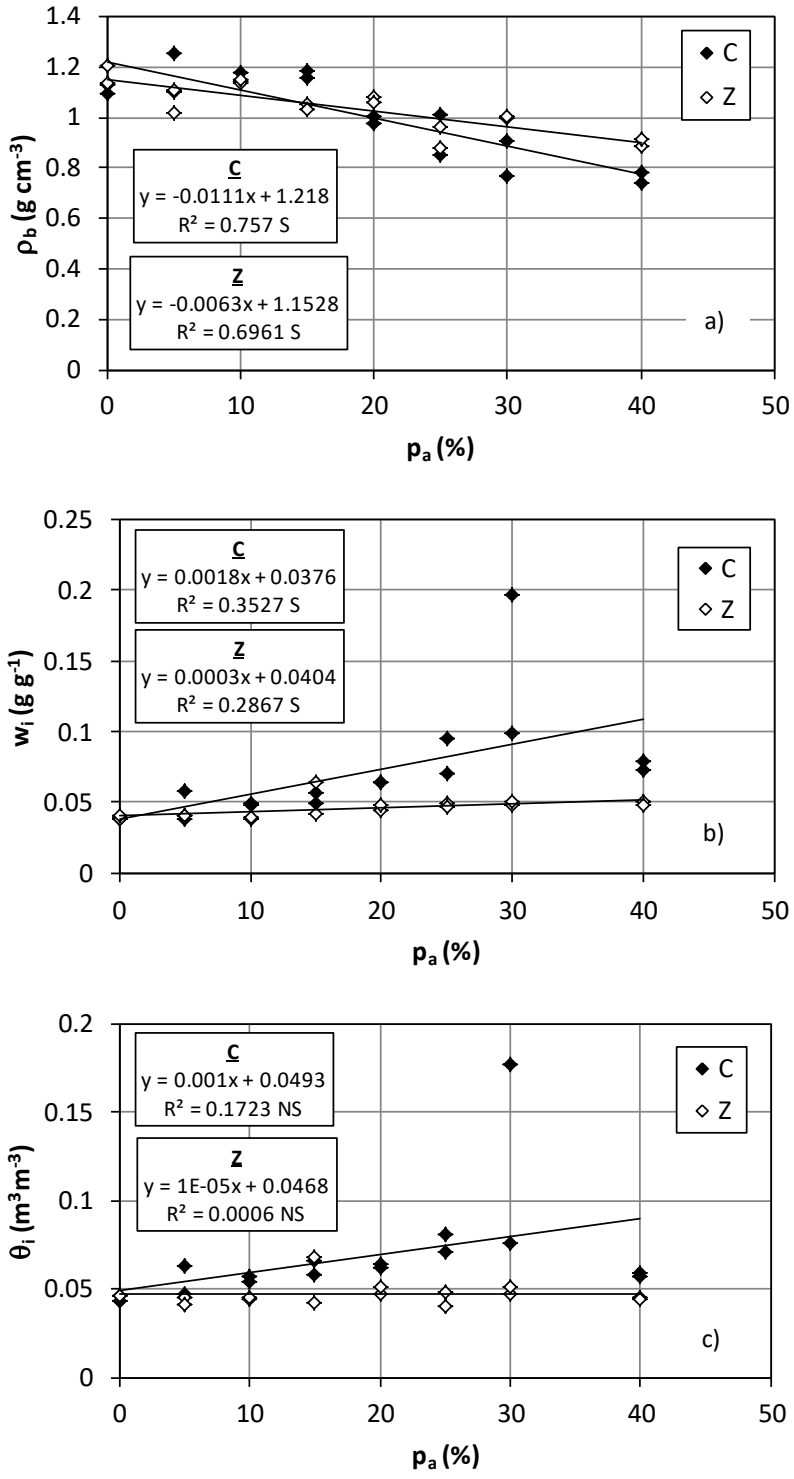

Figure 4. Dry soil bulk density, ρ_b, gravimetric, w_i, and volumetric, θ_i, soil water content before starting the second campaign of MDI runs against percentage of applied amendment, p_a (C = compost; Z = zeolite; S: coefficient of correlation, R, significantly greater than zero at $P = 0.05$; NS: R not significantly greater than zero)

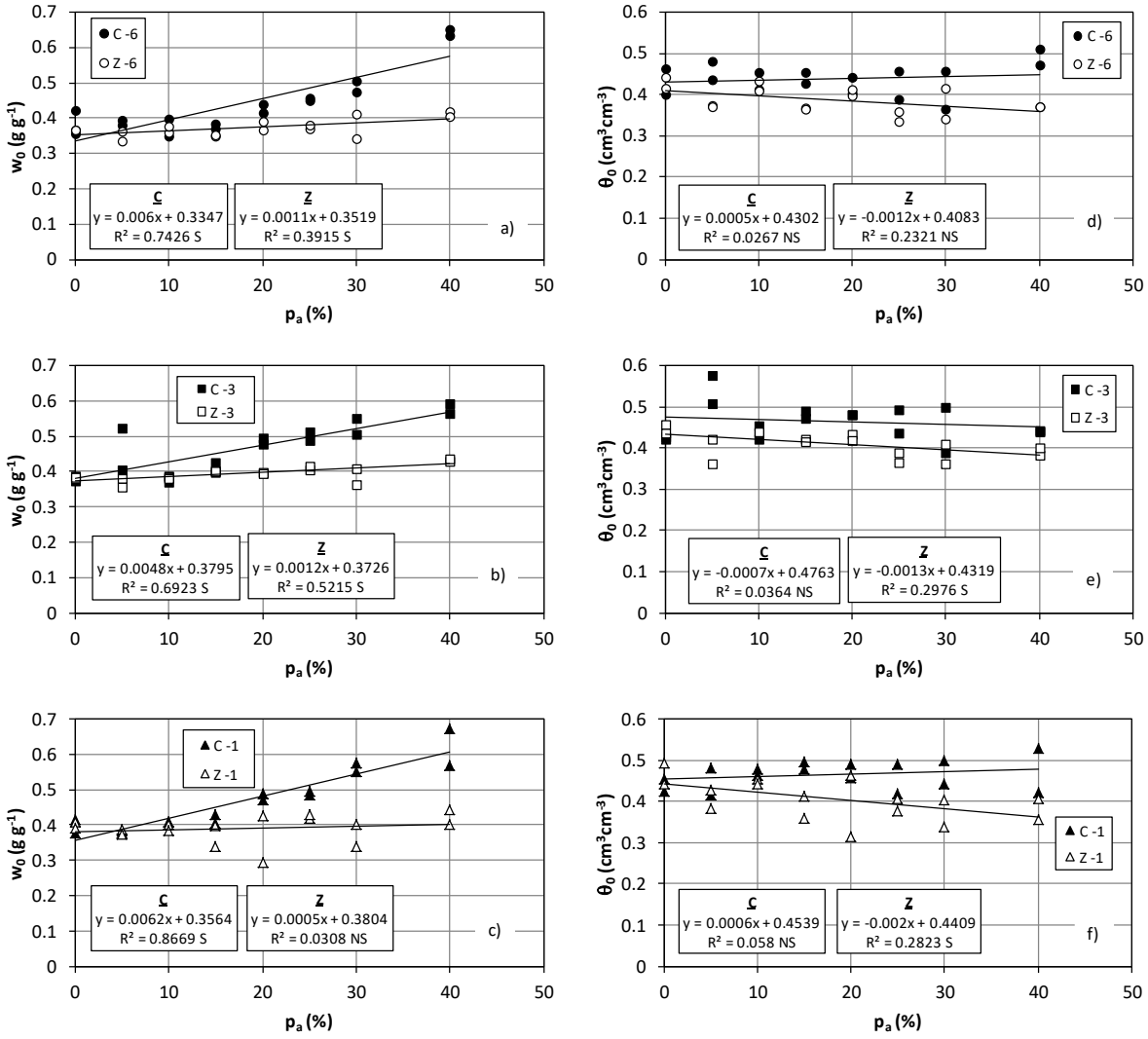

Figure 5. Gravimetric, w_0, and volumetric, θ_0, final soil water content against percentage of amendment, p_a, for the two treatments (C = compost; Z = zeolite) and the three established pressure heads with the MDI, h_0 (h_0 = -6, -3 and -1 cm; S: coefficient of correlation, R, significantly greater than zero at P = 0.05; NS: R not significantly greater than zero)

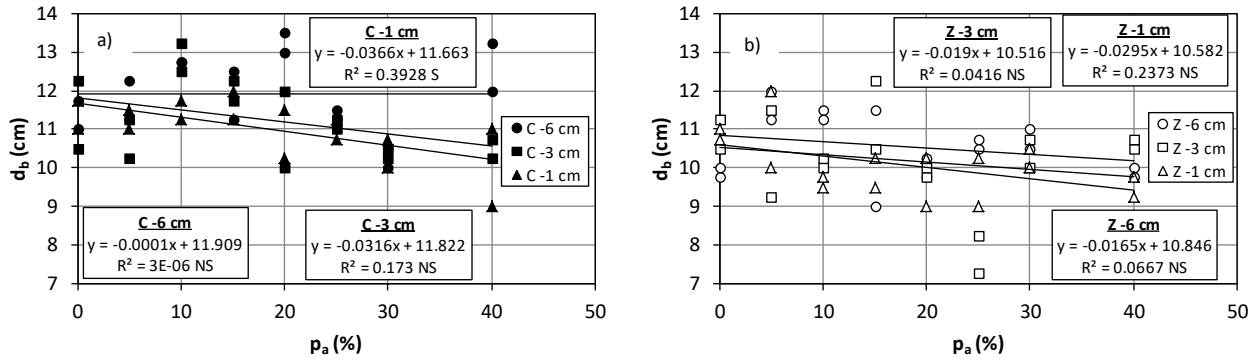

Figure 6. Relationship between the diameter of the wetted bulb at the soil surface after the MDI run, d_b (cm), and the percentage, p_a, of amendment (C = compost; Z = zeolite) for the three established pressure heads on the soil surface, h_0 (h_0 = -6, -3 and -1 cm; S: coefficient of correlation, R, significantly greater than zero at P = 0.05; NS: R not significantly greater than zero)

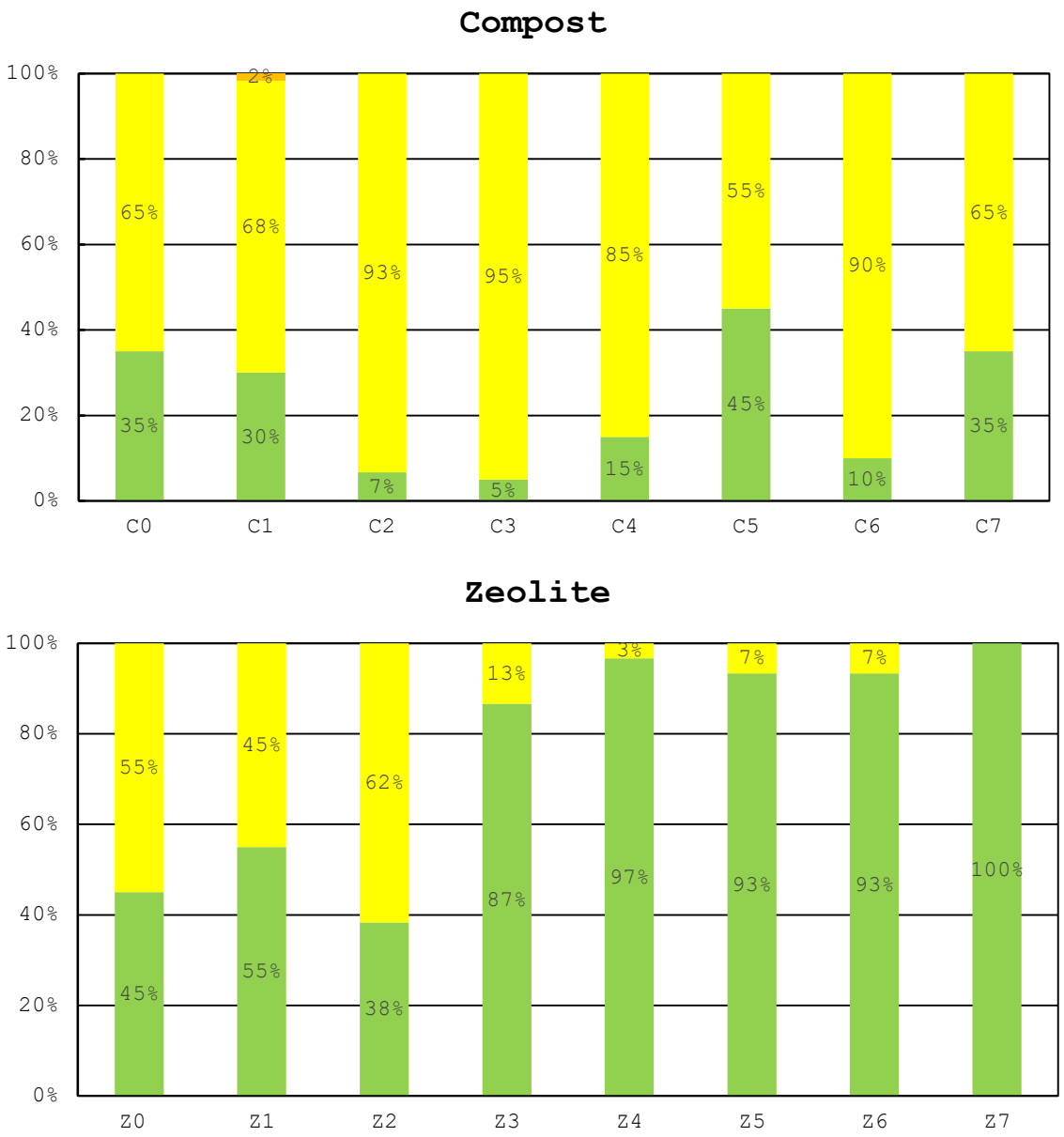

Figure 7. Classification of soil water repellency according to Bisdom et al. (1993) for different concentrations of compost and zeolite (green: wettable; yellow: slightly water repellent; orange: strongly water repellent)

Table 1. Properties of the amendments used in this investigation provided by the manufacturer

Compost	EC (dS m^{-1})	C (%)	N (%)	pH	P (%)	Ash (%)
	2.0	48	2.6	8.4	<1.0	12.3
Zeolite	CEC (Cmol kg^{-1})	SiO_2 (%)	Al_2O_3 (%)	K_2O (%)	CaO (%)	Fe_2O_3 (%)
	230	50	17	6	6	3

EC = electrical conductivity; *CEC* = cation exchange capacity.

Table 2. Summary statistics of the soil hydraulic conductivity values, K_{-6}, K_{-3} and K_{-1} (mm/h), obtained on the soil treated with compost, C, or zeolite, Z, by establishing, in two sampling campaigns, three different pressure head, h_0, values with the Mini-Disk Infiltrometer (sample size, N = 16 for each dataset except for C and h_0 = -1 cm in the second sampling campaign for which N was equal to 15)

Statistic	h_0 = -6 cm				h_0 = -3 cm				h_0 = -1 cm			
	First sampling campaign		Second sampling campaign		First sampling campaign		Second sampling campaign		First sampling campaign		Second sampling campaign	
	C	Z	C	Z	C	Z	C	Z	C	Z	C	Z
Min	5.7	12.6	1.0	7.8	36.1	34.2	14.1	15.5	62.8	52.1	28.5	48.1
Max	24.9	27.7	16.3	33.2	63.5	81.2	45.0	68.4	126.3	207.4	81.5	106.7
Mean	16.1 a A	19.6 a A	8.0 b A	15.1 b B	46.5 a A	51.1 a A	27.8 b A	39.4 b B	87.0 a A	97.4 a A	51.4 b A	76.7 a B
CV (%)	38.3	21.9	48.6	39.0	19.3	25.6	36.6	29.1	23.4	44.2	31.9	24.3

Min = minimum value; *Max* = maximum value; *CV* = coefficient of variation.

For a given pressure head and sampling date, two means followed by the same upper case letter were not significantly different according to an F test and a two-tailed t test at P = 0.05. Two means followed by a different upper case letter were significantly different.

For a given pressure head and amendment, the lower case letter was the same when two means were not significantly different according to an F test and a two-tailed t test at P = 0.05, and different when the two means were significantly different.

Table 3. Summary statistics of the dry soil bulk density, ρ_b, gravimetric, w_i, and volumetric, θ_i, soil water content values before starting the second campaign of MDI runs for the two amendments (sample size, $N = 16$ for each dataset)

Parameter	Statistic	Compost	Zeolite
ρ_b ($g\ cm^{-3}$)	Min	0.74	0.88
	Max	1.26	1.21
	Mean	1.02 a	1.04 a
	CV (%)	16.1	9.3
w_i ($g\ g^{-1}$)	Min	0.038	0.038
	Max	0.196	0.064
	Mean	0.070 a	0.046 b
	CV (%)	55.2	14.8
θ_i ($m^3 m^{-3}$)	Min	0.043	0.041
	Max	0.178	0.068
	Mean	0.068 a	0.047 b
	CV (%)	46.1	13.5

For a given parameter, two means followed by the same lower case letter were not significantly different according to an F test and a two-tailed t test at $P = 0.05$. Two means followed by a different lower case letter were significantly different.

Table 4. Summary statistics of the gravimetric, w_0, and volumetric, θ_0, final soil water content values after a MDI run at different pressure heads, h_0, on a soil treated with compost, C, or zeolite, Z (sample size, $N = 16$ for each dataset)

Statistic	h_0 = -6 cm				h_0 = -3 cm				h_0 = -1 cm			
	w_0 (g g^{-1})		θ_0 (m^{3}m^{-3})		w_0 (g g^{-1})		θ_0 (m^{3}m^{-3})		w_0 (g g^{-1})		θ_0 (m^{3}m^{-3})	
	C	Z	C	Z	C	Z	C	Z	C	Z	C	Z
Min	0.350	0.336	0.365	0.334	0.370	0.355	0.390	0.362	0.377	0.295	0.417	0.313
Max	0.650	0.418	0.510	0.443	0.591	0.437	0.577	0.458	0.673	0.443	0.528	0.492
Mean	0.443a	0.373b	0.439a	0.386b	0.466a	0.395b	0.464a	0.409b	0.469a	0.390b	0.465a	0.404b
CV (%)	20.1	6.3	8.5	8.4	15.8	5.5	9.7	7.3	18.3	9.7	7.2	12.1

Min = minimum value; *Max* = maximum value; *CV* = coefficient of variation.

For given pressure head and variable (w_0 or θ_0), two means followed by a different lower case letter were significantly different according to an F test and a two-tailed t test at $P = 0.05$.

Table 5. Summary statistics of the values of the diameter of the wetted bulb at the soil surface after the MDI run, d_b (cm), for the two amendments and the three established pressure heads on the soil surface, h_0 (sample size, N = 16 for each dataset)

Parameter	Compost			Zeolite		
	h_0 = -6 cm	h_0 = -3 cm	h_0 = -1 cm	h_0 = -6 cm	h_0 = -3 cm	h_0 = -1 cm
Min	10.0	10.0	9.0	9.0	7.3	9.0
Max	13.5	13.3	12.0	12.0	12.3	12.0
Mean	11.9 a A	11.3 ab A	11.0 b A	10.5 a B	10.2 a B	10.0 a B
CV (%)	8.5	8.7	6.8	7.8	11.8	7.8

For a given amendment, two means followed by the same lower case letter were not significantly different according to an F test and a two-tailed t test at P = 0.05. Two means followed by a different lower case letter were significantly different.

For a given pressure head, two means followed by a different upper case letter were significantly different according to an F test and a two-tailed t test at P = 0.05.

Table 6. Summary statistics of the soil sorptivity values, S_{-6}, S_{-3} and S_{-1} (mm $h^{-0.5}$), obtained, in the second sampling campaign, on a soil treated with compost, C, or zeolite, Z, by establishing three different pressure head, h_0, values (sample size, N = 16 for each dataset except for C and h_0 = -1 for which N was equal to 15)

Statistic	Pressure head					
	-6 cm		-3 cm		-1 cm	
	C	Z	C	Z	C	Z
Min	4.1	13.0	5.3	36.8	13.0	43.7
Max	30.2	66.2	52.6	77.4	64.8	106.5
Mean	18.0 a	29.1 b	30.4 a	48.4 b	40.7 a	69.1 b
CV (%)	50.6	41.8	50.2	26.2	43.0	21.2

Min = minimum value; *Max* = maximum value; *CV* = coefficient of variation.

For a given pressure head, two means followed by the a different lower case letter were significantly different according to an F test and a two-tailed t test at P = 0.05.

Chapter 6 – Discussion

The research activities carried out during the PhD addressed a set of issues concerning how soil hydraulic properties are modified by natural process and anthropogenic actions. Alterations to these properties therefore have long-term consequences for agricultural productivity, soil conservation, and environmental stability, they can either enhance or impair soil functionality, leading to reduced water availability for crops, increased runoff and erosion risk. Thus, the ability to interpret and quantify changes in soil hydraulic properties is central to understanding soil resilience and vulnerability under contemporary agri-environmental conditions. In this framework, this PhD research contributed to the broader discussion on soil–water interactions by analysing a range of realistic situations representative of agricultural and forest systems.

The work adopted a dynamic view of soils as systems whose hydrological behaviour evolves in response to both external disturbances and internal structural changes. Moreover, a deliberate site-based approach was adopted, focusing on Sicilian soils and on issues typical of mediterranean environments, where water scarcity, intense rainfall events, and land degradation coexist. This choice allowed the investigation of soil hydraulic responses under conditions that are both environmentally critical and highly relevant from a management perspective. Overall, this approach supports a more realistic interpretation of soil functioning and contributes to the development of management strategies better aligned with the inherent complexity of soil processes under field conditions.

In discussing soil alterations, a first distinction was made between modifications affecting the soil surface and those occurring within the soil matrix. Although conceptually different, both types of alteration showed to have profound and sometimes comparable effects on soil hydraulic behaviour. In both cases, a common outcome can be the reduction of soil hydraulic conductivity, driven by changes in pore continuity and effective flow pathways. For instance, the results obtained from the study on layered soils indicate that the presence of a less permeable layer in the upper part of the profile plays a dominant role in controlling infiltration processes, regardless of the hydraulic properties of the underlying material. Even when the subsoil was more conductive, a thin surface layer with reduced permeability was sufficient to limit water entry and slow down the overall infiltration process. Comparable indications emerged from the laboratory experiments focused on soil column preparation. When different compaction procedures were compared, the lowest hydrodynamic responses were consistently associated with methods that induced more surface impacts, resulting in a more compacted upper layer, leading to reduced sorptivity and hydraulic

conductivity, despite similar bulk densities considering the entire column. Together, these results underline the critical role of surface conditions in regulating soil–water interactions and highlight how relatively subtle modifications can propagate into substantial changes in infiltration dynamics. These findings have clear relevance for both agricultural and forest contexts, as they highlight how relatively small alterations in the upper soil layers can heavily affect infiltration and runoff processes. From a management perspective, this highlights the importance of preserving or restoring surface soil structure, particularly in environments exposed to intense rainfall or mechanical disturbance.

Moving from surface-related modifications to internal soil alterations, the discussion shifts toward soils modified through the incorporation of external materials, either intentionally or unintentionally. In this case as well, the investigations focused on Sicilian soils, reflecting the strong site-specificity of the hydraulic response to amendments and contaminants. The effects of internal alterations on soil hydraulic properties showed to be highly variable and strongly dependent on both the intrinsic characteristics of the added materials and the physical and chemical properties of the receiving soil. Whether related to the unintended introduction of contaminants, such as microplastics, or to the deliberate application of agronomic amendments, both types of inputs represent anthropogenic modifications of the soil matrix and therefore have the potential to alter pore structure, water flow paths, and soil–water interactions.

About microplastics, the results obtained for the analysed soils indicate that, under the tested conditions, their overall effect on soil hydraulic behaviour was limited. However, this apparent lack of a strong response should not be interpreted as evidence of negligible impact. As highlighted in the corresponding study, the hydraulic response to microplastic inclusion varied with soil type and applied pressure head, even when the same polymer type and concentration were considered. This variability confirms that no general conclusions can be drawn from a single experimental framework. Nevertheless, the study represents a meaningful step forward in current knowledge, as it is among the few investigations addressing microplastic effects under near-saturated conditions, a hydraulic domain that remains largely unexplored in the literature. On the other hand, results obtained for compost, zeolite, and biochar indicate that these materials can significantly modify soil hydraulic behaviour, although with contrasting effects depending on amendment type, application rate, and hydraulic regime. Compost addition tended to reduce near-saturated hydraulic conductivity, particularly at higher amendment rates, suggesting a partial obstruction of the pore network or the development of finer, more tortuous flow paths. Zeolite showed a more limited and less consistent influence, while biochar generally enhanced soil water transmission, especially under conditions governed by smaller pores. These findings confirm that agronomic amendments cannot be treated as

a homogeneous category and that their hydraulic effects must be evaluated in relation to both soil texture and the dominant pore size domain involved in water flow.

From a management perspective, these findings are particularly relevant for agricultural soils, where amendments are often applied primarily to improve chemical fertility, organic matter content, or soil pH, with limited consideration of their hydrological consequences. The results presented in this thesis highlight that such materials can also induce non-negligible changes in soil hydraulic behaviour, which may either support or hinder water movement depending on the type of material and the application rate. Therefore, the hydraulic effects of amendments should be explicitly considered when designing soil management strategies, especially in mediterranean environments where water availability and infiltration dynamics are critical constraints. The results also suggest that certain amendments may be intentionally exploited to improve soil hydraulic functioning. In particular, biochar showed the potential to enhance hydraulic conductivity under near-saturated conditions, adding a further benefit to the range of positive effects already documented for this material. This indicates that, beyond their agronomic and chemical roles, some amendments could be integrated into management practices with the specific aim of improving soil hydrological performance, provided that their effects are evaluated in relation to local soil properties and environmental conditions. This perspective reinforces the need for an integrated approach to soil management, in which physical, chemical, and hydrological processes are jointly considered rather than treated as independent components.

Across the studies presented in this thesis, methodological aspects emerged as a cross-cutting element that strongly influenced the interpretation of soil hydraulic behaviour. Both laboratory and field investigations confirmed that infiltration measurements are highly sensitive to the experimental framework adopted, often to a degree comparable with the effects induced by soil alterations themselves. In laboratory conditions, the preparation of repacked soil columns proved to be a critical step for ensuring meaningful and comparable results. As discussed in the context of surface compaction, different packing strategies can lead to distinct near-surface conditions, which in turn exert a dominant control on infiltration dynamics. These findings emphasize that laboratory methodologies cannot be treated as neutral technical steps, but rather as integral components of the experimental system that directly shape the observed hydraulic response.

Moreover, automation emerged as a central element for improving experimental efficiency and reproducibility. Manual reading procedures, commonly adopted in infiltration measurements, can be time-consuming and subject to operator-related variability, especially during prolonged field

campaigns. The development and testing of an automated Mini Disk Infiltrometer addressed these limitations by providing a more standardized and efficient measurement process. Although some technical aspects, such as the characteristics of the porous disk, require further refinement, the automated system demonstrated the potential to reduce experimental uncertainty and facilitate data acquisition in both laboratory and field contexts.

Overall, these methodological insights underline that progress in soil hydrology is closely linked to the refinement of experimental tools and protocols. By contributing to the optimization of laboratory procedures and exploring innovative measurement solutions, this PhD work provides a methodological foundation that can support future studies aimed at characterizing soil hydraulic behaviour under realistic and complex conditions.

Chapter 7 – Conclusion

Overall, the studies discussed in this thesis provide a coherent picture of soil hydraulic behaviour as the outcome of interacting physical, structural, and management-related factors. Rather than singular mechanisms, the research adopted an integrative perspective, addressing soil responses under realistic conditions representative of common agricultural and forest scenarios. Across the different case studies, a recurring outcome was the marked sensitivity of infiltration and near-saturated flow processes to relatively small alterations in soil structure, surface conditions, or amendments inputs.

A first major contribution of this PhD concerns methodological aspects of infiltration measurements. Part of the research was devoted to improving the clarity, reliability, and reproducibility of experimental procedures, particularly in laboratory conditions. The results demonstrated that, when a shared manual protocol is applied, comparable infiltration data can be obtained by different operators using the Mini Disk Infiltrometer. In addition, the way repacked soil columns are prepared was shown to significantly influence hydrodynamic responses: preparing the soil in successive layers reduced variability among repeated measurements, contributing to more robust experimental outcomes. Although these findings are specific to the tested soil and conditions, they represent an important step toward more standardized laboratory methodologies. Methodological advancement was further achieved through the development and validation of a low-cost, automated Mini Disk Infiltrometer. This manufactured device, produced using accessible 3D-printing technology and inexpensive sensors, yielded infiltration results largely comparable to those obtained with a commercial instrument. This confirms the feasibility of alternative, cost-effective measurement solutions that can enhance experimental efficiency and accessibility in both laboratory and field applications.

Beyond methodological aspects, this thesis examined how different forms of soil alteration influence hydraulic behaviour. Results consistently showed that modifications affecting near-surface conditions play a dominant role in controlling infiltration, with even thin, low-permeability layers substantially limiting water entry into the soil profile. The analysis of internally modified soils further demonstrated that anthropogenic inputs could induce contrasting hydraulic effects depending on both material characteristics and soil context. Microplastic experiments highlighted the relevance of particle shape, with fibrous forms exerting the strongest influence under near-saturated conditions, representing an early contribution to understanding microplastic–soil–water interactions. Similarly, agronomic amendments produced material-specific responses: biochar generally enhanced soil

hydraulic performance, whereas compost reduced unsaturated conductivity at higher application rates, and zeolite showed limited or variable effects. Overall, these findings emphasize the need to explicitly account for hydraulic impacts when soils are altered through management or external inputs.

Taken together, the research conducted during this PhD advances current understanding of how soil hydraulic properties respond to both external disturbances and internal modifications. Rather than providing universal formulations, the work contributes well-documented experimental evidence that strengthens the conceptual framework needed to interpret soil–water interactions under realistic management and environmental conditions. This represents a solid basis for further developments in soil hydrology, water resource management, and sustainable agroecosystem planning.

The results previously presented represent a step forward in the understanding of soil hydraulic behaviour under a range of realistic disturbances and management conditions. At the same time, the results obtained highlight several directions along which future investigations could further advance current knowledge. From a methodological perspective, additional research is needed to consolidate and extend the procedures developed in this work. The effects of soil column preparation and packing methods should be tested across a wider range of soil textures and structural conditions, in order to assess the transferability of the proposed approaches beyond the loam soils investigated here. Similarly, the automated 3D-printed Mini Disk Infiltrometer developed during this PhD offers promising opportunities for improving the efficiency and repeatability of infiltration measurements, but its performance should be evaluated under different environmental settings, soil types, and moisture conditions to fully assess its potential for both laboratory and field applications. With respect to soil structural alterations, further studies could explore more complex layering configurations and their interaction with natural rainfall regimes, particularly under repeated wetting–drying cycles. Extending these analyses to different pedological contexts would help clarify how the thickness, position, and hydraulic contrast of soil layers jointly control infiltration and runoff processes under Mediterranean climatic conditions. Regarding internally modified soils, future research should aim to deepen the understanding of soil-specific responses to anthropogenic inputs. In the case of microplastics, further experimental work is required to investigate the combined effects of particle shape, concentration, and polymer type particularly under near-saturated conditions, as well as their interaction with different soil matrices. Such studies would contribute to clarifying whether the observed effects are transient or persistent and how they evolve over time. Similarly, the hydraulic implications of agronomic amendments deserve further attention, particularly under field conditions and over longer time scales. The results obtained for biochar, compost, and zeolite suggest that

amendments applied for chemical or structural benefits may also induce relevant hydraulic changes, which should be explicitly considered in soil management strategies. Long-term and field-based experiments would be especially valuable to assess the persistence of these effects and their interaction with natural climatic forcing.

Overall, future research building on the outcomes of this thesis should continue to adopt integrated and site-specific approaches, combining methodological refinement with realistic experimental conditions. Such efforts are essential to improve the understanding of soil–water interactions in agri-forest systems and to support more effective and sustainable land and water management practices, particularly in environmentally sensitive mediterranean regions.

Appendix

This chapter presents two experimental studies that were carried out during the PhD research and have reached the stage of data analysis and preliminary interpretation.

The first study extends the laboratory investigation on amended soils to field conditions, aiming to assess how the effects of compost and zeolite evolve over the medium term after exposure to natural atmospheric agents. The second study focuses on the occurrence and development of soil water repellency following wildfire in a forest soil.

Although the experimental activities have been completed, data processing and in-depth discussion are still ongoing. These studies are included in this chapter because they represent an essential component of the overall research path, and their finalisation is expected to lead to the preparation of manuscripts for submission to international peer-reviewed journals

Field experiment on amendments

Following the study on the short-term effects of compost and zeolite addition on the hydrodynamic properties of a sandy loam soil, presented in Chapter 5, this subsequent work was designed to assess the medium-term effects of these amendments in order to evaluate the evolution of their influence on soil hydraulic behaviour over time. Unlike the previous experiment, which focused on freshly prepared and tightly controlled laboratory conditions, this phase aimed to reproduce more realistic environmental conditions, allowing the amended soils to undergo natural weathering and ageing processes. The study also sought to extend the investigation to field-scale applications, thereby bridging the gap between laboratory findings and the complex dynamics occurring in situ. The overall objective was to better understand how compost and zeolite interact with the soil matrix over time, and how these interactions may alter the near-saturated hydraulic properties when subject to environmental weathering and natural wetting–drying cycles.

Two experimental plots were created in the citrus orchard from which the original soil had been collected. Each plot corresponded to one amendment type (compost or zeolite) and was divided into four subplots receiving different amendment rates: 0%, 5%, 10%, and 15% by volume. The soil in each subplot was excavated to a depth of 15 cm, thoroughly mixed with the designated amendment (or left unamended for the control), and then returned to its original position. The plots were left undisturbed for approximately six months (January–June 2025) to allow the system to stabilize and

to permit the natural development of soil–amendment interactions. At the end of this period, infiltration trials were performed using the Mini Disk Infiltrometer under 3D conditions. For each subplot, six infiltration tests were conducted at each of the three pressure heads (h_0 = −6, −3, and −1 cm), resulting in a comprehensive dataset to evaluate the influence of both amendment type and application rate on the soil's near-saturated hydraulic properties. The raw results are here reported in Fig. 7a-f.

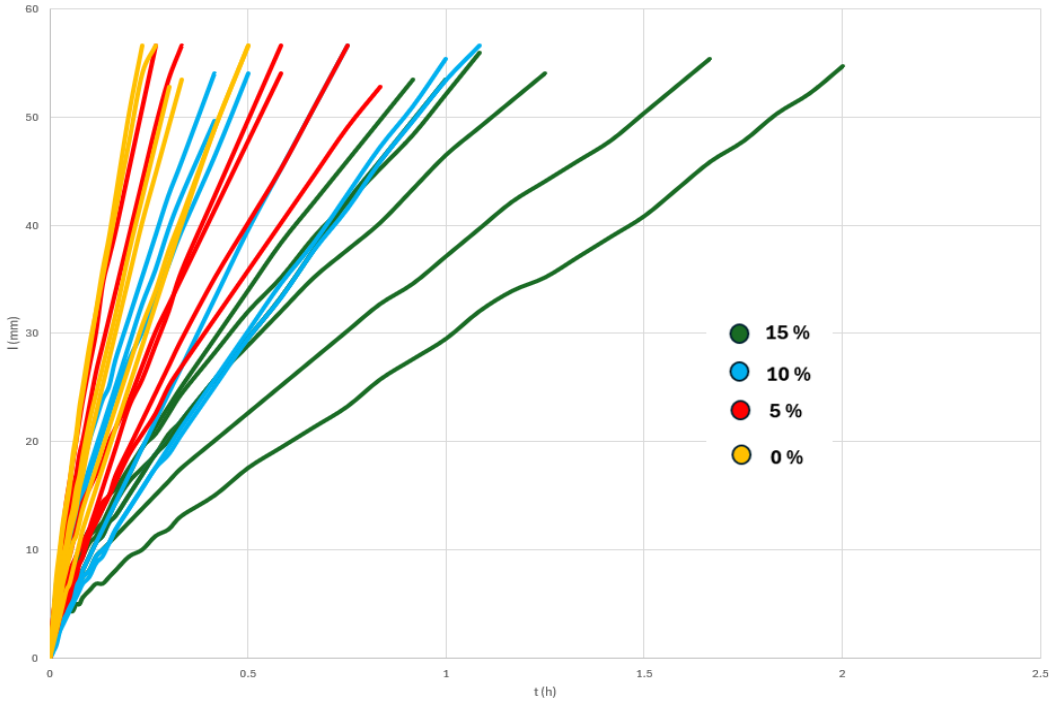

Fig 7a: cumulative infiltration curve for compost amended parcel with pressure head h_0 = -6 cm

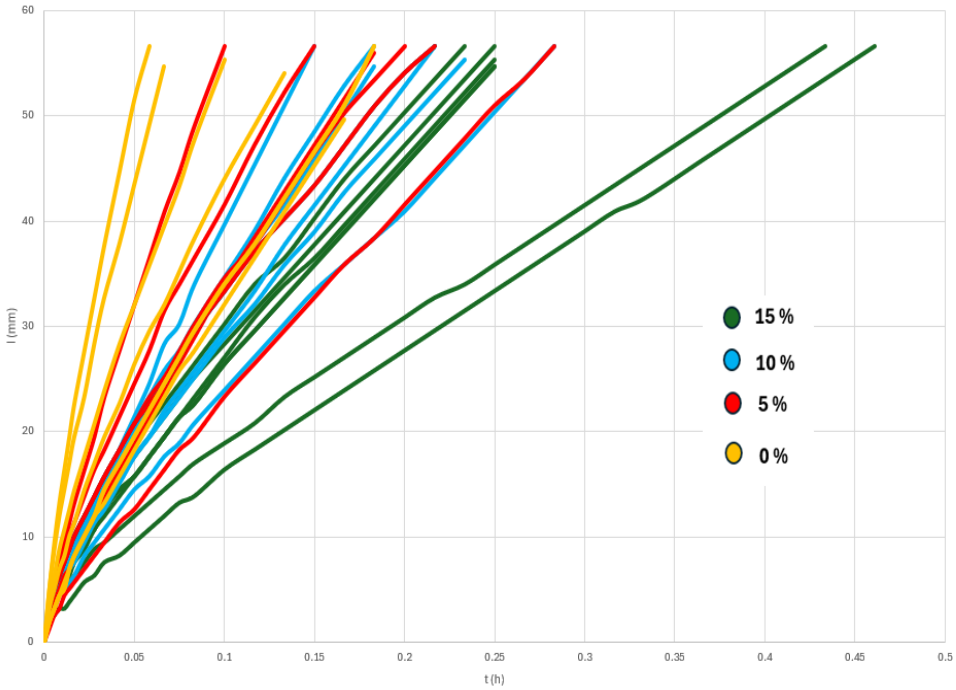

Fig 7b: cumulative infiltration curve for compost amended parcel with pressure head h_0 = -3 cm

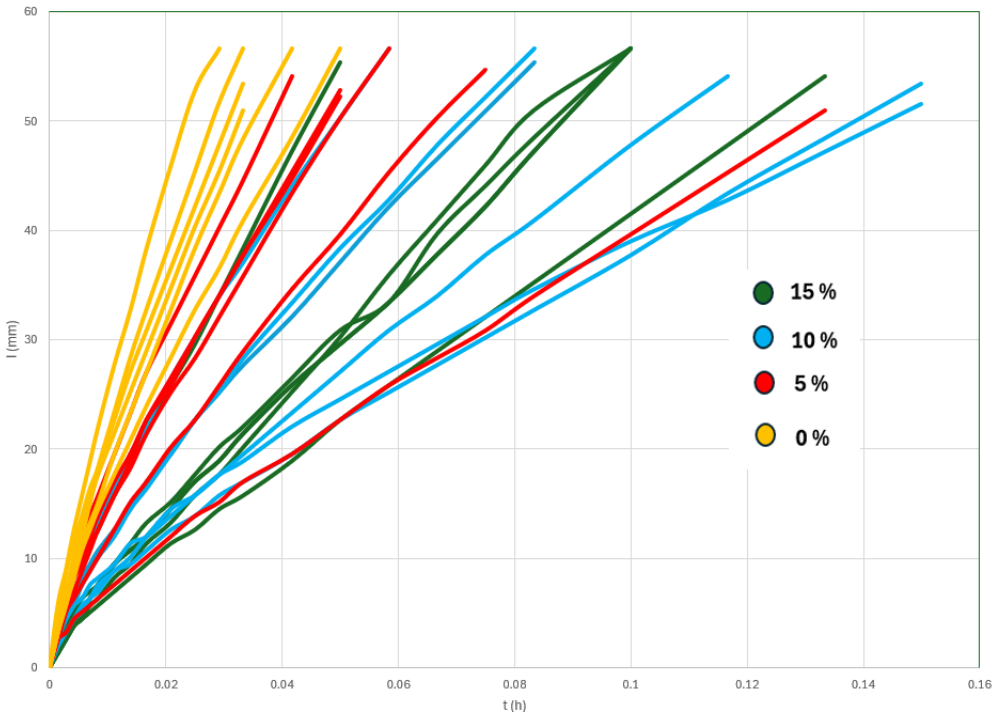

Fig 7c: cumulative infiltration curve for compost amended parcel with pressure head h_0 = -1 cm

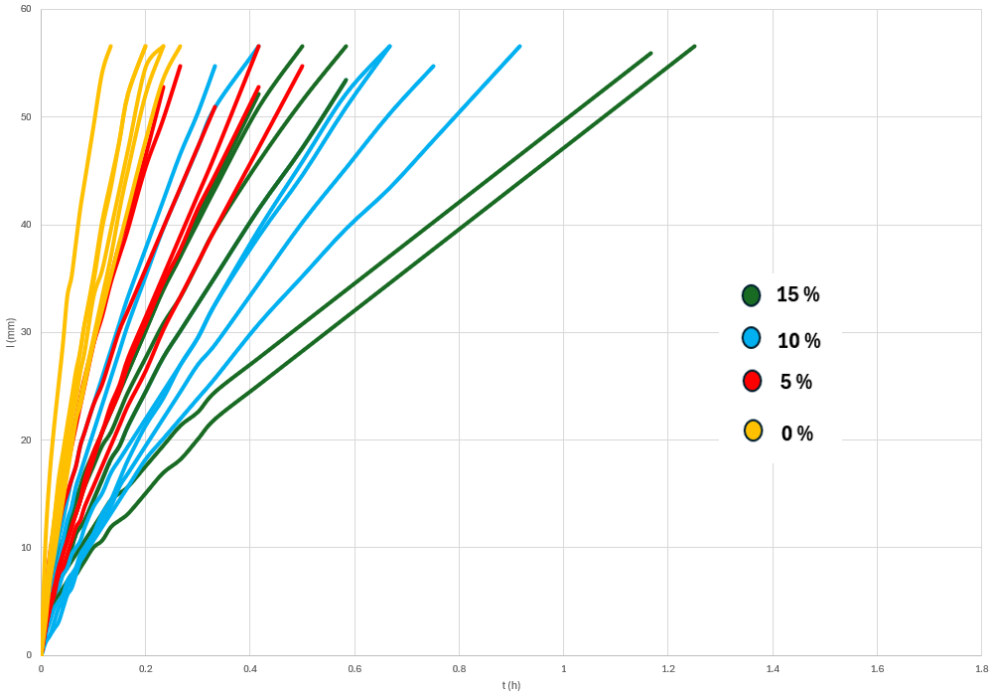

Fig 7d: cumulative infiltration curve for zeolite amended parcel with pressure head h_0 = -6 cm

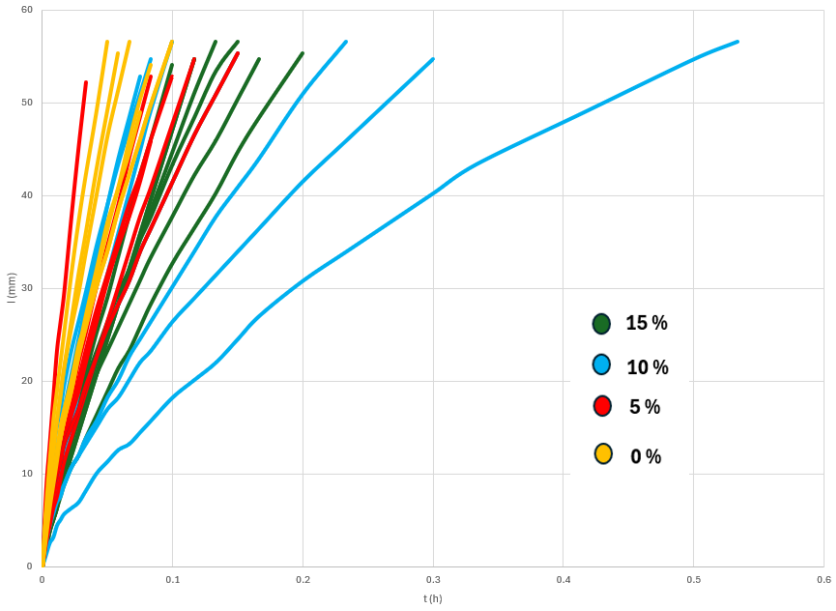

Fig 7e: cumulative infiltration curve for zeolite amended parcel with pressure head h_0 = -3 cm

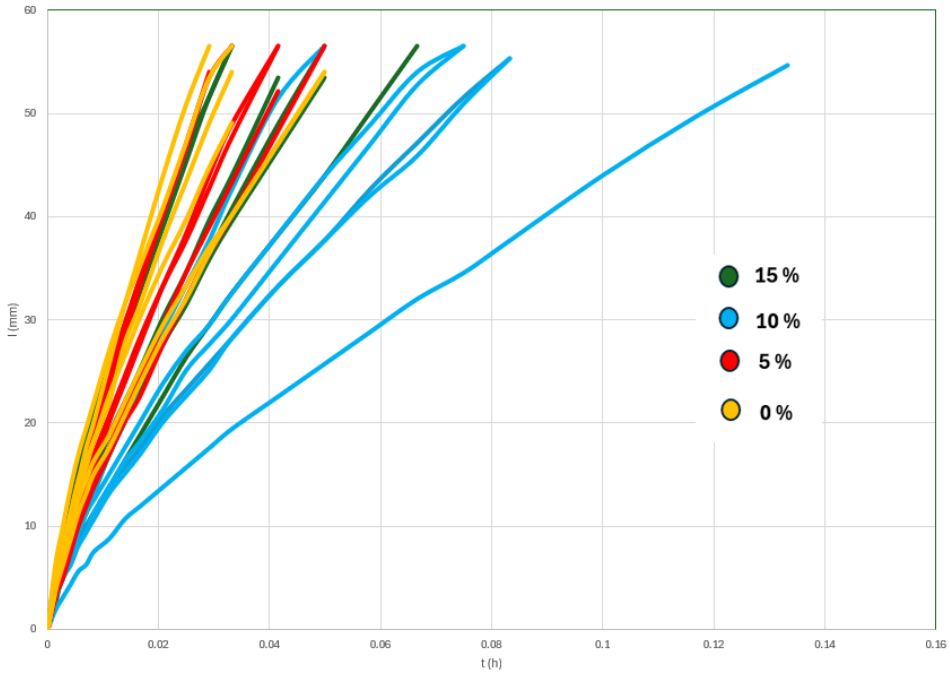

Fig 7f: cumulative infiltration curve for zeolite amended parcel with pressure head h_0 = -1 cm

Preliminary results from field tests conducted on compost- and zeolite-amended plots are consistent with the general trends observed in the previous laboratory experiment. In particular, compost addition tended to reduce unsaturated hydraulic conductivity, especially at higher amendment rates and under more negative pressure heads, suggesting a partial obstruction of the pore network or the onset of mild water repellency effects. In contrast with the laboratory findings, zeolite appeared to reduce hydraulic conductivity under field conditions, although further statistical analyses are needed to confirm and better interpret this behaviour. These analyses will provide a more complete and reliable understanding of the observed effects. This ongoing work represents a crucial step toward linking laboratory findings with field-scale hydrological responses, providing a more realistic understanding of how soil amendments may affect infiltration dynamics, water retention, and the sustainability of soil–water interactions in agricultural systems.

Post-wildfire Water Repellency

Wildfires represent one of the main disturbances affecting Mediterranean forest ecosystems, often leading to profound changes in the physical and hydrological properties of soils. Among these, soil water repellency (SWR) plays a key role, as it can markedly reduce the soil's infiltration capacity, promoting surface runoff and increasing the risk of erosion (Imeson et al., 1992; Wang et al., 2000). Understanding the spatial and vertical variability of SWR after fire events is therefore essential to

assess post-fire hydrological response and to support soil conservation strategies and sustainable forest management. In this context, this work conducted during the doctoral period aims to investigate the occurrence and intensity of water repellency in forest soils affected by wildfires, focusing on how the recent fire history and the organic matter content influence the development of hydrophobic layers in the soil profile.

Soil samples were collected in October 2023 from four areas within Monte Pellegrino Natural Reserve (R.N.O. Monte Pellegrino), located in the municipality of Palermo. The four areas were selected based on the historical occurrence of wildfires, with reference to the wildfire in 2016, which affected a large portion of the mountain, and two more localized events in summer 2023. An additional selection criterion aimed at targeting areas with similar forest cover, ensuring a hypothetical consistency in soil litter and chemico-physical properties. Thus, four soils were sampled (Tab. 3).

Tab 3: Sampling areas characterization

	SOIL A	SOIL B	SOIL AB	SOIL C
Coordinates	38°09’23’’N 13°21’18’’E	38°10’38’’N 13°20’26’’E	38°09’08’’N 13°21’23’’E	38°10’17’’N 13°20’38’’E
Elevation	282 m.s.l.	325 m.s.l.	289 m.s.l.	353 m.s.l.
Exposure	S-O	O	E	O
WIldfire	2016	2023	2016 -2023	NO
Forest cover	Present	Present	Absent	Present
Vegetation species	C. sempervirens, P. halepensis	C. sempervirens, P. halepensis	P. setaceum, A. alba	C. sempervirens P. halepensis
Litter	Present	Present (burned)	Absent	Present

Following a quick manual removal of the litter, with efforts to preserve the integrity of the soil surface, undisturbed samples were collected using steel cylinders with a diameter of 8 cm and a height of 5 cm from the top 5 cm of soil. Fifteen samples were taken from each area, along with approximately 4-5 kg of soil from the same depth, for textural analysis and to measure organic matter content. The steel cylinders were sealed on both ends with plastic caps and wrapped in plastic film;

once transported to the laboratory, they were air-dried until they reached equilibrium. During transport, one sample from Soil B was lost, so only 14 samples were considered for the Soil B subset.

Prior to testing, each sample was carefully weighed, then water repellency was measured using the Water Drop Penetration Time (WDPT) approach, conducted on the surface as well as through the full soil profile at 1 cm increments, thereby identifying 5 layers. To achieve this, the cylinders were opened, placed on a plastic plunger, and held upright by wooden supports of varying heights depending on the profile analysed. Starting with 5 cm supports for the surface, each profile was characterized with 10 drops (N=150 per depth for each soil), timed individually. Once all drops infiltrated, the wooden supports were removed, and the sample was pushed out of the cylinder by 1 cm using the plunger. At this point, 4 cm wooden supports were placed at the base, and the first centimetre of soil was carefully cut with a knife to expose the next layer for analysis. This procedure was repeated until reaching the -4 cm layer from the surface; in some samples it was not possible to characterize all layers due to the presence of large rocks that obstructed the proper cutting procedure. During each phase, all material was gathered to preserve the integrity of the sample content after testing, subsequently each sample was dried in an oven at 105°C for 24 hours to determine its initial water content. Additionally, the four soil types were characterized for their clay, sand, and organic matter content (Tab 2)

Tab 2: Clay, sand and organic matter percentage in the fur soils.

Soil	Clay %	Sand %	O.M %
A	26.02	21.84	6.1
B	12.25	35.85	16.5
AB	26.46	13.28	5.5
C	27.6	14.9	13.9

SOIL A: TEMPORAL COMPARISON

The Soil A area has been the focus of several studies investigating the evolution of soil water repellency following the 2016 wildfire. The first assessments, conducted through field WDPT tests in August 2016 and May 2017 (Tinebra et al., 2019), revealed a marked persistence of extreme water repellency (EXH) throughout the first post-fire year. These results suggested that the recovery of the

soil's wettability is strongly related to fire severity: in severely burned soils, such as Soil A, even a full year was insufficient for the soil to regain its pre-fire hydrological conditions.

Subsequent investigations carried out in 2018 by Bagarello et al. (2020) confirmed a gradual decline in repellency intensity. While some residual repellency (classified as STR) was still detected in two sampling points, most of the tested sites (five out of seven) had already returned to wettable (WET) conditions.

The 2023 observations for Soil A further support this interpretation, with the soil exhibiting complete wettability (WET class). Seven years after the fire, a full return to undisturbed conditions can be assumed, as the temporary alterations induced by the 2016 event—whose hydrophobic effects persisted for at least one year and were still partially detectable in 2018—had entirely disappeared by 2023

WATER REPELLENCY PROFILES

To characterize the water repellency profiles of each soil, the WDPT data were divided into 20 subsets based on the soil type (A, B, AB, C) and depth layer along the profile (0, -1, -2, -3, -4 cm).

As an exploratory analysis, the Lilliefors (1967) test was applied to each data subset to determine whether the distribution was normal. Additionally, the same test was applied to the logarithmically transformed variable to assess lognormality. In both cases, the null hypothesis of normality and lognormality was consistently rejected. Due to these results, each subset was characterized by a median value, which was assigned to a water repellency class considered representative of the subset (*wettable soil*, WET, WDPT <5 s; *slightly water repellent*, SLI, 5-60 s; *strongly water repellent*, STR, 60-600 s; *severely water repellent*, SEV, 600-3600 s; *extremely water repellent*, EXT, >3600 s). The interquartile range was also measured to provide an indication of data variability within each subset.

Tab 3: WDPT of every soil profile for each sampling zone

	Soil A (16)	Soil B (23)	Soil AB (16-23)	Soil C (NO)
	Median (s)	Median (s)	Median (s)	Median (s)
0	1 (WET)	2610 (SEV)	4 (WET)	1020 (SEV)
-1	1 (WET)	13020 (EXT)	15 (SLI)	2220 (SEV)
-2	1 (WET)	9900 (EXT)	30 (SLI)	900 (SEV)
-3	1 (WET)	2970 (SEV)	35 (SLI)	30 (SLI)
-4	1 (WET)	195 (STR)	32 (SLI)	12 (SLI)

As shown in Tab 3, notable differences between the four soils under examination are immediately evident: Soil B exhibits the highest water repellency (EXT in -1 and -2 cm), followed by Soil C (SEV in 0, -1 and -2 cm), Soil AB (SLI in -1, -2, -3 and -4 cm), and finally Soil A, which is entirely wettable (WET). The interquartile range (IQR) values reveal substantial variability across all soils except for Soil A, which is not surprising given the nature of the phenomenon being investigated.

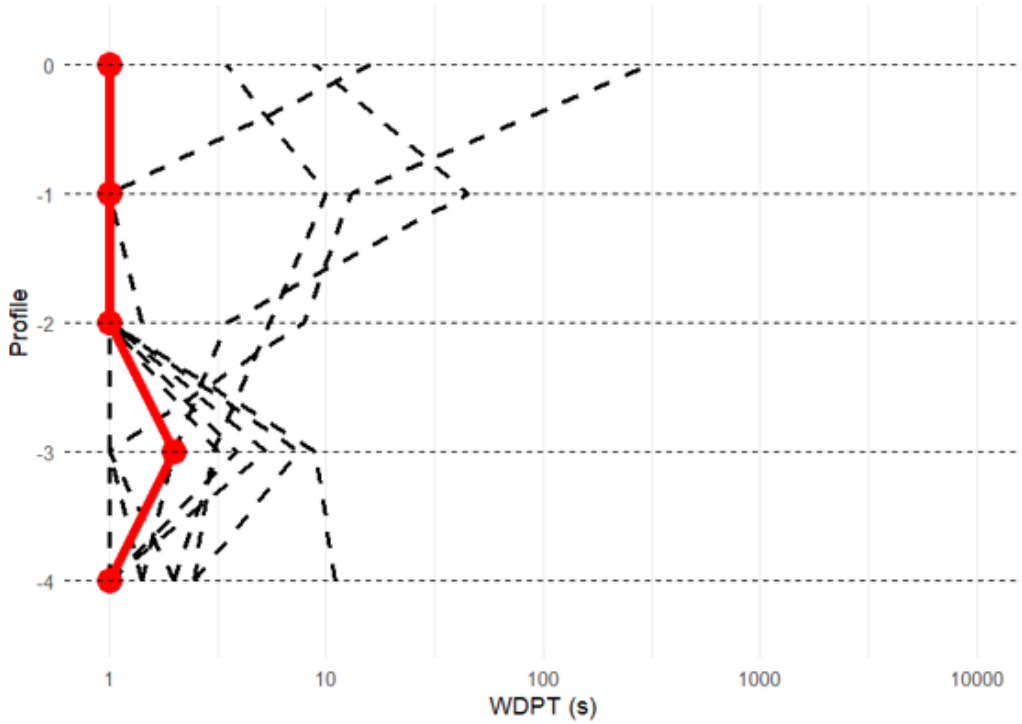

Fig 2: SWR profile of Soil A (16)

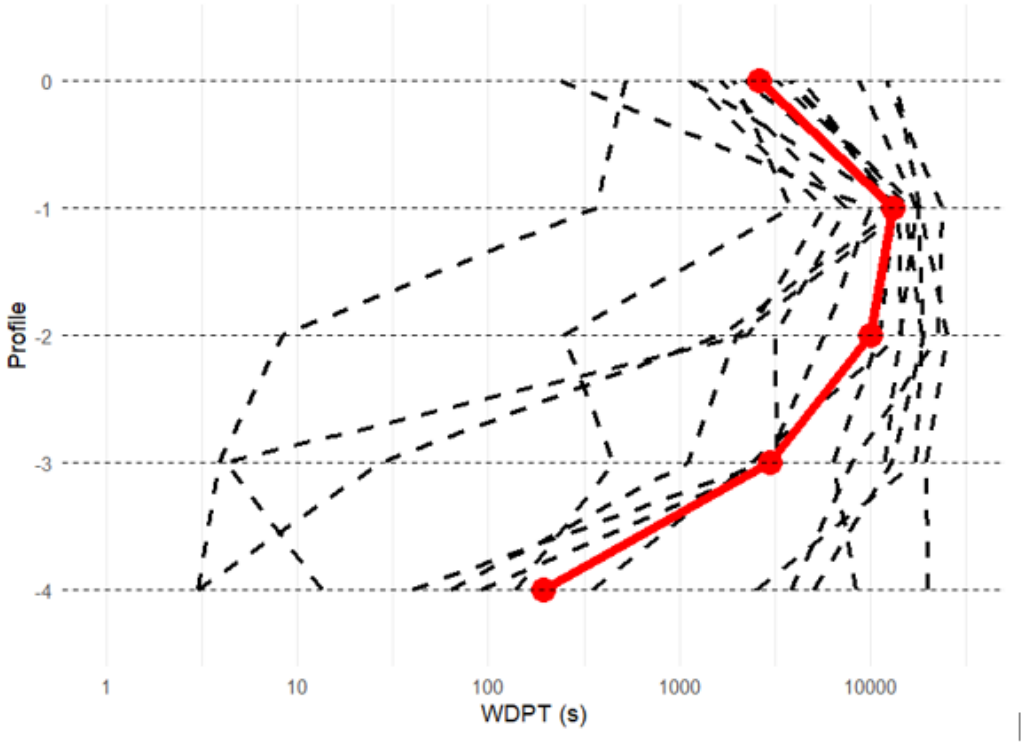

Fig 3: SWR profile of Soil B (23)

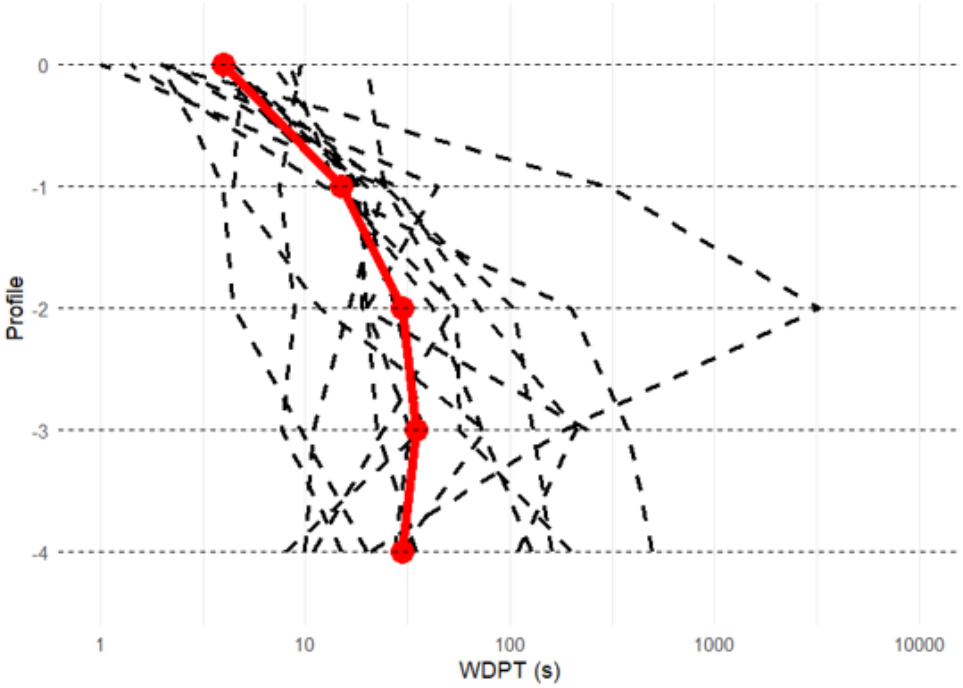

Fig 4: SWR profile of Soil AB (16-23)

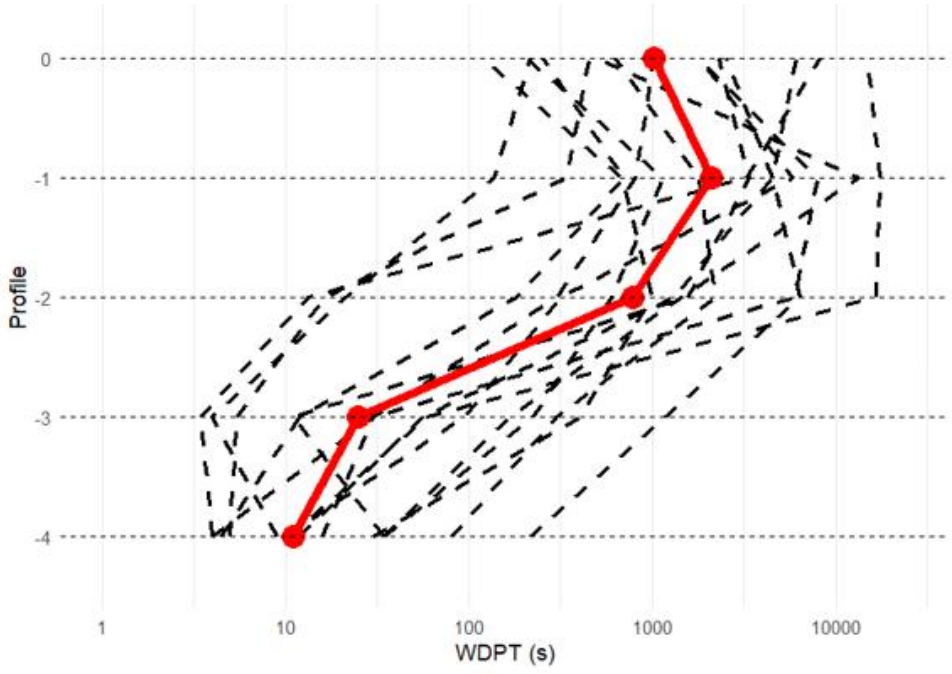

Fig 5: SWR profile of Soil C (NO)

Figures 2–5 show the soil water repellency profiles for the four investigated soils. The x-axis represents the water drop penetration time (WDPT, s) on a logarithmic scale, while the y-axis indicates the soil profile depth. The red solid line connects the median WDPT values calculated from all 150 drops at each depth, whereas the black dashed lines represent the mean values obtained for each individual sample (10 drops per sample). Overall, the signal appears consistent among samples, suggesting a reliable agreement between the general mean and the individual sample means along the soil profiles.

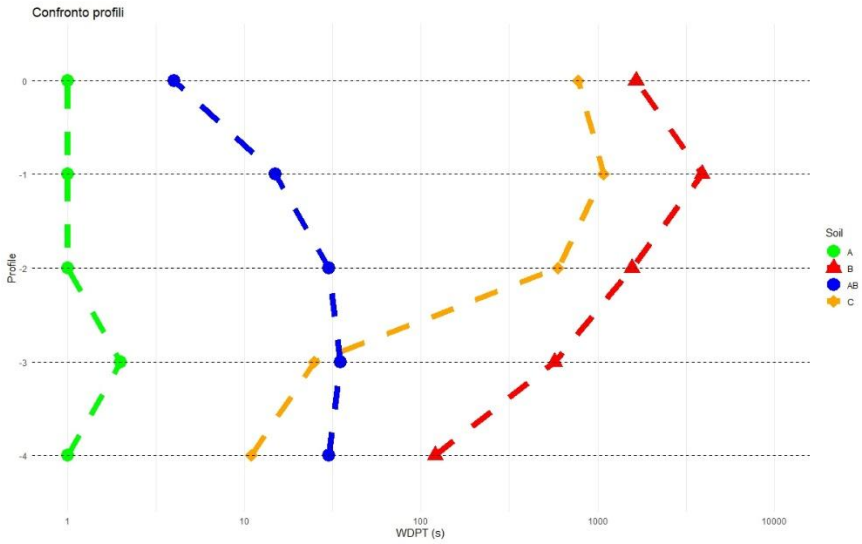

Fig 6: comparison of each SWR profile

In Fig.6, soils were compared in pairs according to their organic matter content and exposure to the 2023 wildfire. Specifically, Soils A and AB are characterized by low organic matter content, with only AB having been burned, whereas Soils B and C have higher organic matter content, with B affected by the fire and C remaining unburned.

In the A vs. AB comparison, the burned soil (AB) exhibits greater water repellency along the entire profile compared to the unburned soil (A), particularly in the subsurface layers. Similarly, in the B vs. C comparison, higher WDPT values are observed in the burned soil (B) across most depths, with the strongest differences again found below the surface. These results indicate that the soils affected by the 2023 wildfire (AB and B) tend to be more hydrophobic throughout the profile, especially below the topmost centimeters. This supports the hypothesis, consistent with Caltabellotta (2022), that the fire primarily enhanced water repellency in the deeper layers rather than at the surface

References:

Bagarello, V., Basile, G., Caltabellotta, G., Giordano, G., & Iovino, M. (2020). Testing soil water repellency in a Sicilian area two years after a fire. *Journal of Agricultural Engineering*, *51*(2), 64-72.

Caltabellotta, G., Iovino, M., & Bagarello, V. (2022). Intensity and persistence of water repellency at different soil moisture contents and depths after a forest wildfire. *Journal of Hydrology and Hydromechanics*, *70*(4), 410-420.

Dohnal, M., Dusek, J., & Vogel, T. (2010). Improving hydraulic conductivity estimates from minidisk infiltrometer measurements for soils with wide pore-size distributions. *Soil Science Society of America Journal*, 74, 804–811.

Imeson, A. C., Verstraten, J. M., Van Mulligen, E. J., & Sevink, J. (1992). The effects of fire and water repellency on infiltration and runoff under Mediterranean type forest. *Catena*, *19*(3-4), 345-361.

Lilliefors, H. W. (1967). On the Kolmogorov-Smirnov test for normality with mean and variance unknown. *Journal of the American statistical Association*, *62*(318), 399-402.

Princ, T., Fideles, H. M., Koestel, J., & Snehota, M. (2020). *The impact of capillary trapping of air on satiated hydraulic conductivity of sands interpreted by X-ray microtomography. Water, 12, 2, 445*.

Sacha, J., Snehota, M., Trtik, P., & Hovind, J. (2019). Impact of infiltration rate on residual air distribution and hydraulic conductivity. *Vadose Zone Journal*, *18*(1), 1-15.

Snehota, M., Jelinkova, V., Sobotkova, M., Sacha, J., Vontobel, P., & Hovind, J. (2015). Water and entrapped air redistribution in heterogeneous sand sample: Quantitative neutron imaging of the process. *Water Resources Research*, *51*(2), 1359-1371.

Tinebra, I., Alagna, V., Iovino, M., & Bagarello, V. (2019). Comparing different application procedures of the water drop penetration time test to assess soil water repellency in a fire affected Sicilian area. *Catena*, *177*, 41-48.

Wang, Z., Wu, Q. J., Wu, L., Ritsema, C. J., Dekker, L. W., & Feyen, J. (2000). Effects of soil water repellency on infiltration rate and flow instability. *Journal of Hydrology*, *231*, 265-276.

Zhang, R. (1997a). Determination of soil sorptivity and hydraulic conductivity from the disk infiltrometer. *Soil Science Society of America Journal*, 61, 1024–1030.